

Dissertation zur Erlangung des Doktorgrades  
der Fakultät für Chemie und Pharmazie  
der Ludwig-Maximilians-Universität München

# Metabolic and Genomic Annotations in Halophilic Archaea

Tanja Margret Oberwinkler

aus Fürstenfeldbruck



2011



## Erklärung

Diese Dissertation wurde im Sinne von Paragraph 13 Abs. 3 bzw. 4 der Promotionsordnung vom 29. Januar 1998 (in der Fassung der sechsten Änderungssatzung vom 16. August 2010) von Herrn Prof. Dr. Dieter Oesterhelt betreut.

## Ehrenwörtliche Versicherung

Diese Dissertation wurde selbständig und ohne unerlaubte Hilfe angefertigt.

München, am 26.7.2011

Tanja Oberwinkler

Dissertation eingereicht am: 26.7.2011

1. Gutachter: Prof. Dr. Dieter Oesterhelt
2. Gutachter: Prof. Dr. Helga Stan-Lotter

Mündliche Prüfung am: 17. Oktober 2011



*Zur lieben Erinnerung an meine Oma Antonia Bernthaler*

To see a world in a grain of sand  
And a heaven in a wild flower,  
Hold infinity in the palm of your hand  
And eternity in an hour.

*William Blake, 'Auguries of Innocence', 1803*



# Contents

<b>Summary</b>	<b>xix</b>
<b>1 Background</b>	<b>1</b>
1.1 Introduction to halophilic archaea as model organisms . . . . .	1
1.1.1 Diversity of halophilic archaea . . . . .	1
1.1.2 Ecological distribution of halophilic archaea . . . . .	2
1.1.3 Why use halophilic archaea as model organisms? . . . . .	4
1.2 Physiology and metabolism . . . . .	5
1.2.1 Adaptation to and protective mechanisms in extreme environments	5
1.2.1.1 Protections against dehydration . . . . .	5
1.2.1.2 Adaptation to oxygen deficiency . . . . .	6
1.2.1.3 Protections against photo-oxidation . . . . .	7
1.2.2 Metabolic analysis . . . . .	7
1.3 Motivation and objectives . . . . .	9
<b>2 Material and methods</b>	<b>11</b>
2.1 General materials . . . . .	11
2.1.1 Instruments . . . . .	11
2.1.2 Chemicals . . . . .	11
2.1.3 Kits and enzymes . . . . .	11
2.1.4 Software . . . . .	11
2.2 Microbiological methods . . . . .	11
2.2.1 Strains and culture conditions . . . . .	11
2.2.1.1 Overview of strains . . . . .	11
2.2.1.2 Culturing and storage of <i>Hbt. salinarum</i> , <i>Nmn. pharaonis</i> and <i>Nmn. moolapensis</i> strains . . . . .	14
2.2.2 Media . . . . .	14
2.2.2.1 Media for <i>Hbt. salinarum</i> . . . . .	14
2.2.2.2 Minimal medium for <i>Nmn. pharaonis</i> . . . . .	16
2.2.2.3 Modified growth medium for Haloarchaea (MGM) . . . . .	16
2.2.2.4 Synthetic medium 'DBCM2' for <i>Nmn. moolapensis</i> . . . . .	16
2.3 Molecular biological methods . . . . .	18
2.3.1 Preparation of unpurified ('crude') DNA from halobacterial cells	18
2.3.2 Gel-electrophoresis of DNA . . . . .	18
2.3.3 Isolation of DNA fragments from agarose gels . . . . .	19

2.3.4	Determination of DNA concentration . . . . .	19
2.3.5	Polymerase chain reaction (PCR) . . . . .	19
2.3.6	Sequencing of DNA . . . . .	19
2.3.7	Isolation of total RNA . . . . .	20
2.3.8	DNase digestion of extracted RNA . . . . .	20
2.3.9	DNA microarrays for gene expression profiling . . . . .	21
2.3.9.1	Synthesis of fluorescent-labeled cDNA . . . . .	21
2.3.9.2	Production and pretreatment of microarray slides . . . . .	22
2.3.9.3	Prehybridization and hybridization of microarrays . . . . .	22
2.3.9.4	Washing of the slides . . . . .	22
2.3.10	Reverse Transcription PCR (RT-PCR) . . . . .	23
2.3.10.1	Synthesis of cDNA . . . . .	23
2.3.10.2	Gel extraction and DNA sequencing . . . . .	24
2.4	Protein chemical methods . . . . .	25
2.4.1	Isotope coded protein labeling (ICPL) . . . . .	25
2.4.1.1	Isolation of cytosolic proteins of <i>Hbt. salinarum</i> . . . . .	25
2.4.1.2	Reduction, alkylation and nicotinoylation . . . . .	25
2.4.2	Membrane isolation by sucrose gradient . . . . .	26
2.4.3	Protein precipitation by trichloroacetic acid (TCA) . . . . .	26
2.4.4	SDS-Polyacrylamide Gel-Electrophoresis (SDS-PAGE) . . . . .	26
2.4.4.1	ICPL samples . . . . .	26
2.4.4.2	Analysis of proteins from sucrose gradient bands . . . . .	27
2.4.5	Tryptic in-gel-digestion and desalting of protein samples after SDS-PAGE . . . . .	27
2.4.5.1	ICPL labeled protein samples . . . . .	27
2.4.5.2	Proteins from sucrose gradient . . . . .	27
2.5	Analytical methods . . . . .	28
2.5.1	Amino acid analysis of <i>Hbt. salinarum</i> . . . . .	28
2.5.1.1	Calculations of the intracellular change of concentration of ornithine ( $\Delta_{orn}$ ) and arginine ( $\Delta_{arg}$ ) per cell . . . . .	28
2.5.2	Stable Isotope Labeling in <i>Nmn. pharaonis</i> with $^{13}C$ carbon sources . . . . .	29
2.5.3	Preparation of lipids . . . . .	29
2.5.3.1	Cell harvest and disruption . . . . .	29
2.5.3.2	Lipid extraction . . . . .	29
2.5.3.3	Extraction of polar lipids by acetone precipitation . . . . .	30
2.5.3.4	Cleavage of ether lipids with boron trichloride . . . . .	30
2.5.4	Preparation of amino acids . . . . .	30
2.5.4.1	Hydrolysis . . . . .	31
2.5.4.2	Derivatization . . . . .	31
2.5.5	Isolation of intracellular solutes . . . . .	31
2.5.6	Thin layer chromatography (TLC) . . . . .	32
2.5.6.1	Analytical TLC . . . . .	32



2.5.6.2	Preparative TLC with iodine staining . . . . .	32
2.5.7	Mass spectrometry . . . . .	32
2.5.7.1	Analysis of extracted lipids by negative-ion electro-spray ionization (ESI) mass spectrometry (MS) . . . . .	32
2.5.7.2	Analysis of alkyl chains and amino acids with gas chromatography mass spectrometry (GC/MS) . . . . .	33
2.5.7.3	Analysis of proteins extracted from sucrose gradient with NanoLC-MS/MS . . . . .	33
2.5.7.4	Analysis of nicotinoylated proteins (ICPL) . . . . .	34
2.5.8	Nuclear magnetic resonance . . . . .	35
2.5.8.1	NMR measurements of extracted lipids . . . . .	35
2.5.8.2	NMR measurements of extracted osmolytes . . . . .	36
2.6	Bioinformatics environment . . . . .	36
2.6.1	Data analysis of microarrays . . . . .	36
2.6.2	Carbon fate modeling in <i>Nmn. pharaonis</i> . . . . .	36
2.6.3	Bioinformatic analysis . . . . .	37
2.6.4	Genome annotation of <i>Nmn. moolapensis</i> . . . . .	37
2.6.4.1	Genome sequencing and assembly . . . . .	37
2.6.4.2	Gene prediction and annotation . . . . .	37
<b>3</b>	<b>Lipid metabolism in halophilic Archaea</b>	<b>39</b>
3.1	Introduction . . . . .	39
3.1.1	Archaeol - the basic structure of all archaeal membrane lipids . . . . .	41
3.1.2	Polar lipids . . . . .	42
3.1.3	Biosynthetic pathways of lipids . . . . .	42
3.1.3.1	Synthesis of the glycerol phosphate backbone from dihydroxyacetone phosphate (DHAP) . . . . .	42
3.1.3.2	Isoprenoids are synthesized via the mevalonate pathway . . . . .	44
3.2	Results and discussion . . . . .	46
3.2.1	Lipidomics in <i>Hbt. salinarum</i> , <i>Nmn. pharaonis</i> and <i>Nmn. moolapensis</i> . . . . .	46
3.2.1.1	Analytical and preparative TLC of lipid extracts identified different glycolipids . . . . .	46
3.2.1.2	Identification of archaeal lipids by negative-ion ESI-mass spectrometry . . . . .	48
3.2.2	Stable isotope labeling of isoprenoid chains . . . . .	58
3.2.2.1	Assignment of all carbons from the isoprenoid chain by natural abundance $^{13}\text{C}$ NMR . . . . .	58
3.2.2.2	$^{13}\text{C}$ NMR spectra resulting from differently labeled carbon sources . . . . .	62
3.2.2.3	GC/MS measurements of cleaved isoprenoids supported NMR data . . . . .	77

3.3	Conclusions . . . . .	83
<b>4</b>	<b>Amino acid metabolism in halophilic Archaea</b>	<b>85</b>
4.1	Introduction . . . . .	85
4.1.1	Overview of the haloarchaeal amino acid metabolism . . . . .	85
4.1.1.1	Glutamate family (glutamate, glutamine, proline, arginine) . . . . .	85
4.1.1.2	Aspartate family (aspartate, alanine, asparagine, threonine, methionine, lysine) . . . . .	86
4.1.1.3	Serine family (serine, glycine, cysteine) . . . . .	86
4.1.1.4	Branched-chain amino acids (valine, leucine, isoleucine) . . . . .	87
4.1.1.5	Aromatic amino acids (phenylalanine, tyrosine, tryptophan, histidine) . . . . .	87
4.1.2	Carbon fate maps for analysis in metabolic labeling . . . . .	87
4.1.3	Arginine fermentation - a unique way to gain energy . . . . .	88
4.2	Results and discussion . . . . .	89
4.2.1	Distribution of carbons via TCA cycle indicated non-classical amino acid biosynthesis pathways in <i>Nmn. pharaonis</i> . . . . .	89
4.2.1.1	Incorporation of the label in single amino acids derived from 1- <sup>13</sup> C- or 2- <sup>13</sup> C-acetate . . . . .	91
4.2.2	Carbon fate modeling in BNet resulted in mixed label types of amino acids . . . . .	96
4.2.2.1	Cysteine biosynthesis as an example of a carbon fate map . . . . .	97
4.2.3	Few alternative carbon sources - other than acetate - support growth of <i>Nmn. pharaonis</i> in minimal medium . . . . .	101
4.2.4	Characterization of the arginine/ornithine metabolism in <i>Hbt. salinarum</i> . . . . .	103
4.2.4.1	<i>Hbt. salinarum</i> can grow without arginine and ornithine in synthetic medium . . . . .	103
4.2.4.2	Amino acid uptake experiments with the wild-type <i>Hbt. salinarum</i> . . . . .	105
4.2.4.3	Experiments with a deletion strain verified ArcD as the main arginine uptake system . . . . .	106
4.2.4.4	Analysis of arginine fermentation by RNA microarrays and Isotope Coded Protein Labeling (ICPL) . . . . .	108
4.3	Conclusions . . . . .	111
<b>5</b>	<b>Carbon fixation in halophilic Archaea</b>	<b>113</b>
5.1	Introduction . . . . .	113
5.1.1	Calvin cycle (Calvin-Benson-Bassham cycle) . . . . .	113
5.1.2	Reductive acetyl-CoA pathway . . . . .	114

---

5.1.3	Fatty acid degradation via propionyl CoA - 3-hydroxypropionate cycle . . . . .	115
5.1.4	Reductive citrate cycle . . . . .	116
5.1.5	CO <sub>2</sub> fixation in halophilic Archaea . . . . .	117
5.2	Results and discussion . . . . .	118
5.2.1	Homology comparison in archaeal genomes . . . . .	118
5.2.1.1	Different potential CO <sub>2</sub> fixation pathways were found in halophilic archaea . . . . .	119
5.2.1.2	Calvin cycle could be excluded . . . . .	119
5.2.1.3	Improbable CO <sub>2</sub> fixation by the reductive acetyl-CoA pathway . . . . .	123
5.2.1.4	3-hydroxypropionate cycle . . . . .	124
5.2.1.5	The reductive citrate cycle is possible in <i>Hbt. salinarum</i> . . . . .	127
5.2.1.6	Reductive condensation of carbon dioxide by the glycine cleavage system . . . . .	129
5.2.2	Stable isotope labeling with <sup>13</sup> C carbonate in <i>Nmn. pharaonis</i> . . . . .	130
5.2.2.1	NMR spectra showing possible CO <sub>2</sub> fixation . . . . .	130
5.2.2.2	GC/MS derived data does not confirm carbon incorporation from CO <sub>2</sub> in <i>Nmn. pharaonis</i> . . . . .	134
5.2.3	Transcriptional analysis verifies active RuBisCO in <i>Nmn. pharaonis</i> . . . . .	137
5.3	Conclusions . . . . .	141
<b>6</b>	<b>Genomic and metabolic features of <i>Nmn. moolapensis</i></b> . . . . .	<b>143</b>
6.1	Introduction . . . . .	143
6.1.1	Haloarchaeal retinal proteins . . . . .	143
6.1.2	Osmoprotection in halophiles by compatible solutes and inorganic cations . . . . .	145
6.1.3	<i>Nmn. moolapensis</i> and its comparison to other halophilic archaea . . . . .	146
6.2	Results and discussion . . . . .	148
6.2.1	Conclusions of the genome of <i>Nmn. moolapensis</i> and comparison to its haloalkaliphilic relative <i>Nmn. pharaonis</i> . . . . .	148
6.2.1.1	Comparison and synteny analysis of retinal protein genes with associated regulators in halophilic archaea . . . . .	151
6.2.1.2	Metabolic pathway comparison in the genus <i>Natronomonas</i> . . . . .	159
6.2.2	Energy metabolism in <i>Nmn. moolapensis</i> . . . . .	164
6.2.2.1	Different illuminations showed phototrophic growth of <i>Nmn. moolapensis</i> . . . . .	164
6.2.2.2	Sucrose gradients of cell membranes resulted in differently colored bands . . . . .	166
6.2.3	NMR revealed glutamate as the sole compatible solute . . . . .	169
6.3	Conclusions . . . . .	170

<b>7 Supplementary material</b>	<b>173</b>
<b>Bibliography</b>	<b>199</b>
<b>Appendix</b>	<b>217</b>
Abbreviations . . . . .	217
Publications . . . . .	220
Danksagung . . . . .	221
Curriculum vitae . . . . .	223

## List of Figures

1.1	Representatives of the family <i>Halobacteriaceae</i> . . . . .	1
1.2	Possible environments of haloarchaea . . . . .	3
1.3	How it all started in 2005 ... . . . .	10
3.1	Comparison of archaeal and bacterial / eukaryotic cell membrane lipids	40
3.2	Structure of archaeol . . . . .	41
3.3	Pathways for the biosynthesis of archaeal ether lipids in halophiles . . .	45
3.4	Analytical TLC of total lipid extracts . . . . .	47
3.5	Preparative TLC of total lipid extract . . . . .	49
3.6	TLC plate from recovered lipids of <i>Nmn. pharaonis</i> . . . . .	49
3.7	Comparison of MS spectra of striking PGP-Me C <sub>20</sub> -C <sub>25</sub> between halophilic archaea . . . . .	52
3.8	MS spectrum of total lipid extract of <i>Nmn. moolapensis</i> . . . . .	55
3.9	MS/MS spectrum of a new glycolipid in <i>Nmn. moolapensis</i> . . . . .	56
3.10	Structures of isoprenoid chains in <i>Nmn. pharaonis</i> . . . . .	59
3.11	Natural abundance <sup>13</sup> C NMR spectra of extracted lipids . . . . .	60
3.12	{ <sup>1</sup> H, <sup>13</sup> C}-FHSQC NMR spectrum of extracted unlabeled lipids . . . . .	62
3.13	Workflow of <sup>13</sup> C labeling experiments . . . . .	64
3.14	Broadband decoupled NMR spectrum of fully labeled lipids . . . . .	65
3.15	Comparison of a 1 D natural abundant <sup>13</sup> C spectrum with a broadband carbon spectrum . . . . .	66
3.16	2 D FHSQC NMR of extracted <sup>13</sup> C labeled lipids . . . . .	67
3.17	Carbon and FHSQC spectra of lipids from cells grown in presence of either 1- <sup>13</sup> C or 2- <sup>13</sup> C acetate . . . . .	69
3.18	1 D carbon spectrum of <sup>13</sup> C labeled lipids with <sup>12</sup> C lysine as an addi- tional carbon source . . . . .	70
3.19	FHSQC U- <sup>13</sup> C <sub>2</sub> acetate with <sup>12</sup> C lysine . . . . .	71
3.20	Integrated NMR signals after normalization of <sup>13</sup> C labeled lipids in addition to 5 mM, 10 mM and 30 mM lysine in the growth medium . . .	72
3.21	Main possible degradation pathways of lysine . . . . .	74
3.22	Model for formation of isoprenoids in the mevalonate pathway in <i>Nmn. pha- raonis</i> in comparison to <i>Hbt. salinarum</i> . . . . .	76
3.23	Demonstration of the fragmentation process during ionization. . . . .	79
3.24	GC/MS spectra of <sup>13</sup> C labeled lipids with 1- <sup>13</sup> C acetate and 2- <sup>13</sup> C acetate	80

3.25	GC/MS spectra of isoprenoids extracted from cells grown in the presence of U- <sup>13</sup> C acetate and <sup>12</sup> C lysine. . . . .	81
4.1	Biosynthetic families of amino acids . . . . .	86
4.2	ADI pathway and gene cluster of <i>Hbt. salinarum</i> . . . . .	88
4.3	Derivatives of amino acids . . . . .	89
4.4	GC/MS spectra of derivatized and labeled alanine . . . . .	90
4.5	GC/MS spectra of amino acids resulted in specific clusters with similar labeling arrangements . . . . .	92
4.6	Problems in metabolic labeling of amino acids . . . . .	94
4.7	Biosynthesis diagram of cysteine and threonine . . . . .	99
4.8	Model of carbon fates of cysteine and threonine biosynthesis . . . . .	100
4.9	Alternative carbon sources in <i>Nmn. pharaonis</i> minimal medium . . . . .	102
4.10	Growth curves of three different strains of <i>Hbt. salinarum</i> : R1 (or R-), R+ and $\Delta arcD$ . . . . .	104
4.11	Conversion of arginine to ornithine by <i>Hbt. salinarum</i> R1 cells in basal salt medium . . . . .	105
4.12	Uptake experiments with deletion strain $\Delta arcD$ and wild-type <i>Hbt. salinarum</i> R1 in basal salt medium . . . . .	107
4.13	The arginine deiminase (ADI) pathway in <i>Hbt. salinarum</i> and possible connections to other pathways . . . . .	110
5.1	Calvin cycle . . . . .	115
5.2	Reductive acetyl-CoA pathway . . . . .	116
5.3	Propionate cycle . . . . .	117
5.4	Reductive citrate cycle . . . . .	118
5.5	Phylogenetic tree of the archaeal RuBisCO. . . . .	120
5.6	CO <sub>2</sub> fixation cycle using RuBisCO in <i>Nmn. pharaonis</i> . . . . .	121
5.7	Hypothetical CO <sub>2</sub> fixation pathway via propionyl-CoA . . . . .	127
5.8	Comparison of NMR spectra of lipids extracted from cells grown in the presence of (A) unlabeled carbon sources ( <sup>12</sup> C), (B) U- <sup>13</sup> C <sub>2</sub> acetate or (C) <sup>13</sup> C carbonate. . . . .	132
5.9	Integrated NMR signals after normalization of nonlabeled lipids, labeled lipids from <sup>13</sup> C acetate or <sup>13</sup> C carbonate. . . . .	133
5.10	GC/MS spectra of lipids with incorporated carbons from (i) <sup>12</sup> C acetate, <sup>12</sup> C carbonate, (ii) <sup>12</sup> C acetate <sup>13</sup> C carbonate, (iii) <sup>13</sup> C acetate, <sup>12</sup> C carbonate . . . . .	135
5.11	Check-PCR of primers designed for RT-PCR . . . . .	138
5.12	Check-PCR with 40 cycles of extracted RNA analyzed by agarose gel-electrophoresis . . . . .	139
5.13	Analysis of PCR products for genes involved in the AMP-CO <sub>2</sub> fixation pathway by agarosegel-electrophoresis . . . . .	139

---

6.1	Overview of haloarchaeal retinal proteins . . . . .	144
6.2	Phase contrast micrograph of <i>Nmn. moolapensis</i> . . . . .	148
6.3	Function categories and function classes for the classification of <i>Nmn. moolapensis</i> proteins . . . . .	150
6.4	Phylogenetic tree of all known haloarchaeal retinal proteins from sequenced genomes . . . . .	153
6.5	Genome location of retinal genes and genes involved in their regulatory network in <i>Nmn. moolapensis</i> : bacteriorhodopsin and halorhodopsin . .	156
6.6	Genome location of retinal genes and regulators in <i>Nmn. moolapensis</i> : sensory rhodopsin and transcription regulator brz . . . . .	158
6.7	Proposed respiratory chain for the genus <i>Natronomonas</i> . . . . .	161
6.8	Methionine metabolism in <i>Nmn. moolapensis</i> in a KEGG map and annotated with PRIAM . . . . .	162
6.9	Growth curves of <i>Nmn. moolapensis</i> , growing under different conditions	165
6.10	Sucrose gradients of <i>Nmn. moolapensis</i> membranes . . . . .	166
6.11	Absorption spectra of isolated membrane bands from sucrose gradient of <i>Nmn. moolapensis</i> . . . . .	167
6.12	NMR spectrum of extracted solutes of <i>Nmn. moolapensis</i> . . . . .	169
S1	Comparison of total lipid extracts by ESI-MS . . . . .	174
S2	Catalogue of lipid fragments from MS/MS spectra . . . . .	180
S3	Lipid fragments from MS/MS spectra of unknown MS peaks in <i>Nmn. moolapensis</i> . . . . .	184
S4	2D proton-COSY experiment of fully <sup>13</sup> C labeled lipids. . . . .	185
S5	Chromatogram of a typical GC/MS measurement of isoprenoids. . . . .	186
S6	Overview of all quantified proteins using the ICPL method . . . . .	188

*List of Figures*

---



# List of Tables

1.1	Summary of representative halophilic archaea from different habitats . . . . .	4
1.2	Energy-generating processes utilized by extreme halophiles . . . . .	8
2.1	Instruments . . . . .	12
2.2	Chemicals . . . . .	13
2.3	Kits and enzymes . . . . .	13
2.4	Software . . . . .	13
2.5	Complex medium for <i>Hbt. salinarum</i> . . . . .	14
2.6	Synthetic medium for <i>Hbt. salinarum</i> . . . . .	15
2.7	Minimal medium for <i>Nmn. pharaonis</i> . . . . .	16
2.8	Concentrated salt water - 30% (w/v) . . . . .	16
2.9	MGM - 23% . . . . .	17
2.10	Synthetic medium DBCM2 . . . . .	17
2.11	Trace element solution SL10 . . . . .	17
2.12	Vitamin 10 stock . . . . .	18
2.13	PCR reaction mixture . . . . .	19
2.14	Thermocycling conditions for 'Check PCR' . . . . .	19
2.15	Thermocycling conditions for sequencing PCR . . . . .	20
2.16	Primers for 'Check-PCR' . . . . .	21
2.17	TE buffer . . . . .	21
2.18	Hybridization solutions for microarrays . . . . .	23
2.19	Washing solutions for microarrays . . . . .	23
2.20	Primers for RT-PCR and corresponding 'Check-PCR' . . . . .	24
3.1	TLC $R_f$ in solvent system $\text{CHCl}_3/\text{MeOH}/90\%$ acetic acid, 65:4:35, v/v/v. . . . .	48
3.2	ESI-MS (negative mode) ion peaks. . . . .	50
3.3	Chemical shifts of carbons in solvents and isoprenoid chains . . . . .	61
3.4	Integrated all ("a") and positive ("+") signals of FHSQC spectra of lipids from <i>Nmn. pharaonis</i> grown in presence of $\text{U-}^{13}\text{C}_2$ acetate and $^{12}\text{C}$ lysine . . . . .	71
5.1	Comparison of autotrophic $\text{CO}_2$ fixation pathways . . . . .	114
5.2	Corresponding gene homologs found in <i>Nmn. pharaonis</i> , <i>Hbt. salinarum</i> and <i>Nmn. moolapensis</i> encoding enzymes of the AMP- $\text{CO}_2$ fixation cycle . . . . .	123
5.3	Homolog genes found in <i>Nmn. pharaonis</i> , <i>Hbt. salinarum</i> and <i>Nmn. moolapensis</i> encoding enzymes for $\text{CO}_2$ fixation via propionyl-CoA . . . . .	126

5.4	Homolog genes found in <i>Nmn. pharaonis</i> , <i>Hbt. salinarum</i> and <i>Nmn. moolapensis</i> encoding enzymes for the reductive citrate cycle . . . . .	128
5.5	Genes found in <i>Nmn. pharaonis</i> , <i>Hbt. salinarum</i> and <i>Nmn. moolapensis</i> encoding enzymes of the reductive glycine cleavage system . . . . .	129
5.6	Integrated all ("a") and positive ("+") signals of FHSQC spectra of lipids from <i>Nmn. pharaonis</i> grown in presence of U- <sup>13</sup> C <sub>2</sub> acetate or <sup>13</sup> C carbonate . . . . .	134
5.7	Genes of <i>Nmn. pharaonis</i> selected for transcription analysis . . . . .	137
5.8	Overview of possible fixation pathways in halophilic archaea . . . . .	140
6.1	Genes encoding retinal proteins and associated regulators in <i>Nmn. moolapensis</i> . . . . .	152
6.2	Genomic and physiologic comparison of <i>Nmn. moolapensis</i> to <i>Nmn. pharaonis</i> and <i>Hbt. salinarum</i> R1 . . . . .	159
S1	Protein sequence analysis of lysine decarboxylase . . . . .	173
S2	Summary of arginine and ornithine uptake experiments in <i>Hbt. salinarum</i>	187
S3	Enzymes encoded in <i>Nmn. pharaonis</i> (Napha) and <i>Hbt. salinarum</i> (Hasal) capable of CO <sub>2</sub> fixation. . . . .	189
S5	Genes of <i>Nmn. moolapensis</i> annotated for pathway comparison . . . . .	193

## Summary

The metabolic diversity of microorganisms is far wider than that of higher plants and animals. Prokaryotes can gain energy from an enormous variety of chemical reactions, with or without oxygen, or from light. They can use even simple carbon and nitrogen sources for biosynthesis, such as CO<sub>2</sub> and N<sub>2</sub>. This incredible metabolic flexibility has enabled microbes to colonize many extreme environments, where conditions severely limit the growth of other organisms, and many of these extremophiles belong to the domain Archaea. Haloarchaea (family *Halobacteriaceae*) are one such group. They inhabit the waters of salt lakes where the salt concentration can reach saturation and the pH can vary between neutral and extremely alkaline.

In most Archaea metabolic pathways have not been examined experimentally, but considerable insights can be gained from the complete set of genes predicted from their genome sequences. Often, this information can be used to reconstruct conserved metabolic networks used for synthesis of cell components and degradation of organic matter.

The aims of this study were (i) to predict metabolic capabilities of specific halophilic archaea based on genomic data; (ii) to perform comparative analysis of particular gene sets within the family *Halobacteriaceae*; (iii) to elucidate still unknown or ambiguous pathways involved in lipid biosynthesis, CO<sub>2</sub> fixation and amino acid metabolism; and (iv) to integrate data from biochemistry, molecular biology and genome annotation using a system's biological approach in order to provide a basis for metabolic flux profiling.

In a first step, the genome of the recently described extremely halophilic archaeon *Natronomonas moolapensis*, was sequenced and annotated. This neutrophilic species was chosen in order to compare its metabolism to that of the type species of this genus, *Natronomonas pharaonis* which grows in salt saturated soda lakes, at pH 11. A comparison of the pathway maps of both organisms revealed some differences in amino acid and cofactor biosynthesis, as well as a major difference in their energy metabolism. A synteny analysis of genes involved in energy metabolism showed that although *Nmn. moolapensis* possesses the same genes for retinal proteins (bacteriorhodopsin, halorhodopsin and sensory rhodopsin) and their regulators as *Halobacterium salinarum*, their synteny was more related to the corresponding genes encoded in the genome of the closely related *Nmn. pharaonis*.

*Nmn. moolapensis* was proven to be able to grow phototrophically, and mass analysis of cell membranes identified the presence of bacteriorhodopsin, confirming a major difference in energy production between *Nmn. moolapensis* and *Nmn. pharaonis*, which

lacks bacteriorhodopsin.

*Nmn. moolapensis* can synthesize membrane glycolipids while *Nmn. pharaonis* (and other haloalkaliphiles) cannot. The next objective of this study was to analyze and identify the membrane lipids of *Nmn. moolapensis* and correlate this data with known biosynthetic pathways. It was determined by MS/MS analysis that the glycolipid of *Nmn. moolapensis* represents a novel structure. This lipid was shown to differ from the glycolipid S-TGD-1 in *Hbt. salinarum* in the number of attached sugars as well as in the proposed phosphate group in *Nmn. moolapensis*. Phosphoglycolipids have not been detected in haloarchaea before. The presence and structure of this glycolipid might have implications for the stability of bacteriorhodopsin, as the trimeric arrangement of this protein in the purple membrane of *Hbt. salinarum* has been shown to be stabilized by glycolipids.

Archaeal membrane lipids are based on isoprenoids which are synthesized via the mevalonate pathway. It was found that this pathway is not identical in *Nmn. pharaonis* and *Hbt. salinarum*. Analysis by NMR and MS of  $^{13}\text{C}$  labeled isoprenoids revealed that lysine could be channeled into isoprenoid synthesis in *Nmn. pharaonis* with no specific preference for position in the carbon skeleton. Labeling with U- $^{13}\text{C}$  acetate yielded uniformly labeled isoprenoids. In contrast, it has been shown before that in *Hbt. salinarum* the central carbon unit of the isoprenoid was always supplied from amino acids and not from acetate. This difference can be explained by a thiolase with different specificity in *Hbt. salinarum* involved in the first step of the mevalonate pathway and the equilibration of acetyl-CoA with the cellular pool. How lysine is degraded to acetoacetyl-CoA remains unknown.

It was not known whether haloarchaea can use  $\text{CO}_2$  as a carbon source for biosynthesis, but this is most likely the case in *Nmn. pharaonis*, which lives in a carbonate-rich environment. Metabolic labeling with  $^{13}\text{C}$  was used to investigate whether *Nmn. pharaonis* is capable of  $\text{CO}_2$  fixation. After the addition of  $^{13}\text{C}$  labeled carbonate in the medium, NMR spectra showed an enrichment of  $^{13}\text{C}$  in membrane lipids and thus demonstrated  $\text{CO}_2$  fixation in *Nmn. pharaonis*. A search for genes encoding enzymes that are predicted to fix  $\text{CO}_2$  identified a variety of potential carbon fixation mechanisms in *Nmn. pharaonis*, *Nmn. moolapensis* and *Hbt. salinarum*.

The combination of modern analytical tools to identify cell components and pathways and a systems biology approach to the analysis of genomic data has provided a powerful means of investigating the metabolism of haloarchaea.  $^{13}\text{C}$ -based flux analysis supported by carbon-fate modeling was performed in order to shed light on the amino acid metabolism of haloarchaea. The results indicate that cysteine and lysine are synthesized by non-classical amino acid pathways in *Nmn. pharaonis*. In *Hbt. salinarum*, the arginine ornithine metabolism was characterized, since this organism is the only archaeon known to have an arginine deiminase gene cluster. Translational analysis showed an upregulation of the arginine deiminase (*arcA*, OE5208R) and the ornithine carbamoyltransferase (*arcB*, OE5205R) in *Hbt. salinarum* while omitting ornithine and arginine in the synthetic medium indicating an active ADI-pathway. Furthermore,

---

arginine-ornithine uptake experiments could verify ArcD, the respective antiporter, as the main arginine uptake system in *Hbt. salinarum*. These results demonstrate again that after a particular time of adaptation *Hbt. salinarum* has a very flexible physiology, allowing it to grow well even under harsh conditions.

Overall, these results reveal the metabolic flexibility of haloarchaea, and show important differences even between species of the same genus. Furthermore, they raise many questions regarding the biosynthetic pathways and point to promising areas of further research that may uncover novel biological processes.



# 1 Background

## 1.1 Introduction to halophilic archaea as model organisms

### 1.1.1 Diversity of halophilic archaea

Extremely halophilic bacteria were already described in the beginning of the 20<sup>th</sup> century (Klebahn, 1919; Petter, 1931), being common organisms found on salted fish. At this time they were considered as highly adapted bacteria. But it was not until the late 1970's (Magrum *et al.*, 1978) that their special phylogenetic position was understood, as member of the Archaea (Woese & Fox, 1977).

Archaea form the third domain of life, alongside the two other domains, the Bacteria and the Eukarya.

All currently known halophilic archaea belong to the phylum Euryarchaeota. Halophilic species have been identified in the families *Methanospirillaceae*, the *Methanosarcinaceae* and the *Halobacteriaceae*.

The *Halobacteriaceae* are the halophiles par excellence. They consist of one order, the *Halobacteriales*. Over the intervening years, 30 genera have been de-

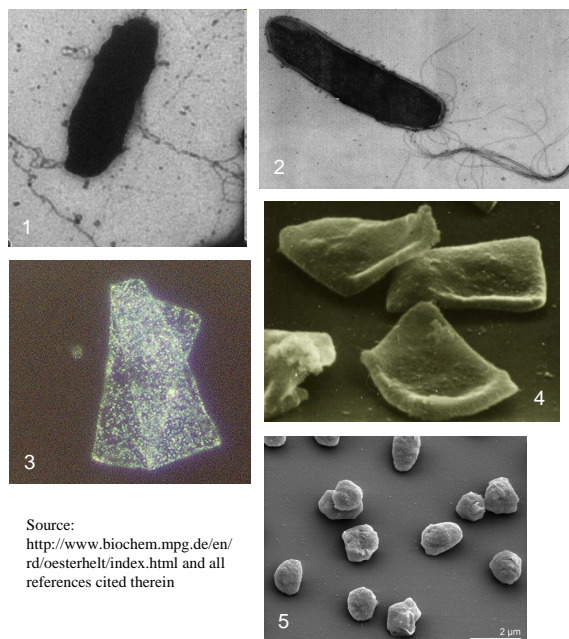


Figure 1.1: **Representatives of the family *Halobacteriaceae*:** (1) *Natronomonas pharaonis*, (2) *Halobacterium salinarum*, (3) *Haloquadratum walsbyi*, (4) *Haloarcula quadrata*, (5) *Halogeometricum borinquense*

scribed which can be divided into two groups (present status of genera within the order *Halobacteriales* can be seen in <http://www.the-icsp.org/taxa/halobacterlist.htm>). Some members belong to a neutrophilic group (e.g. *Halobacterium*, *Halococcus*, *Haloferax* and *Haloarcula*) which grow well between pH 5 and 8 and others form a alkaliphilic group (e.g. *Halorubrum* and *Natronococcus*) thriving optimally from pH 8.5 to 11. The genus *Natronomonas* is unusual in having two species with different pH optima: the haloalkaliphilic *Natronomonas pharaonis* and the halophilic *Natronomonas moolapensis*.

Halophilic archaea show a great variety of morphological types, including rods, cocci, disc-shaped cells, flat triangles and squares. Most of the species within the *Halobacteriaceae* family are pleomorphic. The lack of a strong cell wall polymer like bacterial peptidoglycan in many haloarchaea enables them to adapt to their changing environment by changing their cell form to optimize oxygen absorption (Norton, 1992).

Other habitats where halophiles could set up a niche in a hostile environment are described below.

### 1.1.2 Ecological distribution of halophilic archaea

Originally, Archaea were thought to be restricted to specific, often extreme environments, but DeLong & Pace (2001) showed that Archaea are much more widespread and might constitute as much as 20% of the total biomass. The *Halobacteriaceae* are the main component of the microbial biomass of such environments like the the Dead Sea, hypersaline soda lakes such as Lake Magadi, Kenya, the Great Salt Lake in Utah and saltern crystallizer ponds. The red coloration of virtually all of these lakes arises from C<sub>40</sub> carotenoid pigments, like lycopene, and C<sub>50</sub> carotenoids, like bacterioruberin, found in high concentrations in the membranes of most members of the family (Oren, 1994).

Additional hypersaline environments inhabited by halophilic microorganisms are salted food products, such as salted fish (McGenity *et al.*, 2000), and animal hides treated with salt for preservation. Moreover, various halobacteria have been isolated from salt mines where salt deposits date back from the Triassic and Permian periods in Bad Ischl, Austria, (Stan-Lotter *et al.*, 1999; McGenity *et al.*, 2000) or from ancient halite in Death Valley, California (Schubert *et al.*, 2010). *Haloarcula* species have been tested under astrobiological conditions suggesting that these organisms could survive





Sources: (1) <http://de.wikipedia.org/wiki/Halophile> (2) <http://earthobservatory.nasa.gov> (3) + (4) private

Figure 1.2: **Possible environments of haloarchaea.** (1) Solar salterns in the San Francisco Bay. (2) Utah Great Salt Lake: A sharp line across its center is caused by the restriction in water flow from the railroad causeway. North of the causeway salinities are higher, and the water appears red because of the pigments of halophiles. (3) and (4) Death Valley, Badwater basin.

exposure to the space environment (Rothschild & Mancinelli, 2001) and hence could possibly spread between planets.

Total salt concentration and ionic composition of a given environment determine its quality as a biotope. So-called thalassohaline brines reflect the ionic composition of the sea. Although it has been detached from the world ocean for a long time the Great Salt Lake in Utah still reflects ionic composition of seawater (pH 7-8). The Dead Sea is an example for an athalassohaline environment (pH 5.8-6), dominated by divalent cations (presently around 1.9 M  $Mg^{2+}$  and 0.4 M  $Ca^{2+}$ , in addition to about 1.7 M  $Na^{+}$  and 0.14 M  $K^{+}$ ). Alkaline soda lakes are stable habitats where pH values remain commonly above 10. The solubility of divalent cations is very low and carbonate and bicarbonate ions dominate the anion sum in such lakes (Oren, 2002a). In Table 1.1 an overview of typical halophilic habitats and their archaeal residents is given.

Table 1.1: **Summary of representative halophilic archaea from different habitats.** (Chaban *et al.*, 2006)

<b>Habitat</b>	<b>Representative genera</b>
Salterns, crystallizer pools	<i>Halorubrum</i> , <i>Haloarcula</i> , <i>Halogeometricum</i>
Dead Sea	<i>Halorubrum</i> , <i>Haloferax</i>
Soda lakes	<i>Haloarcula</i> , <i>Natronomonas</i> , <i>Natronococcus</i>
Salt lakes	<i>Natrinema</i>
Hypersaline Antarctic lakes	<i>Halorubrum</i>
Salted fish and hides	<i>Halobacterium</i>
Ancient salt deposits	<i>Haloarcula</i> , <i>Halococcus</i> , <i>Halorubrum</i>
Saline soils	<i>Halorubrum</i> , <i>Haloferax</i> , <i>Haloterrigena</i>
Low-salinity habitats	<i>Haloferax</i> , <i>Halogeometricum</i>

### 1.1.3 Why use halophilic archaea as model organisms?

The haloarchaea are amongst the easiest archaea to grow and manipulate in the laboratory. Neither do they require extreme temperatures for growth nor strict absence of oxygen. Since many molecular biological methods have been adapted for application under high salt conditions (DasSarma & Fleischmann, 1995; Dyall-Smith, 2009), several haloarchaeal species are excellent model organisms that are used for the investigation of many biological questions. For a long time the haloarchaea were the only archaea which could be transformed. Thus they possess many advantages as models for studying the archaeal domain (Soppa, 2006).

The independent evolutionary history of Archaea provides new insights into the evolution of cellular metabolism. Furthermore, organisms living under extreme environmental conditions are gaining increasing importance for biotechnological applications (Davis, 1998) and the analysis of their metabolism constitutes a prerequisite for possible future metabolic engineering (Bailey, 1991). So far, there are no examples of an archaeon being directly responsible for a human or plant disease. Their harmlessness but special intrinsic features, which are assumed to prevent archaea from posing a threat to vertebrates, are utilized in biotechnological applications. For example, liposome adjuvants prepared from archaeal membranes elicit a much greater immune response than bacterial liposomes (Krishnan & Sprott, 2008). Ether lipids from archaea have been suggested as drug carriers or non-caloric fats due to their increased stability towards thermal and enzymatic hydrolysis. Other halophilic archaea have been detected as efficient degradable plastic ("biological polyesters") producers of poly-3-hydroxybutyrate (Lillo & Rodriguez-Valera, 1990) and other polyhydroxyalkanoates

(Legat *et al.*, 2010). Since the retinal protein bacteriorhodopsin (BR) maintains its photochemical properties over long periods it is the most prominent case of a haloarchaeal "product" and therefore it has a large number of possible uses (summarized in Hampp & Oesterhelt, 2004) such as holographic image storage (Oesterhelt *et al.*, 1991) or "secure labeling" for identification and authentication of security documents ([www.u-nica.com](http://www.u-nica.com)).

The ability of halophilic archaea to thrive at high salinity has sparked considerable research of their principles that allow their proteins function under conditions that 'salt out' normal proteins. The halotolerance of many enzymes derived from haloarchaea can be exploited wherever enzymatic transformations are required to function at low water activities, e.g. in the presence of high salt conditions. Archaea combine bacteria-like and eukaryote-like features to regulate cellular processes. The machinery for basal transcription, for example, is much simpler than in eukaryotes, and therefore also more amenable to analysis. This list of possible biotechnological uses of haloarchaea is by no means exhaustive and is reviewed in a several articles (Rodriguez-Valera, 1992; Ventosa & Nieto, 1995).

## 1.2 Physiology and metabolism

### 1.2.1 Adaptation to and protective mechanisms in extreme environments

Organisms living in a hypersaline environment are not only exposed to a high ionic strength but also to a permanent water stress. Moreover, salt lakes and brines commonly occur in hot climates where water temperatures can reach 50 °C. Oxygen is often scarce in hypersaline habitats. Due to the high salt concentration and high temperatures, the solubility of oxygen is limited, restricting aerobic growth. Without protective mechanisms and adaption strategies, like the ones halophilic archaea have developed, survival under the mentioned conditions would not be possible.

#### 1.2.1.1 Protections against dehydration

To avoid losing cell water to the ion rich environment - halophilic archaea can accumulate ions at high concentrations inside the cell. To maintain the osmotic balance,

they keep the  $\text{Na}^+$  concentration low and accumulate  $\text{K}^+$  and  $\text{Cl}^-$  ions to a level at least equating the extracellular NaCl concentration. All halophilic microorganisms contain potent transport mechanisms, carrier-proteins and ion pumps (Oren, 2000, 2002c) (e.g.  $\text{Na}^+/\text{H}^+$  antiporters). Another strategy for osmotic adaptation is the accumulation of organic solutes (e.g. glycerol, sugar alcohols, amino acids). In contrast to the above-mentioned "salt-in" strategy, the use of compatible solutes requires much less far-reaching adaptations of the intracellular enzymatic machinery. However, the production of such solutes is energetically expensive, while osmotic adaptation by accumulation of KCl in the cytoplasm costs relatively little energy (Oren, 2002c). Halophilic archaea also use compatible solutes (e.g. glutamate). More information about osmoprotection in halophiles can be also read in subsection 6.1.2.

The abundance of acidic amino acids in halophilic proteins is biased towards the surface. Acidic residues were found to be far more abundant on the protein surface as compared to the interior (Lanyi, 1974; Rao & Argos, 1981; Madern *et al.*, 1995; Fukuchi *et al.*, 2003). This means that in contrast to non-halophilic proteins halophilic proteins bind significant amounts of salt and water in order to remain in solution. The high surface negative charge also keeps proteins from aggregating and precipitating.

### 1.2.1.2 Adaptation to oxygen deficiency

The solubility of molecular oxygen is greatly reduced at high salt concentrations (Rodriguez-Valera *et al.*, 1985). Halophilic microorganisms have evolved different strategies to thrive under these conditions. Some halophiles like *Hbt. salinarum*, for instance, are capable of forming gas vesicles which decrease the net specific gravity of the cells, enabling them to rise towards the brine-air interface. Gas vesicles are intracellular microbial flotation devices that consist of mainly one protein, GvpA. They provide buoyancy to the cell and promote flotation to the surface, where the presence of oxygen and light is favorable for the growth of these cells (Pfeifer *et al.*, 1997, 2002). Besides the possession of gas vesicles, these organisms have evolved also other strategies to thrive under low oxygen conditions.

Due to the presence of the retinal protein bacteriorhodopsin (BR) the organism can use light directly to drive bioenergetic processes, i.e. to grow photoorganotrophically (Hartmann *et al.*, 1980; Oesterhelt & Krippahl, 1983). BR can be expected to be especially valuable in stressful habitats in which intense illumination is combined with

oxygen limitation - a situation halobacteria may encounter on bright sunny days in saturated brines. Several studies have shown that BR is produced only at low growth rates and that low oxygen concentrations are stimulatory (Rogers & Morris, 1978). Even under totally anaerobic conditions, it has been demonstrated that *Hbt. salinarum* can grow phototrophically (Hartmann *et al.*, 1980). Halophilic archaea can use a number of alternative compounds serving as terminal electron acceptors for respiration: nitrate (Mancinelli & Hochstein, 1986), dimethylsulfoxide, trimethylamine *N*-oxide (Oren & Trüper, 1990), fumarate (Oren, 1991), elemental sulfur, and thiosulfate.

### 1.2.1.3 Protections against photo-oxidation

Solar radiation poses a physiological challenge for microbial communities that colonize habitats exposed to the sun. Protection against photo-oxidation (UV radiation) is achieved by bacterioruberins and carotenoids, which are part of the membrane lipids and cover the whole cell surface. Carotenoids act as antioxidants, preventing photooxidation by quenching singlet oxygen ( $^1\text{O}_2 + \text{carotenoid} \rightarrow ^3\text{O}_2 + ^3\text{carotenoid} \rightarrow \text{carotenoid} + \text{heat}$ ), which could otherwise damage DNA, lipids and enzymes.

## 1.2.2 Metabolic analysis

Metabolism is a fundamental cellular process. Chemical reactions, which are organized in metabolic pathways, allow organisms to grow, break down organic matter (catabolism) and use energy to construct cell components (anabolism). The high conservation of pathways concerning the central metabolism throughout all domains of life suggests they were an early evolutionary invention. While the information-processing machinery resembles eukaryotic systems, the core metabolic functions of archaea are more similar to bacteria (Allers & Mevarech, 2005).

Haloarchaea have evolved a broad repertoire of energy generating strategies. Since hypersaline environments are often rich in organic nutrients it is most likely that under normal conditions only the aerobic chemoorganotrophic mode of nutrition is used by haloarchaea. However, some have evolved a broad repertoire of energy-generating processes for survival under changing conditions (Table 1.2). Most microbial processes that occur at low salt concentrations can be found up to considerably high salinities, often up to NaCl saturation.

Table 1.2: **Energy-generating processes utilized by extreme halophiles.** Modified from Chaban *et al.* (2006)

Process	Representative genera
<b>Aerobic respiration (carbon sources)</b>	
Amino acids	Most genera
Glycerol	<i>Haloarcula</i> , <i>Haloferax</i>
Sugars	<i>Halobacterium</i> , <i>Haloferax</i> , <i>Halorubrum</i> , <i>Natrialba</i>
Hydrocarbons	<i>Halobacterium</i> , <i>Haloferax</i>
<b>Aerobic respiration (terminal electron acceptors)</b>	
Nitrate	<i>Haloarcula</i> , <i>Haloferax</i> , <i>Halogeometricum</i>
Trimethylamine <i>N</i> -oxide	<i>Halobacterium</i> , <i>Haloarcula</i> , <i>Haloferax</i>
Dimethylsulfoxide	<i>Halobacterium</i> , <i>Haloarcula</i> , <i>Haloferax</i>
Fumarate	<i>Halobacterium</i> , <i>Haloferax</i>
<b>Fermentation of arginine</b>	<i>Halobacterium</i>
<b>Photosynthesis</b>	<i>Halobacterium</i>

Variations in pathways between the three domains *Archaea*, *Bacteria* and *Eukarya* reflect not only phylogeny but also particular lifestyles and requirements (Danson *et al.*, 2007). This means that special features of haloarchaeal metabolism do not only represent ancestral metabolic characteristics in a primitive organism. In fact, they illustrate evolutionary adaptation of microorganisms to survival in a variety of different hostile environments.

The advent of genome sequencing in the past decade has resulted in a new approach to the study of metabolic pathways. Before sequencing of genomes was possible, metabolism studies relied mainly on enzymological data retrieved from the traditional techniques of enzyme purification and characterization or growth experiments, testing different substrates. Today, the "systems biology" approach integrates data from biochemistry, molecular biology, microbiology with information from genome sequences, providing a much more powerful tool than relying on just the single disciplines. Publication of a new genome sequence often includes an integrated metabolic overview of nutrient uptake and energy production.

The comparison of complete genome sequences has revealed that archaea are more than a sum of their (eukaryotic and bacterial) parts (Graham *et al.*, 2000). A high fraction (as much as 50%) of archaeal genes are non-orthologous enzymes, i.e. they have an unknown function. This can be explained by independent, convergent evolution (Jain *et al.*, 1999; Allers & Mevarech, 2005). Some archaea-specific genes have

unique functions not found in bacteria or eukarya.

Global analysis of cell function, also based on data retrieved from genome annotation, is usually performed by using DNA/RNA microarrays (transcriptomics) and by 2D gel electrophoresis or high-performance liquid chromatography (HPLC) and mass spectrometry (MS) (proteomics).

Metabolic labeling experiments are still indispensable for the elucidation of metabolic pathways. Stable isotope labeling of small-molecule metabolites, either measured by nuclear magnetic resonance (NMR) or MS, is a powerful tool for characterizing pathways and reaction fluxes in a metabolic network (Mu *et al.*, 2007).

In terms of systems biology, structure and flux data yielded by metabolic labeling are used to reconstruct metabolic networks. The final goal of this approach is to integrate genomics and proteomics with quantitative kinetic information on enzyme activities and metabolite levels, moreover to construct a metabolic model. However, at present we are far from a situation where the function of every open reading frame can be confirmed experimentally in addition to kinetic and regulatory information (Danson *et al.*, 2007).

This thesis deals with the reconstruction of metabolic pathways in halophilic archaea using several of the above-mentioned approaches.

## 1.3 Motivation and objectives

The research into extreme environments has important implications for biology and may lay the foundations for applications in the biotechnology industry. Studying the metabolism of haloarchaea provides insights into the history of life on earth and the origin of life.

The principal aim of this thesis was to describe degradative and biosynthetic pathways of halophilic archaea and to identify the unique or unusual features of their metabolism. Although metabolic pathway reconstruction continuously improved with the release of new annotated genome sequences, there are still many pathway gaps in the metabolic network of archaea. To avoid adopting annotation errors of genes (misassigned functions by automatic annotation), one focus of this work was set on confirming or refuting genomic data in order to provide a basis for metabolic modelling and flux analysis for halophilic archaea in the future.



Figure 1.3: **How it all started in 2005 ...** "my" discovery of extremophiles during my stay as a graduate student in Iceland.

Different approaches were taken to reach these goals:

- tracing the fate of small-molecule metabolites by metabolic labeling in (i) the isoprenoid biosynthesis pathway (chapter 3); (ii) the amino acid metabolism (chapter 4); and (iii) the carbon fixation pathways (chapter 5)
- carbon fate modelling using a bioinformatical approach (chapter 4)
- performing transcriptional analyses (e.g. role of archaeal RuBisCO, chapter 4)
- combining manual annotation data with experimental results (e.g. metabolic and genomic characterization of a new halophilic archaeon, chapter 6)
- genome comparison of *Halobacterium salinarum*, *Natronomonas pharaonis* and *Natronomonas mooolapensis* with each other and with further haloarchaea.

Experimental results were integrated with genomic data in order to provide a basis for metabolic modeling and flux analysis for halophilic archaea in the future.



## 2 Material and methods

### 2.1 General materials

#### 2.1.1 Instruments

In Table 2.1 general tools are listed that were applied during different kinds of experiments.

#### 2.1.2 Chemicals

Chemicals were purchased in the grade 'pro analysis' from Merck, Sigma-Aldrich, Riedel de Hën or Fluka. Exceptions as well as chemicals of particular importance for the presented results are listed in Table 2.2.

#### 2.1.3 Kits and enzymes

All enzymes or kits used in this study are listed in Table 2.3.

#### 2.1.4 Software

Programs and the bioinformatics environment used in this study are itemized in Table 2.4.

## 2.2 Microbiological methods

### 2.2.1 Strains and culture conditions

#### 2.2.1.1 Overview of strains

In the course of this study experiments were undertaken with three halophilic archaeal organisms, *Hbt. salinarum* (strain R1, DSM 671), *Nmn. pharaonis* (strain Gabara, DSM 2160) and *Nmn. moolapensis* (DSM 18674).

Table 2.1: **Instruments**

<b>Instrument</b>	<b>Distributor</b>
Analytical balance HL52	Mettler Toledo
Autoclave Varioklav 500 EP-Z	H+P Labortechnik
Balance PB3002-SDR	Mettler Toledo
BCA Protein Assay	Thermo Scientific Pierce
Bioanalyzer 2100	Agilent
Bottle top filter, 500 ml, 0.22 $\mu$ m	Costar
Centrifuge 5417R, rotor FA45-30-11	Eppendorf
Centrifuge RC5C Plus, rotor GS3, SS34	Sorvall
Centrifuge Rotixa 120 R	Hettich
Centrifuge TL-100	Beckmann
Glass Filter OG 515 (Orange)	Schott
GC/MS	Finnigan Trace Ultra Gas Chromatograph Finnigan PolarisQ Mass Spectrometer
Glass vials for $\text{BCl}_3$ cleavage	Pierce
Gradient mixer	Bromma
ICPL Kit	Serva Electrophoresis
Incubator BK5060E	Heraeus
Klett photometer	Klett-Summerson
LC for amino acid analysis	Biotronik LC 3000
NanoDrop ND-1000	peqLab
Nitrogen evaporator station	Pierce Reacti Therm
NMR Spektrometer, 500 MHz	Bruker Daltonics
PCR Thermocycler PCR System 9700	GeneAmp
pH meter microprocessor pH 211	Hanna Instruments
Photometer	Shimadzu UV 1700
Pipettes	Eppendorf Research 2 $\mu$ l, 20 $\mu$ l, 200 $\mu$ l, 1000 $\mu$ l
Power supply EPS 200	Pharmacia Biotech
Q-TOF Ultimate Massenspektrometer	Waters
Reflow gadget	Büchi
Rotation evaporator	Büchi Rotovapor -R
Shaker Unimax 2010	Heidolph
Sonifier 250	Branson
Steriflip Filter	Millipore
Thermomixer	Eppendorf
Ultracentrifuge	Beckmann Coulter
Ultrapure water apparatus	Millipore
Ultrasonic bath	Sonorex Bandelin
UV/Vis spectrometer Ultrospec 3000	Pharmacia Biotech
Vacuum concentrator Speedvac Concentrator	Savant
Water bath	Julabo C

Table 2.2: **Chemicals**

<b>Chemical</b>	<b>Distributor</b>
<sup>13</sup> C labeled substances and solvents	Euriso-Top
DNA Ladder, GeneRuler	Fermentas
Fluted filter	Schleicher
MSTFA	Macherei-Nagel
Protein Marker, PageRuler unstained	Fermentas
Protease Inhibitor Cocktail Tablets	Roche

Table 2.3: **Kits and enzymes**

<b>Kits and enzymes</b>	<b>Distributor</b>
ABI Prism BigDye v3.1	Applied Biosystems
BCA protein assay kit	Pierce
Cyscribe	Pharmacia
DNA- <i>free</i> DNase Treatment Kit	Applied Biosystems
ICPL Duplex Kit	Serva
peqGOLD RNAPure	peqlab
Phusion Flash Mix	Finnzymes
QIAquick Gel Extraction Kit	Qiagen
QIAquick PCR Purification Kit	Qiagen
RNA 6000 Nano Chip kit	Agilent Technologies
Superscript III reverse transcriptase	Invitrogen

Table 2.4: **Software**

<b>Software</b>	<b>Source</b>
BNet	Gonzalez O., MPI Biochemistry
ClustalX2	<a href="http://www.clustal.org">http://www.clustal.org</a>
FigTree	<a href="http://tree.bio.ed.ac.uk/">http://tree.bio.ed.ac.uk/</a>
HaloLex	<a href="http://www.halolex.mpg.de/">http://www.halolex.mpg.de/</a>
Inkscape	<a href="http://www.inkscape.org/">http://www.inkscape.org/</a>
LATEX2	<a href="http://www.latex-project.org/">http://www.latex-project.org/</a>
MDL Isis/Draw 2.5	<a href="http://www.symyx.com/">http://www.symyx.com/</a>
PRIAM	<a href="http://priam.prabi.fr/">http://priam.prabi.fr/</a>
Primer3	<a href="http://frodo.wi.mit.edu/primer3/">http://frodo.wi.mit.edu/primer3/</a>
TeXnicCenter	<a href="http://www.texniccenter.org/">http://www.texniccenter.org/</a>
TIGR MeV	<a href="http://www.tigr.org">http://www.tigr.org</a>
Xcalibur	<a href="http://www.thermo.com/finnigan">http://www.thermo.com/finnigan</a>
XWin-NMR	Bruker

Table 2.5: **Complex medium for *Hbt. salinarum***

<b>Ingredient</b>	<b>Amount</b>
MgSO <sub>4</sub>	81 mM
Na <sub>3</sub> citrate	10 mM
KCl	27 mM
NaCl	4.3 M
Peptone (L34, Oxoid)	1 % (w/v)
H <sub>2</sub> O	to 1 l

### 2.2.1.2 **Culturing and storage of *Hbt. salinarum*, *Nmn. pharaonis* and *Nmn. moolapensis* strains**

Halophilic cells were grown in complex or synthetic medium and unless stated otherwise were incubated aerobically in the dark under constant shaking at 100 rpm and 37 °C. Typically, 35 ml of medium in a 100 ml Erlenmeyer flask inoculated with 1 ml of a starter culture. To measure turbidity (cell density), a Klettphotometer was used (578 nm fixed wavelength). Cell growth of 1 l cultures was monitored by measuring the optical density at 600 nm (OD<sub>600</sub>) in a spectrophotometer (Ultrospec 3000, Pharmacia Biotech). As a rule of thumb 1 ml of culture of an OD<sub>600</sub> = 1.0 contains  $1.34 \times 10^9$  cells. Calculation of the internal cell volume was performed as published earlier: 1 ml of a culture of *Hbt. salinarum* at OD<sub>578</sub> = 1 (= Klett 100) corresponds to 1.36 µl internal cell volume (Hartmann & Oesterhelt, 1977; Michel & Oesterhelt, 1976). This was treated as a linear correlation, even when in the late stationary phase precipitating salt as well as cell fragments obviously contributed to the optical density. For storage, the culture was left in the dark at room temperature.

## 2.2.2 **Media**

All media were either sterilized by filtration into sterile bottles through sterile 0.2 µm pore-size filters or autoclaved at 101 kPa for 15 min.

### 2.2.2.1 **Media for *Hbt. salinarum***

#### **Complex medium for *Hbt. salinarum*** (Oesterhelt & Krippahl, 1983)

The pH of the complex medium in Table 2.5 was adjusted to 7.0 with NaOH.

#### **Synthetic medium for *Hbt. salinarum*** (Oesterhelt & Krippahl, 1973; Grey & Fitt, 1976)

The pH of the synthetic medium in Table 2.6 was adjusted to 7.0 with NaOH.

Table 2.6: Synthetic medium for *Hbt. salinarum*

<b>Ingredient</b>	<b>Amount</b>
NaCl	4.020 M
MgSO <sub>4</sub> × 7 H <sub>2</sub> O	81.14 mM
KCl	26.83 mM
KNO <sub>3</sub>	0.99 mM
Sodium citrate	1.7 mM
Glycerol	109 mM
KH <sub>2</sub> PO <sub>4</sub>	0.42 mM
K <sub>2</sub> HPO <sub>4</sub> × 3 H <sub>2</sub> O	0.58 mM
CuSO <sub>4</sub> × H <sub>2</sub> O	0.0002 mM
FeCl <sub>2</sub> × 4 H <sub>2</sub> O	0.0116 mM
MnSO <sub>4</sub> × H <sub>2</sub> O	0.0018 mM
ZnSO <sub>4</sub> × 7 H <sub>2</sub> O	0.0015 mM
Na <sub>2</sub> MoO <sub>4</sub> × 2 H <sub>2</sub> O	0.001 mM
CoCl <sub>2</sub> × 6 H <sub>2</sub> O	0.001 mM
Thiamine	0.0165 mM
Biotin	0.0021 mM
Folic acid	0.0115 mM
L-arginine	2.30 mM
L-isoleucine	3.35 mM
L-leucine	6.10 mM
L-lysine × HCl	1.37 mM
L-methionine	1.34 mM
L-threonine	4.20 mM
L-serine	5.80 mM
L-phenylalanine	0.61 mM
L-alanine	2.5 mM
Glycine	1 mM
L-proline	0.9 mM
L-aspartic acid	3 mM
L-glutamic acid	9 mM
L-tyrosine	1.1 M
L-valine	2.50 mM

Table 2.7: **Minimal medium for *Nmn. pharaonis***

<b>Ingredient</b>	<b>Amount</b>
NaCl	3,4 M
Na <sub>2</sub> CO <sub>3</sub>	175 mM
Sodium acetate	20 mM
KCl	27 mM
MgSO <sub>4</sub> × 7 H <sub>2</sub> O	1 mM
Na <sub>2</sub> HPO <sub>4</sub> × H <sub>2</sub> O	2 mM
NaH <sub>2</sub> PO <sub>4</sub> × 7 H <sub>2</sub> O	2 mM
FeSO <sub>4</sub> × 7 H <sub>2</sub> O	5 μM
CuSO <sub>4</sub> × 5 H <sub>2</sub> O	4 μM
MnCl <sub>2</sub>	4 μM
CaCl <sub>2</sub> × 2 H <sub>2</sub> O	3 μM
ZnSO <sub>4</sub> × 7 H <sub>2</sub> O	3 μM
NH <sub>4</sub> Cl	12 mM

Table 2.8: **Concentrated salt water - 30 % (w/v)**

<b>Salt</b>	<b>g per 1 l</b>
NaCl	240
MgCl <sub>2</sub> × 6 H <sub>2</sub> O	30
MgSO <sub>4</sub> × 7 H <sub>2</sub> O	35
KCl	7
1M Tris x Cl, pH 7.5	5 ml

#### 2.2.2.2 Minimal medium for *Nmn. pharaonis*

The pH of the medium shown in Table 2.7 was adjusted to 9.2 before filter sterilization.

#### 2.2.2.3 Modified growth medium for Haloarchaea (MGM)

(Dyall-Smith, 2009)

##### **Concentrated salt water (SW) stock solution**

After salts were completely dissolved in pure water, CaCl<sub>2</sub> × 2 H<sub>2</sub>O was slowly added from a 1 M sterile stock solution (final concentration = 0.5 g/l). The pH was adjusted up to 7.5 with a minimum volume of 1 M Tris base (Table 2.8).

##### **23 % MGM**

The pH was adjusted up to 7.5 with 1 M Tris.Cl, pH 7.5, using 5 ml per Liter (Table 2.9).

#### 2.2.2.4 Synthetic medium 'DBCM2' for *Nmn. moolapensis*

To 1 l of autoclaved 25 % salt water (Table 2.8) (ie. 833 ml 30 % SW + 167 ml pure water) the following volumes of filter sterilized solutions were added (Table 2.10) and

Table 2.9: **MGM - 23 %**

<b>Ingredient</b>	<b>1 l</b>
Salt Water (30 % stock)	833 ml
Pure Water	134 ml
Peptone (Oxoid)	5 g
Yeast Extract	1 g

Table 2.10: **Synthetic medium DBCM2**

<b>Ingredient</b>	<b>ml</b>
1 M Tris x Cl, pH 7.4	10
1 M NH <sub>4</sub> Cl, (53.4 g/l)	5
K <sub>2</sub> HPO <sub>4</sub> buffer, pH 7.4	2
SL10 trace elements	1
Vit10 vitamin solution	3
1 M pyruvate	10
salt water 25 %	to 11

the pH was adjusted to 7 - 7.5 (Dyall-Smith, 2009).

### **K<sub>2</sub>HPO<sub>4</sub> buffer**

30 ml of 0.5 M KH<sub>2</sub>PO<sub>4</sub> solution were initially mixed with 100 ml of 0.5 M K<sub>2</sub>HPO<sub>4</sub>. Then 2 ml aliquots of the KH<sub>2</sub>PO<sub>4</sub> solution were added until the pH was close to 7.5.

### **Trace element solution SL10 and vitamin 10 stock**

The components of the trace element solutions SL10 (Widdel et al., 1983) were added and dissolved as listed in Table 2.11. Then a stock solution of all vitamins was prepared (Table 2.12).

Table 2.11: **Trace element solution SL10**

<b>Ingredient</b>	<b>Amount</b>
25 % HCl	10 ml
FeCl <sub>2</sub> × 4H <sub>2</sub> O	1.5 g
H <sub>2</sub> O	1.0 l
CoCl <sub>2</sub> × 6H <sub>2</sub> O	190 mg
MnCl <sub>2</sub> × 4H <sub>2</sub> O	100 mg
ZnCl <sub>2</sub>	70 mg
H <sub>3</sub> BO <sub>3</sub>	6 mg
Na <sub>2</sub> MoO <sub>4</sub> × 2H <sub>2</sub> O	36 mg
NiCl <sub>2</sub> × 6H <sub>2</sub> O	24 mg
CuCl <sub>2</sub> × 2H <sub>2</sub> O	2 mg
H <sub>2</sub> O	to 1 l

Table 2.12: **Vitamin 10 stock**

<b>Ingredient</b>	<b>Amount</b>
4-aminobenzoate	13 mg
Biotin	3 mg
Nicotinic acid	33 mg
Hemicalcium D-(+)-pantothenate	17 mg
Pyridoxamine hydrochloride	50 mg
Thiamine chloride hydrochloride	33 mg
Cyanocobalamin	17 mg
D,L-6,8-thioctic acid	10 mg
Riboflavin	10 mg
Folic acid	4 mg
H <sub>2</sub> O	to 1 l

## **2.3 Molecular biological methods**

### **2.3.1 Preparation of unpurified ('crude') DNA from halobacterial cells**

Halobacterial DNA for PCR was prepared by water lysis of cells without further purification. 1.2 ODml of a fresh halobacterial culture were spun down (10 600 g, 2 min) and the supernatant removed. After an additional short spinning step, residual liquid was removed with a pipette tip to get rid of most of the salt. The pellet was then lysed by adding 400  $\mu$ l of sterile deionized water and rapid up- and down pipetting until all lumps were dissolved and a uniform solution was obtained. 1  $\mu$ l of this DNA contained approx. 10 ng of DNA from  $4 \times 10^6$  cells. The DNA preparation was stored at 4 °C and was used as a template in PCRs for approximately 3 months.

### **2.3.2 Gel-electrophoresis of DNA**

Analytical and preparative separations of DNA were carried out by gel-electrophoresis, in which negatively charged nucleic acid molecules are moved through an 1 - 2% agarose matrix with an electric field. Prior to pouring the molten agarose/TAE solution into the horizontal unit, ethidium bromide was added from a stock solution (10 mg/ml in water) to a final concentration of 0.5  $\mu$ g/ml. A 1 x Tris/Acetate/EDTA (TAE, 40 mM Tris/Acetate, 2 mM EDTA,) buffer was used at 5 V/cm. The samples were applied to the gels dissolved in 1 x DNA sample buffer (0.2% (w/v) bromophenol blue, 30% glycerol) and a DNA ladder was run in parallel. Afterwards bands of samples were examined by transillumination with ultraviolet light at 302 nm relative to the DNA ladder.



Table 2.13: **PCR reaction mixture**

'crude' DNA	1 $\mu$ l (10 ng)
Phusion Flash-mix (1 x)	12.5 $\mu$ l
Forward primer (10 $\mu$ M)	1.25 $\mu$ l
Reverse primer (10 $\mu$ M)	1.25 $\mu$ l
H <sub>2</sub> O	ad 25 $\mu$ l

Table 2.14: **Thermocycling conditions for 'Check PCR'**

Initial denaturation	98 °C, 1 min
Denaturation	98 °C, 10 sec
Annealing	60 °C, 20 sec
Elongation	72 °C, 1 min/1000 bases
Storage	4 °C
35 - 40 cycles between denaturation and elongation	

### 2.3.3 Isolation of DNA fragments from agarose gels

To isolate specific DNA fragments from agarose gels, the QIAquick Gel Extraction kit was used. In brief, a gel slice containing only the desired fragment was excised from the gel and treated according to the manufacturer's protocol.

### 2.3.4 Determination of DNA concentration

The concentrations of solutions of PCR products after purification via agarose gels were determined with a micro-volume UV-Vis Spectrophotometer (NanoDrop) by measuring the absorption at 260 and 280 nm. Protein-free samples should achieve the ratio OD<sub>260/280</sub> of about 2.0 (dsDNA). Alternatively, if only an approximate concentration was needed, PCR fragments were applied on an agarose gel that was stained with ethidium bromide. The brightness of the UV signals of the corresponding bands was then compared to that of the 1.6 kb band of the 1 kb DNA ladder (1.6 kb band contained 50 ng DNA per 10  $\mu$ l DNA marker) assuming a linear relationship between brightness and amount of DNA.

### 2.3.5 Polymerase chain reaction (PCR)

Depending on the purpose of the PCR, different polymerases and temperature profiles were used. The standard protocol for a typical 'Check-PCR' is shown in Table 2.13 and Table 2.14.

### 2.3.6 Sequencing of DNA

Sequencing of DNA was performed using the chain-termination method with fluorescence labeled 2',3'dideoxynucleotides. The sequencing reaction was performed with

Table 2.15: **Thermocycling conditions for sequencing PCR**

Denaturation	94 °C, 3 min
Annealing	94 °C, 10 sec
Elongation	60 °C, 4 min
Storage	4 °C
25 cycles between denaturation and elongation	

a BigDye Terminator Cycle Sequencing Ready Reaction Kit (Perkin Elmer Applied Biosystems). A typical reaction mixture was prepared from 4  $\mu\text{l}$  (100-500 ng) DNA of the PCR-product, 1  $\mu\text{l}$  of primer (20 pmol), 2  $\mu\text{l}$  of BigDye mix, 1  $\mu\text{l}$  of BigDye buffer, 2  $\mu\text{l}$  of 5 M betaine and  $\text{H}_2\text{O}_{\text{bidest}}$  to a final volume of 10  $\mu\text{l}$ . The temperature program is listed up in Table 2.15. After amplifying the DNA in the thermocycler the product was diluted with another 10  $\mu\text{l}$  of  $\text{H}_2\text{O}$  and samples analyzed in house on a capillary sequencer (ABI Prism 377 DNA Sequencer).

### 2.3.7 Isolation of total RNA

Depending on the turbidity of the culture, 3-6 ml were removed and the cells spun down for 5 min at 10 500 g and 4°C, in a Sorvall centrifuge. The supernatant was removed completely with a pipette and discarded. Then the cell pellet was resuspended in 3 ml peqGold RNA Pure (Peqlab) solution and incubated at rt for 5 min. The homogenate was split into aliquots of 1 ml and 200  $\mu\text{l}$  of chloroform was added to each portion. The suspension was mixed well and incubated for another 10 min at rt. Centrifugation at 15 000 g and 21 °C for 5 min yielded proper phase separation. From this step onwards, samples were always kept on ice. The upper aqueous layer was carefully transferred into a new reaction tube. A 0.5 volumes of isopropanol was added and this solution incubated at -20 °C for 15 min before centrifuging again at 18 000 g for 10 min. From the resulting pellet, isopropanol was removed by washing twice with 1 ml of 75 % ethanol<sub>DEPC</sub> (centrifugation at 15 000 g and 4 °C for 10 min). The pellet was dried for about 10 min at rt (until it turned transparent) and finally dissolved in 50  $\mu\text{l}$  of RNase-free  $\text{H}_2\text{O}_{\text{DEPC}}$ . To preserve the RNA the pellet was quickly frozen with dry ice and stored at -80 °C.

### 2.3.8 DNase digestion of extracted RNA

50  $\mu\text{l}$  of RNA (0.2  $\mu\text{g}/\mu\text{l}$ ) were treated with 2  $\mu\text{l}$  DNase I (Ambion) and the appropriate buffer from a 10 x for 30 min at 37 °C. Then another 2  $\mu\text{l}$  of DNase I was added and the solution incubated for 30 min at 37 °C. After adding 0.2 volumes of the inactivation reagent, the sample was incubated for 5 min at rt with occasional mixing. The mixture was centrifuged at 10 000 g for 1.5 min and the supernatant was transferred to a fresh tube. To confirm the complete digestion of DNA, a 'Check-PCR' was performed with primers of *sdhA* (succinate dehydrogenase, NP4264A) for *Nmn. pharaonis* and primers

Table 2.16: Primers for 'Check-PCR'

Primers for <i>Nmn. pharaonis</i>	
sdhA-for	TAGCGATGGTCACGAAACTG
sdA-rev	ATTCCCCAGTGTTCAAGCTG
Primers for <i>Hbt. salinarum</i>	
BopPrXba-for	TTTCGAGTCTAGACACGCGTGCACGCATCGACT
BopPrBgIII-rev	CAACATAGATCTGCAACAGTACCTAACGAGGA

Table 2.17: TE buffer

Tris-HCl	10 mM
EDTA	1 mM
H <sub>2</sub> O <sub>bidest</sub>	to 1000 ml
pH	8.0

of the *bop* promoter for *Hbt. salinarum* (listed in Table 2.16). RNA was quantified by absorption at 260 and 280 nm using a NanoDrop spectrophotometer (before and after DNase digestion). Ideally, the 260/280 ratio should be close to 2 for high quality nucleic acid. To control the quality and integrity of the RNA, the samples were analyzed with the 2100 Bioanalyzer using the RNA6000-Nano-LabChip-Kit. Electrophoresis in this microfluidics-based platform was performed and the Integrity Number (RIN), a quantitation estimate, was calculated.

## 2.3.9 DNA microarrays for gene expression profiling

### 2.3.9.1 Synthesis of fluorescent-labeled cDNA

For transcription of RNA into stable fluorescently-labeled cDNA the CyScribe First-Strand cDNA Labeling Kit and the two dyes Cy3 (green) and Cy5 (red) were used. For primer annealing, 1  $\mu$ l of a nonamer-mix, 1-5  $\mu$ g of RNA and H<sub>2</sub>O<sub>bidest</sub> to 11  $\mu$ l were incubated for 5 min at 70 °C and afterwards cooled down for 10 min to rt. Due to light sensitivity of the dyes, all further steps were conducted in the dark. 4  $\mu$ l of 5x CyScript buffer, 2  $\mu$ l of DTT, 1  $\mu$ l of a dUTP mix (desoxyuridintriphosphate), 1  $\mu$ l of Cy3 or Cy5 and 1  $\mu$ l of Cy-Script-Reverse transcriptase were added and finally incubated for 90 min at 42 °C. The reverse transcription reaction was stopped by adding 2.5  $\mu$ l of 0.5 M EDTA, pH 8. RNA was hydrolyzed by adding 5  $\mu$ l 1 M NaOH and incubating for 30 min at 65 °C. After cooling down the reaction mix to rt, 12.5  $\mu$ l of 1 M Tris\HCl pH 7.5 was added to stop the hydrolysis. To eliminate excess primers, unintegrated dyes and RNA fragments, 1  $\mu$ l of yeast tRNA (4 mg/ml, Roche) and TE-buffer (Table 2.17) to 500  $\mu$ l were added to the labeled cDNA solutions. Ultra filtration of the cDNA was performed in Microcon YM 30-columns (Millipore) until the volume of the cDNA solution was reduced to 17  $\mu$ l.

### 2.3.9.2 Production and pretreatment of microarray slides

*Hbt. salinarum* DNA-gene probes were produced from PCR products (Twellmeyer, 2007) and printed on CMT-GAPS II coated slides (Corning) with the ChipWriter Pro printer (Virtek) according to a protocol of M. Panhuysen (Max Planck Institut of psychiatry). Five purified replicates of every DNA-gene probe were printed on the slide (Diehl *et al.*, 2001). Slides were heated for 10 sec at 80 °C and covalent binding of DNA to the slide resulted from UV-crosslinking (3000 x 100 µJ) (Twellmeyer, 2007).

1.25 g of succinic anhydride was dissolved in 250 ml 1,2-dichlorine ethane. Afterwards, 3.1 ml of 1-methylimidazole was added and the slides kept in this solution for 1 h. They were washed with the same volume of 1,2-dichlorine ethane and dipped twice into 95 °C H<sub>2</sub>O for 2 min and into 95 % ethanol for 1 min. For drying, the slides were centrifuged for 5 min at 1500 rpm in 50 ml tubes (Falcon) in a Hettich centrifuge (Rotixa 120R).

### 2.3.9.3 Prehybridization and hybridization of microarrays

Before incubating the slides for 25 min in the prehybridisation solution (Table 2.18), the solution itself was heated to 50 °C for 1 h. Then the slides were dipped first into H<sub>2</sub>O<sub>bidest</sub> and second into isopropanol, each 30 sec. To dry them, they were centrifuged again for 5 min at 1500 rpm in 50 ml tubes (Falcon) in a Hettich centrifuge (Rotixa 120R).

The hybridization solution (Table 2.18) was incubated at 98 °C and then cooled down to rt. To avoid background noise, 2 µl of 1 % SDS was added to the hybridisation solution and pipetted to the center of a coverslip. This was applied on the prehybridized microarray, covering the entire printed area with the solution. Each microarray was packed into a hybridization chamber (Corning) and additionally wrapped in aluminium foil to protect it from dehydration. The hybridization took place over night at 64 °C.

### 2.3.9.4 Washing of the slides

Unbound or non-specifically bound DNA was removed by washing the array in two steps. The arrays were washed twice 5 min in washing solution I, and afterwards in washing solution II, respectively (Table 2.19). Drying was achieved by centrifuging for 5 min at 1500 rpm in 50 ml tubes (Falcon) in a Hettich centrifuge (Rotixa 120R). Detection took place after incubation of the slides for 1 h at rt in the dark.

Table 2.18: **Hybridization solutions for microarrays**

<b>Prehybridisation solution</b>	
BSA fraction V	2.5 g
20 x SSC	43.75 ml
10 % SDS	2.5 ml
H <sub>2</sub> O <sub>bidest</sub>	to 250 ml
<b>Hybridization solution</b>	
cDNA	ca. 17 µl
20 x SSC	3.75 µl
50 x Denhardts-reagent	1.25 µl
H <sub>2</sub> O <sub>bidest</sub>	to 30 µl
<b>50x Denhardts-reagent</b>	
Ficoll 400	2% (w/v)
Polyvinylpyrrolidon	2% (w/v)
BSA fraction V	2% (w/v)
H <sub>2</sub> O <sub>bidest</sub>	to 500 µl, pH 7.0

Table 2.19: **Washing solutions for microarrays**

<b>Washing solution I</b>	
20x SSC	12.5 ml
10% SDS	500 µl
H <sub>2</sub> O <sub>bidest</sub>	to 500 ml
<b>Washing solution II</b>	
20x SSC	1.5 ml
10% SDS	500 µl
H <sub>2</sub> O <sub>bidest</sub>	to 500 ml

### 2.3.10 Reverse Transcription PCR (RT-PCR)

The extracted RNA (chapter 2.3.7) was digested with DNase I (chapter 2.3.8), a 'Check-PCR' was performed for determining possible contaminating DNA and the purity and quality of the RNA was measured by the Bioanalyzer.

#### 2.3.10.1 Synthesis of cDNA

The synthesis of cDNA from extracted RNA was carried out by reverse transcriptase SuperScript III (Invitrogen) with 3 µg RNA, 1 µl dNTPs (10 mM each) and 2 µl of the corresponding reverse primer. The reaction solution was incubated for 5 min at 70 °C and cooled down for another 5 min on ice. 4 µl of a 5 x buffer, 2 µl of DTT and 1 µl of the reverse transcriptase were added and filled up with H<sub>2</sub>O<sub>bidest</sub> to 20 µl. The reaction mix was kept at rt for 5-10 min and then incubated for 50 min at 55 °C and for 15 min at 70 °C. A 'Check-PCR' (chapter 2.3.8) including a non-template control reaction (NTC) and a positive control with genomic DNA for every gene of interest was performed. The positive control of the PCR was a reaction using primers for *sdhA* (Table 2.16). To determine if there was residual genomic DNA, a NTC was performed

Table 2.20: Primers for RT-PCR and corresponding 'Check-PCR'

<b>NP1254A, apt<sub>2</sub></b>	
<b>adenine phosphoribosyltransferase,</b>	
apt <sub>2</sub> -for	CACCGGACACCGTACTGAC
apt <sub>2</sub> -rev	CTGTCTGGCCTCGATGAACT
<b>NP1426A, apt<sub>1</sub></b>	
<b>adenine phosphoribosyltransferase</b>	
apt <sub>1</sub> -for	AGCTTCAGCAGTCGCTTCTC
apt <sub>1</sub> -rev	ATAACGACGAGCGGAATGTC
<b>NP2770A, rbcL</b>	
<b>type III RuBisCO</b>	
rbcL-for	CGACCTCGTCTGTACGTTCC
rbcL-rev	GGTTACCTGCGTACCGTGTT
<b>NP3202A, -</b>	
<b>ribose-1,5-biphosphate isomerase</b>	
NP3202A-for	CGAGGAGACACATGAGGACA
NP3202A-rev	GAACAGCTCTCGCATCAGTG
<b>NP3958A, deoA</b>	
<b>AMP phosphorylase</b>	
deoA-for	GGCGGACATCATCTTCGATA
deoA-rev	ACTACGAGGCCGTCAGTGTC
<b>NP4264A, sdhA</b>	
<b>succinate dehydrogenase</b>	
sdhA-for	TAGCGATGGTCACGAAACTG
adhA-rev	ATTCCCAGTGTTCAAGCTG
<b>NP1314, citZ</b>	
<b>acitrate (si)-synthase</b>	
citZ-for	AAGGGCTGGAGGGAGTTTTA
citZ-rev	GATTTGAACGACCCGAGTTC

with H<sub>2</sub>O<sub>bidest</sub> instead of a template RNA. The primers of all genes of interest are listed in Table 2.20. All oligonucleotides were purchased from Metabion (purification grade 'desalted'). Oligonucleotides were designed with the software Primer3 and an optimal melting temperature was preset to 60 °C. Oligonucleotides were stored at -20 °C.

### 2.3.10.2 Gel extraction and DNA sequencing

The cDNA was loaded on an agarose gel. If the RT-PCR was successful, the PCR product was cut out of the gel with a scalpel, and the DNA extracted as described in chapter 2.3.3 and the subsequent sequencing in chapter 2.3.6.

## 2.4 Protein chemical methods

### 2.4.1 Isotope coded protein labeling (ICPL)

This method provides relative quantitation of two different protein samples in one experiment by isotopic labeling of free amino groups of isolated intact proteins by amine specific reagents (Kellermann, 2008).

#### 2.4.1.1 Isolation of cytosolic proteins of *Hbt. salinarum*

##### Extraction of proteins

35 ml of freshly grown cells were harvested, until an OD value of 0.4 was reached, by centrifugation at 6500 g for 10 min at 4 °C. Every subsequent step was processed on ice. The cells were placed in a sonication bath for 1 min and then resuspended in lysis buffer (50 mM Tris/HCl, pH 7.5; 5 mM phosphatase inhibitors (sodium fluoride, 2-glycerol phosphate, sodium vanadate, sodium pyrophosphate), protease inhibitor mixture (1 tablet/10 ml, EDTA-free Protease Inhibitor Cocktail Tablet, Roche), 100 µg/mL DNase I (Sigma-Aldrich) and 1 % N-octylglucoside). Afterwards the cell suspension was again placed in the sonication bath for 1 min. Then the cell suspension was incubated for 30 min at rt on a shaker (1 000 rpm) and centrifuged at 25 000 g for 30 min at 4 °C to remove cell debris and cell envelope fragments.

##### Determination of protein concentration by BCA assay

The protein concentration of the sample was determined using a bicinchoninic acid (BCA) protein assay kit (Pierce). The experiment was performed according to user's manual and the absorption was measured at 562 nm at the spectrometer Ultrospec 3000.

##### Purification of proteins by acetone precipitation

Proteins of the supernatant (cytosolic fraction) were first diluted with H<sub>2</sub>O<sub>bidest</sub> 1:1 and precipitated by adding a five-fold excess of 100 % ice-cold acetone. After incubation at -20 °C over-night the precipitated proteins were centrifuged at 20 000 g for 30 min at 4 °C and the supernatant was carefully removed. The pellet was washed twice with 100 µl of 80 % ice-cold acetone, dried and stored at -80 °C until use.

#### 2.4.1.2 Reduction, alkylation and nicotinoylation

Reduction and blocking of cysteine residues (carbamidomethylation), alkylation with iodacetamide and isotope labeling of the protein samples were performed according to the manufacturer's protocol (ICPL Kit, Serva Electrophoresis). After nicotinoylation, the samples were purified again by acetone precipitation.

## 2.4.2 Membrane isolation by sucrose gradient

After harvesting the culture by centrifugation at 8000 rpm for 30 min and 10 °C in a SS34 rotor, the pellet was resuspended in 3-4 ml basic salt. Then the cells were disrupted by homogenizing in a glass homogenizer and sonification in an water bath (3 x 1 min, 5 min break respectively, 50 % duty cycle in ice water). Insoluble cell components were removed by centrifugation at 6200 rpm for 15 min at 10 °C in the same rotor. Membranes were pelleted from the supernatant by centrifugation at 30 000 rpm for 1 h at 10 °C in a Ti50 rotor. Finally the pellet was resuspended in 1 ml H<sub>2</sub>O<sub>bidest</sub> and applied on a 30 % - 50 % (w/w) sucrose gradient (dissolved in H<sub>2</sub>O). The gradient was centrifuged at 25 000 rpm for 14 h at 10 °C in a TST-41 rotor. Significantly visible bands were sucked off with a pasteur pipette and transferred into a borosilicate glass cuvette. The absorption of the sucrose solution was measured in a spectrophotometer (Pharmacia Biotech). To test if there were carotinoids located in the bands, tetrahydrofuran (THF) was added 1:1 to the sucrose suspension and the absorption measurements repeated again.

## 2.4.3 Protein precipitation by trichloroacetic acid (TCA)

Proteins remaining in the bands of the sucrose gradients were precipitated with TCA. To the sucrose solution, an equal volume of 20 % TCA was added and the solution mixed and incubated on ice for 30 min. The solution was centrifuged in an Eppendorf microcentrifuge for 30 min at 14 000 rpm and the pellet with the precipitated proteins washed twice with H<sub>2</sub>O<sub>bidest</sub> (centrifuging it for 15 min). Before freezing it for storage at -20 °C it was dried in a speed vac.

## 2.4.4 SDS-Polyacrylamide Gel-Electrophoresis (SDS-PAGE)

4-12 % Bis-Tris Mini Gels (NuPAGE, Novex) were used for the separation of the proteins before mass analysis.

### 2.4.4.1 ICPL samples

The sample (300 µg = 150 µg of each labeling state) was resuspended in 10 µl sample buffer (NuPAGE). The protein pellet underwent a 5 min long sonication and then it was heated for 30 min at 70 °C. 10 µl of the sample was applied to the gel and electrophoresed at 200 V. The SDS-PAGE gel was stained for half an hour with Coomassie R (fixation solution: 45 % v/v methanol, 10 % v/v acetic acid) and destained overnight for several hours (destaining solution: 10 % v/v ethanol, 7.5 % v/v acetic acid). While destaining, the gel was rotated and the destaining solution exchanged frequently. Protein bands were excised from the gel in thin slices. These were reduced to small pieces, transferred into 0.5 ml LoBind Eppendorff tubes with 150 µl H<sub>2</sub>O<sub>bidest</sub> in it (to avoid drying-out of the gel) and destained by adding 100 µl 50 % (v/v) acetonitrile



and 50 mM  $\text{NH}_4\text{HCO}_3$  for 20 min, which was alternated until the gel pieces were completely destained. The gel pieces were incubated in 100  $\mu\text{l}$  10 mM dithiothreitol (DTT) in 50 mM  $\text{NH}_4\text{HCO}_3$  at 59 °C, followed by 30 min in the dark in 100  $\mu\text{l}$  iodacetamide (IAA) in 50 mM  $\text{NH}_4\text{HCO}_3$ . Finally, the gel pieces were washed again by incubation in 100  $\mu\text{l}$  50 % (v/v) acetonitrile and 50 mM  $\text{NH}_4\text{HCO}_3$  for 20 min, which was repeated three times.

### 2.4.4.2 Analysis of proteins from sucrose gradient bands

Depending on the concentration of the precipitated proteins, samples were dissolved in 40 - 200  $\mu\text{l}$  sample buffer (NuPAGE, 4x). Sample reducing agent (NuPAGE, 10x) was added and 10 - 40  $\mu\text{l}$  of each sample was heated for 10 min at 70 °C before loading onto the gel. Electrophoresis was at 180 V. Finally, the gel was stained for 3 h with 0.1 % Coomassie Brilliant Blue R250 (40 % v/v EtOH, 10 % v/v acetic acid) on a shaker and destained with solution I (40 % v/v EtOH, 10 % acetic acid) for 1 h and solution II (10 % v/v acetic acid) for 30 min. The gel was stored in a 1 % acetic acid solution at 4 °C, until tryptic in-gel-digestion.

### 2.4.5 Tryptic in-gel-digestion and desalting of protein samples after SDS-PAGE

(Shevchenko *et al.*, 1996)

#### 2.4.5.1 ICPL labeled protein samples

The gel pieces were dried in a SpeedVac centrifuge and 4.7 ng/ $\mu\text{l}$  trypsin (Promega) added. Digestion was carried out overnight at 37 °C at 1000 rpm. The supernatant was collected into LoBind Eppendorf tubes and combined with the eluates of the following three elution steps: (i) water; (ii) 50 % v/v acetonitrile; and (iii) 50 % v/v acetonitrile with 0.1 % v/v trifluoroacetic acid (TFA). The combined eluates were frozen in liquid nitrogen and dried in a SpeedVac centrifuge. Before starting with the desalting process, the pellets were dissolved in 100  $\mu\text{l}$   $\text{H}_2\text{O}_{\text{bidest}}$ , frozen and dried again. Each sample was dissolved in 20  $\mu\text{l}$  5 % formic acid and desalted using C18 Extraction Disk Cartridges (3M Empore High Performance Extraction Disk Cartridges, 7 mM/3 ml cartridges, St. Paul). The column was first equilibrated with 10  $\mu\text{l}$  isopropanol and washed twice with 10  $\mu\text{l}$  5 % formic acid. The dissolved sample was added to the column and the column was washed twice with 10  $\mu\text{l}$  5 % formic acid. The proteins were eluted with 20  $\mu\text{l}$  5 % formic acid in 80 % methanol. The eluates were dried in a SpeedVac centrifuge.

#### 2.4.5.2 Proteins from sucrose gradient

Gel bands were cut into 1 mm<sup>3</sup> cubes and washed two times with 50 mM ammonium bicarbonate, 50 % ethanol. For protein reduction, gel pieces were incubated with 10 mM

DTT in 50 mM ammonium bicarbonate for 1 h at 56 °C. Alkylation of cysteines was performed by incubating the samples with 10 mM iodoacetamide in 50 mM ammonium bicarbonate for 45 min at 25 °C in the dark. Gel pieces were washed two times with 50 mM ammonium bicarbonate, 50 % ethanol, dehydrated with 100 % ethanol, and dried in a vacuum concentrator. The gel pieces were rehydrated with 12.5 ng/ $\mu$ l trypsin (sequencing grade, Promega) in 50 mM ammonium bicarbonate and incubated overnight at 37 °C for protein digestion. Supernatants were transferred to fresh tubes, and the remaining peptides were extracted by incubating gel pieces two times with 30 % acetonitrile in 3 % TFA followed by dehydration with 100 % acetonitrile (MeCN). The extracts were combined and desalted using RP-C18 StageTip columns, and the eluted peptides used for mass spectrometric analysis.

## 2.5 Analytical methods

### 2.5.1 Amino acid analysis of *Hbt. salinarum*

For determination of the amino acids, cells were grown (growth conditions described in subsection 2.2.1.2) in synthetic medium with defined composition (Koch, 2005), with and without glycerine. The cell culture was harvested at stationary phase ( $OD_{600} = 1.5$ ) by centrifugation for 20 min at 8000 rpm (10 °C in a Sorvall RC5C centrifuge with a GS3 rotor).

Afterwards the pellet was suspended in basal salt (like complex medium for *Hbt. salinarum* (section 2.2.2.1) but without peptone) till an  $OD_{600}$  of 4.5 was reached and 35 ml of the cell suspension were given in a klett-flask. Arginine, ornithine or both (0.5 %) were added to the concentrated cell suspension and again incubated at 37 °C, aerobically or anaerobically in the dark or in the light.

For cells cultured under anaerobic growth conditions, 1 ml of a 1 M sodiumcarbonate solution was added into the sidearm of the klett-flask. The cell suspension was flushed with nitrogen for 5 min and finally the flask made airtightly closure with a plug containing a septum inside. At various times, 0.5 ml samples were taken (in case of anaerobic conditions, samples were taken with a syringe through the septum), and the cells were removed by centrifugation (14 000 rpm, 5 min, Eppendorf desk centrifuge). Aliquots of the supernatant (400  $\mu$ l) were frozen and later analyzed for arginine or ornithine on an amino acid analyzer (Biotronik LC3000).

#### 2.5.1.1 Calculations of the intracellular change of concentration of ornithine ( $\Delta$ orn) and arginine ( $\Delta$ arg) per cell

Parameters (calculated by Ricardo Del Rosario from the internal Cell Database):

- cell density: 450 Klett/ml = 4,59 OD/ml

- 1 OD<sub>600</sub> ml = 1,36\*10<sup>9</sup> cells
- cell water volume : 0.59 fl

First, the absolute number of the measured amino acid molecules was converted into a number per 1 ml. After calculating the number of cells in 1 ml using the optical density, the absorption or secretion of the amino acid per cell could be determined.

### 2.5.2 Stable Isotope Labeling in *Nmn. pharaonis* with <sup>13</sup>C carbon sources

Instead of <sup>12</sup>C carbon sources, <sup>13</sup>C labeled acetate or/and <sup>13</sup>C labeled amino acids and <sup>13</sup>C labeled sodium carbonate were added to the minimal medium for *Nmn. pharaonis* (subsubsection 2.2.2.2). All isotopomers and deuterated solvents were ordered from Euriso-Top. *Nmn. pharaonis* cells were inoculated twice consecutively in 35 ml minimal medium containing the respective labeled carbon source before inoculation into 350 ml medium.

### 2.5.3 Preparation of lipids

Before extracting lipids it was necessary to separate the membrane fraction of the harvested cells from the remaining cell components.

#### 2.5.3.1 Cell harvest and disruption

For labeling experiments, lipids yielded from at least 350 ml cell culture in stationary phase were required. Upon reaching the stationary phase, the cells were harvested by centrifugation in a Sorvall RC 5c plus centrifuge (4 °C, 10500 rpm, Rotor SS34) for 30 min. The pellet was resuspended in basal salts (NaCl 3.4 M, KCl 13 mM, KH<sub>2</sub>PO<sub>4</sub> 7.3 mM, pH 9) and then homogenized for 2 h by adding a small quantity of DNase I and mixing it with a magnetic stir bar. Finally the cells were broken up by osmotic shock (Oesterhelt & Stoeckenius, 1971): the cell suspension was dialyzed against 30 l water in dialysis cassettes (Pierce Slide-A-Lyzer, 10 000 MWCO) over night at 4 °C. After dialysis, lipids were separated from proteins, DNA and RNA by ultra-centrifugation at 40 000 rpm for 2.5 h at 4 °C (Beckman Coulter LE-80K, Ti50 rotor).

#### 2.5.3.2 Lipid extraction

Lipids were extracted according to Bligh and Dyer (Bligh & Dyer, 1959). The polar fraction of lipids was obtained by extraction with chloroform, methanol and citric acid (2:2:1.8; v/v/v). The pellet was dissolved in 40 ml citric acid and transferred into a separatory funnel. 50 ml chloroform and 50 ml methanol were added and mixed by shaking the funnel. 50 ml of both, chloroform and citric acid were added again and

the solution allowed to separate into two layers after shaking. After collecting the chloroform layer in a round flask, additional chloroform was added into the funnel. Extractions were repeated for as long as this layer stayed colored. To exclude the water in the solution, some  $\text{Na}_2\text{SO}_4$  was added to the chloroform layer and finally filtered through a fluted filter. The solvent was removed by rotary evaporation.

### 2.5.3.3 Extraction of polar lipids by acetone precipitation

Total lipid extracts were dissolved by shaking in 600  $\mu\text{l}$   $\text{CHCl}_3$  and 100  $\mu\text{l}$  MeOH (6:1). The solutions were transferred into precooled ( $-20^\circ\text{C}$ ) glass centrifuge tubes (COREX) after prior flushing of the tubes twice with 300  $\mu\text{l}$  of solvents. Then, 4 ml of ice-cold acetone was added and the solution incubated at  $-20^\circ\text{C}$  over night. The solution was centrifuged (Sorvall centrifuge, SS 34 rotor) at 2900 g, 30 min at  $5^\circ\text{C}$  and the lipid precipitate was removed with a metal spatula and resuspended again in 2 ml ice-cold acetone. The suspension was sonicated in a water bath. After centrifugation, acetone precipitation was repeated twice and the sample incubated at  $-20^\circ\text{C}$  for 1 h after every repetition.

### 2.5.3.4 Cleavage of ether lipids with boron trichloride

For analyzing the alkyl chains of extracted ether lipids, cleavage with  $\text{BCl}_3$  (dissolved in methylene chloride) was performed (Nishihara & Koga, 1988; Kates *et al.*, 1965; Gerrard & Lappert, 1952). After drying the lipids in glass vials (Pierce) under stream of nitrogen, 1 ml of  $\text{BCl}_3$  in  $\text{CH}_2\text{Cl}_2$  was added and the vial closed by an appropriate screw top. The reaction was allowed to proceed for 30 min with occasional shaking of the tube. Afterwards, the solution was evaporated and the  $\text{BCl}_3$  and borate removed by two rounds of suspension in MeOH and drying. Cleaved lipids were dissolved in 1.5 ml  $\text{CHCl}_3/\text{MeOH}/\text{H}_2\text{O}$  (1:1:0.9; v:v:v) and then the upper phase, which contained the polar headgroups, was removed. The phytanoylchloride (attached chloride to the isoprenoid chain) which was dissolved in  $\text{CHCl}_3$  was evaporated again before 1 ml petroleum ether was added. The solution was shaken well and sonified in a water bath. To avoid taking up precipitates, the solution was transferred into a new glass vial and washed with 1 ml  $\text{H}_2\text{O}$ . The upper phase containing the phytanoylchloride in petroleum ether was again transferred into a new vial and finally dried off under a nitrogen stream.

### 2.5.4 Preparation of amino acids

After dialysis of the cell extract (subsubsection 2.5.3.1), 20% TCA was added to the supernatant to a final concentration of 2% and incubated on ice for 30 min. The precipitated proteins were collected by centrifugation at 20 000 rpm for 15 min at  $4^\circ\text{C}$  (SS34 rotor), and the protein pellet dried in a speed vac.

#### 2.5.4.1 Hydrolysis

The protein pellet was dissolved in 1 ml 25 % HCl and mixed well. The dissolved pellet was transferred into a test tube, which was flushed with nitrogen and sealed by heating. After incubating the sample for 24 h at 110 °C it was cooled and opened again. Drying was achieved by incubating it 4 h in an desiccator under vacuum and a heating lamp. To avoid oxidation of tryptophane for some samples 2.5 % (v/v) thioglycolic acid was added to the HCl (Matsubara1969, Penke1974).

#### 2.5.4.2 Derivatization

Since functional groups (hydroxyl, carboxylic acid, amine, thiol, phosphate) present a problem in gas chromatographic separation derivatization of the sample was necessary.

##### Methoximation of carbonyl groups

Keto groups were derivatized by methoxyamine hydrochloride, 20 mg/ml (Pierce), which was dissolved in pyridine (Alfa Aesar). After hydrolysis, the dried pellet was dissolved in 10 µl of derivatization reagent and incubated at 30 °C for 1.5 h at 900 rpm on a shaker.

##### Silylation of labile hydrogens

Protic sites of amino acids (OH-, NH-, and SH-groups) were blocked by silylation to reduce dipole-dipole interactions and to increase volatility for GC separation (Poole *et al.*, 1980). The use of *N*-(*tert*-butyldimethylsilyl)-*N*-methyl-trifluoroacetamide (MTBSTFA) had the advantage that mostly neutral and volatile byproducts are formed that did not react with the column, hence enabling direct GC-MS analysis (Evershed, 1993). The silylation reagent MTBSTFA was diluted with pyridine 1:9 and 90 µl was pipetted onto the methoximated sample. After thorough mixing, the sample was incubated at 75 °C for 30 min at 900 rpm.

#### 2.5.5 Isolation of intracellular solutes

Cells were grown in 200 ml of medium in 500 ml flasks at 37 °C and shaken at 100 rpm. The following media were used: complex medium of *Hbt. salinarum* (Table 2.5), synthetic medium of *Nmn. pharaonis* (Table 2.7) and synthetic medium of *Nmn. moolapensis* (Table 2.10) respectively. When the culture reached mid-exponential phase (OD 0.3 - 0.4), cells were harvested by centrifugation (6000 g, 30 min). The cell pellet was washed three times with 3.4 M NaCl and dried in a speed vac centrifuge. Cell pellets were suspended in 1.5 ml 70 % (v/v) EtOH and mixed intensively for 5 min. After 5 min in a water bath sonicator the mixture was centrifuged at 11 000 g, for 10 min at 4 °C in an Eppendorf microcentrifuge. The extraction step was repeated twice and the ethanolic supernatants were pooled in a small flask. Most of the solvent was removed

by rotary evaporation and final sample drying was achieved by centrifugation in a speed vac. For NMR analysis, samples were redissolved in 160  $\mu\text{l}$   $\text{D}_2\text{O}$  (99.9%) and centrifuged for 10 min at 10 000 rpm in an Eppendorf centrifuge. The thin top layer was discarded and the rest of the aqueous supernatant taken for measurements.

### 2.5.6 Thin layer chromatography (TLC)

#### 2.5.6.1 Analytical TLC

Lipids dissolved in  $\text{CHCl}_3$  (20  $\mu\text{g}/\mu\text{l}$ ) were applied on a DC plate (Merck, silica gel 60 glass) with borosilicate glass capillaries (Clark GC120). After the solvent was evaporated completely, the plate was placed in a TLC chamber. The glass chamber was filled with the mobile phase ( $\text{CHCl}_3/\text{MeOH}/90\%$  acetic acid, 65:4:35, by volume) to a depth of about 2 cm and a filter paper (Carl Schleicher and Schüll) was placed behind the plate. After the mobile phase reached almost the end of the plate, it was removed from the chamber and dried at 120 °C in a ventilated oven. A sulfuric acid spray (15%  $\text{H}_2\text{SO}_4$  in EtOH) was used to detect the lipids. Using a heat gun, lipids were charred at maximum heat until brownish bands appeared. Finally, the retention factor ( $R_f$ ), which is defined as the distance traveled by the compound divided by the distance traveled by the solvent, was determined for each visible spot.

#### 2.5.6.2 Preparative TLC with iodine staining

For preparative TLC, extracted lipids were applied on PLC plates (Merck, silica gel 60 glass). After development, the plates were removed from the chamber and heat dried (subsubsection 2.5.6.1). Since the detection method with sulfuric acid is destructive and the solutes cannot be recovered after detection, iodination was chosen as a proper reversible staining method for lipids (Sims & Larose, 1961). The dry plate was placed in covered chromatography jars containing iodine crystals in a glass dish. Due to the hydrophobic character of both the halogen and lipids, samples adsorb iodine and readily appear on plates as brownish spots. Once they were visible, the colored spots were fixed by scraping around their periphery with a sharp pencil before the iodine coloration faded. Sublimation of iodine took several hours. The bands were cut out with a scalpel and the extract leached with the solvents  $\text{CHCl}_3$  and MeOH (6:1, v/v) in a frit again. Finally the sample was dried under a stream of nitrogen.

### 2.5.7 Mass spectrometry

#### 2.5.7.1 Analysis of extracted lipids by negative-ion electrospray ionization (ESI) mass spectrometry (MS)

*Hbt. salinarum* was grown in 2 l of complex medium, *Nmn. pharaonis* in 2 l of minimal medium and *Nmn. moolapensis* in 2 l of DBCM2 (recipes for all media are listed in

subsection 2.2.2). Total lipids were extracted by the modified method of Bligh and Dyer (subsubsection 2.5.3.2) after harvesting the cells. Dried lipids were dissolved in 10 ml 100 % CHCl<sub>3</sub> and then 10 µl of the samples of *Hbt. salinarum* and *Nmn. pharaonis* were diluted in 990 µl solvents (CHCl<sub>3</sub>/MeOH/H<sub>2</sub>O, 20:20:7, v/v/v) and 5 µl of the sample of *Nmn. moolapensis* was diluted in 995 µl solvents. The specified volume was taken up with a Hamilton syringe and subjected to ESI-MS analysis on a Q-ToF Ultima mass spectrometer (Waters) equipped with an ion-spray interface. The samples were continuously introduced into the mass spectrometer at a flow rate of 5 µl/min by an internal syringe pump. The instrumental conditions were as follows: cone gas flow, 100 l/h; desolvation gas flow at 150 °C, 400 l/h; capillary voltage 1.75 kV; mass range, 50-2000 amu. Collision-induced dissociation mass spectra (CID-MS) were obtained with a voltage of 10.0 kV showing [M - H]<sup>-</sup> and [M - 2H]<sup>2-</sup> parent ions as well as some fragmentation ions. The instrument was calibrated with 0.1 % phosphoric acid and washed with the solvents between sample application to avoid procrastination of former samples. As an external standard for the negative mode leucine enkephalin (Sigma-Aldrich) was injected and MS and MS/MS spectra recorded.

#### 2.5.7.2 Analysis of alkyl chains and amino acids with gas chromatography mass spectrometry (GC/MS)

For the analysis of <sup>13</sup>C labeled isoprenoids and amino acids, GC/MS was carried out using a Finnigan TRACE GC Ultra Gas Chromatograph equipped with a Rtx-5 Sil MS column (Restek: 30 m, 0.25 mm, 0.25 µm) that was coupled to a Finnigan PolarisQ Mass Spectrometer. Depending on the concentration of the samples, amino acids were diluted with pyridine to different levels and isoprenoids were dissolved in methanol. The injection volume was 1 µl at a carrier gas flow of 1.20 ml/min helium in the splitless mode. The initial oven temperature of 40 °C was maintained for 1 min and then raised to 300 °C at 15 °C/min and held at this final temperature for 1 min. Other settings were 220 °C base temperature, a surge pressure of 3.00 kPa, 200 °C ion source temperature and electron impact ionization (EI) at 70 eV. Mass spectra were analyzed in the range of 25.0 - 550.0 and till 760.0 atom mass units (amu) respectively. Before starting the measurements, three runs with ethyl acetate were performed for flushing the column.

#### 2.5.7.3 Analysis of proteins extracted from sucrose gradient with NanoLC-MS/MS

All digested peptide mixtures were separated by on-line NanoLC and analyzed by electrospray tandem mass spectrometry. The experiments were performed on an Agilent 1200 nanoflow system connected to an LTQ Orbitrap mass spectrometer (Thermo Electron) equipped with a nanoelectrospray ion source (Proxeon Biosystems). Binding and chromatographic separation of the peptides took place in a 15-cm fused sil-

ica emitter (75  $\mu\text{m}$  inner diameter from Proxeon Biosystems) in-house packed with reversed-phase ReproSil-Pur C18-AQ 3  $\mu\text{m}$  resin (Dr. Maisch GmbH, Ammerbuch-Entringen, Germany). Peptide mixtures were injected onto the column with a flow of 500 nL/min and subsequently eluted with a flow of 250 nL/min from 2% to 40% MeCN in 0.5% acetic acid, in a 100 min gradient. The precursor ion spectra were acquired in the Orbitrap analyzer ( $m/z$  300-1800,  $R = 60\,000$ , and ion accumulation to a target value of 1 000 000), and the five most intense ions were fragmented and recorded in the ion trap. The lock mass option enabled accurate mass measurement in both MS and Orbitrap MS/MS mode as described previously (Olsen *et al.*, 2005). Target ions already selected for MS/MS were dynamically excluded for 90 s.

The data analysis was performed with the MaxQuant software as described (Gruhler *et al.*, 2005) supported by Mascot as the database search engine for peptide identifications. Peaks in MS scans were determined as three-dimensional hills in the mass-retention time plane. MS/MS peak lists were filtered to contain at most six peaks per 100 Da interval and searched by Mascot (Matrix Science) against a concatenated forward and reversed version of the *Hbt. salinarum* R1 or *Nmn. pharaonis* DSM 2160 (extracted from NCBIInr and contained frequently observed contaminants like proteases and human keratins). The initial mass tolerance in MS mode was set to 7 ppm and MS/MS mass tolerance was 0.5 Da. Cysteine carbamidomethylation was set as a fixed modification, whereas N-acetyl protein and oxidized methionine were set as variable modifications.

Analysis was performed by C. Boulegue (core facility of the MPI of Biochemistry).

### 2.5.7.4 Analysis of nicotinoylated proteins (ICPL)

Peptide separation was achieved using a capillary liquid chromatography system (Ultimate, LC Packings) containing a reversed-phase column (LC Packings Pepmap reversed-phase C18 column, 75  $\mu\text{m}$  i.d., 15 cm) coupled online to a MALDI target spotter (Probot, LC Packings). After the injection of a sample volume of 30  $\mu\text{l}$  the peptides were trapped on a short reversed-phase column (300  $\mu\text{m}$  i.d., 5 mM). The mobile phase consisted of (i) 0.05% TFA and (ii) 0.04% TFA in 80% (v/v) ACN/water. For separation of the peptides, a 65 min linear gradient from 10% to 45% (ii) at a flow rate of 200 nl/min was used, followed by a 20 min wash step of the column with 100% (ii). The analytical column was directly connected to a MicroTee (Upchurch, Oak Harbor, WA) where the eluent was mixed with matrix solution (5 mg/mL  $\alpha$ -cyano-4-hydroxycinnamic acid, 50% (v/v) ACN/water, 5 mM ammonium dihydrogen phosphate, 0.1% (v/v) TFA) at a flow rate of 1.3  $\mu\text{L}/\text{min}$  and deposited onto a blank MALDI plate. 400 MALDI spots per plate resulted from the LC-eluent which was automatically spotted in 10 sec fractions over a time period of 67 min. These spots dried at rt. Mass-spectrometric analysis was performed on a 4700 Proteomics Analyzer (Applied Biosystems, Framingham, MA) equipped with an Nd-YAG laser that produces pulsed power at 355 nm at pulse rates of 200 Hz. MS-spectra were acquired



by accumulation of 2500 laser shots using a positive reflector mode with a deflection cut off range of  $m/z$  700. Subsequently, the MS-spectra were automatically analyzed by the Peakpicker-software (a generous gift from ABI) to detect and quantify isotopic peptide pairs and generate a list of precursor ions for MS/MS-analysis. Only the more intense MS-signal of an isotopic labeled pair was selected for MS/MS-Analysis. For precursor selection, the S/N-threshold for peptide pairs was set to 20 and to 50 for single MS-peaks. Furthermore, the total amount of precursors for each MALDI-spot was not allowed to exceed 40. A total of 1500 laser shots were carried out for each high-energy MALDI-TOF/TOF CID spectra utilizing collision energy of 1 keV and nitrogen as collision gas. For assistance in statistical analysis an in-house program, developed by A. Brunner (MPI of Biochemistry, Lottspeich Group) was employed.

## 2.5.8 Nuclear magnetic resonance

### 2.5.8.1 NMR measurements of extracted lipids

**1 D carbon/proton and 2 D Fast Heteronuclear Single Quantum Coherence (FHSQC) spectra** NMR spectra were recorded with a Bruker DRX 500 spectrometer equipped with TCI triple resonance probehead, operating in the Fourier transform mode at 500 MHz for the  $^1\text{H}$  nucleus and 125 MHz for the  $^{13}\text{C}$  nucleus at 300 K. The solutions were prepared dissolving the samples in  $d_4$ -MeOD and  $d$ - $\text{CDCl}_3$  2:5 (v/v). 1D  $^{13}\text{C}$  spectra were recorded with  $^1\text{H}$  on-resonance decoupling. For 2D spectra, gradient-enhanced HSQC pulse sequence was used. In combination to every 2D measurement also 1D  $^1\text{H}$  spectra were measured.

**Additional measured spectra of lipids** In the beginning of this study different NMR methods were tested to achieve maximum sensitivity. The following techniques were applied on the same sample:

- $^{13}\text{C}$  broadband (BB) spectrum decoupled on  $^1\text{H}$
- $^{13}\text{C}$ -dept-135 spectrum (DEPT = distortionless enhancement by polarization transfer)
- homonuclear correlation spectroscopy  $^1\text{H}$ ,  $^1\text{H}$ -COSY (CORrelated SpectroscopY)

**Integration and normalization of signals in FHSQC spectra** A crucial step in data pre-processing of spectra from metabonomic studies is normalization. The normalization step tries to account for variations of the overall concentrations of samples. In this experiment two different normalization steps were performed in the 2D spectra. A program of Bruker (XwinNMR) integrates all marked peaks and calculates the "a"-values which include all, positive and negative integrals. The "+"-values only represent

positive integrals, which are not so prone to artefacts compared to negative integrals, that can occur during phasing or baseline correction of the spectra.

Normalization step (1): Since the samples were always solved in the same amount of *d*<sub>4</sub>-MeOD, it was used as an internal standard. The intensities of the 2D spectra were normalized in respect to concentration of methanol (in order to have constantly the same value of methanol intensity). This step corrects acquisition parameters of the instrument such as shimming (adjust the homogeneity of the magnetic field) and different scan numbers (signal grows proportional to number of scans).

Normalization step (2): To correct different concentrations of samples, to make them comparable between each other, an approximate estimation of each concentration was performed. Proton spectra of every sample were superimposed pairwise at a specific region (significant peaks) and intensities of peaks were compared to calculate a specific ratio.

### 2.5.8.2 NMR measurements of extracted osmolytes

A <sup>1</sup>H WALTZ-decoupled <sup>13</sup>C-NMR spectrum was recorded with a Bruker DRX 500 spectrometer at 500 MHz with a 5 mM TXI probe head. Acquisition parameters included 33.3 kHz sweep width, 32 k datapoints, 90° pulse angle, 100 k transients and a temperature of 298 K. Chemical shifts were measured relative to dioxane (67 ppm).

## 2.6 Bioinformatics environment

### 2.6.1 Data analysis of microarrays

Fluorescence intensities of each probe on the array were scanned with GenePix 4000B (Biozym Scientific GmbH) at 532 nm and 635 nm and extracted with the software Genepix Pro V6 (same company). Using MS Excel, the relevant data were retrieved from raw data and saved in a text-file. This file included the gene-ID, the exact coordinates of the probes as well as the fluorescences of every gene. The data collection was processed in the R environment using a custom service routine written by G. Welzl (Helmholtzzentrum, Neuherberg, Germany). From the normalized, noiseless data, significance values (ttest) with TIGR-MEV were calculated.

### 2.6.2 Carbon fate modeling in *Nmn. pharaonis*

Stable isotope tracer experiments were based on a comprehensive analysis of cellular metabolism by labeling pattern analysis in all amino acids (Sauer *et al.*, 1999; Szyper-ski, 1995). Therefore an analysis tool for tracking individual atoms in a bioreaction network was required. Carbon-fate maps (Mu *et al.*, 2007) were updated and extended with organism specific reaction data and connected to the internal annotation tool BNET (programmed by O. Gonzalez, MPI of Biochemistry) for reconstructing

metabolic pathways. MDL Mol files were downloaded from the KEGG COMPOUND database (Kanehisa & Goto, 2000) for molecules not included in the network. The information about the 2D chemical structure was converted into InChI files, which is an unique identifier for a metabolite.

### 2.6.3 Bioinformatic analysis

For analysis of new or unknown pathways in archaea, information from KEGG (Kanehisa & Goto, 2000), organism-specific data from HaloLex (Pfeiffer *et al.*, 2008a) as well as experiments described in the literature were combined. Homology search on amino acid sequences was performed with Blast (Altschul *et al.*, 1997). Multiple alignments were calculated using the ClustalX program (Thompson *et al.*, 1994). For phylogenetic analysis, a neighbor-joining tree was calculated from the multiple alignment applying the program FigTree. Standard parameters were used.

### 2.6.4 Genome annotation of *Nmn. moolapensis*

#### 2.6.4.1 Genome sequencing and assembly

The genome of *Nmn. moolapensis* (DSM 18674) was sequenced using the whole-genome-shotgun pyrosequencing method '4-5-4' (Margulies *et al.*, 2005; Rothberg & Leamon, 2008) and assembled with the PHRED-PHRAP-CONSED package (Gordon *et al.*, 1998). While PHRED was calculating the quality value for each sequenced base (in the case of '4-5-4' quality is calculated from results of different reads covering the same region), PHRAP was building the assembly of the sequenced reads. CONSED was representing the viewer and editor of the PHRAP assembled sequences. Scaffolding of the contigs was performed by cosmid end sequencing. To achieve gap closure between the scaffolds, cosmid walking and PCRs on chromosomal DNA across contig boundaries was used.

#### 2.6.4.2 Gene prediction and annotation

The genome of *Nmn. moolapensis* was analyzed with REGANOR (McHardy *et al.*, 2004) from the annotation package GENDB (Meyer *et al.*, 2003) for gene prediction. For each coding sequence an automatic function prediction was performed by Metanor (Goesmann *et al.*, 2005). In this study, the main focus was on genes involved in metabolic pathways. Starting from the raw set of sequenced ORFs, bidirectional best blast (BBB) hits were generated of these predicted *Nmn. moolapensis* genes against the ORF set of *Nmn. pharaonis*. Genes without BBB hits but with a predicted EC number were annotated manually by BLAST (Altschul *et al.*, 1997) and searches in the literature. The software system HaloLex (Pfeiffer *et al.*, 2008a) served as a platform during the whole annotation process. Each *Nmn. moolapensis* enzyme was assigned to a functional class and category. Blast results against *Nmn. pharaonis* and other

organisms were carefully evaluated for annotation of gene functions or descriptions. Using PRIAM (Caudel-Renard *et al.*, 2003), an automatic enzyme detection method, it was possible to compare the metabolic potential between different species.

## 3 Lipid metabolism in halophilic Archaea

### 3.1 Introduction

Halophilic archaea have to cope with high salt concentrations and some species also live at an alkaline pH of 11. To survive in such harsh conditions, these organisms must maintain the structural integrity of the cell, and have biochemical mechanisms to sustain growth.

The archaeal cell membrane is unusual, and well adapted to resist extreme conditions. One of the major characteristics that separate Archaea from Bacteria is the abundance of ether lipids (Kates, 1993b), which form the main component of the archaeal cell membrane. Four structural properties characterize the differences between archaeal and bacterial / eukaryotic lipids (Figure 3.1): (i) Archaeal lipids are based on isoprenyl glycerol ethers and thus dissimilar from the ester based bacterial and eukaryotic lipids; (ii) isoprenoid side chains are bound at the *sn*-2 and *sn*-3 positions (G-1-P) of the glycerol moiety in archaeal lipids, while bacterial and eukaryotic lipids have *sn*-1 and 2-fatty acid chains (G-3-P). In order to designate the configuration of glycerol derivatives, the prefix 'sn' (for stereospecifically numbered, according to the IUPAC recommendations for nomenclature of lipids) is used, which is shown in Figure 3.2. The opposite glycerol stereochemistry in Archaea is the most definitive feature of archaeal lipids in phylogenetic and evolutionary significance (Koga *et al.*, 1998; Peretó *et al.*, 2004). (iii) Hydrocarbon chains of polar lipids are highly methyl-branched isoprenoids in Archaea whereas Bacteria mostly exhibit straight-chain fatty acids; (iv) a bigger part of the archaeal domain, including thermoacidophiles, thermophilic anaerobes, and some methanogens, can build bipolar lipids with a tetraether core that span the membrane, forming a lipid monolayer rather than the usual bilayer.

No tetraether has yet been detected in halophilic archaea, including haloalkaliphiles, but small amounts of fatty acids have been found in membrane proteins of *Hbt. salinarum* (Pugh & Kates, 1994). The fatty acids are not part of archaeal membrane lipids

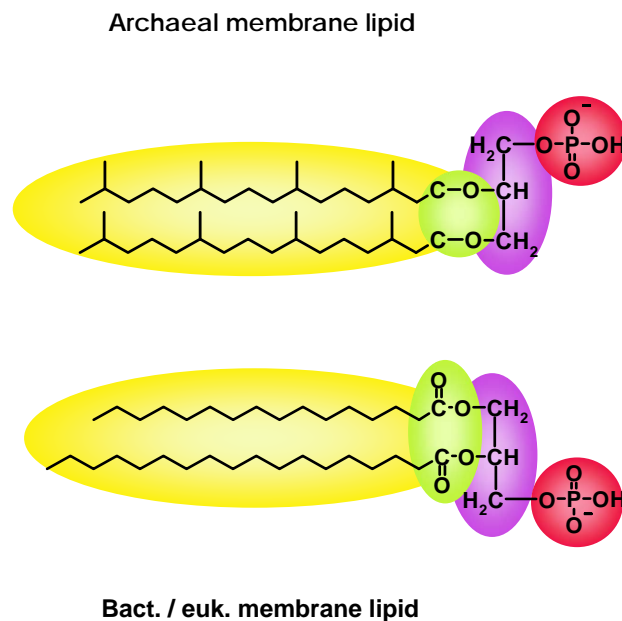


Figure 3.1: **Comparison of archaeal and bacterial / eukaryotic cell membrane lipids.** Adaptation of archaeal cell membrane lipids to extreme environmental conditions by: (i) Ether linkages between the polar headgroups and lipid tails whereas bacteria and eukaryotes use ester bonds (ii) Isoprenoid chains instead of fatty acids (iii) Glycerol stereochemistry opposite of that in Bacteria and Eukarya (iv) Single monolayer membranes in some Archaea rather than the usual phospholipid bilayer (not shown).

(Kolbe *et al.*, 2000) and the origin of them is still unclear because no enzymes exist in Archaea (like the fatty acid synthase complex) that possibly could synthesize these. The ether bonds, isoprenoid chains, and bipolar tetraether lipids have a significant effect on the physicochemical properties of archaeal lipid membranes (Koga & Morii, 2005). For example, ether lipids are much more stable to chemical attack via oxidation or acid/base treatment than ester lipids. Moreover, the distinctive lipid-membrane composition is considered primarily as an adaptation to energy stress, since archaea like the halophilic members rely on environmental exclusivity at extreme conditions (Valentine, 2007). There is increasing evidence that ether lipids have a major role in archaeal membranes in enabling the organisms to tolerate extremes of temperature, salt concentrations and pH.

### 3.1.1 Archaeol - the basic structure of all archaeal membrane lipids

Archaeal membrane phospholipids and glycolipids are entirely derived from archaeol or from its dimer, caldarchaeol. Archaeol (Figure 3.2) is a fully saturated, isoprenoid glycerol diether and halophilic archaea display many variants of it (Kates, 1993b). This archaeal 'core lipid' represents the diphytanylglycerol diether (modified by adding the appropriate alkyl group designations, such as C<sub>20</sub>, C<sub>25</sub>, etc). Specifically, membranes of *Hbt. salinarum* contain archaeol derivatives with two phytanyl side chains (C<sub>20</sub>), and, to lesser extents, other isoprenoid constituents such as squalenes (C<sub>30</sub>), phytoenes (C<sub>40</sub>), menaquinones (C<sub>40</sub>), and dolichol (C<sub>60</sub>) (Oesterhelt, 1976; Lechner *et al.*, 1985; Kushwaha *et al.*, 1976a).

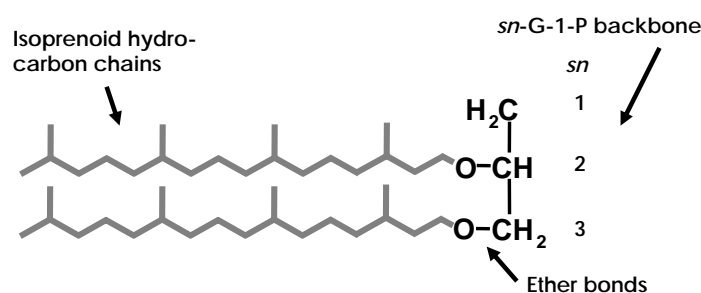


Figure 3.2: **Structure of archaeol.** Archaeol is a double ether of *sn*-1-glycerol where positions 2 and 3 are bound to phytanyl residues. The archaeols are Archaea homologs of diacylglycerols (DAGs). The sugars or polar head groups that are frequently attached to the *sn*-1 position of the glycerol moiety in archaeal diether lipids are not shown.

In alkaliphilic species of extreme halophiles, such as *Nmn. pharaonis*, both the C<sub>20</sub>-C<sub>20</sub> diether and C<sub>20</sub>-C<sub>25</sub> (C<sub>25</sub> = sesterterpanyl) diether occur (Tindall *et al.*, 1984). Sometimes the C<sub>25</sub>-C<sub>25</sub> diether is encountered as a minor component as well (Rosa *et al.*, 1982, 1983). In most cases the hydrophobic chains are fully saturated, but double bonds appearing transiently during the biosynthesis of the phytanyl chains were observed in *Hbt. salinarum* (Moldoveanu & Kates, 1988; Fredrickson *et al.*, 1989).

The abundance of unsaturated lipids seems to be a general feature of cold adaptation in psychrophilic archaea. Similar studies on the psychrotolerant haloarchaeon *Hrr. lacusprofundi* indicated that the proportion of unsaturated lipids correlates with growth temperature. The unsaturated lipids ensure membrane fluidity, and thereby membrane function, is maintained (Gibson *et al.*, 2005; Cavicchioli, 2006).

### 3.1.2 Polar lipids

Polar lipids may represent up to 90 % of the total cell lipid content of halophilic archaea (Kamekura & Kates, 1988). All halophilic archaea known so far contain the diether derivatives of phosphatidyl glycerol (PG), the methyl ester of phosphatidyl glycerophosphate (Me-PGP) (Kates, 1996) and biphosphatidyl glycerol (BPG, an analogue of eukaryotic and bacterial cardiolipin) (Lattanzio *et al.*, 2002). Phosphatidylglycerosulfate (PGS) is present in most of the neutrophilic species like *Hbt. salinarum* (Hancock & Kates, 1973), but all alkaliphilic archaea seem to lack PGS. It has also been shown that this phospholipid was required for the functioning of cytochrome c oxidase activity in *Halorubrum* sp. (Corcelli *et al.*, 2007) .

For unknown reasons, also substantial amounts of glycolipids are missing in most haloalkaliphilic members. An exception is the alkaliphilic strain *Natrialba* SSL1, isolated from a soda lake in India, which possesses a diglycosyl diether (DGD-4) lipid (Upasani *et al.*, 1994). Also, new glycolipids have been detected recently by NMR and TLC (Corcelli *et al.*, 2000; Corcelli, 2009), but some of them, like glycocardioplipin GlyC, seem not to be part of an archaeal membrane and are generated during lipid extraction and preparation (Renner *et al.*, 2005). The major membrane glycolipid of *Hbt. salinarum* is sulfated-triglycosyl diether (S-TGD-1) (Kates, 1993b). It has been shown that archaeal glycolipids play an important role in the stabilization and assembly of bacteriorhodopsin (Bop) in the PM (Essen *et al.*, 1998; Weik *et al.*, 1998; Hüseyin, 2001).

### 3.1.3 Biosynthetic pathways of lipids

While there is much experimental evidence of unusual diether-derived and tetraether-derived archaeal lipids the biosynthetic pathways underlying this diversity are largely unknown. A brief summary of the current understanding in this field is presented below.

#### 3.1.3.1 Synthesis of the glycerol phosphate backbone from dihydroxyacetone phosphate (DHAP)

In Figure 3.3 it is displayed that the glycerol phosphate backbone of archaeal diether lipids is formed from glycerol 1-phosphate, derived from DHAP via glycerol-1-



phosphate dehydrogenase (EC 1.1.1.261) (Nishihara *et al.*, 1999). Linking the first side chain to the backbone is catalyzed by geranylgeranylgeranyl phosphate (GGGP) synthase (Soderberg *et al.*, 2001). The second chain is attached by digeranylgeranylgeranyl phosphate (DGGGP) synthase (Chen *et al.*, 1993) and the saturation of double bonds occurs after adding a cytidine group at the *sn*-1 position of the glycerol moiety (Koga & Morii, 2006).

Enzymes catalyzing the linkage of sugar moieties are not known, and only one enzyme responsible for adding headgroups has been characterized (Morii & Koga, 2003). Little is known about enzymes involved in the saturation (hydrogenation) of isoprenoid side chains and the formation of cyclic tetraether lipids (Boucher *et al.*, 2004).

### 3.1.3.2 Isoprenoids are synthesized via the mevalonate pathway

Like other archaea, halophiles derive their isoprenoids from mevalonate, as shown by tracer studies (Kates & Kushwaha, 1978; Ekiel *et al.*, 1986). In eukarya and some bacteria, which synthesize isopentenyl diphosphate (IPP) and its isomer dimethylallyl diphosphate (DMAPP) through this pathway (Lange *et al.*, 2000), five steps have been described (Figure 3.3): (i) 3-hydroxy-3-methylglutaryl-CoA (HMG-CoA) is formed from acetyl-CoA and acetoacetyl-CoA; (ii) HMG-CoA is reduced to mevalonate; (iii) mevalonate is phosphorylated to phosphomevalonate; (iv) phosphomevalonate is phosphorylated to diphosphomevalonate; (v) this is converted to IPP.

While most archaea lack genes for phosphomevalonate kinase (EC 2.7.4.2) and diphosphomevalonate decarboxylase (EC 4.1.1.33), haloarchaea operate a chimeric mevalonate pathway combining bacterial-type and archaeal-type enzymes (Smit & Mushegian, 2000). For instance, *Nmn. pharaonis* encodes an archaeal isopentenyl phosphate kinase (NP2852A) and a bacterial diphospho-mevalonate decarboxylase (NP1580A).

For conversion of IPP to DMAPP in the last mevalonate step, two analogous types of isopentenyl diphosphate isomerases (IDI) exist (Boucher, 2007). Both the archaeal-type and the bacterial-type are present in *Nmn. pharaonis* (NP0360A, NP4826A, NP5124A) and in *Hbt. salinarum* (OE3560F, OE6213R, OE7093R) (Falb *et al.*, 2008), but in other haloarchaea only a bacterial type IPP isomerase is present (Boucher *et al.*, 2004).

An unusual first step in the mevalonate biosynthesis was revealed by labeling studies (Ekiel *et al.*, 1986) where instead of mevalonate being synthesized from three molecules acetyl-CoA, the reaction used two of these and a C<sub>2</sub>-unit derived from degraded amino acids.

The products of the mevalonate pathway (IPP and DMAPP) are then used as building blocks for lipid side chains by polycondensation to trans- and cis-polyprenyl chains in head-to-tail fashion by (E)- and (Z)-prenyltransferases (EC 2.5.2.-). Farnesylgeranyl diphosphate synthase was found in the alkaliphilic *Nmn. pharaonis* (Rosa *et al.*, 1982) and the hyper-thermophilic *Aeropyrum pernix*, whose polar lipids contain C<sub>25</sub> alkyl chains (Morii *et al.*, 1999).

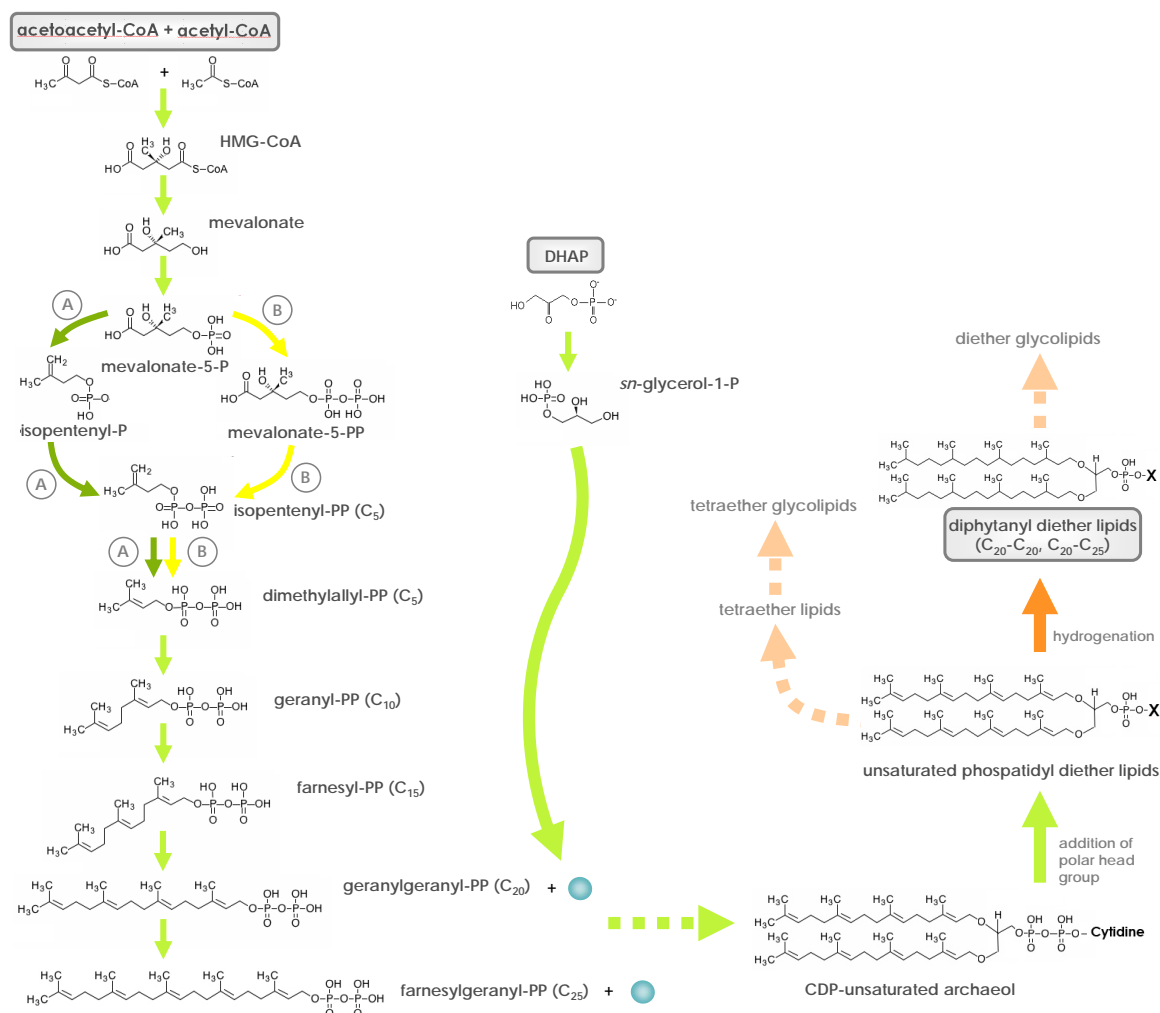


Figure 3.3: **Pathways for the biosynthesis of archaeal ether lipids in halophiles.** While the glycerol phosphate backbone of ether lipids is synthesized from dihydroxyacetone phosphate (DHAP), the according isoprenoids are synthesized via the mevalonate pathway from acetoacetyl-CoA and acetyl-CoA. Archaeal- (A) and bacterial-type (B) enzyme variants (according to (Falb *et al.*, 2008)) are indicated with circles. Compounds: HMG-CoA - 3-hydroxy-3-methylglutaryl-CoA; P and PP are phosphate and pyrophosphate; DHAP - dihydroxyacetone phosphate; CDP - cytidine diphosphate

## 3.2 Results and discussion

### 3.2.1 Lipidomics in *Hbt. salinarum*, *Nmn. pharaonis* and *Nmn. moolapensis*

#### 3.2.1.1 Analytical and preparative TLC of lipid extracts identified different glycolipids

Total lipid extracts of three halophilic archaea, *Hbt. salinarum*, *Nmn. pharaonis* and *Nmn. moolapensis*, were extracted according to Bligh and Dyer (Bligh & Dyer, 1959) with chloroform, methanol and citric acid. Afterwards they were analyzed and compared by thin layer chromatography (TLC) on silica gel plates. Because of the many variables in TLC, slight differences in solvent system, adsorbent, thickness of the adsorbent, amount of material spotted and temperature during the mobile phase can affect the observed  $R_f$  values of lipids, and this method only provides presumptive or corroborative evidence as to the identity of a compound. An additional goal of the preparative TLC was a pre-fractionation of the different lipids before measuring them by ESI-MS.

The retention factor ( $R_f$ ) of each lipid in Figure 3.4 was determined by the formula

$$R_f = \frac{D_x}{D_f}$$

( $D_x$  = distance traveled by the compound,  $D_f$  = distance traveled by the solvent front).

$R_f$  values of the lipids detected in total lipid extracts of *Hbt. salinarum*, *Nmn. pharaonis* and *Nmn. moolapensis* were very similar to the published  $R_f$  values of Corcelli and colleagues (Corcelli *et al.*, 2000) and are listed in Table 3.1. An exception was the  $R_f$  of the PGP-Me in the TLC of the current study (0.37 - 0.39), which was lower compared to the published one (0.51). The unknown glycolipid in *Nmn. moolapensis* also showed a lower polarity (higher  $R_f$ , 0.10) compared to S-TGD-1 of *Hbt. salinarum* ( $R_f = 0.053$ ) in this TLC, as was previously reported (Burns *et al.*, 2009).

Comparison of the lipids between the three halophilic archaea in Figure 3.4 showed similar  $R_f$  values for all lipid classes.

The  $R_f$  values of lipids separated on a preparative TLC plate (Figure 3.5) did not

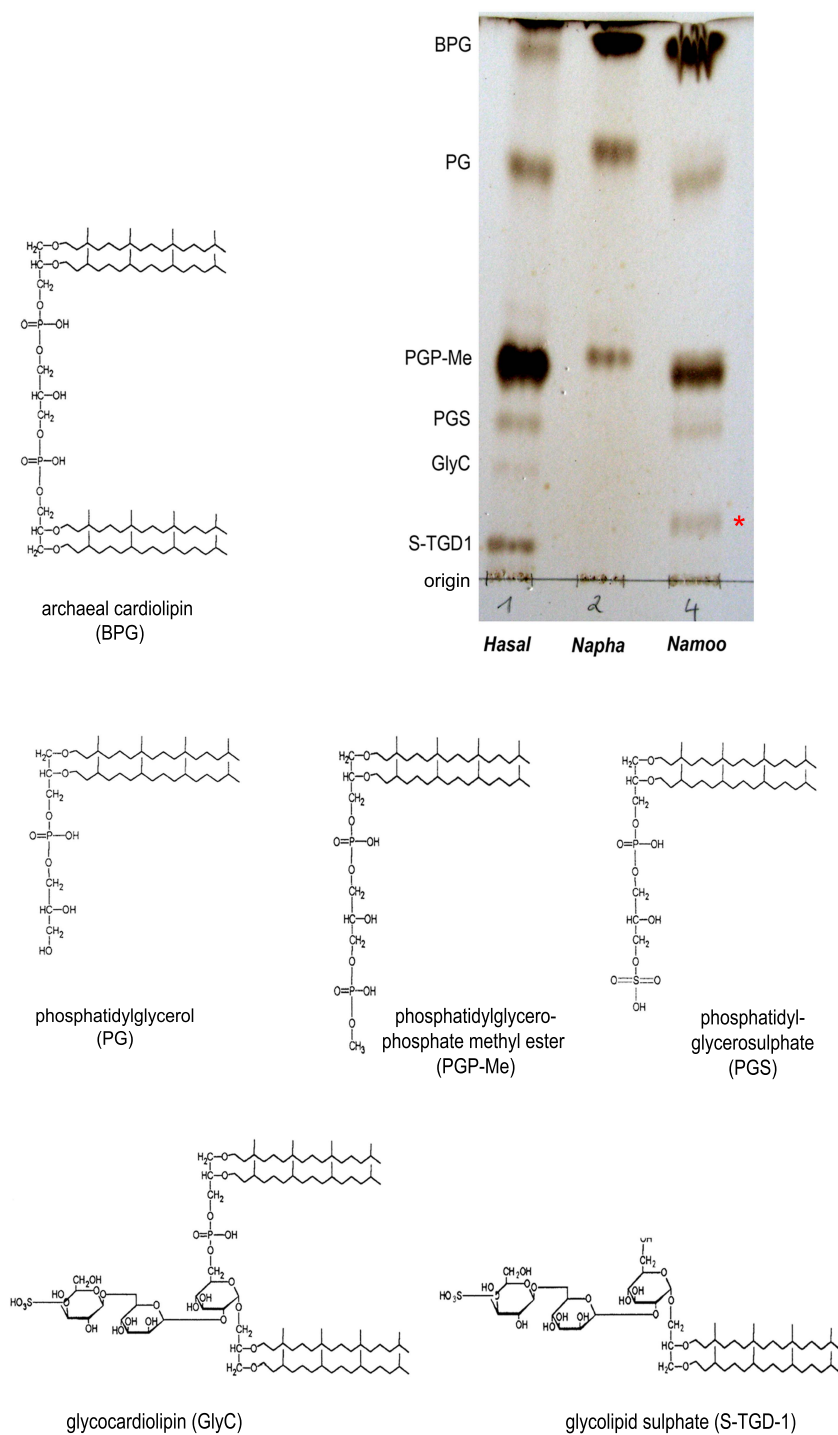


Figure 3.4: **Analytical TLC of total lipid extracts of *Hbt. salinarum* (Hasal), *Nmn. pharaonis* (Napha) and *Nmn. moolapensis* (Namoo).** The red asterisk marks the unknown glycolipid in *Nmn. moolapensis*. The intermediate phosphatidic acid (PA) is a precursor of most lipids, but not visible as a single band on a TLC plate due to its mobility ( $R_f$  0.99). Known glycolipid S-TGD-1 of *Hbt. salinarum*: 3-HSO<sub>3</sub>-Galp $\beta$ 1-6Manp $\alpha$ 1-2Glc $\alpha$ 1-diether

Table 3.1: TLC  $R_f$  in solvent system  $\text{CHCl}_3/\text{MeOH}/90\%$  acetic acid, 65:4:35, v/v/v.

	Hasal	Napha	Namoo
<b>BPG</b>	0.94	0.96	0.94
<b>PG</b>	0.73	0.76	0.71
<b>PGP-Me</b>	0.38	0.39	0.37
<b>PGS</b>	0.28	-	0.27
<b>GlyC</b>	0.20	-	-
<b>S-TGD-1</b>	0.053	-	0.10
<b>neutral lipids + pigments</b>	0.99-1	0.99-1	0.99-1

Extracted and identified lipids of *Hbt. salinarum* (Hasal), *Nmn. pharaonis* (Napha) and *Nmn. moolapensis* (Namoo), compared to  $R_f$  values according to Corcelli *et al.* (2000).

coincide with the values of the analytical TLC plate (Figure 3.4). All lipid spots overlaid each other and no clear separation could be achieved. A band corresponding to the glycolipid sulphate, for example, was only visible in the case of *Nmn. moolapensis*. Reason for the bad lipid separation is due to the higher thickness of the TLC plate.

Recovered lipids of the preparative TLC plate were applied again on an analytical TLC plate (Figure 3.6). Not all lipids could be properly recovered which indicates again a bad separation during the preparative TLC. There were always problems with recovering of PGP-Me, since the visible band was not running at the same  $R_f$  like the one from the standard. Instead, at the front of the mobile phase a big spot appeared. This could indicate a bad separation during the preparative TLC.

### 3.2.1.2 Identification of archaeal lipids by negative-ion ESI-mass spectrometry

Composition of lipid extracts from *Hbt. salinarum*, *Nmn. pharaonis* and *Nmn. moolapensis* as well as recovered lipids of preparative TLC were examined by electrospray mass spectrometry (ESI-MS). A comparison of all spectra is shown in Figure S1.

All significant signals detected in the spectra are listed in Table 3.2, additionally with all calculated masses of lipids that are possibly synthesized in at least one of the three organisms. In addition to the significant main peaks satellites of lower mass were observed in MS spectra of *Nmn. pharaonis* and *Nmn. moolapensis*.

In *Hbt. salinarum*, all known lipids could be found except for the recently described

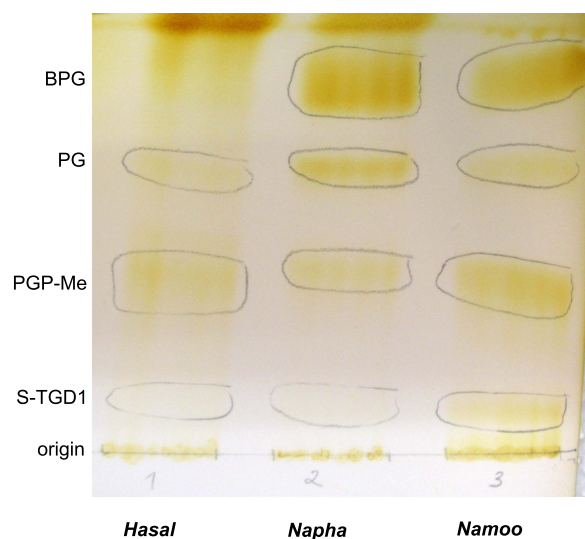


Figure 3.5: Preparative TLC of total lipid extract of *Hbt. salinarum* (Hasal), *Nmn. pharaonis* (Napha) and *Nmn. moolapensis* (Namoo) and stained using iodine vapor. Due to the higher thickness of the TLC plate, lipid bands were less well resolved than on analytical TLC. A partial overlay or mixture of the different groups cannot be avoided in this technique.

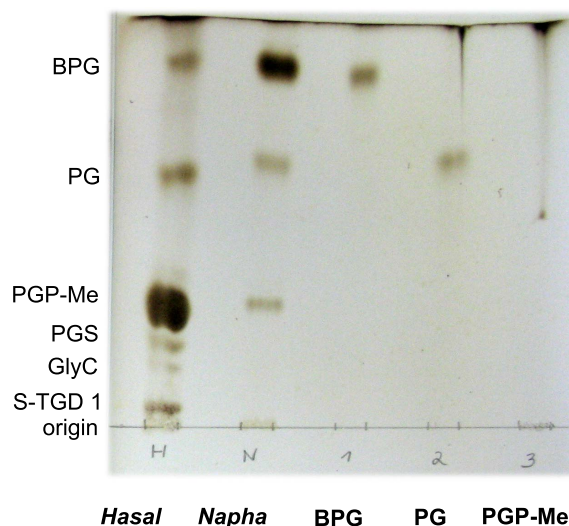


Figure 3.6: TLC plate from recovered lipids of *Nmn. pharaonis* (Napha). Lipids BPG, PG and PGP-Me arose from a preparative TLC of a total lipid extract of *Nmn. pharaonis*. Total lipid extract of *Hbt. salinarum* (Hasal) was applied as an internal standard.

Table 3.2: ESI-MS (negative mode) ion peaks.

Lipid	observed signals ( $m/z$ )						calculated mass		
	<i>Hasal</i>		<i>Napha</i>		<i>Namoo</i>		$C_{20}-C_{20}$	$C_{20}-C_{25}$	$C_{25}-C_{25}$
	$[M - H]^-$	$[M - H]^{2-}$	$[M - H]^-$	$[M - H]^{2-}$	$[M - H]^-$	$[M - H]^{2-}$			
PA	-	-	-	-	731.66	-	731.6	801.7	871.8
BPG	-	-	-	759.65	1520.39	759.65	1521.3	1591.4	1661.5
PG	805.69	-	805.68	-	805.70	-	806.7	876.8	946.9
PGS	-	-	875.77	-	-	-	-	-	-
PGP-Me	-	442.32	-	-	-	442.31	886.6	956.7	1026.8
	899.68	449.32	899.68	449.32	899.68	449.32	900.7	970.7	1040.8
	-	484.37	-	484.37	-	484.36	-	-	-
GlyC	-	-	-	-	-	-	1933.4	2003.5	2073.6
S-TGD-1	1217.83	-	-	-	-	-	1218.8	1288.9	1359.0
Unknown signals	-	-	-	481.34	-	481.34	-	-	-
	489.29	-	489.29	-	489.29	-	-	-	-
	-	-	-	-	-	523.34	-	-	-
	529.48	-	529.48	-	529.47	-	-	-	-
	-	-	-	-	-	555.40	-	-	-
	-	910.67	-	-	-	910.65	-	-	-
	921.67	-	-	-	921.67	-	-	-	-
	967.75	-	967.75	-	967.75	-	-	-	-
	969.76	-	969.76	-	969.76	-	-	-	-
	-	-	-	-	-	1220.94	-	-	-
	-	-	-	-	-	1254.10	-	-	-
	-	-	-	-	1542.42	-	-	-	-
	-	-	1654.53	-	-	-	-	-	-
	-	-	1660.57	-	-	-	-	-	-
	1809.90	-	-	-	-	-	-	-	-
	1844.48	-	-	-	-	-	-	-	-
	1866.47	-	-	-	-	-	-	-	-

Signals from total lipid extracts of *Hbt. salinarum* (Hasal), *Nmn. pharaonis* (Napha) and *Nmn. mooolapensis* (Namoo).



lipids GlyC and BPG (Corcelli *et al.*, 2000). Surprisingly, a peak for PGP-Me with C<sub>20</sub>-C<sub>25</sub> alkyl chains was identified in the mass spectra of all three organisms. Lipids with C<sub>25</sub>-C<sub>25</sub> alkyl chains were not detected.

In *Nmn. pharaonis*, BPG, PG as well as PG-Me were detected.

In *Nmn. moolapensis*, the same lipids as in *Hbt. salinarum* could be detected and, additionally, a peak for the intermediate phosphatidic acid (PA, 731.66) appeared in the spectrum. This is a precursor of most lipids, but not visible as a single band on a TLC plate due to its mobility ( $R_f$  0.99), which is the same as the neutral lipids (Moldoveanu & Kates, 1988). No other C<sub>20</sub>-C<sub>25</sub> chain, besides the one in PGP-Me, in *Nmn. moolapensis* was found. No lipids with C<sub>25</sub>-C<sub>25</sub> alkyl chains were measured.

According to the lipid identification in *Nmn. moolapensis* by TLC, a peak in the MS spectrum for a glycolipid was expected. On TLC it possessed a similar  $R_f$  to S-TGD-1 in *Hbt. salinarum* but more than half of the detected ions in the MS spectrum could not be allotted to a known lipid. This could be due to impurities that were coupled to the hydrophobic part during lipid extraction or indicate novel structures. Among the unknown signals in the MS spectrum, no peak for a *Nmn. moolapensis*-specific glycolipid was found. Therefore, MS/MS spectra were required to scan unknown mass peaks and characterize unknown lipid structure which was performed in section 3.2.1.2.

The satellites which were detected additionally to main peaks in the MS spectra of *Nmn. pharaonis* and *Nmn. moolapensis* might correspond to unsaturated isoprenoids. These are precursors of diphytanyl diether lipids, as even mass differences were observed or still unknown unsaturated lipid species. The latter is consistent with findings of H. Patzelt (Muscat, Oman) and his colleagues, who showed that unsaturated ether lipids are far more common in the halophilic Archaea than generally assumed (Ma *et al.*, 2010). He also revealed that isolates of *Haloarcula* spp. and *Haloferax* sp. obtained from a potash mine crystallization pond in North Germany had unsaturated ether lipids up to 37% of the total membrane lipid content. Whether species from the *Natronomonas* genus have a similar high amount of unsaturated ether lipids has to be determined in future.

In the MS spectrum of *Hbt. salinarum* no peaks for the lipids GlyC and BPG were found. Moreover, they appeared as the two weakest bands on the TLC plate (Fig-

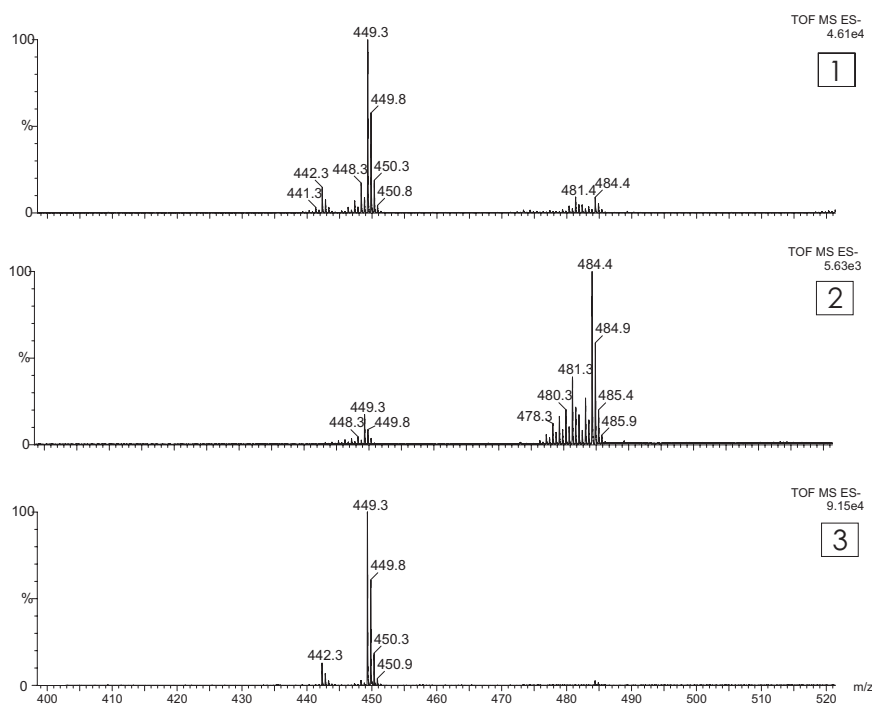


Figure 3.7: **Comparison of MS spectra of striking PGP-Me C<sub>20</sub>-C<sub>25</sub> between halophilic archaea.** MS spectra of total lipid extracts from (1) *Nmn. moolapensis*, (2) *Nmn. pharaonis* and (3) *Hbt. salinarum* show the different ratios between the peaks 449.3 and 484.4 corresponding to the C<sub>20</sub>-C<sub>20</sub> and C<sub>20</sub>-C<sub>25</sub> attached isoprenoids.

ure 3.4). One explanation could be that GlyC and BPG are produced during lipid extraction procedure and generated by transesterification, which was shown by Renner *et al.* (2005). In contrast, Corcelli (2009) presents results on the possible function of GlyC and BPG in halophilic archaea as bioactive lipids, e.g. involvement of BPG in respiratory chain complexes. Corcelli explains that due to the dimeric structure of BPG, it can build ions with a molecular mass of 731.7 and 805.9 after fragmentation which correspond to PA and PG. This fragmentation of BPG into smaller fragments would also explain the lack of the monocharged molecular ion  $[M - H]^-$  at  $m/z$  1521.3 and a bischarged molecular ion  $[M - H]^{2-}$  at  $m/z$  760 in most ESI-MS spectra.

Regarding the literature about lipid research in haloarchaea, *Hbt. salinarum* is not able to synthesize C<sub>25</sub> alkyl chains (Kamekura & Kates, 1999). The corresponding peak (PGP-Me, 484.4 amu) in *Hbt. salinarum* (spectrum 3 in Figure 3.7) was very

weak in comparison to the other spectra. It was already shown in 1982 by de Rosa and colleagues (Rosa *et al.*, 1982) that only *Nmn. pharaonis* is able to synthesize C<sub>25</sub> isoprenoids within the Euryarchaeota.

Clearly recognizable in the spectrum of *Nmn. pharaonis* is that the predominant form of PGP-Me is the lipid with the mixed alkyl chains (C<sub>20</sub>-C<sub>25</sub>).

The spectrum of *Nmn. moolapensis* shows a higher signal for PGP-Me C<sub>20</sub>-C<sub>25</sub> in comparison to the signal for PGP-Me C<sub>20</sub>-C<sub>20</sub> (ratio between the peaks 449.3 and 484.4) than in the spectrum of *Hbt. salinarum*, but not as intense as it could be detected in *Nmn. pharaonis*.

A repetition of the measurement in this study from independently grown cells and separately extracted lipids was performed maintaining the same result. Hence, a contamination of the sample of the GC column could be excluded.

It was already mentioned before that farnesylgeranyl diphosphate synthase (FGPPS, EC 2.5.1.-) could be only detected in *Nmn. pharaonis* (Rosa *et al.*, 1982) and *Aeropyrum pernix* (Morii *et al.*, 1999). We now argue that the corresponding enzyme, FGPPS, is not obligatory for chain-elongation from C<sub>20</sub> to C<sub>25</sub>. Due to a lower substrate specificity small amounts of C<sub>25</sub> chains can also be synthesized by the geranylgeranyl diphosphate synthase (GGPPS, EC 2.5.1.29) in species which do not contain the FGPPS as does *Nmn. pharaonis*.

It might be also that GGPPS of *Nmn. moolapensis* binds the substrates more un-specifically than the enzyme in *Hbt. salinarum*. The substrate specificity of the enzyme routinely escapes annotation.

These small amounts presumably escaped detection due to lower sensitivity of the instruments used formerly. In this study samples were measured by a Q-TOF mass spectrometer which allows precise analysis due to its high resolution.

Apart from the comparable small peak for PGP-Me C<sub>20</sub>-C<sub>25</sub>, no other lipids with C<sub>25</sub> isoprenoids were detected. This would fit with the character of a typical non-alkaliphilic halophile.

In none of the organisms, C<sub>25</sub>-C<sub>25</sub> diether lipids could be identified. They were encountered as a minor component in some halophiles (Rosa *et al.*, 1982, 1983) and Tindall (1985) could show that the amount of C<sub>25</sub>-C<sub>25</sub> lipids was below 1% in haloalkaliphilic archaea. The present results of measured lipids are consistent with the observations of Tindall (1985). The mass ratios of C<sub>20</sub>-C<sub>20</sub> and C<sub>20</sub>-C<sub>25</sub>, and PG and

PGP-Me depend somewhat on the growth conditions. Increasing the salinity of the medium leads to increase the proportion of C<sub>20</sub>-C<sub>25</sub> (Morth & Tindall, 1985).

**Analysis of MS/MS fragments in *Nmn. moolapensis* revealed a new structure for an unknown glycolipid** MS/MS spectra of the main lipids in *Nmn. pharaonis* and *Hbt. salinarum* were recorded. The peaks used for fragmentation were in *Hbt. salinarum*: the singly and the doubly charged ion of PGP-Me, the doubly charged ion of PGS, the singly charged ion of PG and the singly charged ion of S-TGD-1. In addition, in *Nmn. pharaonis* the doubly charged ion of PGP-Me with a C<sub>20</sub> and a C<sub>25</sub> isoprenoid was characterized. For the interpretation of the MS/MS fragments of unknown peaks in the MS spectrum of *Nmn. moolapensis*, a catalogue of possible mass fragments was created and can be seen in Figure S2. By analyzing the mass fragments in MS/MS spectra of already known lipids of *Nmn. pharaonis* and *Hbt. salinarum* specific masses of each fragment were calculated (using the program MDL Isis Draw). This showed that the calculated masses coincide with the measured peaks of an accuracy of 0.05 amu. Since this evidences that the method was very reliable, the proposed structures of the fragments could be used and combined for suggestions of unknown lipid structures in *Nmn. moolapensis*.

The scope of the following MS/MS analysis was to scan unknown mass peaks for the uncharacterized glycolipid in *Nmn. moolapensis*. In Figure 3.8 mass peaks which can be potential candidates for the uncharacterized glycolipid are marked in blue. There are still unknown peaks in the spectrum which are marked in green. The structure of unmarked mass peaks could be already determined in MS spectra and are listed in Table 3.2. MS/MS spectra were taken on the suspicious mass peaks and structures of the fragments could be suggested.

For one mass peak (523 amu, doubly charged), which was exclusively appearing in *Nmn. moolapensis* lipid extracts, a new glycolipid structure was proposed. In Figure 3.9 the suggested structure is depicted and all fragments fit well the observed masses. Also a tetra-hydroxy form of the new glycolipid might exist, which is illustrated in Figure S3. A proposal of the other structures belonging to an unknown peak in a MS spectrum is also given in Figure S3. Since the structure could be only constructed regarding the molecular masses of the ions measured by ESI-MS and fragmentation by MS/MS, it remains unclear which form of sugar is attached to the

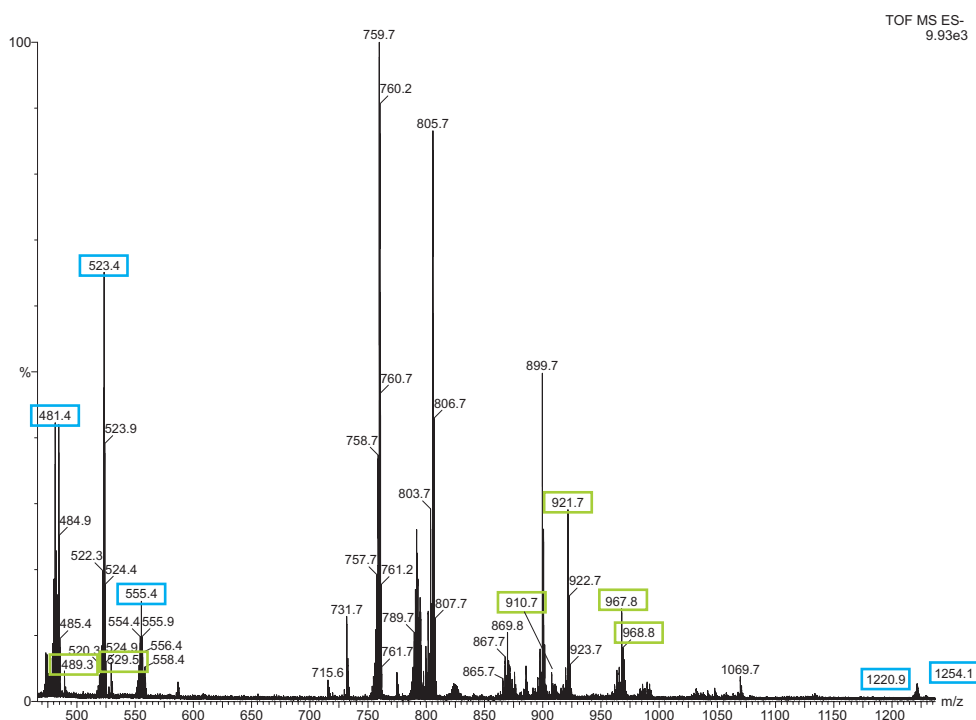


Figure 3.8: MS spectrum of total lipid extract of *Nmn. moolapensis*. For mass peaks marked in blue boxes structures could be proposed. The green mark shows still unclear peaks. Unmarked peaks were already identified during ESI-MS measurements and are listed in Table 3.2.

glycolipid.

In comparison to the glycolipid S-TGD-1 in *Hbt. salinarum*, which has a molecular mass of 1217.8 and three attached sugars (glucose, mannose and galactose), the new glycolipid in *Nmn. moolapensis* has a smaller mass of 1046.7 amu. Therefore it is assumed that it might possess only one sugar. Theoretically, the head group of the unknown glycolipid can be any of a variety of possible sugar compounds (glucose, mannose, galactose, gulose, N-acetylglucosamine, or combinations thereof) (Boucher, 2007).

Other differences between the structure of S-TGD-1 in *Hbt. salinarum* and the proposed lipid structure of the new glycolipid in *Nmn. moolapensis* are the detected phosphate and sulphate group in the newly discovered lipid.

### 3 Lipid metabolism in halophilic Archaea

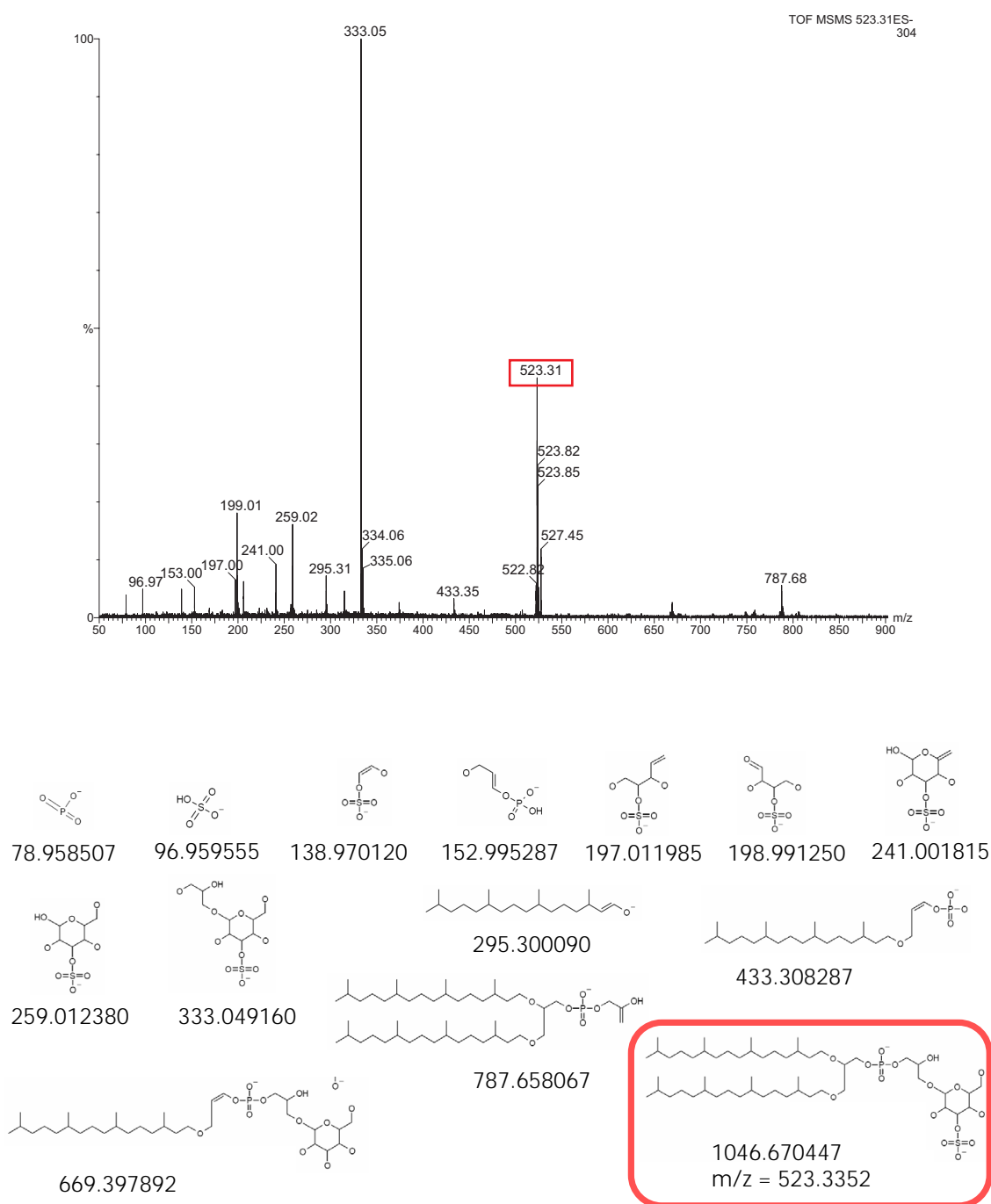


Figure 3.9: **MS/MS spectrum of a new glycolipid in *Nmn. moolapensis*.** Peak 523 of a MS spectrum of lipid extract from *Nmn. moolapensis* was analyzed applying MS/MS. Yielded fragments are displayed beneath the spectrum and the proposed structure of the lipid is highlighted with a red box.

Glycolipids of halophilic archaea are generally multifarious and the biosynthesis of them is not understood at all (Morii & Koga, 2003; Koga & Morii, 2007). In general it is known that in extreme halophiles an unknown glycolipid precursor is stepwise glycosylated with glucose, mannose and galactose followed by sulfation with 3-phosphoadenosine-5-phosphosulfate (PAPS). In this study structures of lipids were identified by analyzing MS peaks and comparing them to results in literature. If no structure could be determined, MS/MS spectra were recorded of unknown peaks and a structure for each fragment could be proposed. Applying MS and MS/MS to a lipid sample cannot solve the structure of the attached sugar moiety, because only the molecular mass of a fragment can be calculated and a possible structure proposed. Only the carbon skeleton of the respective sugar can be determined. Therefore for the unknown lipid in *Nmn. moolapensis* it could be proposed that a hexose is attached to the lipid. Whether this hexose is a glucose, which might be assumed intuitively, because the biosynthesis pathway for S-TGD-1 in *Hbt. salinarum* starts with attaching this sugar, can be only speculated about.

Identification of the sugar component in the unknown glycolipid is only possible by applying NMR. This would imply in the next step of this technique that the lipid has either to be in a pure quality or in such a high concentration that the significant peaks superimpose signals from other lipids.

The proposed structure for the unknown glycolipid of *Nmn. moolapensis* showed a phosphate group which was not expected in a glycolipid. The known lipids in *Hbt. salinarum* as well as *Nmn. pharaonis* either include a phosphate or sugar group, but not both moieties in one molecule. In haloarchaea, biosynthesis of phosphoglycolipids is not known but was detected in methanogenes (Kates, 1993a). *Thermoplasma acidophilum*, for example, is able to synthesize at least eight different species of phosphoglycolipids (Uda *et al.*, 1999, 2000; Shimada *et al.*, 2002). So it is not unthinkable that a similar pathway exists in haloarchaea enabling them to synthesize phosphoglycolipids.

The presence and structure of glycolipids have implications for the stability of bacteriorhodopsin, as the trimeric arrangement of this protein in the purple membrane of *Hbt. salinarum* is stabilized by glycolipids (Renner *et al.*, 2005). To what extent the different structure of the new glycolipid influences the stabilization and hence the function of a BR protein is an exciting question which is further discussed in

subsubsection 6.2.2.2.

The structure of this unusual sulphated phosphoglycolipid in *Nmn. moolapensis* has to be verified and analyzed in more detail by NMR measurements in future.

## 3.2.2 Stable isotope labeling of isoprenoid chains

### 3.2.2.1 Assignment of all carbons from the isoprenoid chain by natural abundance $^{13}\text{C}$ NMR

Before starting with  $^{13}\text{C}$  labeled lipids, NMR measurements with unlabeled samples were performed to annotate each carbon of the isoprenoid and compare the results to the literature. Different NMR techniques were tested and finally the procedure and parameters providing results with the highest quality chosen for further measurements.

About 71 mg of dried lipids were extracted according to Bligh and Dyer (Bligh & Dyer, 1959) from a 5 l culture of *Nmn. pharaonis* that had been grown to stationary phase in minimal medium containing  $^{12}\text{C}$  sodium acetate as the only organic carbon source. The lipids were further fractionated with acetone yielding about 50 mg of polar lipids.

NMR spectra were taken of 2 mg aliquot dissolved in 200  $\mu\text{l}$  *d*<sub>4</sub>-MeOD and 500  $\mu\text{l}$  *d*-CDCl<sub>3</sub>. Tetramethylsilane (TMS) was used as an internal standard for calibrating the chemical shift for  $^1\text{H}$  and  $^{13}\text{C}$  spectroscopy.

Identification of the signals was based on published data on the lipids of methanogenic or other halophilic archaea (Degani *et al.*, 1980; Rosa *et al.*, 1977, 1982; Ekiel *et al.*, 1983).

First, a 1D  $^{13}\text{C}$  NMR spectrum (decoupled on  $^1\text{H}$ , on-resonance) was recorded and chemical shifts of the carbons were found to be consistent with those from literature (Ekiel *et al.*, 1983). Proton spin decoupling has the effect that a series of singlets is produced, one for each different carbon environment, and J-couplings between carbon and hydrogen are suppressed (removing signal splitting). Carbon numbers 1, 2 and 3, which are closest to the polar headgroup (Figure 3.10), were in a rigid situation similar to a solid and therefore harder to determine, while the tail of the lipid (C<sub>4</sub> to C<sub>20</sub>) could move freely and gave a stronger signal in the NMR in Figure 3.11. Diether lipids are composed of two different side chains, (C<sub>20</sub> and C<sub>25</sub>), but the additional carbon



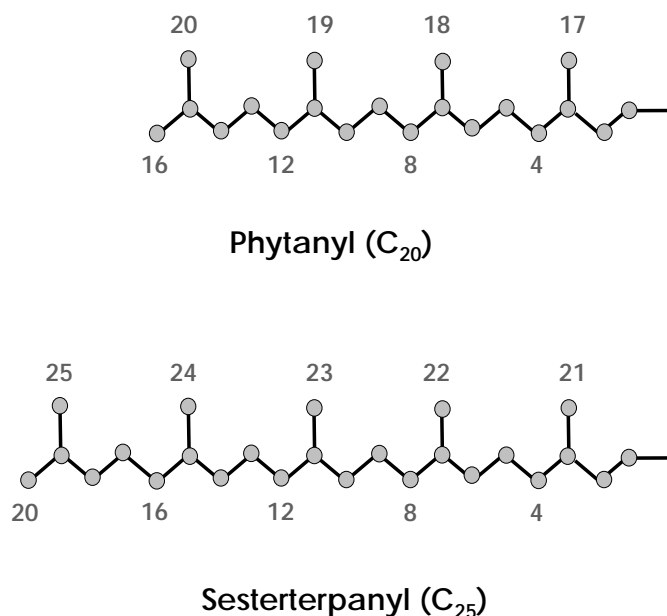


Figure 3.10: **Structures of isoprenoid chains in *Nmn. pharaonis*** All polar membrane lipids of *Nmn. pharaonis* are derivatives of C<sub>20</sub>C<sub>20</sub>, C<sub>20</sub>C<sub>25</sub> or C<sub>25</sub>C<sub>25</sub> diphytanyl glycerol diether (Rosa & Gambacorta, 1988). Therefore, the NMR spectra should contain two sets of signals for two types of lipid chains, assuming only a small influence of the head group on chemical shifts of the phytanyl chains. The signals are produced with respect to the chemical environment of a carbon. Therefore, no difference between signals of chain C<sub>20</sub> and C<sub>25</sub> can be detected.

atoms in the C<sub>25</sub> chain are chemically equivalent to the carbons in the C<sub>20</sub> chain (with respect to attached hydrogens, surrounding spins of <sup>1</sup>H and position in the chain). Therefore, no additional peaks were measured in the 1D <sup>13</sup>C NMR spectrum.

For confirmation of the assignment of the carbon atom, a distortionless enhancement by polarization transfer experiment (<sup>13</sup>C-dept 135) was performed (Figure 3.11). This experiment gives positive signals for all CH and methyl groups in the molecule while CH<sub>2</sub> carbon atoms produce negative signals. Quaternary carbon atoms give no signals at all. The combination of the <sup>13</sup>C-dept 135 and the normal <sup>13</sup>C spectrum were used to determine the number of hydrogen atoms attached to the carbon atom producing each signal in the spectrum. The interpretation of the chemical shifts in the <sup>13</sup>C-dept 135 confirm the assignment of the C<sub>25</sub> chain. In Table 3.3 all chemical shifts of solvents and carbons are listed. For clarity, only carbons of the C<sub>20</sub> chain are mentioned in the

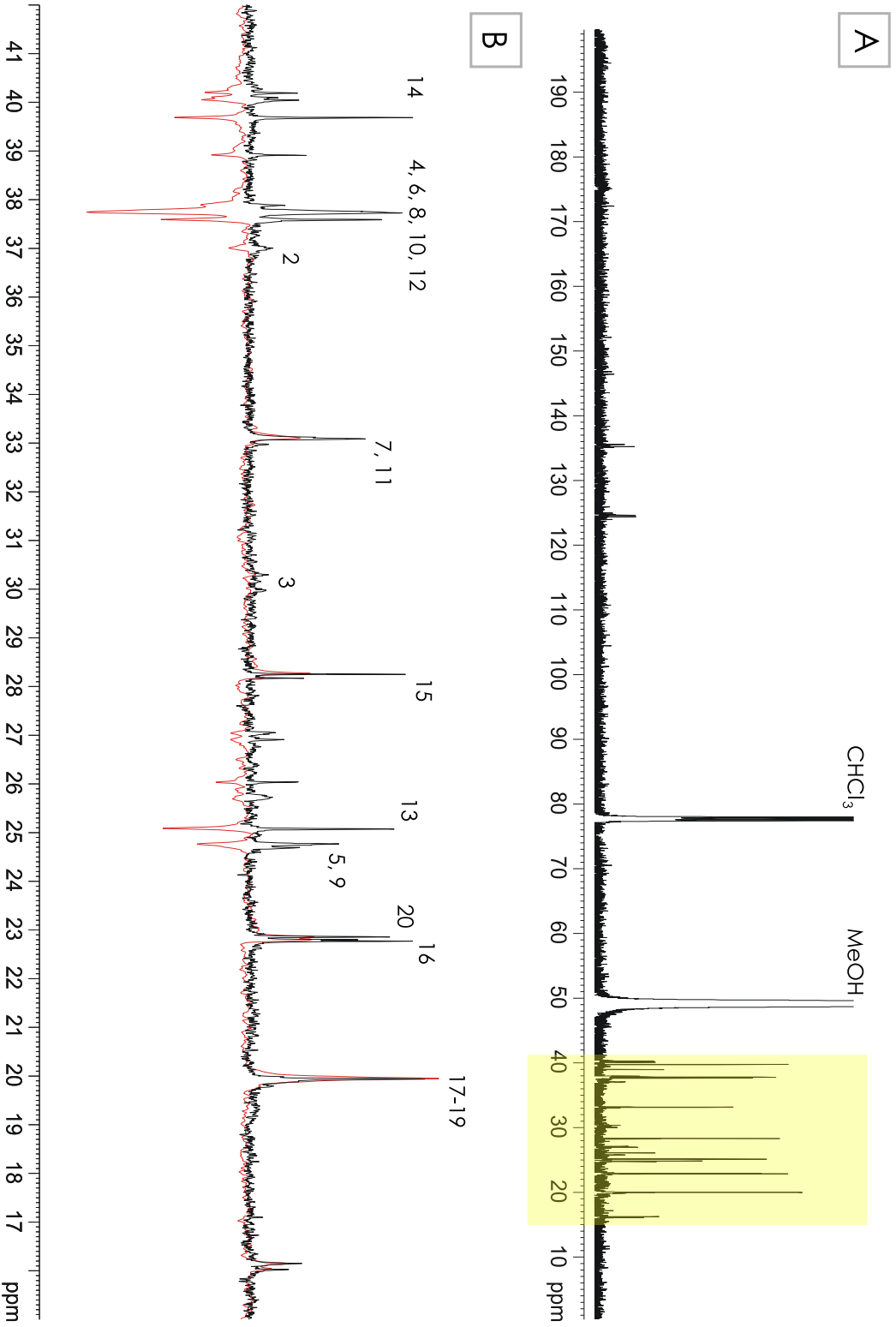


Figure 3.11: **Natural abundance  $^{13}\text{C}$  NMR spectra of extracted lipids of *Nmn. pharaonis*, grown in minimal medium with  $^{12}\text{C}$  acetate. A** 1D  $^{13}\text{C}$  NMR spectrum. **B** Comparison of the region from 42 ppm to 15 ppm (yellow box in A) of the same experiment (in black) with a  $^{13}\text{C}$ -dept-135 experiment (in red). It showed that  $\text{CH}_3$  and  $\text{CH}$  appeared as positive peaks,  $\text{CH}_2$  as negative peaks and C with no H bonded gave no peaks.

Table 3.3: Chemical shifts of carbons in solvents and isoprenoid chains of *Nmn. pharaonis* measured against the internal reference TMS.

Chemical shift (ppm)	C <sub>20</sub> carbon N: 20	C <sub>25</sub> carbon N: 25
19.8-20.0	17-19	21-24
22.8	16	20
22.9	20	25
24.8-24.9	5, 9	5, 9, 13
25.2	13	17
28.5	15	19
30.0, 30.3	3	3
33.3	7, 11	7, 11, 15
36.9-37.2	2	2
37.4-37.7	4, 6, 8, 10, 12	4, 6, 8, 10, 12, 14, 16
39.8	14	18
70.2	1	1

Chemical shifts of solvents that were used (CDCl<sub>3</sub>/CD<sub>3</sub>OD, 5:2, v:v): 49.0 ppm for *d*<sub>4</sub>-MeOD and 77.0 ppm for *d*-CDCl<sub>3</sub>.

following NMR measurements.

A second method, 2D {<sup>1</sup>H, <sup>13</sup>C}-Fast Heteronuclear Single Quantum Coherence (FHSQC) (Sklenar *et al.*, 1993), was then applied, because it is more sensitive and requires a lower sample concentration. Applying FHSQC to the lipids was feasible, since all carbons of interest were connected to at least one hydrogen. A {<sup>1</sup>H, <sup>13</sup>C}-FHSQC spectrum was then determined by measuring the natural abundance of <sup>13</sup>C (1.1%) from 2 mg of the same sample (Figure 3.12).

Together with published data from Ekiel and co-workers (Ekiel *et al.*, 1983), it was possible to assign all the carbons from the chains. In addition to a higher resolution, FHSQC requires a much lower lipid extract concentration, which makes a series of <sup>13</sup>C labeling experiments financially feasible. Furthermore, FHSQC allows quantification of signals by peak integration, which leads to a better comparability of results between different samples. Due to the considerable advantages over 1D NMR techniques, <sup>13</sup>C labeling experiments described in the next sections were analyzed with it.

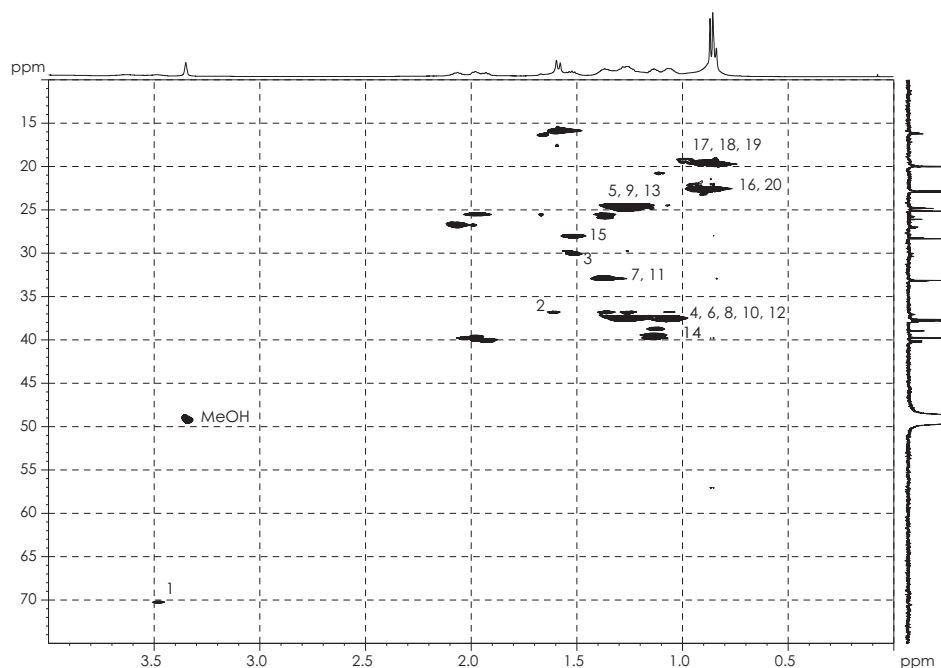


Figure 3.12:  $\{^1\text{H}, ^{13}\text{C}\}$ -FHSQC NMR spectrum of extracted unlabeled lipids of *Nmn. pharaonis*. Signals for all carbons, indicated by numbers, in the isoprenoid chain could be detected. The spectrum also showed that 2 mg of a purified dry lipid extract is sufficient for measuring significant peaks in natural abundance  $^{13}\text{C}$  spectra.

### 3.2.2.2 $^{13}\text{C}$ NMR spectra resulting from differently labeled carbon sources

*Nmn. pharaonis* was fed with different species of  $^{13}\text{C}$  labeled acetate ( $\text{U-}^{13}\text{C}$  acetate,  $1\text{-}^{13}\text{C}$  acetate and  $2\text{-}^{13}\text{C}$  acetate) in order to analyze the incorporation of  $^{13}\text{C}$  into the carbon structure of the lipid.

All  $^{13}\text{C}$  labeling experiments were performed with lipids extracted from 350 ml cultures of cells harvested at stationary phase. Some initial experiments were undertaken with labeled material from 35 ml cultures, but the intensity of NMR signals were too weak (data not shown). Lipid yields varied with growth conditions and media compositions. During extraction and purification procedure also different amounts of lipids could be obtained showing expected technical fluctuations. An overview of the different experimental steps during metabolic labeling of isoprenoids and amino acids is

shown in Figure 3.13. Distribution of the labels in amino acids is presented in detail in subsection 4.2.1.

**Labeling with U- $^{13}\text{C}$  acetate yielded uniformly labeled isoprenoids** Cells were grown in minimal medium containing 20 mM U- $^{13}\text{C}_2$  acetate as the only organic carbon source. Since  $^{13}\text{C}$  labeled substances are comparably expensive, different methodical approaches were tested to minimize culture volume and save costs, while still achieving adequate labeling.

First, a  $^{13}\text{C}$  BB (broadband) spectrum, decoupled on  $^1\text{H}$  was recorded (Figure 3.14). All C-H coupling was suppressed and all split signals of  $^{12}\text{C}$  became singlets similar to the 1D spectra. In this approach, the signal intensity increases while less time is required to obtain a spectrum. As far as sensitivity of the signal is concerned, no differences could be noticed in comparison with the 1D carbon spectrum. Another approach was the employment of two-dimensional NMR to increase sensitivity of the signals. In this method, the interaction of nuclear spins ( $^1\text{H}$  with  $^1\text{H}$ ,  $^1\text{H}$  with  $^{13}\text{C}$ ) are plotted in two dimensions.

A 2D proton-COSY experiment (Figure S4) was performed on a fully labeled sample, which showed scalar couplings between the two nuclei through four signals positioned in a square. The diagonal with all its signals corresponded to the 1D-H-NMR spectrum. Since the aim was to use  $^{13}\text{C}$  labeling, this experiment only proved the sensitivity in comparison to results from a 1D spectrum. H-NMR spectroscopy is the most sensitive method indeed, but is an attractive approach only for smaller non-enriched metabolites.

Using the inverse recording method of Fast Heteronuclear Single Quantum Coherence (FHSQC) only signals of protons directly bound to C atoms appear. Enhancement of the signal to noise ratio is reached by the use of this technique, in which the chemical shift of  $^{13}\text{C}$  is correlated via the large one-bond coupling constant  $^1J_{\text{CH}}$  to the  $^1\text{H}$  chemical shift of the directly bound proton. In Figure 3.16 all carbons were visible at the same chemical shifts of the natural abundance  $^{13}\text{C}$  spectrum (Figure 3.12).

Another advantage of the 2D spectrum, in addition to the high sensitivity, is the possibility to determine and compare the signals in a quantitative way, by integrating the peak area (section 2.5.8.1). This was done for every 2D spectrum and the integrated peaks were compared to the values of the unlabeled natural abundance  $^{13}\text{C}$  spectrum.

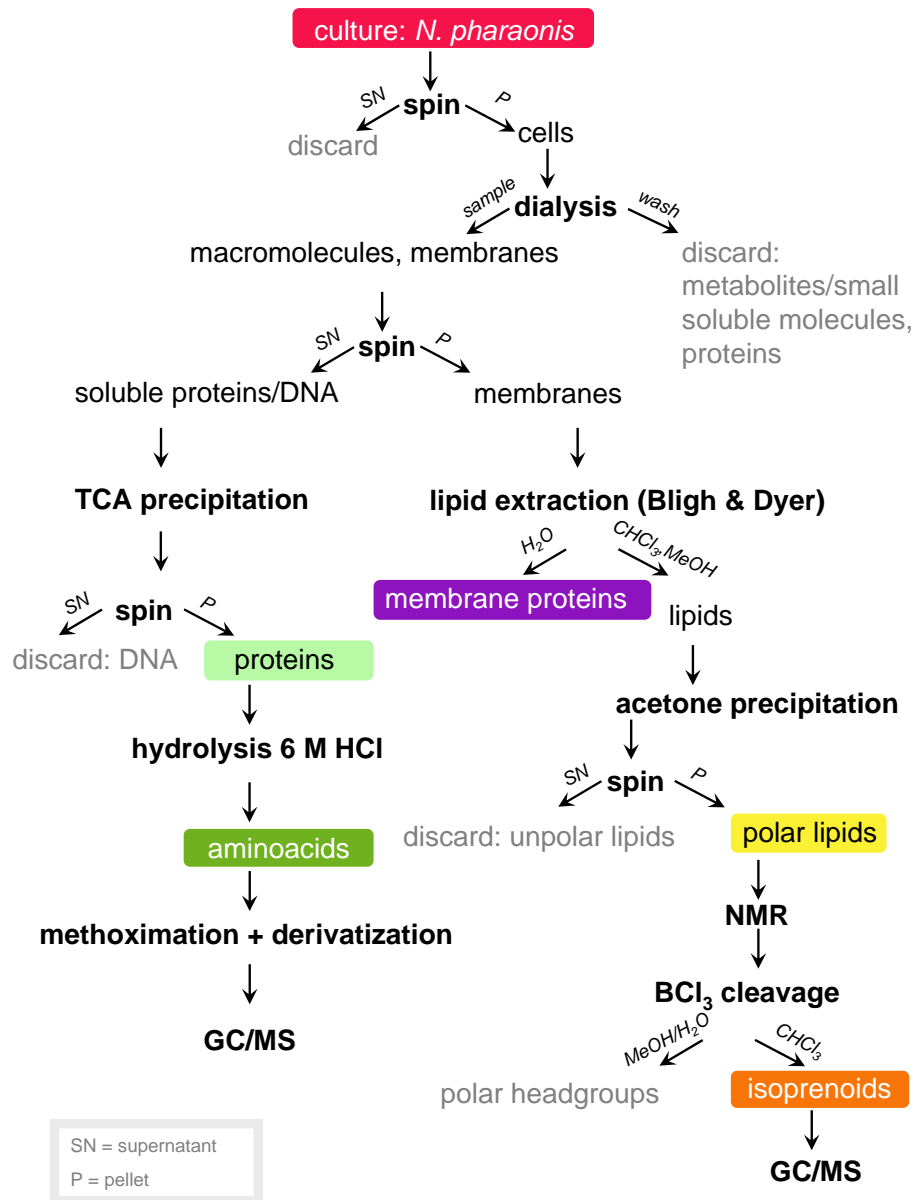


Figure 3.13: Workflow of  $^{13}\text{C}$  labeling experiments in *Nmn. pharaonis*. Introduction of the label into the organism and tracking it to different molecules by extraction of amino acids, lipids and isoprenoids is shown.

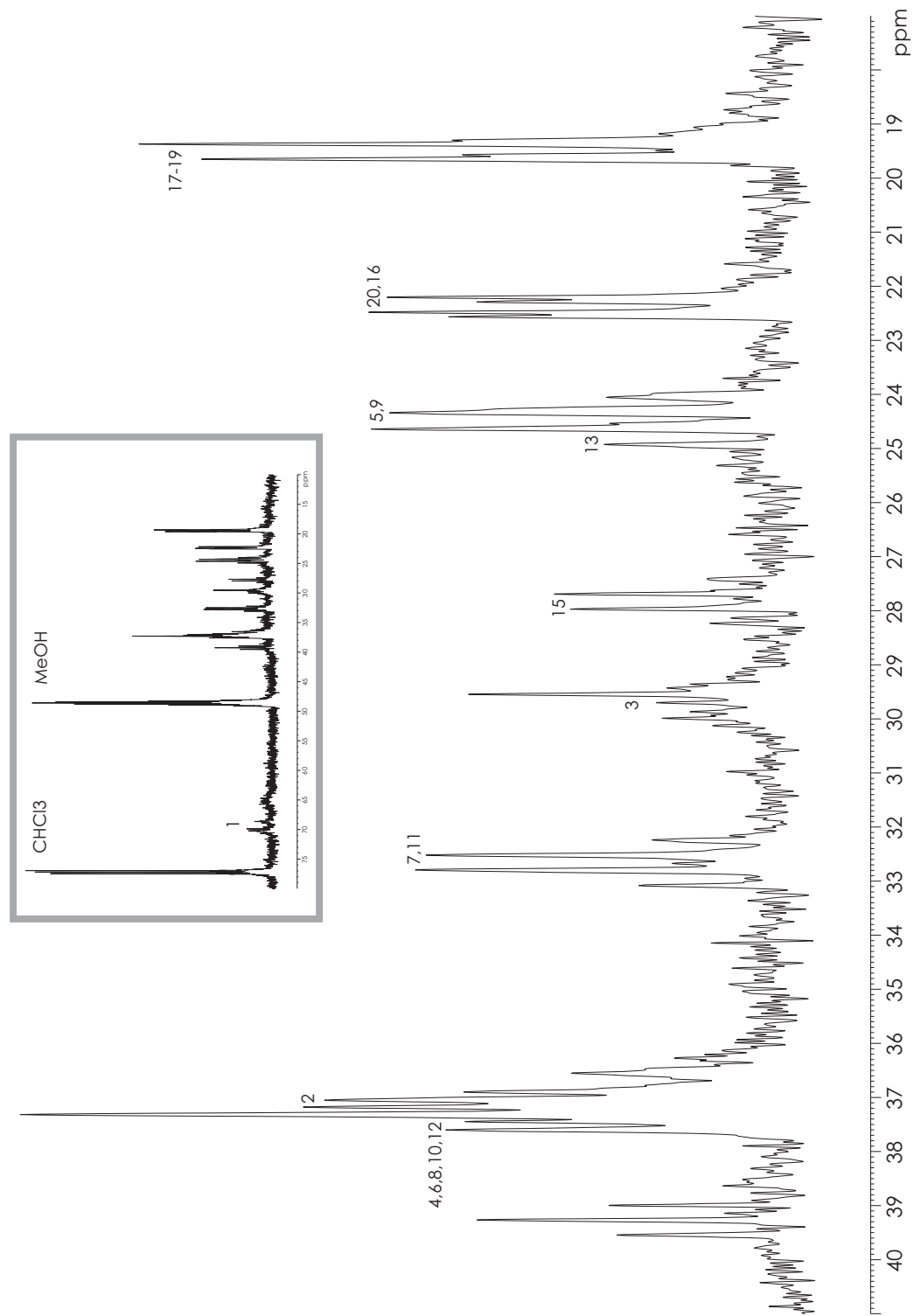


Figure 3.14: **Broadband  $^1\text{H}$  decoupled  $^{13}\text{C}$  NMR spectrum of fully labeled lipids extracted of *Nmn. pharaonis*** Cells were fed with 20 mM U- $^{13}\text{C}_2$  acetate. Spin-spin coupling of adjacent  $^{13}\text{C}$  caused the splitting of NMR signals. This implied that every carbon in the isoprenoid chain was labeled by  $^{13}\text{C}$ .

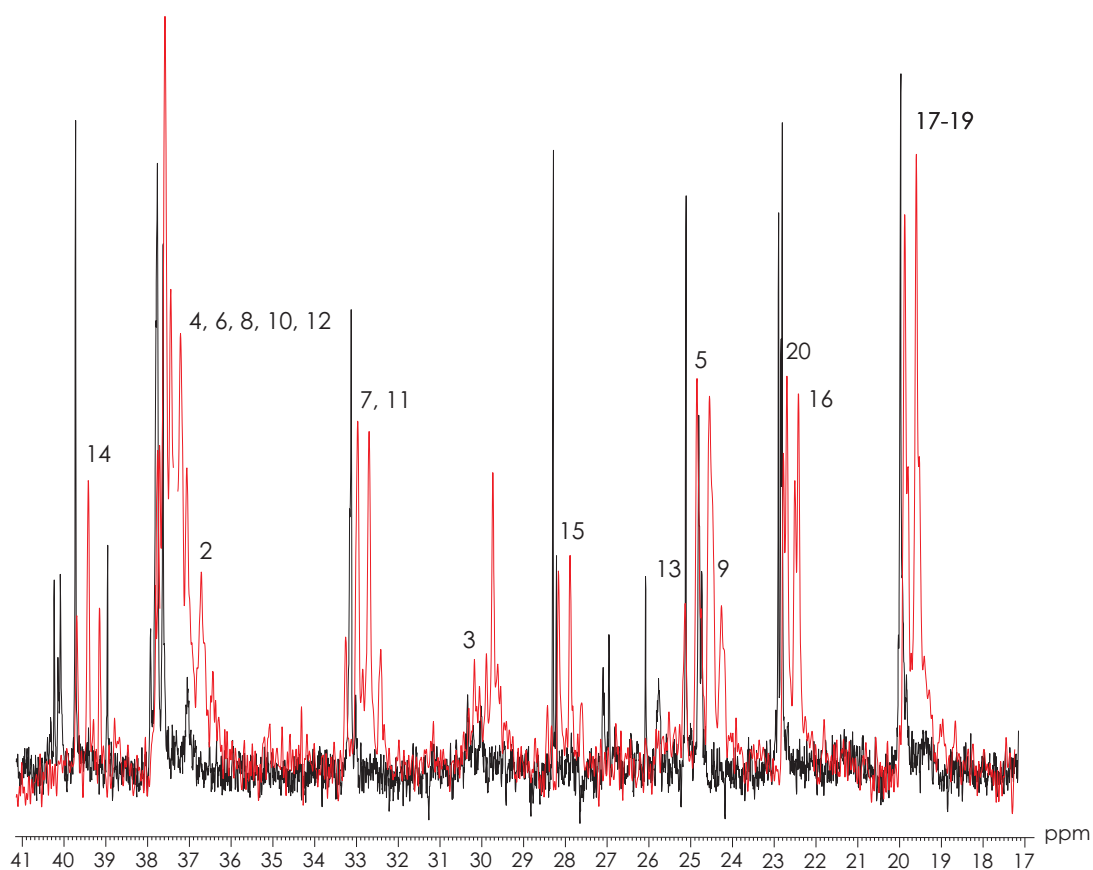
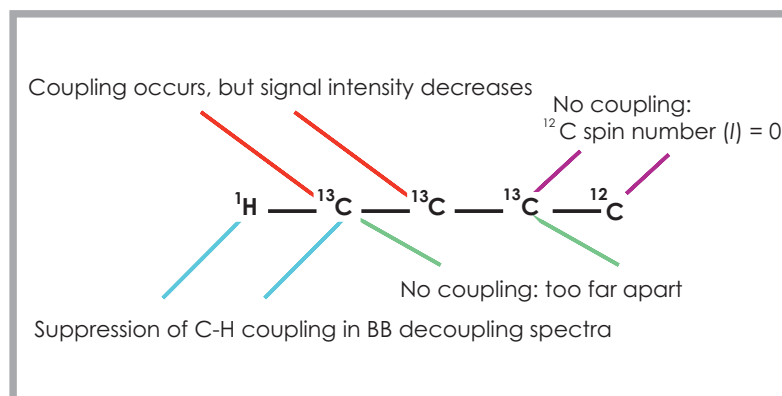


Figure 3.15: **Comparison of a 1D natural abundant  $^{13}\text{C}$  spectrum with a broadband carbon spectrum.** Manual superimposition of a spectrum (black) of unlabeled lipids over a spectrum (red) of lipids with fully  $^{13}\text{C}$  labeled side chains. Grey box above spectra explains that spin-spin coupling and therefore resulting splitting of NMR signals only occurs if two  $^{13}\text{C}$  labeled carbon atoms are adjacent in the alkyl chain.



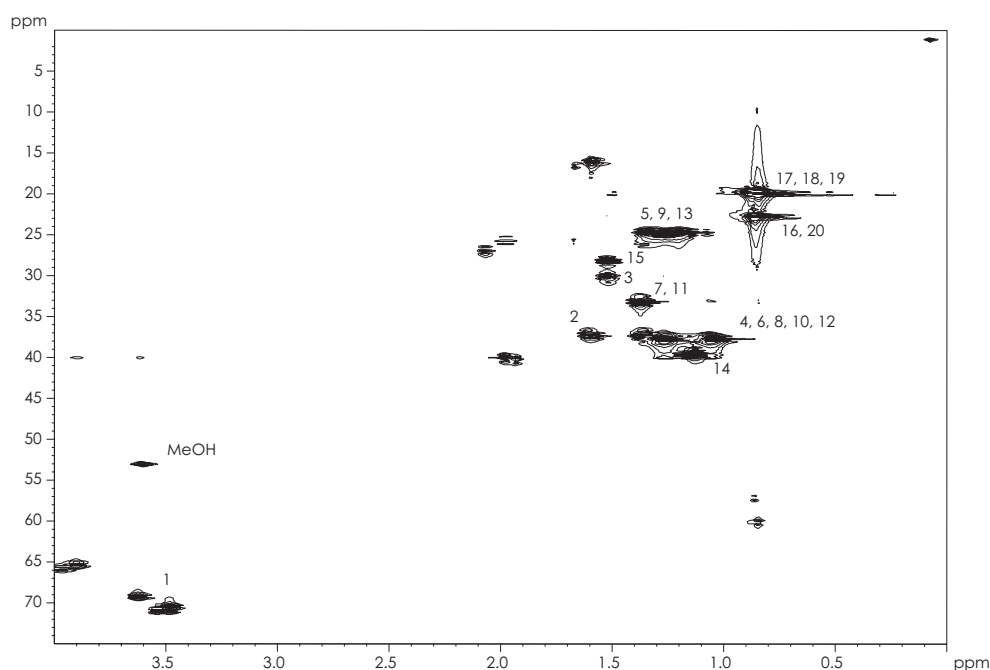


Figure 3.16: **2D FHSQC NMR of extracted  $^{13}\text{C}$  labeled lipids.** Enrichment by  $^{13}\text{C}$  acetate for all carbons in the isoprenoid chain could be determined.

The NMR experiment showed that lipids obtained from the organism grown in the presence of  $^{13}\text{C}$  acetate present a complete labeling with  $^{13}\text{C}$  of the isoprenoid chain. The ratio between the signals of the lipidic chain and the one of the solvent (MeOD used as internal standard) increased significantly. Moreover, these lipids were labeled uniformly, because no significant signal was missing in comparison to the natural abundance  $^{13}\text{C}$  spectrum.

**Introduction of the labels 1- $^{13}\text{C}$  acetate and 2- $^{13}\text{C}$  acetate into *Nmn. pharaonis* indicated a different mevalonate pathway compared to *Hbt. salinarum*** To check if *Nmn. pharaonis* uses the classical mevalonate pathway, enrichment of  $^{13}\text{C}$  by 2D FHSQC was determined in addition to proton decoupled  $^{13}\text{C}$  spectra. Cells were grown in the presence of 20 mM 1- $^{13}\text{C}$  acetate or 2- $^{13}\text{C}$  acetate, respectively. The results were similar to those repeated previously for other archaea (Rosa *et al.*, 1977; Ekiel *et al.*, 1983, 1985). Every second carbon along the lipid chain and branch-methyl

groups were labeled from the methyl group of acetate, and the remaining carbons from the C-1 of acetate (Figure 3.17). It could be also shown that the C-2 unit of acetate is not split during incorporation into the isoprenoid chain. Such labeling is consistent with biosynthesis processing three acetyl-CoA molecules to mevalonic acid as an intermediate of isoprenoids.

This finding contrasts the results from Ekiel and colleagues for *Hbt. salinarum* (Ekiel *et al.*, 1986), who could show in their isoprenoid analysis that only two pairs of carbon atoms of 3-hydroxy-3-methylglutaryl-CoA (HMG-CoA) originate from acetyl-CoA while the central pair of carbon atoms originates from lysine, leucine or serine. Comparing the present experiments of *Nmn. pharaonis* with the spectrum of *Hbt. salinarum*, peaks for carbon numbers 3, 7, 11, 15 [B] and 17, 18, 19 [E] were definitely visible in the 1D as well as in the 2D spectra (Figure 3.17) of *Nmn. pharaonis*, which were absent in the spectrum of *Hbt. salinarum*. In *Nmn. pharaonis*, carbons [B] were delivered from 1-<sup>13</sup>C acetate and carbons [E] from 2-<sup>13</sup>C acetate. Confirmation of the difference in these two organisms was achieved by repeating the experiment with adding <sup>12</sup>C lysine in addition to U-<sup>13</sup>C<sub>2</sub> acetate to the cells of *Nmn. pharaonis*. The results are described below.

**Incorporation of carbons into isoprenoid units originating from U-<sup>13</sup>C acetate or <sup>12</sup>C lysine** To determine if carbons from lysine can be incorporated into the isoprenoid chain, minimal media for *Nmn. pharaonis* were prepared, containing 1,2-<sup>13</sup>C<sub>2</sub> acetate, <sup>12</sup>C sodium carbonate and <sup>12</sup>C lysine. Lysine was added at three different concentrations 5 mM, 10 mM and 30 mM. Carbon atoms from <sup>12</sup>C lysine were incorporated into isoprenoid chains, as shown by the loss of enrichment intensities with increasing concentration of <sup>12</sup>C lysine (Figure 3.18).

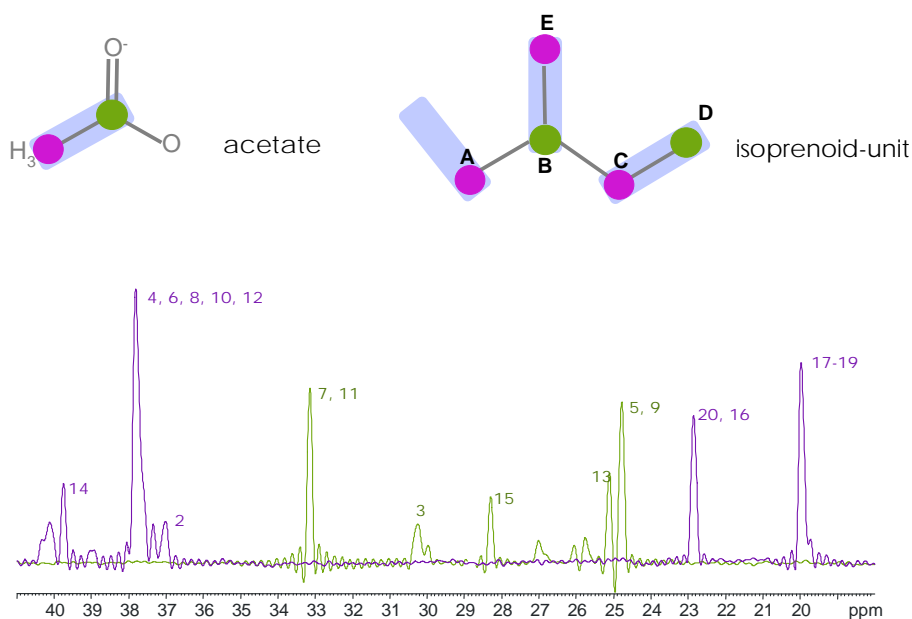
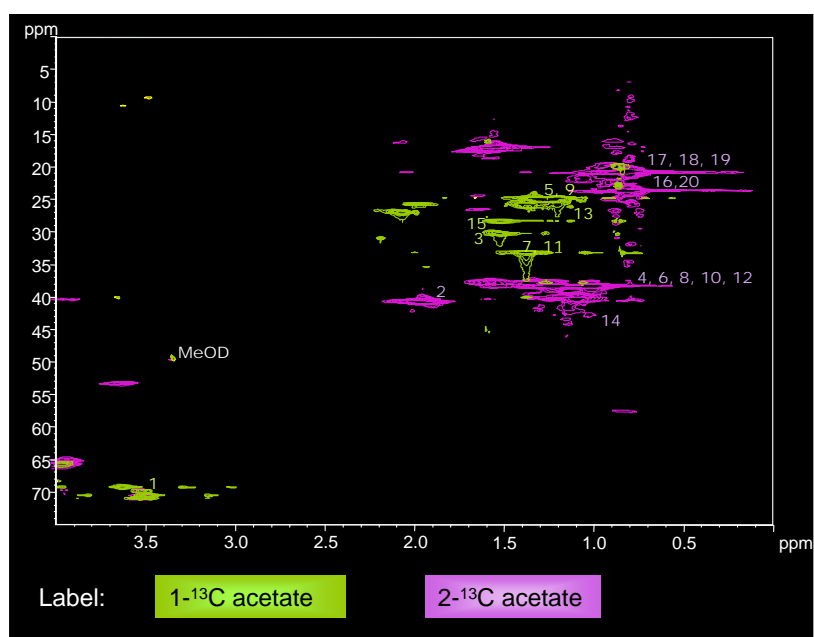


Figure 3.17: Carbon and FHSQC spectra of polar lipids from cells grown in presence of either  $1\text{-}^{13}\text{C}$  or  $2\text{-}^{13}\text{C}$  acetate. The carbons (A-D) of the isoprenoid-unit are labeled according to the IUPAC recommendations for nomenclature of lipids (<http://www.chem.qmul.ac.uk/iupac/lipid/lip1n2.html#112>). The letters of the five-carbon repetitive subunit of phytanyl chains (drawn schematically) correspond to the following signal peaks: [A] = 16, 20; [B] = 3, 7, 11, 15; [C] = 2, 4, 6, 8, 10, 12, 14; [D] = 1, 5, 9, 13; [E] = 17, 18, 19 in the 2D (above) and 1D NMR (below) experiments.

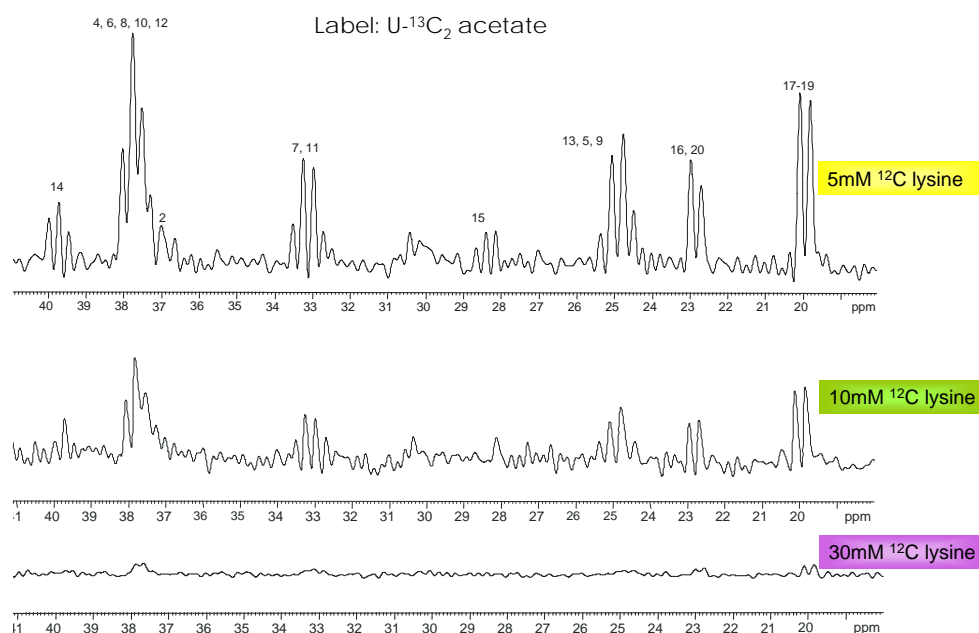


Figure 3.18: **1D carbon spectrum of  $^{13}\text{C}$  labeled lipids with  $^{12}\text{C}$  lysine as an additional carbon source.** With increasing concentration of  $^{12}\text{C}$  lysine in the medium more  $^{12}\text{C}$  carbons were incorporated into the isoprenoid chain and less carbons from  $\text{U-}^{13}\text{C}$  acetate.

2D (Figure 3.19) and 1D spectra (Figure 3.18) showed a significant decrease of peak intensity with increasing concentration of unlabeled lysine in the medium. Both normalization steps, by calculating with "a"-values (all = positive and negative integrals) and "+"-values (only positive integrals) (Table 3.4) were consistent and showed almost constant ratios between the samples with different concentrations of lysine. There was just a slight difference between the analysis in "+" and "a": Calculations using only positive integrals ("+") resulted in smaller standard deviations (5 mM: 0.11; 10 mM: 0.15; 30 mM: 0.30) compared to the results including negative values too ("a") (5 mM: 0.13; 10 mM: 0.19; 30 mM: 0.38). This implied more homogeneous data in analysis of only positive intensity integrals ("+"), which meant also that the probability for artefacts was not so high. Therefore, only graphs for "+"-integrals are shown in Figure 3.20.

*Nmn. pharaonis* was grown in the presence of  $^{13}\text{C}$  labeled acetate and sodium carbonate. Since the concentration of sodium carbonate remained constant between the

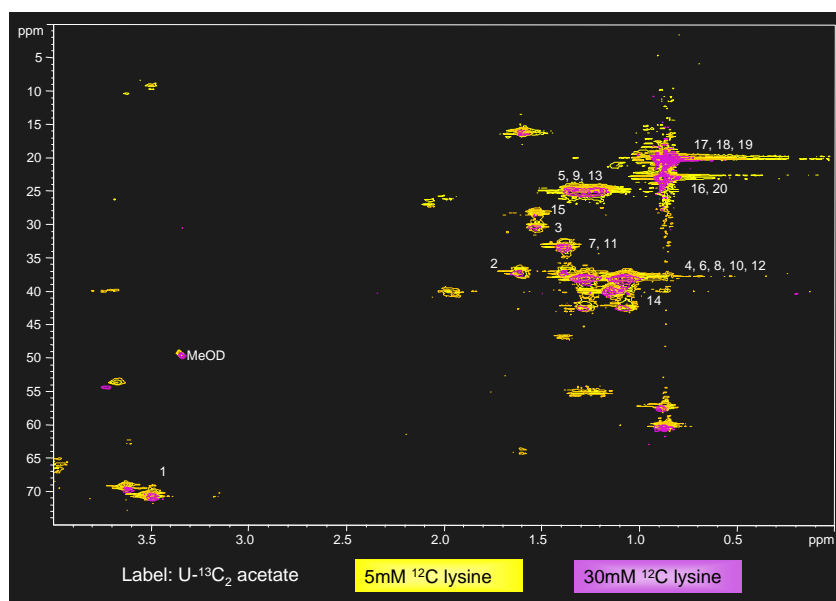


Figure 3.19: **FHSQC U- $^{13}\text{C}_2$  acetate with  $^{12}\text{C}$  lysine.** Equal decrease of signal of enrichments by carbons of U- $^{13}\text{C}_2$  acetate with increasing concentrations of  $^{12}\text{C}$  lysine indicated uniform incorporation of carbons from  $^{12}\text{C}$  lysine in every position of the chain.

Table 3.4: **Integrated all ("a") and positive ("+") signals of FHSQC spectra of lipids from *Nmn. pharaonis* grown in presence of U- $^{13}\text{C}_2$  acetate and  $^{12}\text{C}$  lysine.**

integral	carbon #	5 mM lysine		10 mM lysine		30 mM lysine	
		a	+	a	+	a	+
1	MeOD	1052.8	1538.1	1726.1	2027	1070.1	1487.7
3	17, 18, 19	77979	88015	33536	38337	16818	21271
5	16, 20	49604	58232	22294	26180	13239	15688
7	5, 9, 13	29846	31554	13601	14044	7797.5	8092
9	15	2042.6	3070.4	1132.6	1542.2	863.86	1022
11	3	3691	4006.5	1798.6	2016.8	1210.6	1475.9
13	7, 11	7271.1	9633	3563.9	4504.5	2421.6	2913.4
15	2	4540.6	5075.4	1877.5	2108.5	1123.2	1374.5
17	4, 6, 8, 10, 12	56692	59102	24532	25153	17920	18282
19	14	12324	13058	5123.2	5324.2	3463.6	3566.5
21	1	8155.9	8498.6	3424.7	3491	1701.5	1792.6

normalization by:

	(1) MeOD ("+" values)	(2) concentration in $^1\text{H}$ spectrum
30 mM	100 %	100 %
10 mM	62.00 %	80 %
5 mM	101.64 %	200 %

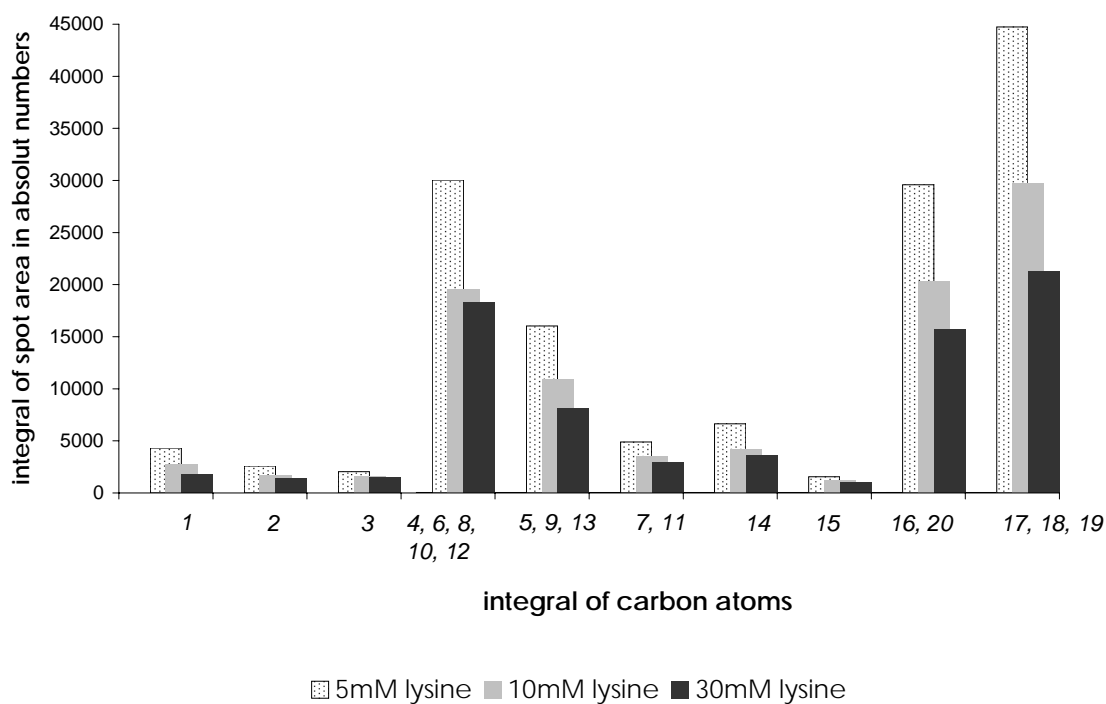


Figure 3.20: **Integrated NMR signals after normalization of  $^{13}\text{C}$  labeled lipids in addition to 5 mM, 10 mM and 30 mM lysine in the growth medium.** Positive integrals of the carbon peaks were compared to each other, after normalization. Some carbons appeared as one big spot in the spectrum like carbons # 5, 9 and 13 for example, resulting in accumulated signals with higher intensities and thus higher integrals.

different samples and only the concentration of lysine was varied, dilution of the enrichment must result from lysine. No conclusions for CO<sub>2</sub> fixation could be made.

The observed incorporation of lysine carbons into the isoprenoid chain was quite surprising, because to date, no specific pathway in halophilic archaea has been described for lysine degradation and channeling of the products into isoprenoid biosynthesis. With "BNet", an in-house programmed annotation tool (Orland Gonzalez, MPI of Biochemistry, Dep. Oesterhelt), no complete pathway for a lysine degradation could be modeled due to the lack of many specific genes. Nevertheless, *Hbt. salinarum* is capable of incorporating carbon atoms from lysine into isoprenoid chains, which was shown by NMR.

In contrast to *Hbt. salinarum*, where the central carbon unit of the isoprenoid is supplied from amino acids (Ekiel *et al.*, 1986) and not from acetate, *Nmn. pharaonis* incorporated carbon atoms from both lysine as well as from acetate in every position of the chain. Although these organisms are close relatives, these results show that they use different pathways for isoprenoid biosynthesis. This implies that in *Nmn. pharaonis* a C<sub>2</sub>-unit from lysine is formed by a till now unknown mechanism and dilutes the C<sub>2</sub>-units derived from acetate.

Three known pathways for lysine catabolism are outlined in Figure 3.21. These are (1) the saccharopine pathway (using transaminase), (2) the 5-aminopentanoate (or oxygenase) pathway and (3) the piperolate pathway. All three lysine degradation pathways merge at crotonoyl-CoA.

The classical lysine degradation pathway in eukaryotes (Higashino *et al.*, 1971) is the reversion of its biosynthesis via saccharopine, 2-oxoadipate and crotonoyl-CoA to acetyl-CoA (pathway number (1) in Figure 3.21). The first two reactions in the saccharopine pathway are catalyzed by lysine-oxoglutarate reductase (EC 1.5.1.7, 1.5.1.8) and saccharopine dehydrogenase (EC 1.5.1.9, 1.5.1.10), respectively. The reductase condenses lysine and 2-oxoglutarate to form saccharopine, which is subsequently oxidized by the dehydrogenase to produce L-2-aminoadipate 6-semialdehyde and glutamic acid (Papes *et al.*, 1999). Further oxidization by aminoadipate-semialdehyde dehydrogenase (EC 1.2.1.31) produces L-2-aminoadipate, which is converted by 2-aminoadipate transaminase (EC 2.6.1.39) to 2-oxoadipate. Oxidative decarboxylation

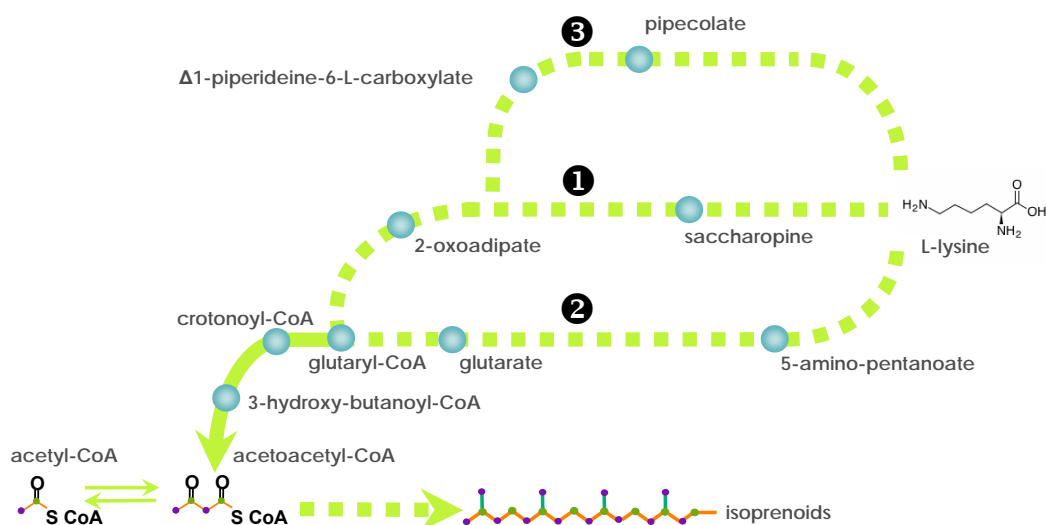


Figure 3.21: **Main possible degradation pathways of lysine.** Three main catabolic pathways (all with a few variational steps in between) in lysine metabolism are known. Eukaryotes degrade lysine first to saccharopine and then further to 2-oxoadipate. Bacteria have developed pathways either from lysine to 5-amino-pentanoate (via cadaverine or 5-amino-pentanamide) and then degradation to glutarate or some species use the pipecolate pathway. The lysine degradation pathway in halophilic archaea is still unclear because a complete pathway could not be annotated in any haloarchaeal genome.

by 2-oxoglutarate dehydrogenase (EC 1.2.4.2; 2.3.1.61) leads to glutaryl-CoA (shown in Figure 3.21).

In the genomes of both, *Nmn. pharaonis* and *Hbt. salinarum*, these important enzymes could not be found by homology search, which implies that there must be another pathway converting lysine into acetyl-CoA. Little is known about lysine degradation pathways in Archaea in general. Only enzymes for the conversion of glutaryl-CoA to acetoacetyl-CoA (glutaryl-CoA dehydrogenase (EC 1.3.99.7, 1.3.99.3), enoyl-CoA hydratase (EC 4.2.1.17), 3-hydroxyacyl-CoA dehydrogenase (EC 1.1.1.35) and acetyl-CoA C-acetyltransferase (EC 2.3.1.9)) are known so far. In *Har. marismortui* the gene encoding saccharopine dehydrogenase was identified. Homology searches showed that this gene is neither present in *Nmn. pharaonis* nor in *Hbt. salinarum*. A gene encoding the saccharopine dehydrogenase was found in genomes of methanogens but only in few halophilic genomes, e.g. *Halomicrobium mukohataei*, *Haloferax volcanii* and *Halorubrum lacusprofundi*.

Several transaminases are encoded in haloarchaea which probably catalyze the con-



version of lysine and other amino acids to TCA cycle intermediates.

Bacteria have evolved completely different strategies for lysine degradation: either via 5-amino pentanamide (Yamanishi *et al.*, 2007) or via cadaverine (Fothergill & Guest, 1977) (both pathways are combined in number (2) in Figure 3.21). Both substrates, which are degradation products of lysine, are converted to 5-amino-pentanoate and then by 5-aminovalerate transaminase (EC 2.6.1.48) and glutarate-semialdehyde dehydrogenase (EC 1.2.1.20) to glutarate, which is converted by glutarate-CoA ligase (EC 6.2.1.6) to glutaryl-CoA - the end point of three pathways. Homology searches of the amino acid sequence of the lysine decarboxylase (EC 4.1.1.18), which converts lysine into cadaverine, found homologies to some archaeal proteins. Among them were some "hypothetical conserved" annotated proteins from *Hrd. utahensis*, *Har. marismortui*, *Nmn. pharaonis*, *Nmn. moolapensis*, *Hqr. walsbyi* and others, but no proteins from *Hbt. salinarum* (Table S1). All sequences included the highly conserved motif "PGGXGTXXE" (alignment not shown), which is always annotated in proteins of the lysine decarboxylase super-family, an indication that lysine is degraded in halophilic archaea via cadaverine and 5-amino-pentanoate. An unusual catabolic pathway for lysine has been detected in anaerobic bacteria such as *Clostridium sp.*, that are able to ferment lysine to acetate, butyrate and ammonia (Stadtman, 1973; Barker *et al.*, 1982) and recently all genes in this pathway could be identified in *Clostridium sp.* (Kreimeyer *et al.*, 2007).

A third distinct route degrades lysine to pipercolate (Chang & Adams, 1974) (number (3) in Figure 3.21). It was first shown in *Pseudomonas sp.* that lysine is degraded in a few steps by  $\Delta$ I-piperideine-2-carboxylate reductase (EC 1.5.1.21) first to L-pipercolate and then by L-pipercolate oxidase (EC 1.5.3.7) (Baginsky & Rodwell, 1967) to  $\Delta$ 1-piperideine-6-L-carboxylate. Regarding these two key enzymes, homology comparisons with amino acid sequences from *Pseudomonas putida* were performed. No homologous gene in any halophilic archaeon could be detected and it remains questionable whether some halophilic oxidoreductases with weak sequence homologies could act in this pathway.

However, for none of these three lysine degradation pathways a complete set of genes was found in haloarchaea. Thus the mechanism of lysine catabolism remains

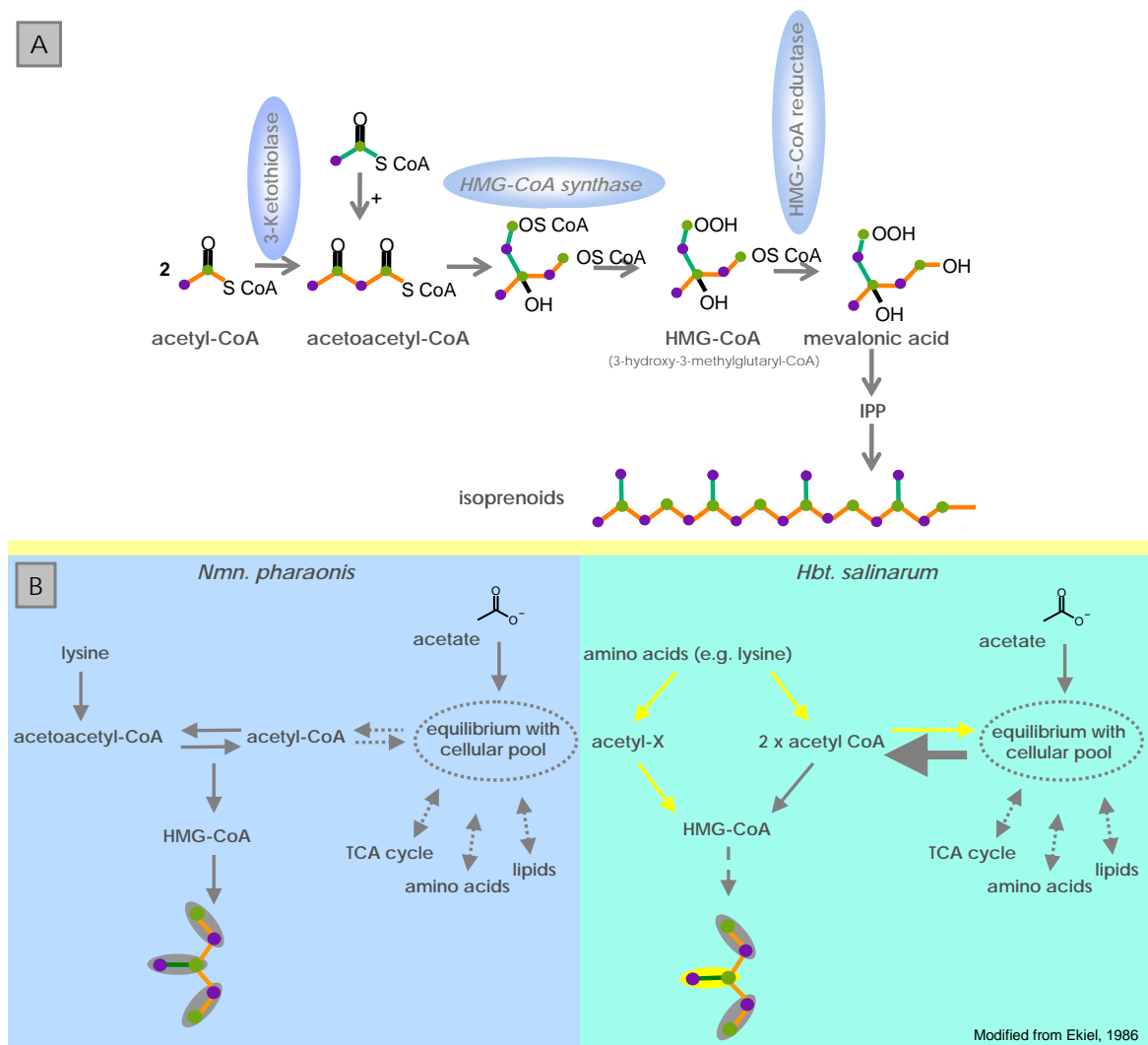


Figure 3.22: **Model for formation of isoprenoids in the mevalonate pathway in *Nmn. pharaonis* in comparison to *Hbt. salinarum*.** **A** Description of the classical mevalonate pathway. **B** Differences in carbon channeling into the isoprenoid biosynthesis between *Nmn. pharaonis* and *Hbt. salinarum*. Carbon atoms from lysine and acetate were incorporated uniformly into isoprenoids in *Nmn. pharaonis*. In contrast, in *Hbt. salinarum* carbon atoms from acetate are never incorporated into the central carbon-unit of the chain. This indicates that *Nmn. pharaonis* uses the classical mevalonate pathway for biosynthesis of isoprenoids, while *Hbt. salinarum* uses a modified pathway. It is assumed that in *Hbt. salinarum* the thiolase, which catalyzes the interconversion of acetyl-CoA and acetoacetyl-CoA, has a different specificity. Ekiel *et al.* (1986) suggested that in a mixed thiolysis reaction acetoacetyl-CoA is synthesized from acetyl-CoA, which equilibrates with the cellular pool, and acetyl-X (where X is a different thiol donor) which is derived from degraded amino acids.

to be unclear. Our experiments demonstrated that carbons from lysine are uniformly incorporated into all positions of isoprenoid chains in *Nmn. pharaonis*. This leads to the conclusion that *Nmn. pharaonis* possesses a canonical thiolase (EC 2.3.1.16, thiolase I) cleaving acetoacetyl-CoA with CoSH to form two units of acetyl-CoA and indicates that *Nmn. pharaonis* uses the classical mevalonate pathway for biosynthesis of isoprenoids.

In Figure 3.22 the biosynthesis of isoprenoids in *Nmn. pharaonis* is presented and compared to the pathway known from *Hbt. salinarum* (Ekiel *et al.*, 1986) and the classical mevalonate pathway found in bacteria and plants (Kanehisa & Goto, 2000).

In *Nmn. pharaonis* carbon atoms from lysine and acetate were incorporated uniformly into isoprenoids while in *Hbt. salinarum* carbon atoms from acetate are never incorporated into the central carbon-unit of the chain (Ekiel *et al.*, 1986). Most likely *Nmn. pharaonis* uses the classical mevalonate pathway for biosynthesis of isoprenoids and *Hbt. salinarum* uses a modified pathway. It is assumed that in *Hbt. salinarum* the thiolase, which catalyzes the interconversion of acetyl-CoA and acetoacetyl-CoA, has a different specificity and can also catalyze in the reverse direction. Ekiel *et al.* (1986) suggested that in a mixed thiolysis reaction acetoacetyl-CoA is synthesized from acetyl-CoA, which equilibrates with the cellular pool, and acetyl-X (where X is a different thiol donor) which is derived from degraded amino acids.

In both models reversibility of a thiolase is essential. Most likely, it will not be possible to draw conclusions about the different specificity of the thiolases in *Hbt. salinarum* and *Nmn. pharaonis* from sequence comparison.

### 3.2.2.3 GC/MS measurements of cleaved isoprenoids supported NMR data

As a complementary method to the NMR analysis, carbon incorporation into isoprenoids was also analyzed by GC/MS.

The lipids were cleaved with  $\text{BCl}_3$  into the polar head groups and isoprenoid chains. This classical reaction yields alkyl chlorides (Nishihara & Koga, 1988; Kates *et al.*, 1965; Gerrard & Lappert, 1952). The alkyl chlorides were first dried and then dissolved in MeOD before injection into a GC/MS system. Electron ionization in GC/MS causes fragmentation of the sample molecules. Different fragments of a molecule are displayed as specific mass peaks in a pattern, which is used for identification of a

sample compound (Figure 3.23). Each fragment delivers a pattern of three peaks, mixed labeled fragments result in an overlay of two different patterns.

#### **Metabolic labeling with $^{13}\text{C}$ acetate resulted in characteristic mass patterns**

Analysis by GC/MS of the isoprenoids after labeling with U- $^{13}\text{C}_a$ acetate revealed that each fragment had a characteristic pattern (demonstrated in Figure 3.23) which was shifted along the x-axis evidencing a complete incorporation of  $^{13}\text{C}$  label.

Results for an unlabeled  $\text{C}_3$  fragment showed masses of 39, 41, 43 (Figure 3.23) in a ratio of 1:2:1 and for a fully labeled  $\text{C}_3$  fragment masses of 42, 44, 46 in similar ratios (overview of GC/MS spectra in Figure 3.24). The ratios remained constant in repeated measurements of the same sample and biological repetitions of different samples. While the pattern could be identified for smaller fragments, this was not always the case for fragmentation patterns for larger fragments.

With increasing size of the fragment the intensity of the mass peaks was decreasing and if the intensity was too low it was not possible to evaluate the pattern. This supports the theory regarding the formation of multiple breaks during ionization: if more breaks occur in a chain, the proportion of smaller fragments ( $\text{C}_3 - \text{C}_5$ ) will increase and show significant pattern signals while larger ions almost vanish in the background of a spectrum.

For drawing metabolic conclusions only the peak with the highest mass (not the highest intensity) in a peak pattern was taken (max-mass peak). The highest mass in a pattern always matched with the calculated mass of a particular fragment (e.g.: 43 Da for the  $^{12}\text{C}_3$  fragment in Figure 3.23). The mass difference between the max-mass peaks for each fragment ( $\text{C}_3, \text{C}_4, \text{C}_5, \text{C}_6$ ) corresponded to the number of carbon atoms (Figure 3.24).

It is not understood in detail which reactions lead to the peaks with smaller masses in a pattern (e.g.: 41 and 39 Da for the  $^{12}\text{C}_3$  fragment in Figure 3.23). Possible are hydrogen eliminations and other rearrangements caused by radical or ionic mechanisms. For example, the loss of two hydrogens during ionic fragmentation in a  $^{12}\text{C}_3$  fragment can lead to a peak with 41 Da.

Degradation of ions formed in the gas phase are matters of thermodynamics and kinetics and have been extensively discussed in many publications (Lefèvre *et al.*, 1992;

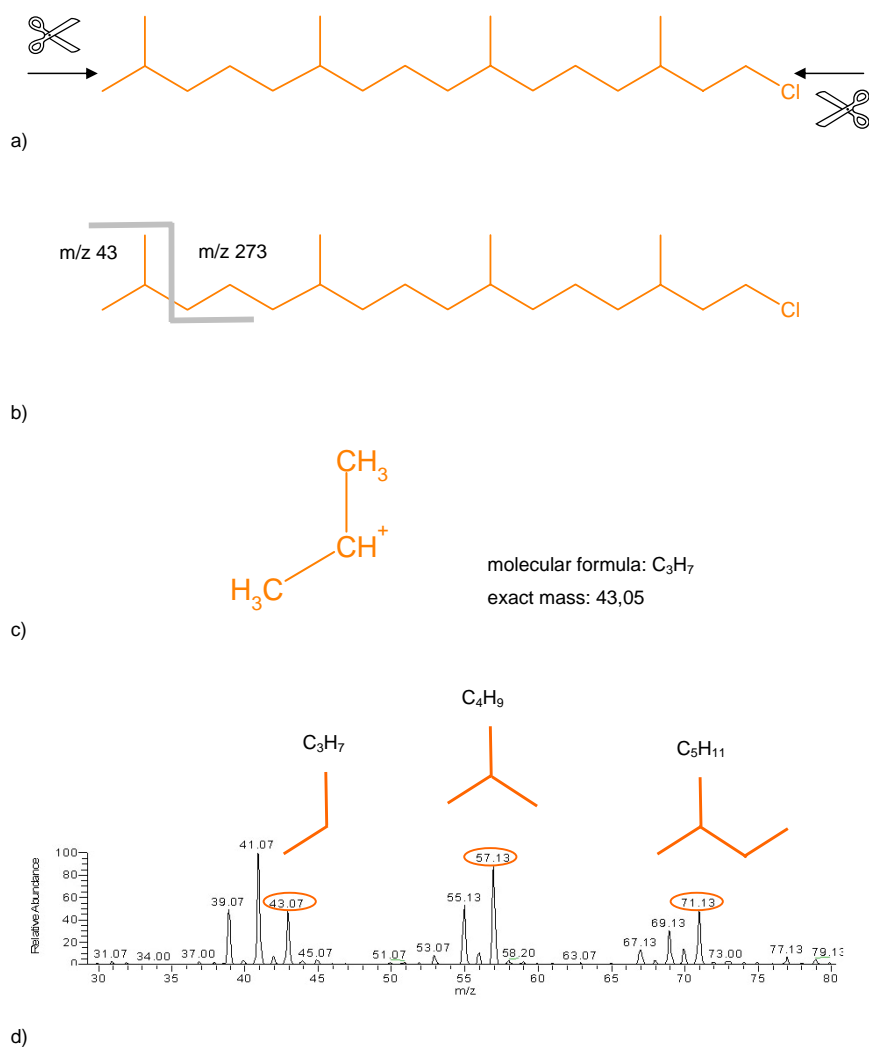


Figure 3.23: **Demonstration of the fragmentation process during ionization.** a) Schematic illustration of fragmentation principle of an alkyl chloride, b) Example of a possible fragmentation of a  $^{12}\text{C}_{20}$  alkyl chain: cleavage of  $\text{C}_{20}\text{H}_{41}\text{Cl}$  into fragment  $\text{C}_3\text{H}_7$  with 43 Da and into fragment  $\text{C}_{17}\text{H}_{34}\text{Cl}$  with 273 Da, c) Example of mass calculation of a  $^{12}\text{C}$  fragment, d) Demonstration of fragmentation pattern analysis in a mass spectrum. The peak with highest mass in every pattern was chosen for further analysis (e.g.  $\text{C}_3\text{H}_7$  - 43.07 m/z), (Oberwinkler, 2006).

### 3 Lipid metabolism in halophilic Archaea

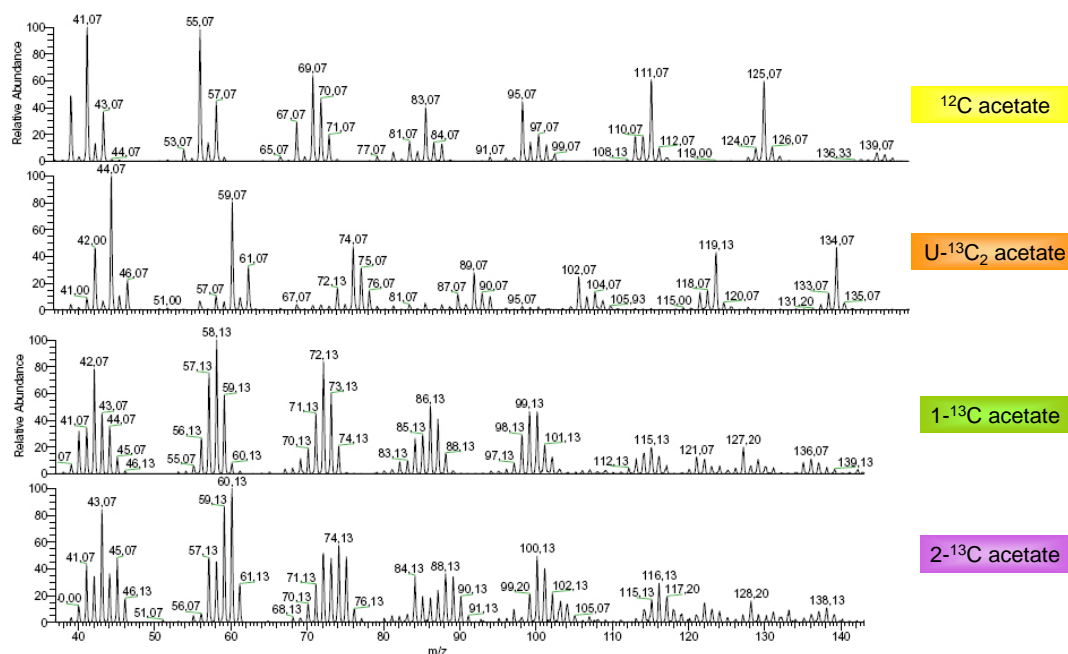


Figure 3.24: GC/MS spectra of  $^{13}\text{C}$  labeled lipids with  $\text{U-}^{13}\text{C}$ ,  $1\text{-}^{13}\text{C}$  acetate and  $2\text{-}^{13}\text{C}$  acetate. To simplify matters, only the peak with the highest mass in every pattern was analyzed (fragmentation is demonstrated in Figure 3.23).

Takayama, 1995; Fagerquist *et al.*, 1999).

Anyhow, analysis based on the peak with the highest mass was sufficient for biological conclusions.

Introducing the  $1\text{-}/2\text{-}^{13}\text{C}$  labeled acetates resulted in mixed patterns of labeled and non-labeled carbons. An hypothetical isoprenoid unit of five carbon atoms with two different states for each carbon ( $^{12}\text{C}$  or  $^{13}\text{C}$ ) results in  $2^5 = 32$  possibilities of arrangements of carbons in one fragment. The NMR experiments confirmed that carbon unit of acetate is not split in the mevalonate pathway (section 3.2.2.2). Every second carbon from the isoprenoid chain was labeled from the methyl group of acetate, and the remaining carbons from the C-1 of acetate. However, no patterns could be detected in the two spectra in Figure 3.24 for  $1\text{-}^{13}\text{C}$  acetate and  $2\text{-}^{13}\text{C}$  and thus no conclusion about the incorporation of C-1 or C-2 from acetate into the isoprenoid chain could be

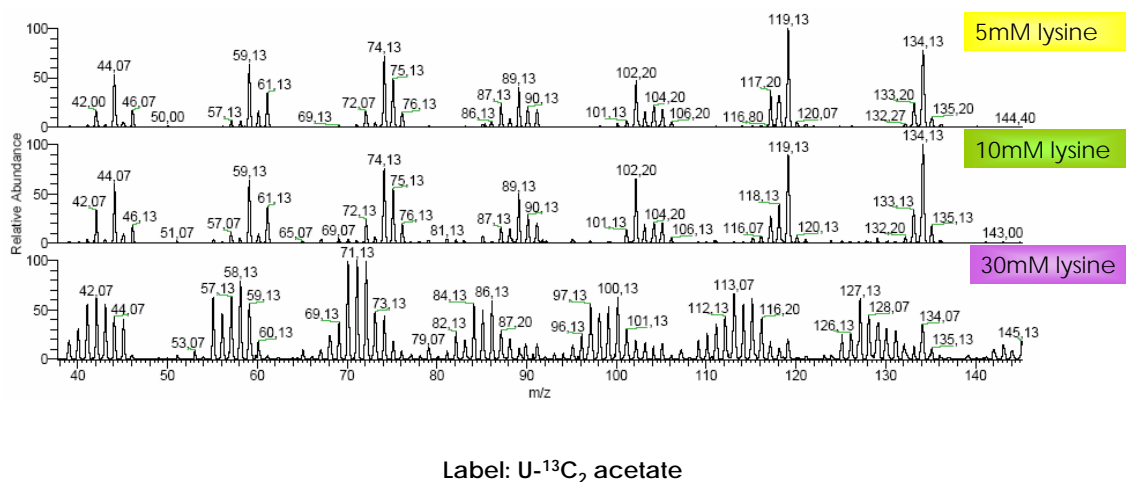


Figure 3.25: GC/MS spectra of isoprenoids extracted from cells grown in the presence of U- $^{13}\text{C}$  acetate and  $^{12}\text{C}$  lysine. Visible dilution of  $^{13}\text{C}$  fragment patterns by  $^{12}\text{C}$  carbons incorporated into isoprenoids.

drawn.

Probably, multiple breaks in one chain resulted in fragments of the same number of carbons but not the same labeling status and thus caused the mixed patterns of the fragments. Therefore, these spectra could not be used for interpretation.

A comparison of the results gained by the NMR-technique and GC/MS of the same sample demonstrates the different weaknesses and power of each technique. GC/MS derived spectra of the experiment with U- $^{13}\text{C}_a$ acetate were consistent with results from NMR, which also showed a fully labeled isoprenoid chain (section 3.2.2.2).

Incorporation of the label introduced by 1-/2- $^{13}\text{C}$  acetate could be tracked into isoprenoids by NMR, but due to complex overlays of differently labeled fragments an interpretation of GC/MS spectra was not possible.

**Incorporation of carbon atoms from lysine proven by GC/MS** Afterwards, isoprenoids consisting of carbons originating from U- $^{13}\text{C}$  acetate or  $^{12}\text{C}$  lysine were investigated by GC/MS originating from the same lipid sample for NMR.

The mass spectra of the isoprenoids showed that carbons from  $^{12}\text{C}$  lysine and  $^{13}\text{C}$  acetate were integrated into the isoprenoid chain (Figure 3.25). A "dilution" by  $^{12}\text{C}$

carbons of an almost pure pattern of  $^{13}\text{C}$  fragments of the isoprenoid chains was observed in the mass spectra in Figure 3.25. With increasing concentration of  $^{12}\text{C}$  lysine in the medium more  $^{12}\text{C}$  carbons were incorporated into the isoprenoid chain and fewer carbons from  $^{13}\text{C}$  acetate.

This is consistent with data obtained by NMR.

At a lysine concentration of 5 mM no incorporation of  $^{12}\text{C}$  carbons could be observed, which is also consistent with the corresponding NMR spectrum.

The 10 mM lysine spectrum showed almost no incorporation of  $^{12}\text{C}$  carbons. This result was quite different from what was measured by NMR where an intense reduction of enrichment was seen. In the 30 mM lysine spectrum however, patterns of mixed fragments ( $^{12}\text{C}$  and  $^{13}\text{C}$ ) demonstrated the "dilution" of  $^{13}\text{C}$  carbons with  $^{12}\text{C}$  carbons.

The reason for the discrepancy between the NMR and the GC/MS data regarding the sample with 10 mM lysine is not known. One explanation might be an overlay of mixed labeled  $^{12}\text{C}$  and  $^{13}\text{C}$  triplets.

Another reason might be contamination. Since contaminated hydrocarbons had to be labeled with  $^{13}\text{C}$  to see an effect in the  $^{13}\text{C}$  pattern of the spectrum in (Figure 3.25), however it might be rather unlikely. Furthermore, as only single alkyl chains were ionized, fragmented and then measured in the mass spectrometer in this experiment, the resulting patterns should only arise from hydrocarbon fragments.

Although an acetone precipitation purification step was performed, after lipid extraction, there were always more than the two expected peaks ( $\text{C}_{20}$ ,  $\text{C}_{25}$ ) visible in the chromatogram (Figure S5). Most of the peaks in a typical isoprenoid chromatogram (peaks with a RT of 14.59; 14.67; 14.73; 14.89; 17.17; 17.30; 17.43), with both labeled or unlabeled samples, showed the same pattern. Lipophilic substances can always be retained with the polar lipids of interest and thus result in extra peaks in the chromatogram.

Nevertheless, impurities and other signals were detected in NMR spectra which is consistent with GC/MS results.

It is concluded that GC/MS is not a stand-alone technique for the measurement of metabolic labeling of lipids if an external standard is not available.



In contrast, GC/MS and not NMR was the method of choice in subsection 4.2.1 for carbon fate modeling to assess whether *Nmn. pharaonis* uses classical pathways for amino acid biosynthesis. Using the NMR technique would have demanded a much more complicated sample preparation in respect to extracting single amino acids. Without a pure sample including just one dominating amino acid spectra would have shown non-interpretable overlaying peaks.

The advantage of NMR in the experiment of the labeled lipids was that it provided precise information on the position of the  $^{13}\text{C}$  label in the carbon skeleton. Since isoprenoids possess a relatively simple structure, and have a NMR spectrum already annotated in the literature (Ekiel *et al.*, 1986), the interpretation of the measured peaks was not too complex.

### 3.3 Conclusions

Although *Nmn. moolapensis* shows a high sequence identity (97.5%, (Burns *et al.*, 2009)) to *Nmn. pharaonis*, *Nmn. moolapensis* presents different capabilities in the biosynthesis of lipids. *Nmn. moolapensis* can synthesize membrane glycolipids (Burns *et al.*, 2009) while *Nmn. pharaonis* (and other haloalkaliphiles) cannot (Kates, 1993a).

Using mass spectrometry, the glycolipid of *Nmn. moolapensis* was shown to differ from the glycolipid S-TGD-1 in *Hbt. salinarum* in the number of attached sugars. Additionally, it was shown to contain a phosphate group. Phosphoglycolipids have not been detected in haloarchaea before and thus this new finding gives insight into the multifarious lipid metabolism of these organisms.

Future NMR analysis of a highly concentrated sample of the *Nmn. moolapensis* glycolipid will deliver exact information about the structure.

To analyze the isoprenoid biosynthetic pathway, *Nmn. pharaonis* was fed with  $^{13}\text{C}$ -labeled substrates to produce labeled lipids, which were then measured by GC/MS and NMR.

Labeling with U- $^{13}\text{C}$  acetate yielded uniformly labeled isoprenoids. This finding and the introduction of labeled carbons from 1- $^{13}\text{C}$  acetate and 2- $^{13}\text{C}$  acetate indicate that *Nmn. pharaonis* uses the classical mevalonate pathway for isoprenoid synthesis. Further labeling experiments with U- $^{13}\text{C}$  acetate and  $^{12}\text{C}$  lysine verified that all car-

bons of the isoprenoid chain are provided from acetate or lysine without detectable preference. This is a major difference to *Hbt. salinarum* where the central carbon unit of the isoprenoid is supplied from amino acids (Ekiel *et al.*, 1986). This showed that there exists no uniform pathway for isoprenoid synthesis in archaea.

Although GC/MS measurements of cleaved isoprenoids supported the spectra gained by the NMR technique, NMR was the method of choice in metabolic labeling. Regardless of the label species NMR provided always precise information on the position of the  $^{13}\text{C}$  label in the carbon skeleton and additionally a quantitative data analysis was possible.

Generally, the results of these studies exhibit numerous facets of archaeal lipids and their biosynthesis pathways that have not been discovered so far.

## 4 Amino acid metabolism in halophilic Archaea

### 4.1 Introduction

#### 4.1.1 Overview of the haloarchaeal amino acid metabolism

Among halophilic archaea the metabolism for amino acids has been well explored for *Har. hispanica* (Hochuli *et al.*, 1999) and *Hbt. salinarum* (Bhaumik & Sonawat, 1994; Ghosh & Sonawat, 1998) but not investigated experimentally in a haloalkaliphilic archaeon like *Nmn. pharaonis*. Some of these studies indicated that many amino acids are synthesized via canonical pathways that had previously been described for bacteria and eukarya (Gottschalk, 1986).

For example, in *Har. hispanica* it was determined by NMR that except for isoleucine, lysine and tyrosine, amino acids are synthesized according to the pathways commonly found in both bacteria and eucarya (Hochuli *et al.*, 1999).

A short introduction of the main canonical amino acid biosynthesis and degradation pathways (Berg *et al.*, 2002; Kanehisa & Goto, 2000; Michal, 1999) is given (Figure 4.1) in the next sections and examples for known alternative pathways in the haloarchaeal amino acid metabolisms are mentioned (described in detail by Falb *et al.* (2008)).

##### 4.1.1.1 Glutamate family (glutamate, glutamine, proline, arginine)

Glutamate serves as a precursor of the amino acids glutamine, proline and arginine. Two main biosynthetic pathways are known (Michal, 1999): (i) Glutamate is synthesized directly from ammonia, 2-oxoglutarate and NADPH; (ii) in the first step glutamine is synthesized from ammonia and glutamate and then the amido group is transferred from glutamine to 2-oxoglutarate yielding two molecules of glutamate.

In haloarchaea, proline might be synthesized via alternative pathways (via 1-pyrroline-5-carboxylate dehydrogenase or by cyclisation of ornithine) and not from

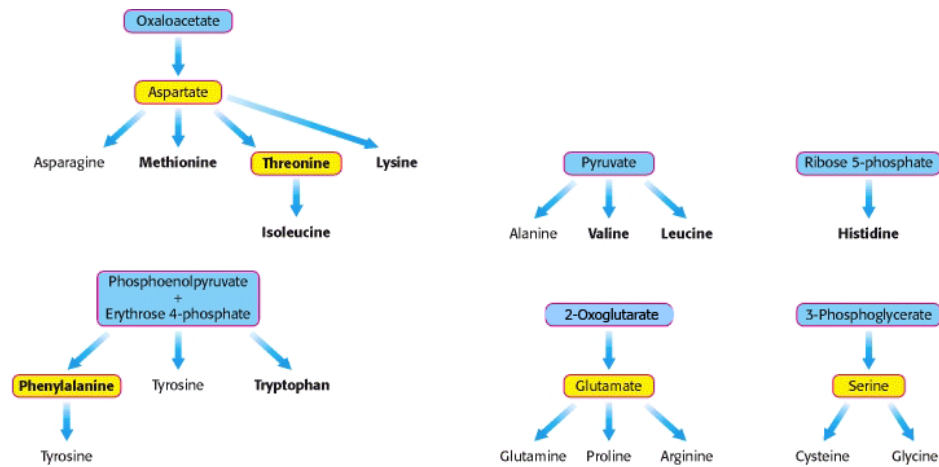


Figure 4.1: **Biosynthetic families of amino acids.** An overview of major metabolic pathways of amino acids in plants and bacteria is given (Berg *et al.*, 2002). Major metabolic precursors are marked blue. Amino acids that give rise to other amino acids are marked yellow.

glutamate (Falb *et al.*, 2008).

In haloarchaea conversion of glutamate in haloarchaea to other amino acids is likely to be catalyzed by several transaminases (Falb *et al.*, 2008). *Hbt. salinarum* employs a unique pathway within the arginine metabolism in Archaea: the arginine deiminase (ADI) pathway in which arginine fermentation takes place (Figure 4.2).

#### 4.1.1.2 Aspartate family (aspartate, alanine, asparagine, threonine, methionine, lysine)

The precursor of aspartate is the TCA cycle intermediate 2-oxoglutarate. Furthermore, aspartate can be converted to asparagine, methionine, threonine and lysine.

In *Har. hispanica* lysine can be synthesized by an alternative pathway the diaminopimelate (DAP) pathway (Hochuli *et al.*, 1999).

#### 4.1.1.3 Serine family (serine, glycine, cysteine)

The biosynthesis of serine starts with 3-phosphoglycerate, an intermediate in glycolysis (Michal, 1999). In further steps glycine and cysteine can be derived.

In haloarchaea an alternative pathway might be possible, in which an oxidation of non-phosphorylated glycerate to hydroxypyruvate takes place (Falb *et al.*, 2008).

The serine degradation pathway consists of conversion of serine to pyruvate and ammonia.

Some haloarchaea encode genes for a glycine-cleavage system (Bender, 1985), enabling them to reversibly cleave glycine (Falb *et al.*, 2008; Oberwinkler, 2006).

#### 4.1.1.4 Branched-chain amino acids (valine, leucine, isoleucine)

Valine, leucine and isoleucine derive their carbon skeleton from pyruvate. The pathways of valine and isoleucine biosynthesis consist of four similar steps with 2-oxoisovalerate as an intermediate. 2-oxoisovalerate can be also converted to leucine (Michal, 1999).

In *Har. hispanica* a threonine pathway has been detected leading to isoleucine (Hochuli *et al.*, 1999).

Branched-chain amino acids have separate degradation and biosynthesis pathways and are catabolized to 2-oxoacids.

#### 4.1.1.5 Aromatic amino acids (phenylalanine, tyrosine, tryptophan, histidine)

Phenylalanine, tyrosine and tryptophan are synthesized from the principal common precursor chorismate in the classical shikimate pathway while histidine derives from ribose 5-phosphate.

It is assumed that in haloarchaea different precursors than in the canonical biosynthesis pathways of aromatic amino acids are used ((Kolog-Gulko & Oesterhelt, 2010)) as already described for *Methanococcus jannaschii* ((White, 2003)).

### 4.1.2 Carbon fate maps for analysis in metabolic labeling

Stable isotope labeling of metabolites (for example  $^{13}\text{C}$ -labeling of acetate or glucose) is a powerful tool for characterizing pathways and reaction fluxes in a metabolic network. The analysis of isotope labeling patterns requires knowledge of the fate of individual atoms. Applications of stable isotope labeling include (i) determination of chemical structures, (ii) characterization of enzymatic reaction mechanisms and (iii) elucidation of metabolic pathways.

In the current study, metabolic labeling was used to assess whether *Nmn. pharaonis* uses classical pathways for amino acid biosynthesis. For this, it is important to accurately model the flows of atoms from substrates to products. The in-house programmed annotation tool "BNet" (Orland Gonzalez, MPI of Biochemistry, Dep. Oesterhelt) was used for pathway modeling.

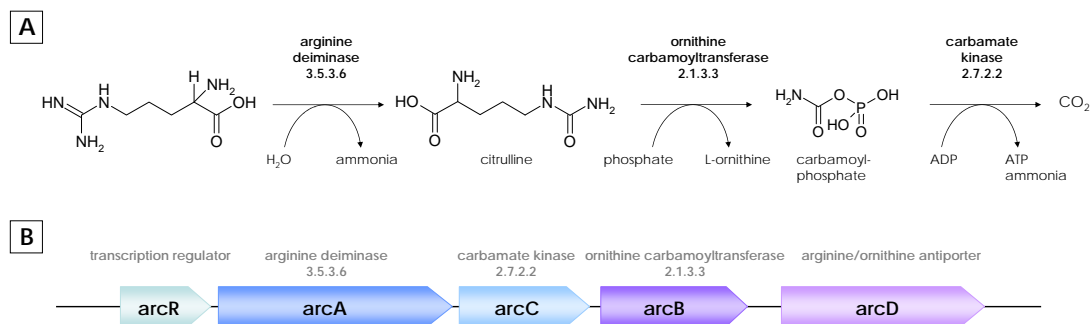


Figure 4.2: **ADI pathway and gene cluster of *Hbt. salinarum*.** In (A) the ADI pathway is illustrated and in (B) the *arc* RACB gene cluster is shown.

### 4.1.3 Arginine fermentation - a unique way to gain energy

Haloarchaea are aerobic chemoorganotrophs that degrade carbon sources such as amino acids, glycerol, and organic acids via the TCA cycle (Ghosh & Sonawat, 1998) and a respiratory electron transport chain (Schäfer, 1996). Due to the low solubility of oxygen in salt-saturated brines, molecular oxygen becomes a limiting factor for oxidative respiration. Therefore, it is not surprising to find that many facultative anaerobes are often halophilic archaea.

One example is *Hbt. salinarum*, which employs two further modes of energy conservation under anaerobic conditions. One is photophosphorylation using the light driven proton pump bacteriorhodopsin, the other is the arginine deiminase (ADI) pathway (Hartmann *et al.*, 1980; Ruepp & Soppa, 1996) where arginine is fermented. In this pathway, arginine is converted to ornithine and carbamoylphosphate, which is further split into carbon dioxide and ammonia with concomitant ATP production (Figure 4.2).

*Hbt. salinarum* is the only archaeon known to have an arginine deiminase gene cluster (*arc* RACB, OE5205R-OE5209R, plasmid PHS3) (Ruepp & Soppa, 1996) encoding all required arginine deiminase pathway enzymes as well as a probable transcription regulator ArcR. The gene for an arginine-ornithine antiporter (OE5204R) (Pfeiffer *et al.*, 2008a; Wimmer *et al.*, 2008) is located next to the arginine deiminase gene cluster.

The ADI pathway is found in a variety of phylogenetic groups within the domain Bacteria, e.g. *Pseudomonas* sp., *Mycoplasma* sp., *Bacillus* sp., and in lactic bacteria (Cunin *et al.*, 1986). This makes it an interesting pathway in *Hbt. salinarum* to explore.

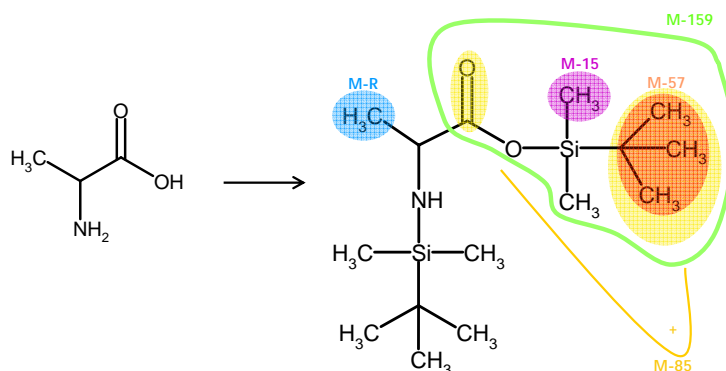


Figure 4.3: **Derivatives of amino acids.** Major ions of tBDMSi amino acids derivatives (e.g. alanine) which can be observed in EI mass spectra. Ions are described by the molecular mass (M) of the respective amino acid less the cleaved fragment, e.g. M-15, M-57, M-85, M-159, M-R.

## 4.2 Results and discussion

### 4.2.1 Distribution of carbons via TCA cycle indicated non-classical amino acid biosynthesis pathways in *Nmn. pharaonis*

In subsection 3.2.2, isotopic tracers provided information about the biosynthetic pathway used by *Nmn. pharaonis* to produce its membrane lipids. In this chapter, the same  $^{13}\text{C}$  substrates,  $1\text{-}^{13}\text{C}$ -,  $2\text{-}^{13}\text{C}$ -, and  $\text{U-}^{13}\text{C}_2$ -acetate were used to produce labeled amino acids.

After hydrolysis of the extracted proteins from *Nmn. pharaonis*, the labeled amino acids were derivatized and analyzed by GC/MS. Accurate GC/MS analysis, however, requires one or more appropriate derivatization procedures to block all active protons and labile keto groups present in both amino acids and carboxylic acids (Halket, 1993). An example of a derivatized amino acid and its detectable ions is shown in Figure 4.3. Possible MS fragmentation pathways of  $\text{N}(\text{O})$ -*tert.*-butyldimethylsilylamino acids were shown by Woo & Chang, 1993. By comparing the chromatograms of the samples with the retention times of an external standard of amino acids, all amino acids could be identified in their labeled form.

As an example, the spectrum of alanine is shown in Figure 4.4. Cells were fed in parallel with one of four different labeled forms of acetate:  $^{12}\text{C}$ -,  $1\text{-}^{13}\text{C}$ -,  $2\text{-}^{13}\text{C}$ -, and  $\text{U-}^{13}\text{C}$ -acetate. The mass spectra of the different amino acids were characterized

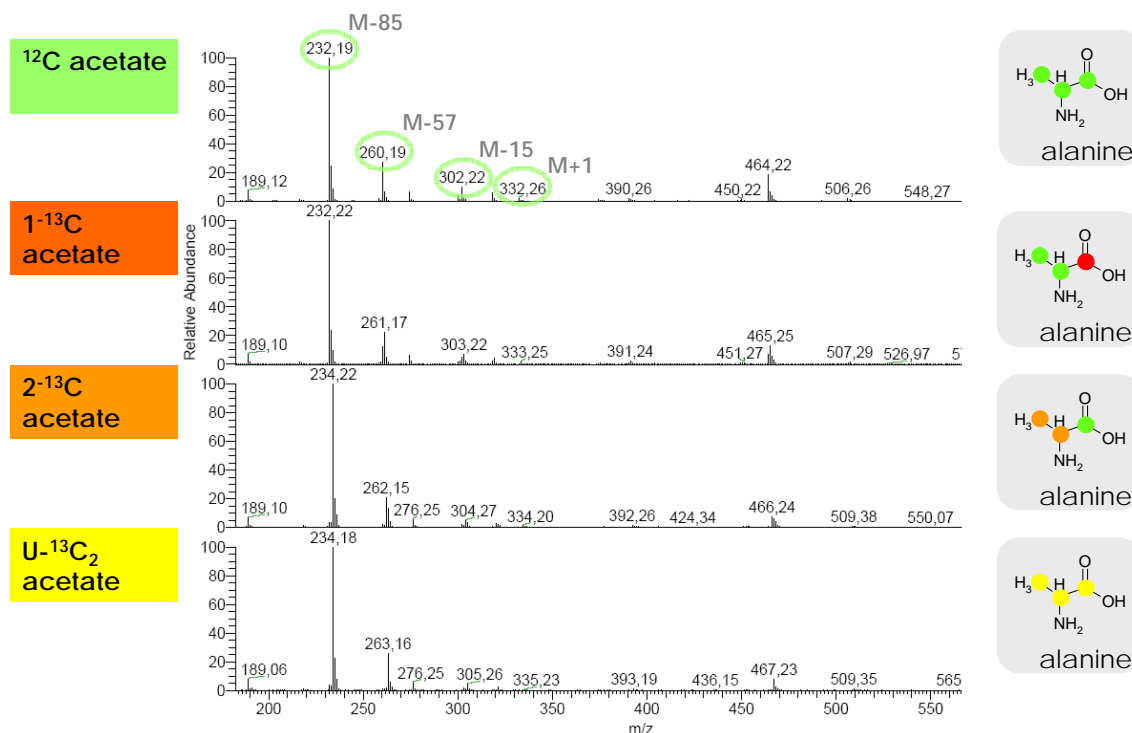


Figure 4.4: **GC/MS spectra of derivatized and labeled alanine.** Extracted amino acids (e.g. alanine) of cells grown in the presence of  $^{12}\text{C}$ -,  $1\text{-}^{13}\text{C}$ -,  $2\text{-}^{13}\text{C}$ -, and  $\text{U-}^{13}\text{C}_2$ -acetate. On the right side of the figure the incorporation of the specific label is shown.

by the main ions M-15 ( $\text{CH}_3$ ), M-57 [ $\text{C}(\text{CH}_3)_3$ ], M-85 [ $\text{C}(\text{CH}_3)_3 + \text{CO}$ ], M-159 [ $\text{COOSi}(\text{CH}_3)_2\text{C}(\text{CH}_3)_3$ ], M-R (Woo & Chang, 1993).

Since the listed ions were not detected for every amino acid in the spectrum, incorporation of a label was tracked only to the two ions with the highest mass intensity, M-57 and M-85.

In other words, the ion M-57 showed how many labeled carbons are incorporated in the amino acid and the ion M-85 gave information whether the carboxy carbon of the amino acid is labeled. The ion M-R determined the label of the alpha carbon.

The spectra of amino acids synthesized from unlabeled and  $\text{U-}^{13}\text{C}$ -acetate were compared with each other. As a result, the peaks of the major ions of the respective amino acid shifted with the corresponding number of labeled carbons (shown in the spectra of alanine in Figure 4.4). A shift of three amu for the ion M-57 could be observed for every amino acid.



Then, the spectra of 1-<sup>13</sup>C-, 2-<sup>13</sup>C-acetate were compared to the unlabeled sample and mass differences between the major ions analyzed. Visual interpretation of the analysis is shown in the next section in Figure 4.5.

In a parallel experiment (data not shown) cells were grown in medium with unlabeled acetate and <sup>13</sup>C carbonate to investigate possible CO<sub>2</sub> fixation. Consistent with the previous data, no shift of the mass peaks could be detected indicating no incorporation of a labeled carbon atom.

#### 4.2.1.1 Incorporation of the label in single amino acids derived from 1-<sup>13</sup>C- or 2-<sup>13</sup>C-acetate

The carbon incorporation of the differently labeled acetate, either from C-1 or from C-2 of acetate, into the amino acids is summarized in Figure 4.5. Analyzing the derivatized amino acid ions in the spectra gave meaningful labeling patterns. Amino acids with similar incorporations of the label were collected in the same group, implying that they were synthesized by the same pathway. The biosynthetic routes predicted on genome annotation were compared to the experimental information.

**Cysteine, methionine, threonine and aspartate** The incorporation of the labels showed that cysteine, methionine, threonine and aspartate are likely to have the same precursor. This is not surprising, because aspartate normally derives from the TCA cycle intermediate oxaloacetate and is further converted to L-aspartate semialdehyde, the precursor of the previously mentioned amino acids (Michal, 1999).

The classical pathway of cysteine synthesis employs serine and glycerate 3-phosphate as precursors (Michal, 1999). However, as shown in Figure 4.5, the carboxy-carbon of cysteine is clearly derived from C-2 of acetate as are the carboxy-carbons from methionine, threonine and aspartate while the carboxy-carbon of glycine and serine originated from the C-1 carbon of acetate. This demonstrates that cysteine and serine do not originate from the same precursor and thus *Nmn. pharaonis* does not use the the classical pathway for cysteine synthesis.

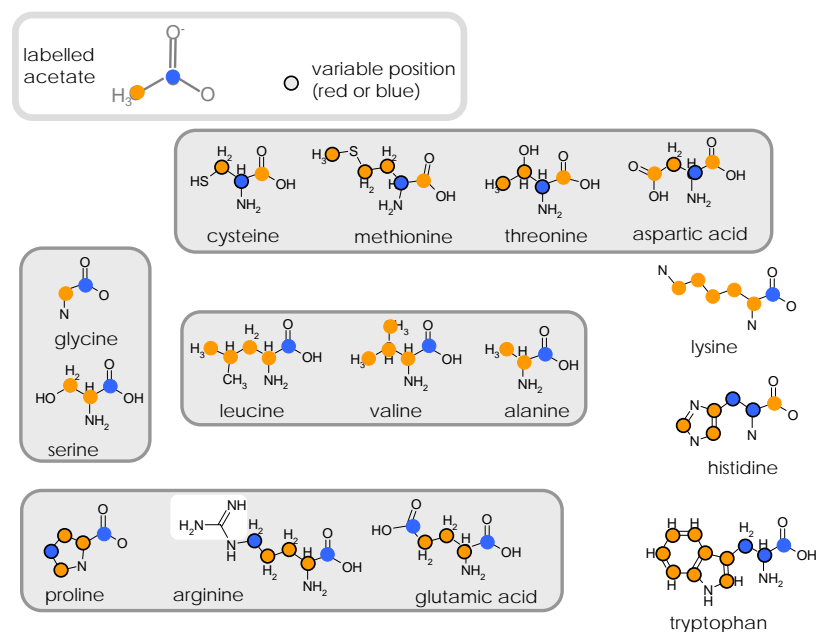


Figure 4.5: **GC/MS spectra of amino acids resulted in specific clusters with similar labeling arrangements.** Carbon C-1 of acetate is marked in blue and C-2 in orange. Due to this ionization method it is not always clear at which position the label is incorporated. In such cases it can be only determined how many of C-1 or C-2 are incorporated. So an unsecure position of the label is marked with a thick black ring around an orange or blue circle. Regarding arginine, the last carbon of the side chain is cleaved off during derivatization (marked with a white box).

In *M. jannaschii*, an alternative cysteine biosynthesis pathway is employed (White, 2003). There, cysteine is synthesized via cystathionine from homocysteine and phosphoserine, which are also involved in the biosynthesis of threonine and methionine. So the results of metabolic labeling of cysteine were consistent with this pathway, meaning that *Nmn. pharaonis* might use the same pathway for cysteine biosynthesis as *M. jannaschii*.

**Lysine** In the classical lysine biosynthesis pathway, lysine is synthesized from L-aspartate semialdehyde. The MS spectra show that lysine receives its carboxy carbon C-1 of acetate and cysteine, methionine, threonine and aspartate from C-2. This demonstrates that lysine might be built from a different precursor than the aspartate family.

Two main classical pathways for lysine biosynthesis are known: (i) Synthesis via the  $\alpha$ -amino adipate pathway (Bhattacharjee, 1985; Schäfer *et al.*, 1989), starting from 2-

oxoglutarate and acetyl-CoA and (ii) synthesis via the diaminopimelate (DAP) pathway relying on aspartic acid and pyruvate as precursors. Since the *dapABD* gene cluster is present in *Nmn. pharaonis* as well as in *Nmn. moolapensis* a functional DAP pathway was assumed and has already been demonstrated for *Har. hispanica* (Hochuli *et al.*, 1999). This contradicts the results of the labeling experiments, which show that lysine cannot have aspartate as a precursor. Since the *dapABD* gene cluster is present in *Nmn. pharaonis* as well as in *Nmn. moolapensis*, a functional DAP pathway was assumed and has already been demonstrated for *Har. hispanica* (Hochuli *et al.*, 1999). This contradicts to the results of the labeling experiments, which show that lysine cannot have aspartate as a precursor.

**Alanine, valine and leucine** According to the common biosynthesis pathways, alanine, valine and leucine are synthesized from pyruvate. The obtained spectra of the  $^{13}\text{C}$  enriched amino acids coincided with the common biosynthetic pathways of the investigated amino acids.

**Glycine and serine** Glycine and serine also seemed to be synthesized by canonical pathways, in which these amino acids originate from glycerate 3-phosphate.

**Glutamate, arginine and prolin** Glutamate, arginine and proline are the only amino acids built from two C-1 carbons of acetate, of which one atom carbon is always incorporated at the carboxy position of the amino acid. Hence, they arise most likely from a common precursor. This precursor is most likely the TCA cycle intermediate 2-oxoglutarate as in the classical biosynthesis pathway for glutamate metabolism. NMR labeling studies showed that this is a major metabolic conversion in haloarchaea (Ghosh & Sonawat, 1998).

**Histidine** In the canonical biosynthesis pathway histidine is synthesized from ribose 5-phosphate. This pathway has been experimentally demonstrated in *Hbt. salinarum* (Ekiel *et al.*, 1986). The mass spectra of histidine showed that this is the only amino acid with two carbon atoms deriving from the C-2 position of acetate without an incorporation of them at the carboxy position. No conclusions about the histidine biosynthesis pathway can be made.

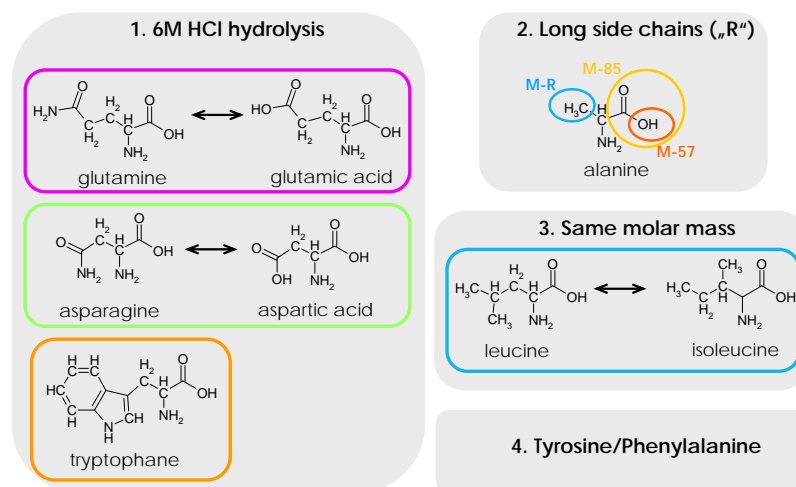


Figure 4.6: **Problems in metabolic labeling of amino acids.** The main problems which emerged during the process of labeling, derivatization and measuring of amino acids are shown.

Summarizing the new findings, most of the investigated amino acids are synthesized via general pathways. Mass spectra indicate that cysteine and lysine have an alternative biosynthesis pathway, which has to be investigated in detail.

**Problematic amino acids** Although for most amino acids the incorporation of the label could be measured, there were still many problems in the procedure of metabolic labeling (Figure 4.6). Due to hydrolysis with hydrochloric acid while cleaving peptide bonds of proteins, acid-weak amino acids like tryptophan were rapidly destroyed and could not be detected. To avoid oxidation of tryptophan, thioglycolic acid was added to the HCl (Matsubara & Sasaki, 1969; Penke *et al.*, 1974). Repetition of the measurement made the detection of the incorporated labels in tryptophan (Figure 4.5) possible.

Another problem is that in long side-chains of amino acids the position of the label could not be annotated if two different carbons (C-1 and C-2 from acetate) were incorporated. Only at the carboxy position of the amino acid the label could be identified by the derivatized ions M - 57 and M - 85 ("double label").

Since the mass of the ion M - R could not be detected in every spectrum, annotation of the alpha carbon in the amino acid was difficult to determine. This is a weakness of the method but could be overcome by application of NMR methods.

Since leucine and isoleucine have the same molecular mass, segregated analysis was

not possible. Analysis of the two aromatic amino acids, tyrosine and phenylalanine, caused many contradictions. Comparison of the spectra of cells grown in the presence of  $^{12}\text{C}$ -,  $1\text{-}^{13}\text{C}$ -,  $2\text{-}^{13}\text{C}$  acetate did not result in consistent positions of the label. One reason for this could be that for every peak detected for a derivatized ion many satellite peaks were measured. The results seem to show a mixture of differently labeled tyrosine and phenylalanine. This could indicate two independent biosynthetic pathways or splitting of one pathway.

The problem with the satellite peaks, but to a lower extent could be also observed in the mass peaks of other amino acids (e.g. alanine in Figure 4.4). This might be due to the presence of mixed labeled pathway precursors (e.g. oxaloacetate, succinate) whose carbons originate from  $1\text{-}^{13}\text{C}$ - or  $2\text{-}^{13}\text{C}$  acetate. Since there were always main peaks observed in each MS spectrum of an amino acid data evaluation was possible. This further implies that there exists a dominant flux. Repetition of amino acid extraction and GC/MS analysis could always show the same dominant fluxes (in spectra with the same main peaks).

The biosynthetic pathways of the aromatic amino acids were not clarified upon genomic annotation (Falb *et al.*, 2008) but experimental data show that L-aspartate-4-semialdehyde and a hexose, rather than PEP and erythrose-4-phosphate, are the precursors used by *Hbt. salinarum* for synthesizing aromatic amino acids (Kolog-Gulko & Oesterhelt, 2010) similar to *Methanococcus jannaschii* (White, 2003).

The question if *Nmn. pharaonis* represents the ideal model organism for flux analysis should be raised. Most of the tested alternative carbon sources, which could have been introduced as specific pathway precursors except glutamate and pyruvate were not absorbed by the cells.  $^{13}\text{C}$ -labeled glucose is also often used as the carbon source in metabolic labeling experiments (Dauner & Sauer, 2000), because during sugar degradation many intermediates serve as a starting point for biosynthesis pathways (e.g. 3-phosphoglycerate, pyruvate). However, *Nmn. pharaonis* and *Hbt. salinarum* growth has not yet been established on glucose as the sole carbon source (Rawal *et al.*, 1988).

GC/MS analysis is much more sensitive than NMR and therefore reduces costs (less labeled material has to be used) and for these reasons it was also applied in this study. However, it has yet to be determined if GC/MS is a better method for providing information on isotopomer distributions than for specific label incorporation

in a metabolite. In contrast, NMR gives information on the position of the label in the carbon chain, and so direct conclusions on the precursor composition can be drawn (Szyperski, 1998).

The question arises, how it is possible to track a carbon atom in the complex network of metabolism at all. Such tracer experiments can be based on the intuitive interpretation of the obtained labeling pattern - this is the most difficult option and requires an abstract modeling framework.

### **4.2.2 Carbon fate modeling in BNet resulted in mixed label types of amino acids**

Another possibility to track carbon atoms in metabolic networks is to construct carbon-fate maps (Mu *et al.*, 2007), which was applied in this study. In carbon-fate maps, the label could be tracked from its introduction into the network, starting at the TCA cycle, until channeling into a specific amino acid pathway. In this chapter, an attempt to track carbons in a metabolic network using an annotation tool is described. The goal was to model pathways and compare the theoretical results to experimental data retrieved by metabolic labeling (subsection 4.2.1).

BNet (programmed by Orland Gonzalez, MPI of Biochemistry) was originally built as an annotation tool to reconstruct metabolic pathways. For applications to carbon fate maps it was connected to a carbon fate database (Mu *et al.*, 2007) and the KEGG Compound database (Kanehisa & Goto, 2000), including information about the molecule's two dimensional structure. Metabolites were downloaded as Mol files, including information about atoms, bonds and coordinates, from the KEGG compound database. The 2D chemical structure information was subsequently converted into "InChI" files which are unique textual identifiers for chemical substances. Homotopic (achiral) atoms are indistinguishable with respect to stable isotope labeling - their groups were treated as equivalents. Therefore, the reactions in which a particular molecule is involved had to be mirrored manually in the database and finally the carbon flow was inverted so that both possibilities were considered.

For every amino acid group in Figure 4.5 it was attempted to construct a carbon fate model. First, a theoretical pathway diagram was constructed with BNet (Figure 4.7),

including well balanced reaction definitions based on enzymes annotated in the genome of *Nmn. pharaonis*. During the modeling process it was recognized that carbon fate modeling has not been fully developed for this purpose. Since BNet relies on genomic data, which are not complete, also the resulting pathways show annotation gaps.

Sodium acetate, the label source, enters the TCA cycle as a two-carbon unit via acetyl-CoA. The problem is that at specific steps of the TCA cycle the labeled carbons get incidentally incorporated into the TCA intermediates. At the beginning of the TCA cycle after new carbons are attached to oxaloacetate to form citrate, the following enzymes can distinguish between the group  $\text{CH}_2\text{-COOH}$  that comes from acetyl-CoA and that which comes from oxaloacetate. After succinyl-CoA is converted into succinate the next enzymes proceed with randomly labeled molecules, because succinate and fumarate contain homotopic carbon atoms. This results in a scrambling of the label at the fumarate-succinate stage.

Since *Nmn. pharaonis* can grow on acetate as the only organic carbon source, it is assumed that the main part of introduced acetate enters the TCA cycle as acetyl-CoA, where it is fully oxidized to  $\text{CO}_2$ . So, the cell can use this molecule in conjunction with respiration as its energy source.

In contrast to *Hbt. salinarum*, *Nmn. pharaonis* has the complete set of enzymes associated with the glyoxylate cycle (isocitrate lyase and malate synthase). The glyoxylate cycle skips the processing of differently labeled achiral molecules. Nevertheless, after isocitrate undergoes cleavage into succinate and glyoxylate, succinate can enter into the citric acid cycle to eventually form oxaloacetate. This again results in a mixture of differently labeled metabolites. Besides carbohydrate biosynthesis, acetate is also the starting point of the mevalonate pathway, the biosynthesis of isoprenoids (subsubsection 3.1.3.2). This pathway bypasses the TCA cycle without scrambling the label. Therefore, interpretable MS spectra could be measured and analyzed in subsubsection 3.2.2.3.

#### 4.2.2.1 Cysteine biosynthesis as an example of a carbon fate map

Since the labeling experiments (subsubsection 4.2.1.1) indicated that cysteine might be synthesized via an alternative pathway a carbon fate map simulating a possible

biosynthesis pathway was constructed.

Cysteine showed the same labeling patterns as methionine, threonine and aspartate (the carboxy-carbon derived from C-2 of acetate, all remaining carbons from C-1 of acetate), and not like serine. Therefore, it is assumed that those amino acids share a similar biosynthesis pathway and carbon fates were tracked starting from acetate to cysteine and threonine.

Carbon fates were calculated and the resulting carbon fate map of cysteine biosynthesis is displayed in Figure 4.8. With the obtained labeling patterns for serine in Figure 4.5, carbon flow in the map in Figure 4.8 was tracked. The positions of the label retrieved from the model do not agree with the measured peaks in the MS spectra.

Since threonine was also included in the carbon fate map, labels of this amino acid were also tracked. Starting from aspartate, the label was tracked via L-aspartate semialdehyde to threonine. In the case of threonine, results of the model (Figure 4.8) coincided with the information flow from experimentally determined mass distributions.

Why the simulated carbon fate map did not show the expected results for the biosynthesis of cysteine, is not quite clear. Since the network is based on genomic data the network is also built up of incomplete, not fully annotated pathways. There are still unknown enzymes without annotation. So maybe there exists a yet unknown cysteine biosynthesis pathway in *Nmn. pharaonis* which cannot be simulated due to lack of genomic data.

Additionally, carbon fate maps (Mu *et al.*, 2007) were constructed for general reactions and maybe do not fit to special archaeal pathways and reactions.

Another possibility is that the analysis of the MS spectra was incorrect due to label scrambling, but on the other hand, modeling carbon fates of biosynthesis pathway of other amino acids (e.g. threonine) worked well.

Due to the inconsistent results of the carbon fate modeling with acetate as the labeling source, no further examples are given. It is concluded that carbon fate modeling in *Nmn. pharaonis* should be carried out with other carbon sources than acetate. To



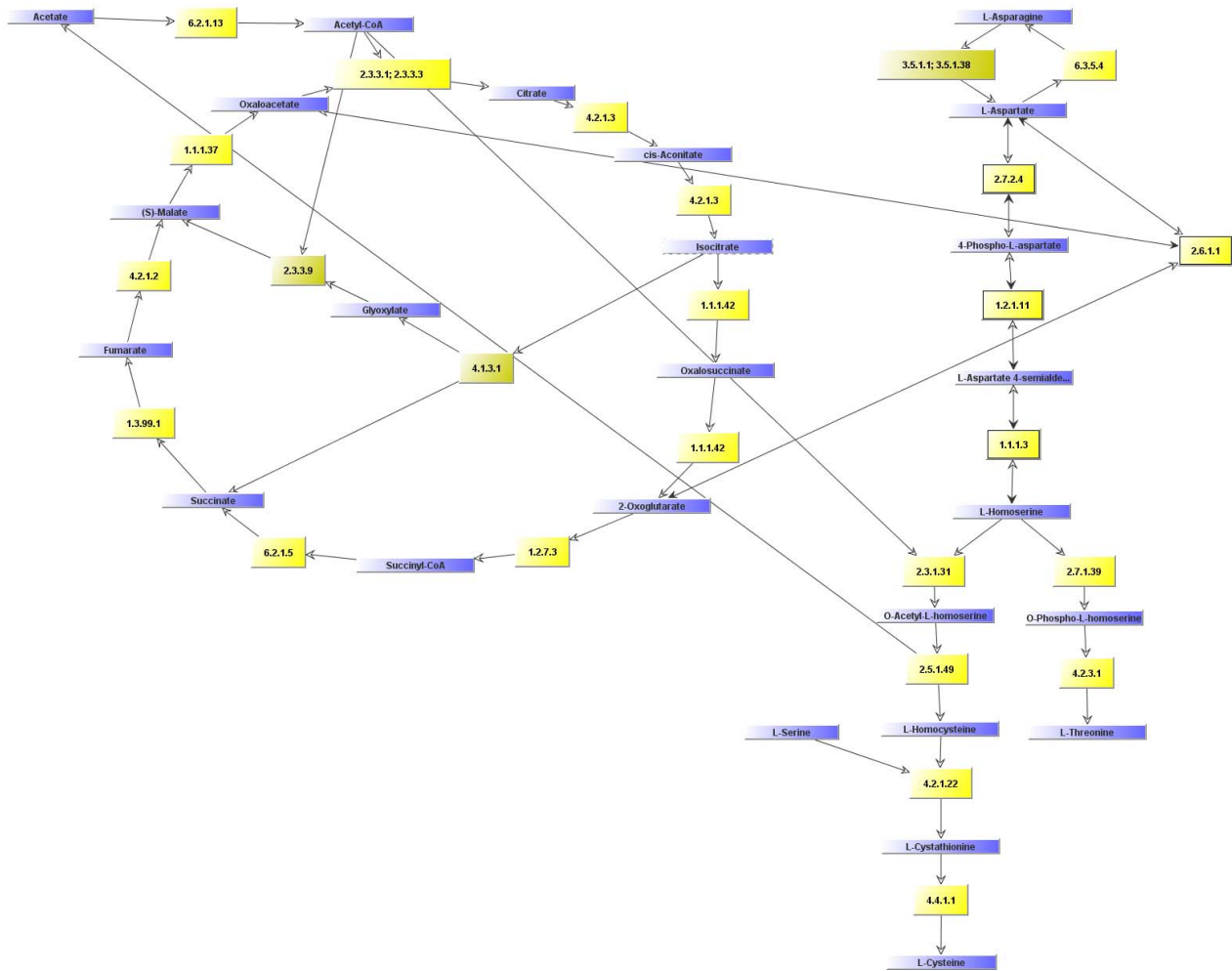


Figure 4.7: **Biosynthesis diagram of cysteine and threonine connected to the TCA cycle.** Compounds of the pathway are shown in blue boxes and EC numbers of each reaction are shown in yellow boxes.

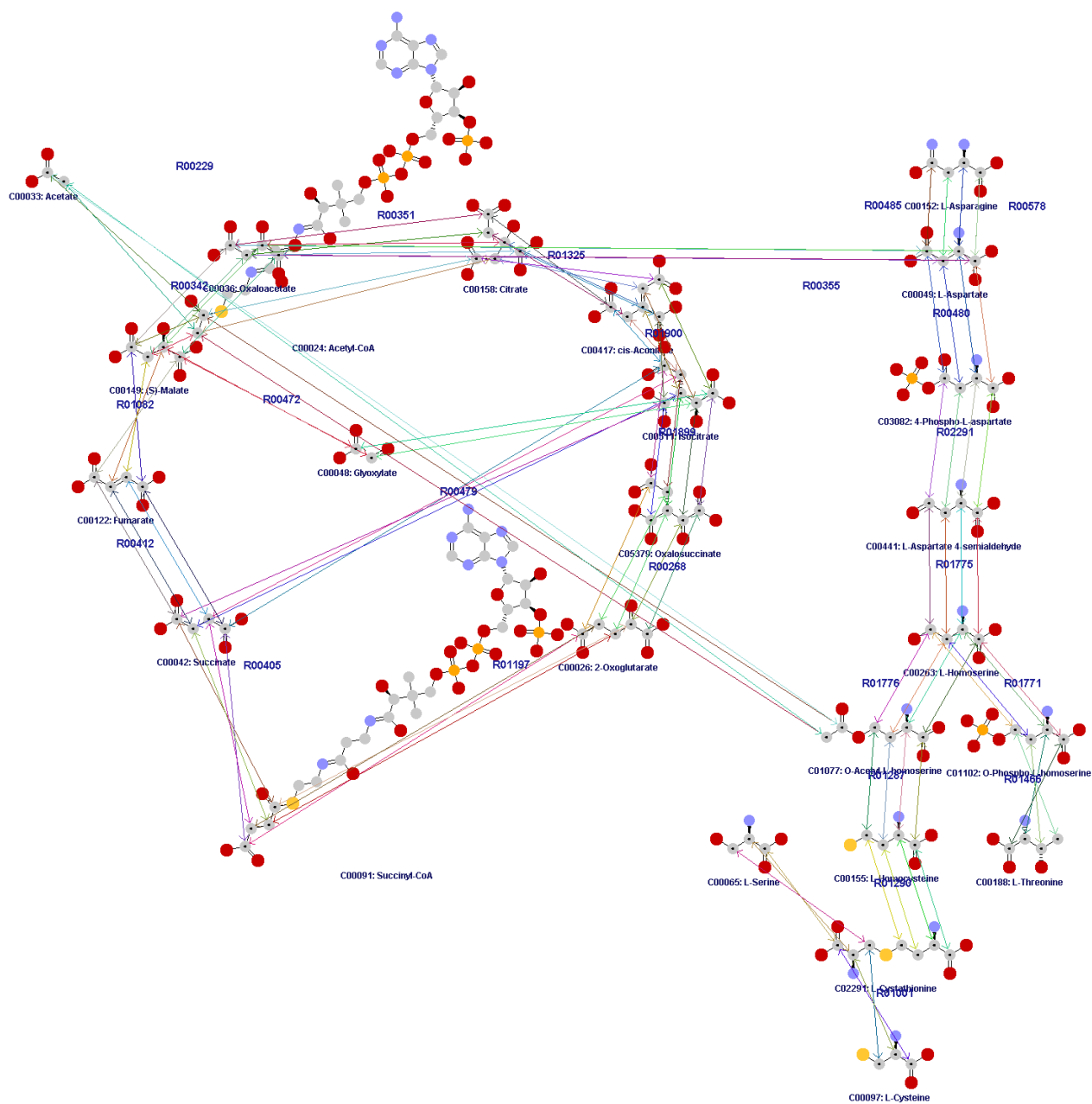


Figure 4.8: **Model of carbon fates of cysteine and threonine biosynthesis.** Legend: carbon - grey, oxygen - red, sulfur - yellow and nitrogen - blue. Colors of fates (connections between the carbons) have no meaning. All possible fates of one carbon can be tracked in this map starting from labeled acetate in the upper left corner to the destinations cysteine and threonine in the lower right corner of the figure.

avoid scrambling of the label by the TCA cycle, different carbon sources with a carbon skeleton consisting of more than two carbons were investigated in minimal medium in the next subsection.

### **4.2.3 Few alternative carbon sources - other than acetate - support growth of *Nmn. pharaonis* in minimal medium**

If an organism needs only one organic carbon source it could be an advantage in metabolic labeling, as is the case with lipid analysis. But if the carbon source, here acetate, is first metabolized in the TCA cycle, yielding mixed labeled precursors for pathways of interest, proper carbon fate modeling is not possible. In this experiment, different carbon sources were tested for their ability to support growth of *Nmn. pharaonis*. The plasticity of the metabolic network of the cell was investigated by inoculating cells into new media from previous cultures at low densities. This allowed to adapt cells in a stepwise manner to new carbon sources.

*Nmn. pharaonis* was cultivated under aerobic conditions in the dark in minimal medium containing only a single organic carbon source. As carbon sources with C-3 skeleton glycerol, dihydroxyacetone (DHA), lactate and pyruvate were tested. Succinate, malate, fumarate and aspartate were chosen as carbon sources with a C-4 skeleton. Glutamate was the only compound tested with 5 and leucin with 6 carbons. All carbon sources except glycerol were used at concentrations between 20 mM and 50 mM; glycerol was used at concentrations between 0.5 and 3 %.

Growth curves of *Nmn. pharaonis*, grown on the previously mentioned carbon sources, are presented in Figure 4.9. *Nmn. pharaonis* was not able to grow on glycerol, DHA or lactate. Pyruvate was the only C-3 compound on which *Nmn. pharaonis* showed growth. None of the carbon sources with a C-4 skeleton supported growth of *Nmn. pharaonis*.

However, glutamate turned out to be the best carbon source for *Nmn. pharaonis*. At a concentration of 50 mM, cells grew faster than in media with 20 mM acetate (the defined standard concentration in the minimal medium in subsection 2.2.2.2) as the carbon source. Growth on leucine was not possible.

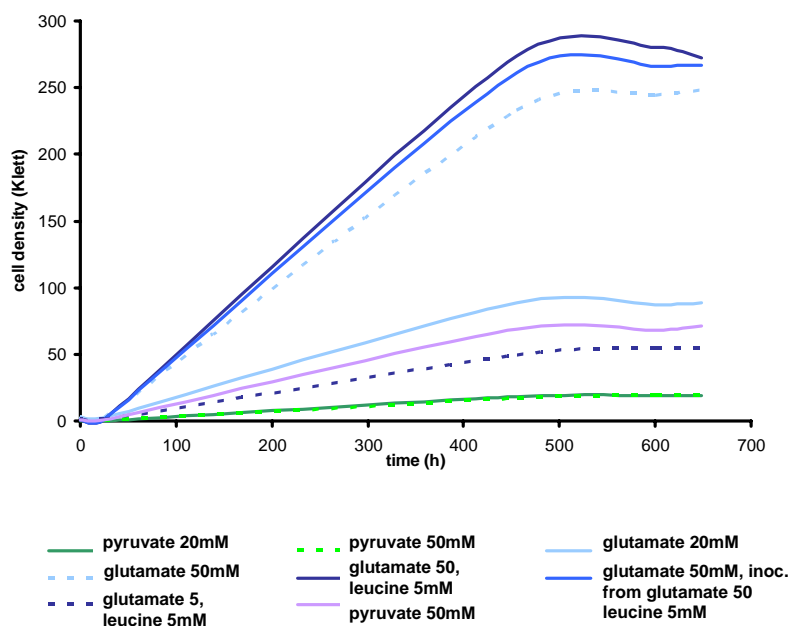


Figure 4.9: **Alternative carbon sources in *Nmn. pharaonis* minimal medium.** Glutamate in combination with leucine seemed to be optimal carbon source after several inoculation steps. No growth could be measured with leucine, aspartate, glycerol, DHA, malate, fumarate, lactate and succinate.

The inability of *Nmn. pharaonis* to grow on glycerol is consistent with its lack of almost every enzyme in glycerol catabolism, except triosephosphate isomerase (NP2182A). Other haloarchaea have different capabilities in metabolizing carbon sources. One reason for the missing enzymes could be its growth in an alkaline environment, where the halotolerant green algae *Dunaliella* does not thrive. *Dunaliella* produces abundant glycerol to protect itself from osmotic pressure (Phadwal & Singh, 2003). *Hbt. salinarum* grows well on glycerol due to two degradation pathways to glyceraldehyde 3-phosphate and subsequent introduction into the Embden-Meyerhoff pathway.

As expected from the missing kinases and uptake-system, *Nmn. pharaonis* could not grow on DHA. In contrast, *Hqr. walsbyi* is able to take up DHA by a cytosolic phosphoenolpyruvate-dependent phosphotransferase system and can grow on it as carbon and energy source (Bolhuis *et al.*, 2006).

Glutamate as well as aspartate are major substrates for halophilic archaea, serving as universal amino donors (Falb *et al.*, 2008) and glutamate is amassed as a compatible

osmolyte (Kokoeva *et al.*, 2002; Desmarais *et al.*, 1997).

The lack of growth on leucine can be explained by the lack of the dehydrogenase complex which is assumed to degrade leucine to 2-oxo-isocaproate in *Hbt. salinarum*.

Lactate degradation has not been described for any haloarchaeon. No clear lactate dehydrogenase homologs could be identified in any haloarchaeal genome, but some aldehyde dehydrogenases show a high similarity to the *M. jannaschii* lactaldehyde dehydrogenase (Falb *et al.*, 2008). The lactate dehydrogenase would be necessary for conversion of lactate into pyruvate. In some bacteria (e.g. *Propionibacterium sp.*), lactate can be fermented to propionate, acetate and CO<sub>2</sub>. However, the respective enzymes for conversion of lactate into Acryloyl-CoA are missing in haloarchaeal genomes.

The inability to grow on fumarate observed here for *Nmn. pharaonis* was also found in *Hbt. salinarum* (Montrone *et al.*, 1993).

Altogether it can be said that glutamate at a concentration of 50 mM served as the best single alternative carbon source for *Nmn. pharaonis*.

#### **4.2.4 Characterization of the arginine/ornithine metabolism in *Hbt. salinarum***

For analysis of the ADI pathway which converts arginine to ornithine to produce ATP, experiments with three different "strains" of the wild-type *Hbt. salinarum* R1 were performed.

##### **4.2.4.1 *Hbt. salinarum* can grow without arginine and ornithine in synthetic medium**

Arginine has long been held as an essential amino acid for *Hbt. salinarum*. But modeling results by Gonzalez (2009) indicated that arginine is not completely indispensable and only supporting growth.

Therefore, growth of *Hbt. salinarum* was investigated in detail with respect to arginine and ornithine supply in synthetic medium.

In Figure 4.10, R1 and  $\Delta arcD$  were grown in synthetic medium with arginine and R+ (= *Hbt. salinarum* R1, adapted to growth in a synthetic medium without arginine

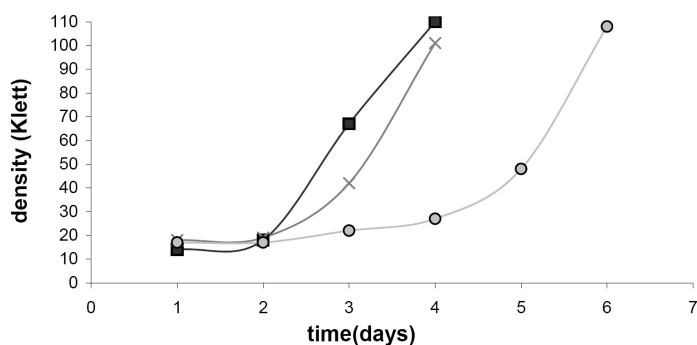


Figure 4.10: **Growth curves of three different strains of *Hbt. salinarum*: R1 (or R-), R+ and  $\Delta arcD$ .** R1 (or R-) growing with arginine, R+, which is the adapted wild-type R1 growing without arginine and ornithine in the synthetic medium and the deletion strain  $\Delta arcD$  are compared in their aerobic growth in the dark. R1 - diamond, R+ - circle,  $\Delta arcD$  - triangle

and its predecessor ornithine) without the two amino acids.

It is easily shown that R+ stayed in a long lag-phase before adapting to the new medium and then starting to grow exponentially as fast as the wild-type. Many inoculation steps of R+ were necessary to train this organism by adapting it to the new medium reaching the same OD as the unadapted wild type R1 in its medium including arginine and ornithine.

In this study it could be demonstrated that *Hbt. salinarum* strain R1 was able to grow under aerobic conditions in the dark in synthetic medium without arginine and ornithine. Moreover, it is clear that arginine is not critical for good growth in terms of speed and the maximum population size reached when *Hbt. salinarum* has adapted its metabolism.

Similar growth experiments of *Hbt. salinarum* in medium with or without arginine and ornithine were performed by Gonzalez (2009) but the doubling time of the cells was much longer and the maximum cell density reached was just about a fourth when either arginine or ornithine was supplied. A reason for these different growth observations is the variable adaptation time (more inoculation steps in the presented experiments of this study).

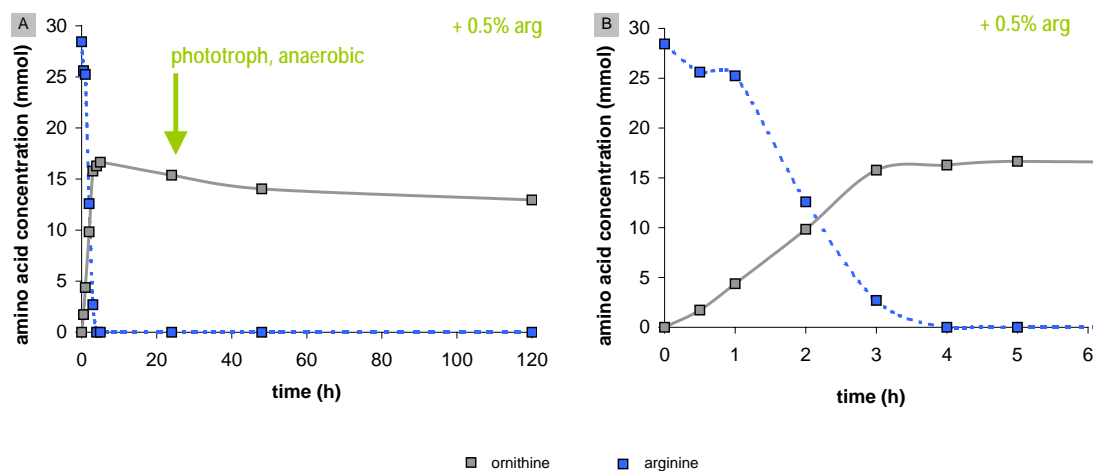


Figure 4.11: **Conversion of arginine to ornithine by *Hbt. salinarum* R1 cells in basal salt medium.** (A) Cells were incubated under aerobic conditions for 24 h in the dark with the supply of 0.5 % arginine and afterwards flushed with nitrogen and incubated in the light. (B) = Detail first figure: Within five hours of adding arginine to the basal salt medium, the amino acid was completely consumed by the cells and ornithine was secreted.

#### 4.2.4.2 Amino acid uptake experiments with the wild-type *Hbt. salinarum*

For a better understanding of the arginine/ornithine uptake mechanisms in the cell, concentration of the amino acids was traced in a set of experiments. Parallel experiments with a concentrated cell suspension under different conditions (e.g. illumination/dark, anaerobe/aerobe) were performed and the change of the intracellular concentration of arginine and ornithine was calculated (all experiments are listed in Table S2).

For these series of experiments halobacterial cells were kept under aerobic conditions in the stationary growth phase in basal salt medium with 0.5 % arginine. In this case, the decreasing concentration of the amino acid in the medium reflects the uptake and consumption of the amino acid by the living cell.

Initially, the experiment of Hartmann *et al.* (1980) was repeated, confirming that the consumption of arginine is coupled to the production of ornithine.

0.5 % arginine were added into the basal salt medium and 1 ml of a 1 M sodium carbonate solution was applied into the side arm of the Klett flask. After 24 h aerobic incubation of the cell suspension (4.5 OD in basal salt medium) in the dark at 37°C, the

culture was transferred into the light shaker and further incubated anaerobically. The concentration of arginine and ornithine were monitored during growth (Figure 4.10). After 4 h all the arginine in the medium was metabolized and converted into ornithine at a ratio of 1.71:1.

Parallel experiments under anaerobic conditions, either constantly incubated in the dark or in the light, did not show any significant differences in arginine uptake or ornithine secretion.

In next experiments the cell suspension was illuminated. As a result, arginine consumption continued and ornithine secretion was observed in similar arginine/ornithine ratios (dark: 2.30; light: 2.65 (Table S2)). It was assumed that phototrophic growth would start after light induction, which would keep the ATP level of the cells at its maximum and therefore ADP would not be available for phosphorylation by carbamoylphosphate. However, this was not the case.

One reason for the differences to the results of Hartmann and colleagues regarding arginine degradation under anaerobic conditions, could be the distinct adaptation between cultures. If the culture has not been adapted to phototrophic conditions (after inoculation from a preparatory culture), it continues fermenting arginine when illuminated as long as the amino acid is present in the medium.

#### 4.2.4.3 Experiments with a deletion strain verified ArcD as the main arginine uptake system

To prove that the decreasing concentration of added amino acid (e.g. arginine) did not result from adsorption to the cell wall or from degradation in basal salt, the experiment (described before) was repeated with the deletion strain  $\Delta arcD$  (deletion of arginine/ornithine antiporter) (Wimmer *et al.*, 2008) and compared to the wild type *Hbt. salinarum* R1.

Panel A in Figure 4.12 shows that for  $\Delta arcD$  the decrease in arginine concentration and the increase in ornithine concentration is drastically slower than in wild type (Figure 4.12). Even after 24 h only 10 % of the arginine had been taken up by the cells. This demonstrates that an uptake of arginine into the cell in the wild type strain



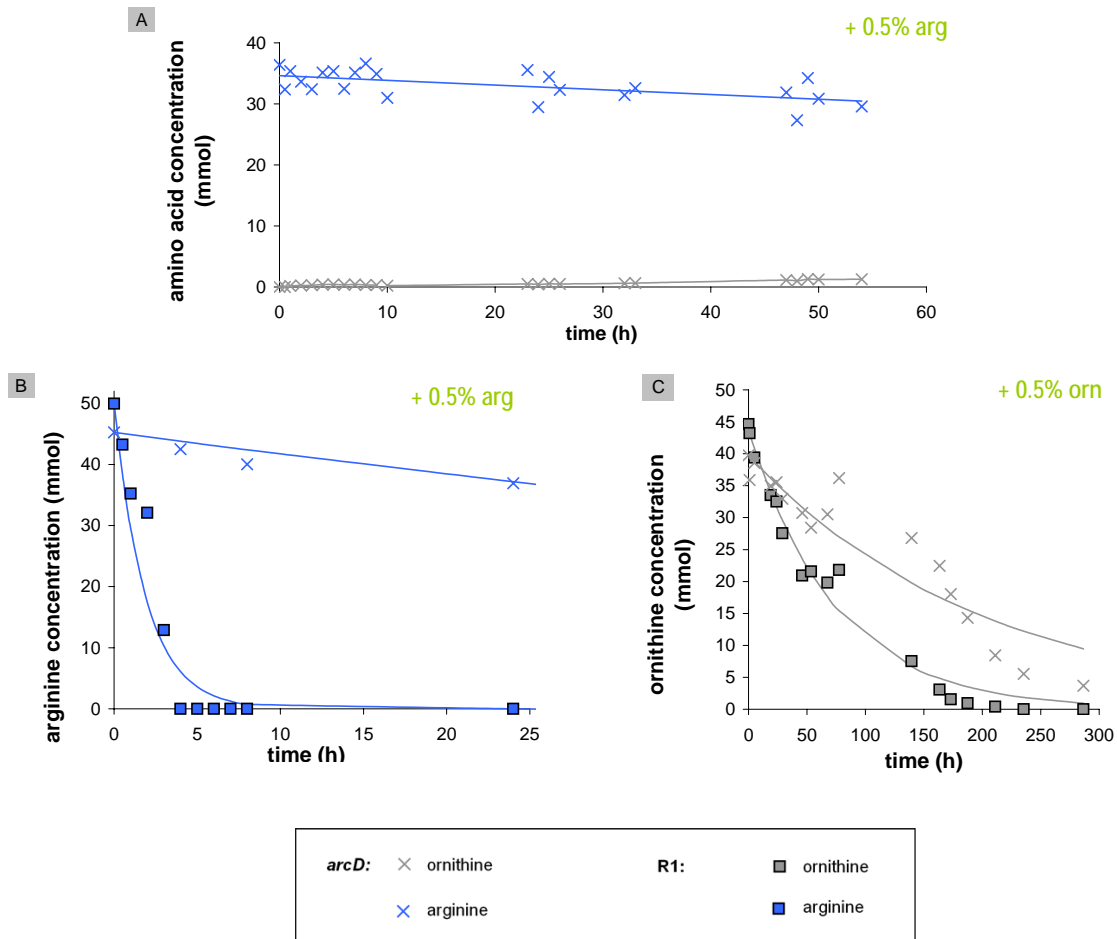


Figure 4.12: Uptake experiments with deletion strain  $\Delta arcD$  and wild-type *Hbt. salinarum* R1 in basal salt medium. (A) Arginine concentration in the basal salt (0.5% arginine) decreased while ornithine was increasing slowly. Cells were incubated anaerobically in the light after 24h aerobically in the dark. (B) Decrease of arginine in basal salt (0.5% arginine) after different times of incubation. (C) Faster uptake of ornithine in the wild-type than in the deletion strain was measured in basal salt with addition of 0.5% ornithine instead of arginine.

causes the rapid depletion of arginine in the medium.

Two additional experiments were performed adding 0.5% arginine (graph B) or 0.5% ornithine (graph C) to the cell suspension (Figure 4.12) while incubating the cells aerobically in the dark. While in the wild type, arginine was depleted from the basal salt medium by active uptake within a time of roughly 2 h, the deletion strain showed limited arginine uptake.

These experiments verified that the arginine/ornithine antiporter ArcD is the main uptake system for arginine and ornithine in halobacterial cells, and that it also works under aerobic conditions. Moreover, ArcD did also operate in reverse direction after excess ornithine was supplied in the medium, as seen by ornithine uptake to resynthesize arginine when the supply of the latter was depleted. Again, the uptake of ornithine was significantly faster (about 50%) in the wild-type than in the deletion strain.

Active uptake of ornithine in *Hbt. salinarum* has already been observed by Gonzalez *et al.* (2008) in metabolic modeling and growth experiments. Together with these studies, it confirms the conversion of arginine to ornithine, which is then accumulated in the medium and begins to deplete when the arginine supply is exhausted (pathway shown in part A of Figure 4.2). Nevertheless, ornithine uptake took place slowly in the deletion strain which implies that, there must be an additional uptake system for ornithine.

Haloarchaeal genomes frequently show annotated ABC-transporters or the Na<sup>+</sup>/H<sup>+</sup> antiporter type, which could possibly take over this function. The ornithine experiment shown here (aerobic in the dark) was repeated under aerobic conditions in the light without any significant differences (data not shown). Under illumination the cells of the deletion strain still showed a much slower ornithine uptake than the wild-type.

#### **4.2.4.4 Analysis of arginine fermentation by RNA microarrays and Isotope Coded Protein Labeling (ICPL)**

Already many insightful investigations on the ADI pathway in *Hbt. salinarum* using proteomic tools have been performed in the past by Tebbe (2005); Damsma (2006) and Aivaliotis *et al.* (2011). In these studies, ICPL (Kellermann, 2008) was applied

to the comparative analysis of two pairs of different cellular states of *Hbt. salinarum* through pairwise comparison.

Quantitation was performed by comparing the MS peptide signals of  $^{12}\text{C}$  and  $^{13}\text{C}$ , isotopic peptide pairs corresponding to different growth conditions.

Additionally, it was attempted to investigate global regulation of the arginine metabolism by microarray analysis.

### **Translational analysis could indicate an active ADI pathway in *Hbt. salinarum***

**R+** According to the published genome annotation (Pfeiffer *et al.*, 2008b; Ng *et al.*, 2000), arginine is believed to be an essential amino acid for *Hbt. salinarum*. Since it could be shown in subsection 4.2.4.1 that *Hbt. salinarum* can grow without both, arginine and ornithine, arginine metabolism was investigated in more detail by ICPL.

Strain R+ exhibited a comparatively long lag-phase of approximately ~3.5 days before starting to grow exponentially, but growth experiments were always reproducible. This indicated a long adaptation time in *Hbt. salinarum* to a medium with less carbon sources.

In further experiments, the same *Hbt. salinarum* strain R1 was grown under the same conditions with 2.30 mM arginine ("R-" = experimental conditions for R1) and compared to R+. Cytosolic proteins of R+ and R- were labeled with ICPL (R+ = heavy label, R- = light label) and analyzed with MALDI TOF/TOF MS.

In this study, 415 proteins were identified of which 34 had significantly different expression levels between R+ and R- (shown in Figure S6). Both the arginine deiminase (*arcA*, OE5208R) and the ornithine carbamoyltransferase (*arcB*, OE5205R) were highly upregulated in R+ (29.7-fold and 4.42-fold, respectively). Neither the carbamate kinase (EC5206R) nor the transcription regulator ArcR (OE5209R) were identified and thus could not be quantified.

In *Pseudomonas aeruginosa*, where the ADI pathway has been studied most extensively (Haas *et al.*, 1990), the genes encoding the ADI pathway are organized in an operon and a polycistronic mRNA is transcribed from a single promoter. Ruepp & Soppa (1996) showed that four individual promoters govern *arc* gene transcription in *Hbt. salinarum* but also an *arcRACB* transcript was found amongst others, demonstrating organisation of the genes in one operon. When the genes of the *arcRACB*

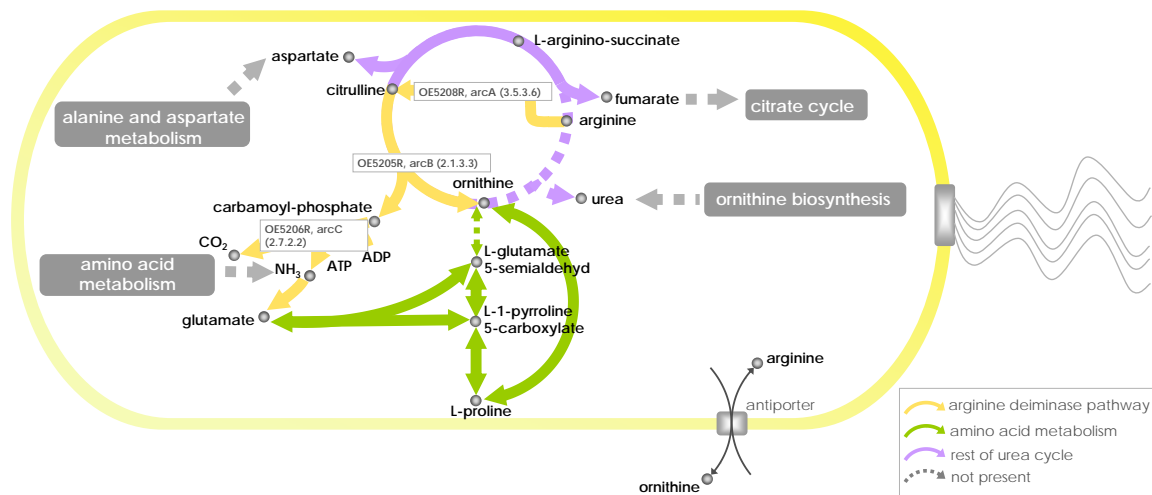


Figure 4.13: **The arginine deiminase (ADI) pathway in *Hbt. salinarum* and possible connections to other pathways.** *Hbt. salinarum* R+ was able to grow in minimal medium without arginine and ornithine. Bridging over the missing components with alternative amino acids (e.g. proline, glutamate) could be one reason for successful growth.

gene cluster (Figure 4.2) were transcribed in one operon under the given conditions, either an upregulation or a downregulation of all four genes would be expected. An upregulation of *arcA* and *arcB* indicated an active ADI pathway in which the cell is trying to compensate the lack of arginine.

Regarding genomic analysis of *Hbt. salinarum* it is clear that all genes required for conversion of ornithine into arginine are present (Gonzalez, 2009). So, the only question is how the organism synthesizes ornithine. *Hbt. salinarum* can convert proline into glutamate.

An upregulation of the ornithine cyclodeaminase (OE2945F) was found by Schwaiger (2009) with *Hbt. salinarum* by a RNA microarray analysis. Since ornithine cyclodeaminase converts proline into ornithine, it is an enzyme of particular interest. However, it was reported in *Clostridium sporogenes* that the ornithine cyclodeaminase only works irreversibly, breaking down ornithine into proline (Costilow & Laycock, 1971) which argues against this hypothesis. In addition, proline can be synthesized by an alternative pathway in *Hbt. salinarum* (Ghosh & Sonawat, 1998).

Another possibility might be the synthesis of ornithine directly via glutamate 5-semialdehyde, using ornithine aminotransferase (EC 2.6.1.13). A candidate for this reaction was found in the genome of *Hbt. salinarum*, OE3168R, which has not been

verified yet experimentally (Gonzalez, 2009).

A model for arginine metabolism in *Hbt. salinarum* summarizing the discussed possibilities is given in Figure 4.13.

Since neither ornithine cyclodeaminase nor ornithine aminotransferase could be identified by GC/MS using ICPL, a characterization of *Hbt. salinarum* R+ by further northern (RNA) blot might offer further insights.

**Microarray analysis did not reveal significant differences in gene expression** RNA microarrays with R- as reference were performed with extracted RNA from the same culture sample from which proteins were isolated for the ICPL experiment above.

The ornithine carbamoyltransferase (ArcB) was detected as the gene with the highest upregulation. This implies that either the ADI pathway or the urea cycle was active but did not give more detailed information about the mechanism of how *Hbt. salinarum* R+ was bridging over the missing arginine/ornithine.

It is assumed that most of the genes of interest relating to the arginine/ornithine metabolism were regulated below a specific threshold of significant regulation. Because of their very low levels of regulation, verification of the microarray data by RT-qPCR was omitted and no further analysis by the microarray technique performed.

## 4.3 Conclusions

In this study, stable isotope labeling of organic carbon sources was used to characterize the amino acid pathways and reaction fluxes of *Nmn. pharaonis*.

Carbon fates were modeled, based on genome annotation data with the program BNet but did not always coincide with the <sup>13</sup>C tracer experiments. These findings indicate that *Nmn. pharaonis* might synthesize some amino acids via alternative biosynthesis pathways (e.g. cysteine and lysine) which has to be investigated in detail. However, it could be shown that the majority of amino acids are synthesized via canonical pathways.

Applying a modeling program for tracking carbon fates in a metabolic network resulted in mixed label types of amino acids. Carbon fates of the modeled pathways were not always consistent with labeling results derived from GC/MS, also due to scrambling of the label in the TCA cycle. Since carbon fate maps (Mu *et al.*, 2007)

used in this study were constructed for general reactions, they might not fit to special archaeal pathways and reactions.

Growth experiments with *Hbt. salinarum* in synthetic medium showed that neither arginine nor ornithine are essential amino acids and also not crucial for good growth (speed and optical density).

Arginine-ornithine uptake experiments with concentrated cell suspensions could verify ArcD, the respective antiporter, as the main arginine uptake system in *Hbt. salinarum*. It is well possible that an additional uptake system for ornithine exists which could eventually be taken over by annotated ABC-transporters or the Na<sup>+</sup>/H<sup>+</sup> antiporter type.

Upregulation of the arginine deiminase (*arcA*, OE5208R) and the ornithine carbamoyltransferase (*arcB*, OE5205R) was observed in *Hbt. salinarum* indicating an active ADI-pathway while omitting ornithine and arginine in the synthetic medium. The translational analysis of the arginine/ornithine metabolism by ICPL led to the conclusion that the adapted *Hbt. salinarum* R+ could grow without arginine and ornithine in synthetic medium, because it might be able to generate ornithine from other amino acids (e.g. proline, glutamate) either catalyzed by an ornithine cyclodeaminase or by an ornithine aminotransferase.

After a particular time of adaptation *Hbt. salinarum* has a very flexible physiology, able to grow well even under harsh conditions (e.g. omitting essential amino acids in medium). This shows again that haloarchaea have evolved many special adaptation strategies to withstand stressful conditions in their natural habitat.

## 5 Carbon fixation in halophilic Archaea

### 5.1 Introduction

The assimilation of carbon dioxide ( $\text{CO}_2$ ) into organic material is quantitatively the most important biosynthetic process on earth. Beside plants and algae, which are known to be solely dependent on the Calvin-cycle to fix  $\text{CO}_2$ , microorganisms also play an important role in autotrophic  $\text{CO}_2$  assimilation. To date, four general pathways are known in autotrophic prokaryotes: (i) the Calvin cycle; (ii) the reductive acetyl-CoA pathway; (iii) the 3-hydroxypropionate cycle; and (iv) the reductive TCA cycle. They all have the ability to reductively transform inorganic carbon into low-molecular-weight building blocks for the biosynthesis of natural compounds.

Generally speaking, the incorporation of inorganic carbon from  $\text{CO}_2$  into cellular carbon requires reducing equivalents and an input of energy. Depending on of energetically unfavorable steps have to be performed by ATP hydrolysis, pathways are differently expensive in energy (listed in Table 5.1). Apart from the Calvin cycle, all known autotrophic pathways start biosynthesis from acetyl-CoA for building blocks, which requires the regeneration of acetyl-CoA using diverse  $\text{CO}_2$  fixation mechanisms. These are introduced in the next subsections.

#### 5.1.1 Calvin cycle (Calvin-Benson-Bassham cycle)

Central to the Calvin cycle (Figure 5.1) is the most abundant enzyme on our planet: the key  $\text{CO}_2$ -fixing enzyme ribulose-1,5-bisphosphate carboxylase-oxygenase (RuBisCO) (Ellis, 1979). Plants, algae, cyanobacteria, and most chemoautotrophic prokaryotes possess type I RuBisCO. A type II enzyme has been identified in only a relatively small number of bacteria. Type III and type IV RuBisCOs have also been described (Hanson & Tabita, 2001). The latter lacks several residues necessary for conventional RuBisCO catalysis and was found in *Bacillus* sp. and oxidizing sulfur bacteria (Tabita *et al.*, 2007). It is referred to as RuBisCO-like protein (RLP) and does not work like

Table 5.1: Comparison of autotrophic CO<sub>2</sub> fixation pathways.

CO <sub>2</sub> fixation pathway	Amount of ATP for synthesis of 1 triose phosphate	Amount of red. equivalents for synthesis of 1 triose phosphate
Calvin cycle	9 ATP	6 NAD(P)H
reductive acetyl-CoA pathway	4 - 5 ATP	3 - 4 NAD(P)H 2 - 3 ferredoxin <sub>red</sub> 1 H <sub>2</sub> (in methanogenes)
3-hydroxypropionate cycle	10 ATP	6 NADPH 1 quinone as e <sup>-</sup> acceptor
reductive TCA cycle	5 ATP	3 NAD(P)H 2 ferredoxin <sub>red</sub> 1 unknown e <sup>-</sup> -donor

An overview of the ATP and reductive equivalents required in the four different pathways of CO<sub>2</sub> assimilation (Lengeler *et al.*, 1999).

RuBisCO enzymes. Type III RuBisCO (Ezaki *et al.*, 1999) is only found in Archaea and has been shown to carboxylate ribulose 1,5-bisphosphate (Maeda *et al.*, 1999, 2002; Finn & Tabita, 2004). The archaeal RuBisCO enzymes possess a unique pentagonal structure essential for their high thermostability (Maeda *et al.*, 2002). They are also unusual in displaying a reversible inhibition by oxygen (Watson *et al.*, 1999). Type I and II enzymes are not oxygen sensitive. However, despite the sequence homology and enzyme activity of type III enzyme, a functional Calvin cycle has not been established and it may instead be involved in AMP metabolism (Sato *et al.*, 2007). The metabolic role of form III RuBisCO is still unclear (Tabita *et al.*, 2007; Berg *et al.*, 2010).

### 5.1.2 Reductive acetyl-CoA pathway

The reductive acetyl-CoA pathway is the only non-cyclic CO<sub>2</sub>-fixation pathway and has the lowest energy consumption (Table 5.1). It is characterized by two key-enzymes (Figure 5.2): the CO-dehydrogenase/acetyl-CoA-synthase complex (Ljungdahl, 1986) and the pyruvate:ferredoxin-oxidoreductase (pyruvate synthase). The enzyme complex catalyzes the reductive synthesis of acetyl-CoA from an enzyme-attached carbonyl group and a methyl group attached to tetrahydropterine. Then the primary CO<sub>2</sub>-fixation product, acetyl-CoA, is carboxylated to pyruvate by an oxidoreductase, which



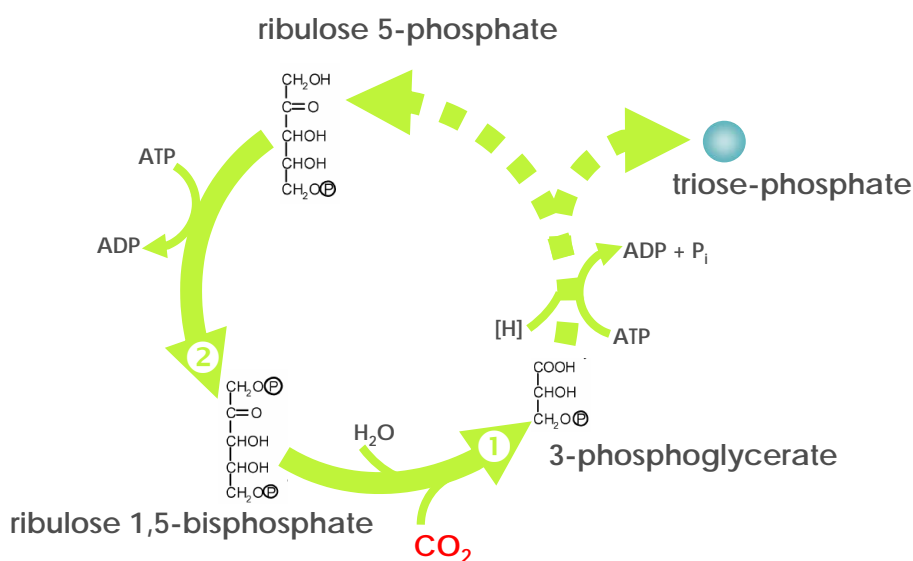


Figure 5.1: **Calvin cycle.** The most important enzyme in the Calvin cycle is the (1) ribulose-1,5-bisphosphate carboxylase-oxygenase (RuBisCO) (EC 4.1.1.39), catalyzing the reductive carboxylation of D-ribulose-1,5-bisphosphate and forming 2 molecules of 3-phosphoglycerate. Besides the RuBisCO, the (2) phosphoribulokinase (EC 2.7.1.19) is also seen as a key-enzyme. It is necessary for replenishment of ribulose-1,5-bisphosphate by phosphorylation of ribulose-5-phosphate.

uses the 2Fe-2S ferredoxin *fdx* as coenzyme. This pathway has been documented in several types of organisms, including homoacetogenic bacteria and methanogenic archaea (Jansen *et al.*, 1982; Stupperich *et al.*, 1983).

### 5.1.3 Fatty acid degradation via propionyl CoA - 3-hydroxypropionate cycle

This pathway was discovered in the green nonsulfur phototrophic bacterium *Chloroflexus aurantiacus* (Holo, 1989). It also seems to operate in a slightly different variant in some acidophilic archaea from the phylum Crenarchaeota, including autotrophic *Acidianus*, *Sulfolobus* and *Metallosphaera* species (Burton *et al.*, 1999; Ishii *et al.*, 1996; Menendez *et al.*, 1999; Norris *et al.*, 1989). In the original 3-hydroxypropionate cycle (Figure 5.3), each turn of the cycle results in the net fixation of two molecules of bicarbonate into one molecule of acetyl-CoA, which is afterwards converted into pyruvate.

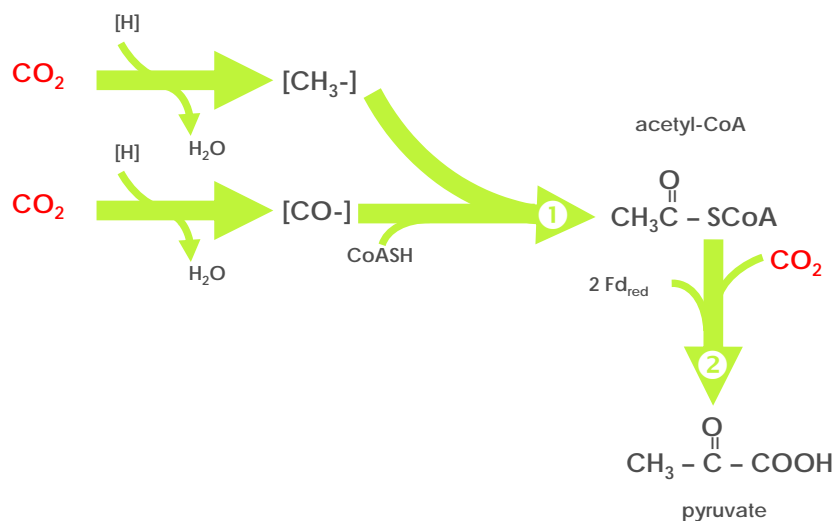


Figure 5.2: **Reductive acetyl-CoA pathway.** The path has both a methyl and carbonyl component. One CO<sub>2</sub> is captured on a special tetrahydrofolate cofactor and reduced to a methyl group. The other CO<sub>2</sub> is reduced to a carbonyl group, and this enzyme-bound carbonyl group is combined with the methyl group to form acetyl CoA by a collection of enzymes termed the (1) CO-dehydrogenase/acetyl CoA synthase complex (EC 1.2.99.2). The (2) pyruvate:ferredoxin-oxidoreductase (pyruvate synthase) (EC 1.2.7.1) carboxylates acetyl CoA to pyruvate (graphic modified from Hügler *et al.* (2003)). [H] reduction equivalent, Fd<sub>red</sub> reduced ferredoxin, [CH<sub>3</sub>-] enzyme-bound methyl group, [CO-] enzyme-bound carbon monoxide group

In the archaeal type, each turn of the cycle captures two molecules of bicarbonate as well, but the carbons are not exported as glyoxylate. Instead, they are converted directly to acetyl-CoA by a route that is similar to that used by *Clostridia* (Kenealy & Waselefsky, 1985) for fermentation of succinate. Enzymes for converting malonyl-CoA first to 3-hydroxypropionate and then to propionyl-CoA by reduction steps are considered to be the key enzymes.

#### 5.1.4 Reductive citrate cycle

The reductive citrate cycle is basically the oxidative, catabolic TCA cycle in reverse (Figure 5.4). Three enzymes, that do not work reversibly in the oxidative TCA cycle, are replaced in the carbon dioxide fixation pathway: ATP-citrate lyase, 2-oxoglutarate:ferredoxin oxidoreductase and fumarate reductase (Schauder *et al.*, 1987). ATP-citrate lyase requires ATP and cleaves citrate (6 carbons) into oxaloacetate (4 carbons) and acetyl CoA (2 carbons). The second important step is the reversible reductive car-

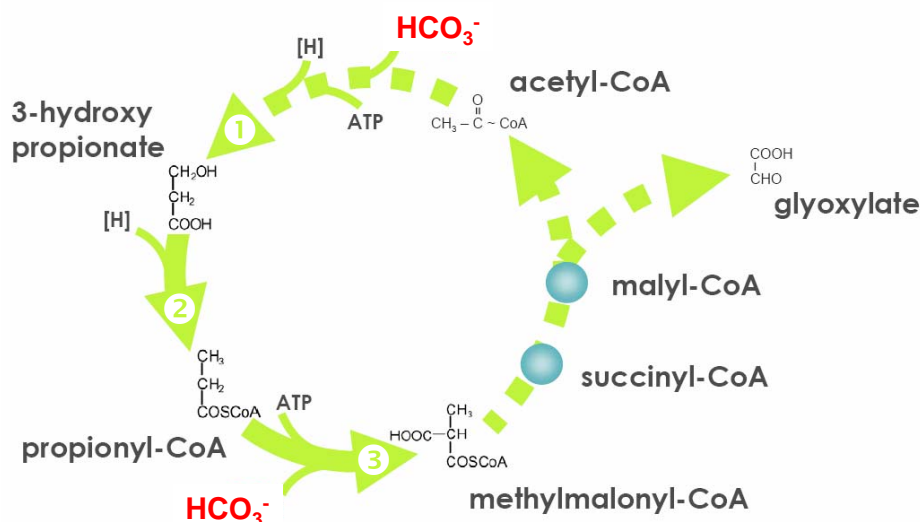


Figure 5.3: **Propionate cycle.** After carboxylation of acetyl-CoA to malonyl-CoA, the latter is reduced with NADPH by (1) malonyl CoA reductase (EC 1.2.1.75, 1.1.1.298) to 3-hydroxypropionate. This is reductively converted to succinyl-CoA by (2) 3-hydroxypropionyl-CoA synthetase (EC 6.2.1.36), 3-hydroxypropionyl-CoA dehydratase (EC 4.2.1.116) and acryloyl-CoA reductase (EC 1.3.1.84). Propionyl-CoA is carboxylated by (3) propionyl-CoA carboxylase (EC 6.4.1.3), fixing another molecule of bicarbonate.

boxylation of succinyl-CoA to 2-oxoglutarate by the 2-oxoglutarate:ferredoxin oxidoreductase. The last of the substituted steps is the reduction of fumarate to succinate. Altogether, two molecules of CO<sub>2</sub> are bound and converted to acetyl-CoA in one cycle, consuming two ATP (Table 5.1).

Green photosynthetic bacteria (*Chlorobium limicola*), thermophilic bacteria (*Hydrogenobacter thermophilus*) growing on hydrogen and certain bacteria that grow by reducing sulfate (*Desulfobacter hydrogenophilus*) have been shown to use the reductive TCA cycle with some minor variations between the species (Evans *et al.*, 1966; Shiba *et al.*, 1985; Schauder *et al.*, 1987).

### 5.1.5 CO<sub>2</sub> fixation in halophilic Archaea

Little research has been done on potential CO<sub>2</sub> assimilation pathways in halophilic Archaea and no convincing evidence for these reactions has been published yet (Oren, 1983). Javor and colleagues showed that *Hbt. salinarum* incorporates CO<sub>2</sub> into cell material (Javor, 1988) and suggested that halobacteria containing purple membrane contribute to light-dependent CO<sub>2</sub> assimilation in the Dead Sea. As a possible mech-

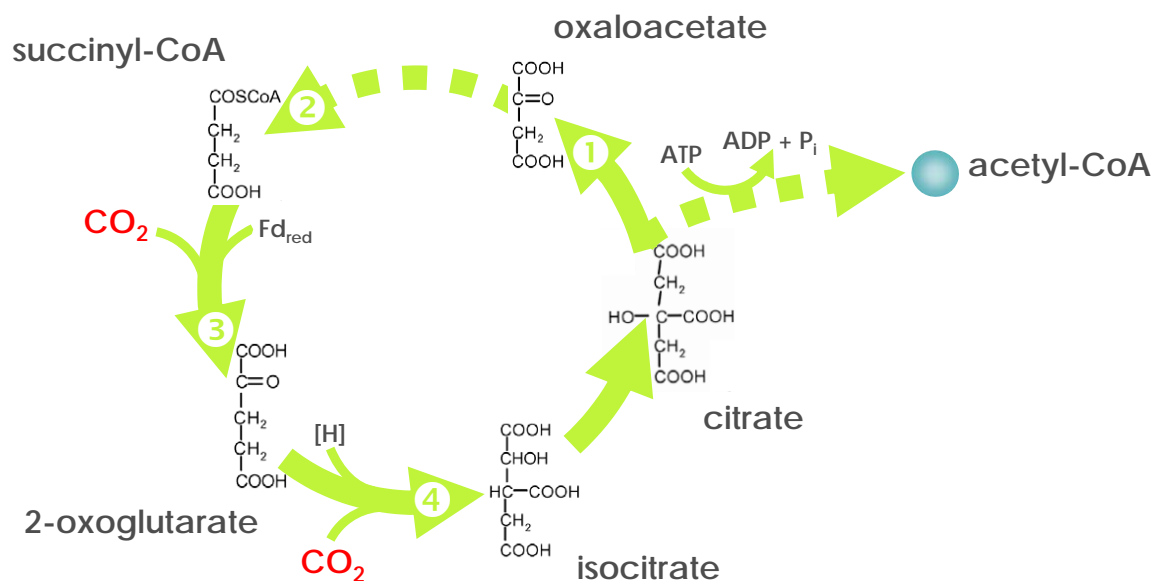


Figure 5.4: **Reductive citrate cycle.** Only three counteracting enzyme pairs are thought to determine the oxidative or reductive direction of the cycle. These three enzymes pushing the cycle in the reductive direction are: (1) ATP-citrate lyase (EC 2.3.3.8), (2) fumarate reductase (EC 1.3.99.1) and (3) 2-oxoglutarate:ferredoxin oxidoreductase (EC 1.2.7.3). Another enzyme, which is indeed reversible but achieves an effective  $\text{CO}_2$  fixation is the (4) isocitrate-dehydrogenase (EC 1.1.1.42).  $[\text{H}]$  reduction equivalent,  $\text{Fd}_{\text{red}}$  reduced ferredoxin

anism, a conversion of  $\text{CO}_2$  and propionyl-CoA into  $\alpha$ -ketobutyrate and CoA was proposed. The aim of the current study was to shed more light on potential  $\text{CO}_2$  fixation pathways in halophilic Archaea. A number of approaches were used including analyses of the gene sequences, stable isotope labeling studies with  $^{13}\text{C}$  carbon sources and transcriptional studies by RT-PCR.

## 5.2 Results and discussion

### 5.2.1 Homology comparison in archaeal genomes

An extensive analysis of the metabolic pathways of halophilic archaea has been reported previously (Falb, 2005). Using this as a starting point, the current study has relied on more recent information from relevant publications, including data from newly annotated genomes. These are described below.

### 5.2.1.1 Different potential CO<sub>2</sub> fixation pathways were found in halophilic archaea

ORFs that were annotated as carboxylating (CO<sub>2</sub> fixating) enzymes were retrieved from the genomes of *Nmn. pharaonis* and *Hbt. salinarum*, and are listed in Table S3. Reactions which proceed spontaneously or cannot be alloted to a specific pathway were not included in this list. Only enzymes specifying reactions that could be meaningfully arranged into one pathway are discussed in the following sections. Whether a pathway is active or not depends not only on the presence of key enzymes but also on other factors, including different energy requirements of the pathways and consequently different growth yield, metabolic flexibility allowing rapid metabolic switches or simultaneous assimilation of specific fermentation products, oxygen tolerance of the key enzymes and affinities for CO<sub>2</sub> or bicarbonate. Another critical issue is the involvement of redox potentials of the individual oxidoreductases and electron carriers in the cell. For example, the conversion of acetyl-CoA into pyruvate by the pyruvate:ferredoxin oxidoreductase depends strongly on the ferredoxin redox potential (subsubsection 5.2.1.5).

### 5.2.1.2 Calvin cycle could be excluded

Some homologous genes in haloarchaea encoding enzymes in the Calvin cycle could be found (Table 5.2), but many steps were missing in the cycle. The following enzymes could not be found in the genomes of *Nmn. pharaonis*, *Hbt. salinarum* and *Nmn. moolapensis*: transketolase (EC 2.2.1.1), fructose-6-phosphate phosphoketolase (EC 4.1.2.22), fructose-1,6-bisphosphatase II / sedoheptulose-1,7-bisphosphatase (EC 3.1.3.11, 3.1.3.37) and phosphoribulokinase (EC:2.7.1.19). RuBisCO has been found in many archaea that were not reported to be able to grow autotrophically as well as in some Euryarchaeota that grow autotrophically but use the reductive acetyl-CoA pathway for CO<sub>2</sub> fixation. Phosphoribulokinase, the second key enzyme of the Calvin cycle, is also absent in archaea, except a few methanogenes (Mueller-Cajar & Badger, 2007). Sequence homology analysis showed that only four species of halophilic archaea carry a RuBisCO gene. These are *Nmn. pharaonis* (NP2770A), *Hfx. volcanii*, *Nab. magadii* and *Hmc. mukohataei*. Homologues could neither be found in *Hbt. salinarum* nor in *Nmn. moolapensis*. A phylogenetic tree (Figure 5.5) constructed based on these sequences shows that the halophilic RuBisCO forms a clade,

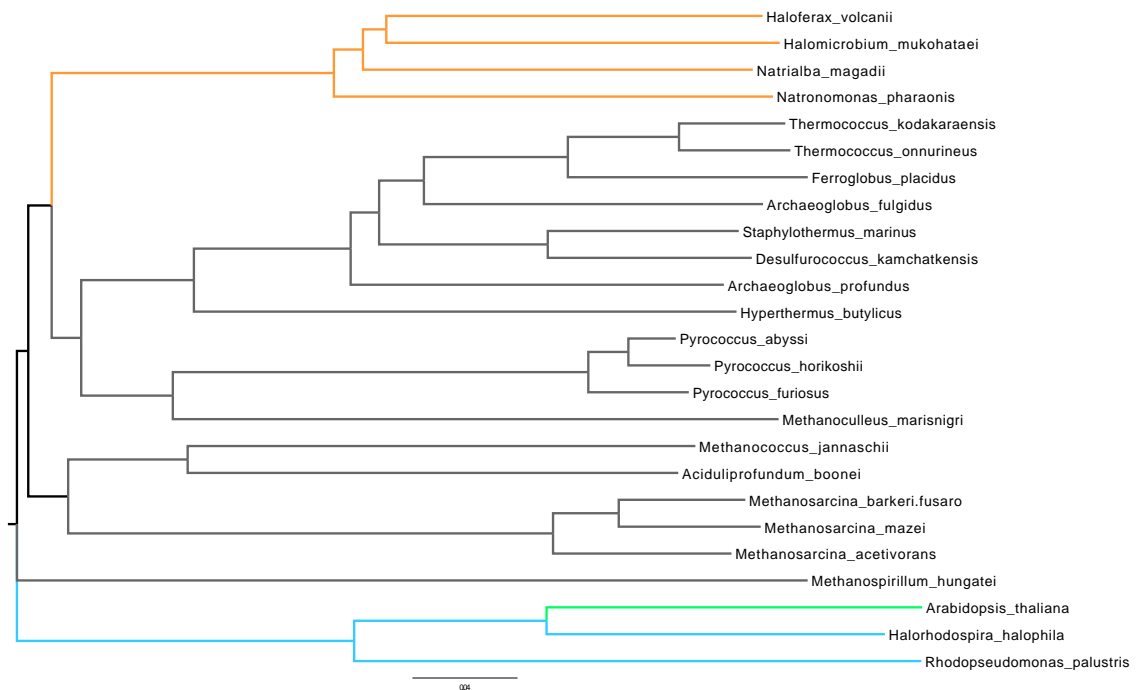


Figure 5.5: **Phylogenetic tree of the archaeal RuBisCO.** The four haloarchaeal RuBisCO proteins (orange) are compared to representative other archaeal (grey), bacterial (blue) and an eukaryotic protein (green). The length of the scale bar (0.04) represents 4% sequence distinction.

distinct from the thermophilic archaea and the methanogens. The tree also shows that the halophilic bacterium *Halorhodospira halophila* has a higher sequence homology to the eukaryotic RuBisCO than to the bacterial type. Other phylogenetic analyses about the archaeal RuBisCO show that it originates from the methanogenic Euryarchaeota (Tabita *et al.*, 2007) and that the Calvin cycle appeared late in evolution (Wächtershäuser, 1990).

Since *Nmn. pharaonis* possess a gene encoding the archaeal RuBisCO with an enigmatic function, its integration in other pathways than the Calvin cycle was investigated.

**Archaeal RuBisCO type III and its involvement in AMP metabolism** In the hyperthermophilic archaeon *Thermococcus kodakaraensis*, the archaeal RuBisCO was linked to the AMP metabolism (Sato *et al.*, 2007) and in *Nmn. pharaonis*, homologs for all the genes of this novel AMP recycling pathway could be detected. Hence, it represents the only known haloarchaeal species able to employ this pathway (reactions # 1

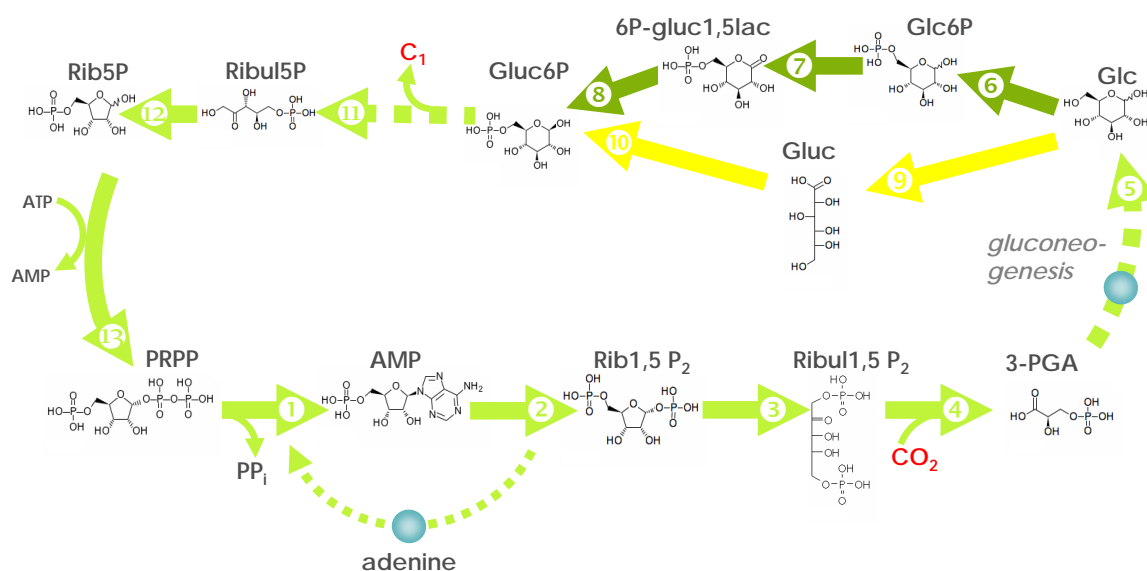


Figure 5.6: **CO<sub>2</sub> fixation cycle using RuBisCO in *Nmn. pharaonis*.** Enzymes: (1) adenine phosphoribosyltransferase, (2) AMP phosphorylase, (3) ribose-1,5-biphosphate isomerase, (4) type III RuBisCO, (5) phosphoglycerate kinase, glyceraldehyde-3-phosphate dehydrogenase, fructose-bisphosphatase, fructose-bisphosphatase, glucose-6-phosphate isomerase, (6) glucokinase, (7) glucose 6-phosphate dehydrogenase, (8) 6-phosphate gluconolactonase, (9) glucose-dehydrogenase, (10) gluconokinase, (11) non-oxidative conversion of C<sub>6</sub> to C<sub>5</sub>, (12) ribose-5-phosphate isomerase, (13) ribose-phosphate pyrophosphokinase. Compounds: AMP - adenosine monophosphate, Rib1,5P<sub>2</sub> - ribose 1,5-bisphosphate, Ribul1,5P<sub>2</sub> - ribulose 1,5-bisphosphate, 3-PGA - 3-phosphoglycerate, Glc - glucose, Glc6P - glucose 6-phosphate, Gluc - gluconate, Gluc6P - gluconate 6-phosphate, 6P-gluco1,5-lac - 6P-glucono 1,5-lactone, Ribul5P - ribulose 5-phosphate, Rib5P - ribose 5-phosphate.

- # 4 in Figure 5.6). Since *Nmn. pharaonis* does not possess an ADP-dependent sugar kinase for AMP production, AMP was generated by the salvage pathway for purines. While AMP is recycled and adenine and 3-phosphoglycerate are released, CO<sub>2</sub> can be fixed by RuBisCO. In the salvage pathway, the free purine bases, adenine, guanine and hypoxanthine, can be reconverted to their corresponding nucleotides by phosphoribosylation. The corresponding enzyme, adenine phosphoribosyl transferase, is annotated in the genome of *Nmn. pharaonis* and transfers pentose phosphate (PP) into the purine precursor 5-phosphoribosyl 1-pyrophosphate (PRPP). 3-phosphoglycerate can be converted by the gluconeogenesis pathway to glucose 6-phosphate. To complete the cyclic pathway a non-oxidative conversion of a C<sub>6</sub> compound into a C<sub>5</sub> is necessary. In Figure 5.6, this step is represented by reaction number 11, where a C<sub>1</sub> compound is released.

However, the presence of the PP pathway is still unclear in haloarchaea. Soderberg

and colleagues performed a phylogenetic analysis of the PP metabolism employing data from several archaeal genomes (Soderberg, 2005). It was suggested that haloarchaea operate part of the non-oxidative and a modified oxidative PP pathway for pentose formation. The oxidative PP was investigated in more detail in *Hbt. salinarum* by enzyme activity assays in cell-free extracts (Daniela Breckau, unpublished results). Enzyme activities could be measured for the following enzymes (numbers in brackets correspond to the enzymes illustrated in Figure 5.6): glucose 6-phosphate dehydrogenase (# 7), glucose-dehydrogenase (# 9) and ribose-5-phosphate isomerase (# 12). Aitken & Brown (1969) have measured activity for the glucose 6-phosphate dehydrogenase too. The assays performed by D. Breckau were able to show a possible oxidative conversion of gluconate 6-phosphate to ribulose 5-phosphate, releasing CO<sub>2</sub> by a 6-phosphogluconate dehydrogenase. Enzyme activity could be measured in the presence of NAD. However, in the presence of NADP, being the common coenzyme of this reaction, no activity could be detected. No homologous genes in any haloarchaeon for the glucose 6-phosphate dehydrogenase (# 7), the 6-phospho gluconolactonase (# 8) nor the gluconokinase (# 10) could be found. But it is assumed that a general sugar kinase with a yet unassigned substrate could function as gluconokinase (e.g. OE1266R, OE3606R, OE4535F in *Hbt. salinarum*) and that one of the general kinases represents # 10. Homologs in *Nmn. pharaonis* and *Nmn. moolapensis* for the mentioned enzymes are listed in Table 5.2.

Two non-oxidative pathways for conversion of a C<sub>6</sub> sugar to a C<sub>5</sub> sugar are known in archaea: (i) a non-oxidative PP pathway and (ii) a reverse ribulose monophosphate (RuMP) shunt, in which a C<sub>1</sub> compound is emitted as formaldehyd. In haloarchaea, only one homolog for the non-oxidative PP, ribose-5-phosphate isomerase and none for the RuMP shunt could be detected by sequence analysis. A possible CO<sub>2</sub> fixation cycle can be only accomplished in *Nmn. pharaonis* without an oxidative conversion to ribulose 5-phosphate. Currently, it is not clear whether or not *Nmn. pharaonis* has such a cycle or if it operates (i) a new conversion or (ii) uses atypical enzymes for an existing conversion pathway. Ribulose 1,5-bisphosphate, the substrate of RuBisCO and at the same time CO<sub>2</sub> acceptor, is not directly synthesized by phosphorylation of ribulose 5-phosphate in a two step reaction with PRPP as intermediate (Finn & Tabita, 2004).

In conclusion, a new cyclic CO<sub>2</sub> fixation pathway (Figure 5.6) might operate in



Table 5.2: Corresponding gene homologs found in *Nmn. pharaonis*, *Hbt. salinarum* and *Nmn. moolapensis* encoding enzymes of the AMP-CO<sub>2</sub> fixation cycle.

Protein name	EC number	Accession number		
adenine phosphoribosyltransferase	2.4.2.7,	NP1254A,	OE1840R,	Nmlp_1547
	2.4.2.22	NP1426A	OE3951R	Nmlp_2103
AMP phosphorylase	2.4.2.-	NP3958A	-	-
ribose-1,5-biphosphate isomerase	5.3.1.-	NP3202A	OE3610R	Nmlp_3882
type III RuBisCO	4.1.1.39	NP2770A	-	-
phosphoglycerate kinase	2.7.2.3	NP4130A	OE2745R	Nmlp_2427
glyceraldehyde-3-phosphate dehydrogenase	1.2.1.59	NP0012A	OE1154F	Nmlp_1502
fructose-bisphosphate aldolase	4.1.2.13	NP1594A	OE2019F	Nmlp_2892
fructose-bisphosphatase	3.1.3.11	NP1592A	OE2020F	Nmlp_2893
glucose-6-phosphate isomerase	5.3.1.9	NP4992A	OE3792F	Nmlp_2148
glucose-6-phosphate 1-dehydrogenase	1.1.1.49	-	<i>a</i>	-
6-phosphogluconate dehydrogenase	1.1.1.44	NP0286A	OE4581F	Nmlp_1412
ribose-5-phosphate isomerase	5.3.1.6	NP0786A	OE4185F	Nmlp_1011
ribose-phosphate pyrophosphokinase	2.7.6.1	NP0606A	OE4085R	Nmlp_3571

Because genes for AMP phosphorylase and type III RuBisCO are absent in the genome of *Hbt. salinarum* and *Nmn. moolapensis*, CO<sub>2</sub> fixation via this pathway can be excluded. Although none of these organisms encodes a gene homolog for glucose-6-phosphate 1-dehydrogenase, this reaction step could be proven experimentally (*a*) in *Hbt. salinarum*. Ordered locus tags (protein) of *Nmn. pharaonis* start with "NP", those of *Hbt. salinarum* begin with "OE" while the tags for *Nmn. moolapensis* are abbreviated with "Nmlp".

*Nmn. pharaonis*, one that includes reaction steps of a non-oxidative pentose phosphate pathway, the Calvin cycle, gluconeogenesis and the purine salvage pathway. Based on these findings, transcriptional analyses were performed to search for experimental evidence for an active RuBisCO enzyme and its biosynthesis pathway, presented in subsection 5.2.3. Since *Nmn. pharaonis* belongs to the small group of haloarchaea harboring a RuBisCO gene (none found in the *Nmn. moolapensis* genome) it was aimed to explain its enigmatic function in this organism.

### 5.2.1.3 Improbable CO<sub>2</sub> fixation by the reductive acetyl-CoA pathway

*Nmn. pharaonis*, *Hbt. salinarum* and *Nmn. moolapensis* contain pyruvate:ferredoxin oxidoreductase (pyruvate synthase) (NP4044A, NP4046A; OE2622R, OE2623R; Nmlp\_3264, Nmlp\_3265) as one potential carboxylating enzyme, but appear to lack homologues of the other key enzyme of the reductive acetyl-CoA pathway. No genes for

the CO-dehydrogenase/acetyl CoA synthase complex could be detected in any of the three organisms. Nevertheless, it is possible that the ferredoxin-dependent oxygen-sensitive pyruvate synthase could catalyze a CO<sub>2</sub> fixation step in combination with the reductive citrate cycle (subsubsection 5.2.1.5). There, one molecule acetyl-CoA is generated from two molecules CO<sub>2</sub>. This could be further carboxylated to pyruvate by the pyruvate synthase.

#### 5.2.1.4 3-hydroxypropionate cycle

Key enzymes such as the malonyl CoA reductase and the 3-hydroxypropionyl-CoA synthetase for a functional 3-hydroxypropionate cycle, as observed in other archaea, are not encoded in the genomes of *Nmn. pharaonis*, *Hbt. salinarum* and *Nmn. moolapensis*. A complete 3-hydroxypropionate cycle could not be established in any of the sequenced haloarchaea (present enzymes are listed in Table 5.3). Since the propionyl-CoA carboxylase is indeed encoded in those halophilic genomes, it is assumed that the enzyme catalyzes the CO<sub>2</sub> fixation via a non-cyclic pathway which is described below and presented in Figure 5.7.

**Fatty acid degradation in haloarchaea** In haloarchaea and most other archaea, genes are present for the degradation of activated fatty acids via the  $\beta$ -oxidation pathway. Since the chain-length specificity of these enzymes is currently unknown, fatty acid degradation might be limited to short chain lengths (e.g. for derivatives of branched-chain amino acids). In comparison to the other halophilic organisms, *Nmn. pharaonis* carries many more genes for paralogs for one particular step of the four-step reaction sequence of the  $\beta$ -oxidation. This was also noted for the genes encoding enzymes for the previous steps in  $\beta$ -oxidation. Consistent with these findings, growth experiments showed that *Nmn. pharaonis* is able to grow on fatty acids of various lengths as the carbon source (especially C<sub>14</sub>). Fatty acids do not appear to be used by *Hbt. salinarum* and the presence of long-chain (C<sub>14</sub>–C<sub>18</sub>) and medium-chain fatty acids (C<sub>14</sub>) has been shown to reduce growth (Königsmaier, 2006). Active carbon assimilation by employing fatty acid degradation in the mentioned halophiles is most likely. However, it is not clear how efficient the incorporation of carbons from CO<sub>2</sub> is in comparison to the whole carbon metabolism via respiration.

Chains with an odd number of carbons are oxidized in the same manner as even-

numbered chains, but the end products of the last cycle of fatty acid degradation of odd-numbered fatty acids are acetyl-CoA and a three chained propionyl-CoA (instead of two molecules acetyl-CoA). Genes for these enzymes could be found in *Nmn. pharaonis*, *Hbt. salinarum* and *Nmn. moolapensis*, indicating a functional degradation pathway for odd-numbered fatty acids Table 5.3.

**Possible CO<sub>2</sub> fixation via propionyl-CoA** Propionyl-CoA is not a common metabolic intermediate in other pathways, so it must be converted into something else to be effectively metabolized. The activated C<sub>3</sub>-unit of it enters the citrate cycle after conversion into succinyl-CoA. Propionyl-CoA is also involved in some amino acid degradation pathways. For example, propionyl-CoA can be derived from the metabolism of the branched chain amino acids by acetyl-CoA acyltransferase. Also glycine, serine, threonine, cysteine and methionine can be catalyzed by cystathionine synthase/lyase to 2-oxobuturate and afterwards converted to propionyl-CoA.

Its conversion to succinyl-CoA is accompanied by CO<sub>2</sub> fixation. If the reductive citrate cycle could take place (subsubsection 5.2.1.5), succinyl-CoA would have been channeled into it allowing further fixation of carbon dioxide.

Three enzymes are essential for the conversion of propionyl-CoA to succinyl-CoA by fixing a bicarbonate ion: propionyl-CoA carboxylase (EC 6.4.1.3), methylmalonyl epimerase (EC 5.1.99.1) and methylmalonyl-CoA mutase (EC 5.4.99.2). Homologous genes for all of them could be found in haloarchaea (Table 5.3). In order to convert a C<sub>3</sub> compound (propionyl-CoA) into a C<sub>4</sub> compound (succinyl-CoA), one of the first steps in this pathway is the carboxylation of propionyl-CoA with an input of energy from ATP. The propionyl-CoA-carboxylase uses biotin as a cofactor.

While *Nmn. pharaonis* expresses most enzymes required for the biosynthesis of biotin, these genes are largely absent in *Hbt. salinarum* and *Nmn. moolapensis* and so biotin must be supplied to the synthetic medium to allow growth. Cobalamin (a derivate of vitamin B<sub>12</sub>) is the coenzyme of methylmalonyl-CoA mutase, which catalyzes an intramolecular shifting of the -CO-S-CoA group. Quantitative proteomic experiments in *Hbt. salinarum* showed an induction of a whole series of genes involved in cobalamin biosynthesis (Tebbe *et al.*, 2009) after shifting from anaerobic to aerobic growth conditions.

Summing up these results, all three haloarchaea have the genetic requirements (Table 5.3) for CO<sub>2</sub> fixation via propionyl-CoA. Quantitative proteomics data of

Table 5.3: Homolog genes found in *Nmn. pharaonis*, *Hbt. salinarum* and *Nmn. moolapensis* encoding enzymes for CO<sub>2</sub> fixation via propionyl-CoA.

Protein name	EC number	Accession number		
propionyl-CoA carboxylase	6.4.1.3	NP3464A	OE1939F	Nmlp_3307
		NP4250A	OE3175F	
		NP4252A	OE3177F	
		NP4364A		
		NP4368A		
methylmalonyl-CoA epimerase	5.1.99.1	NP1228A	OE1718R	Nmlp_2070
methylmalonyl-CoA mutase	5.4.99.2	NP1226A	OE1721R	Nmlp_2010
		NP2320A	OE1972F	Nmlp_2071
		NP2710A	OE2005F	Nmlp_3131
cystathionine synthase/lyase	4.4.1.1	NP4746A	OE2681F	
			OE2173F	
acetyl-CoA acyltransferase	2.3.1.16	NP2214A	OE2011R	Nmlp_2716
		NP2260A	OE3884F	Nmlp_3125
		NP2606A		Nmlp_3314
		NP2612A		
		NP3420A		
		NP3438A		
		NP3650A		
		NP4580A		

Ordered locus tags (protein) of *Nmn. pharaonis* start with "NP", those of *Hbt. salinarum* begin with "OE" while the tags for *Nmn. moolapensis* are abbreviated with "Nmlp".

specific cofactor biosynthesis support an active pathway during aerobic growth of *Hbt. salinarum*. If the derivation of the cell carbon from CO<sub>2</sub> by carboxylation of propionyl-CoA is efficient enough to account for a dectable part of the cell's carbon pool is questionable and discussed further in the experimental part of this chapter.

The CO<sub>2</sub> species assimilated in this pathway distinguishes it from the other mentioned pathways. Here, bicarbonate (HCO<sub>3</sub><sup>-</sup>) is used as the inorganic carbon compound. In alkaline water the concentration of bicarbonate is much higher than the concentration of dissolved CO<sub>2</sub> and therefore the haloalkaliphilic organism *Nmn. pharaonis* might profit from using bicarbonate instead of CO<sub>2</sub>. The biotin-dependent enzyme propionyl-CoA carboxylase, part of the proposed CO<sub>2</sub> fixation pathway via propionyl-CoA introduces bicarbonate into the network.

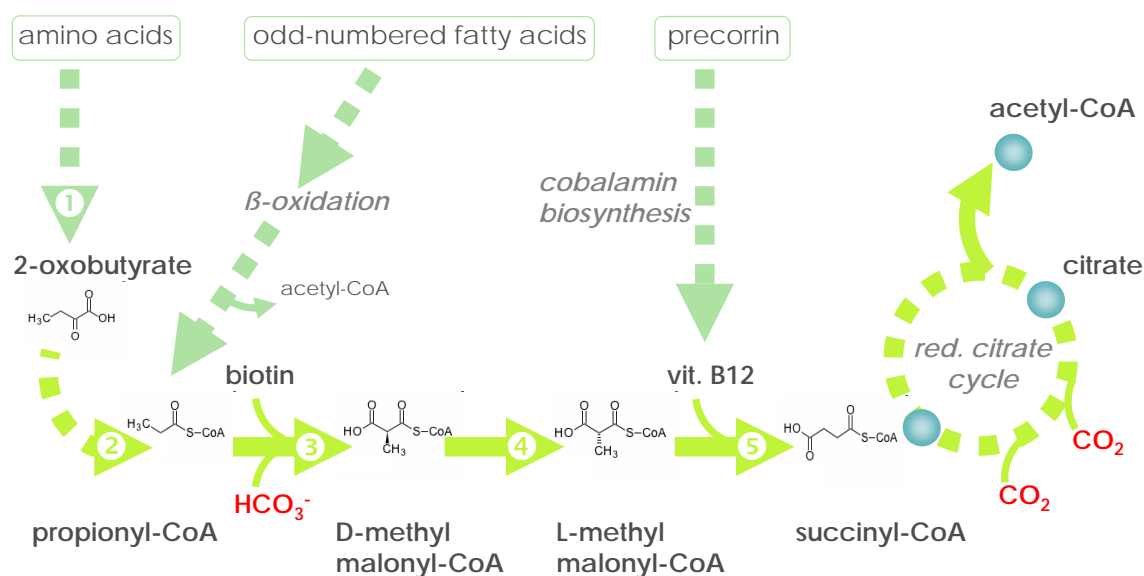


Figure 5.7: **Hypothetical CO<sub>2</sub> fixation pathway via propionyl-CoA.** Enzymes: (1) cystathionine synthase/lyase (EC 4.4.1.1) or acetyl-CoA C-acyltransferase (2.3.1.16) for branched chain amino acids, (2) phosphate acetyltransferase (EC 2.3.1.8), (3) propionyl-CoA carboxylase (EC 6.4.1.3), (4) methylmalonyl-CoA epimerase (EC 5.1.99.1), (5) methylmalonyl-CoA mutase (EC 5.4.99.2)

### 5.2.1.5 The reductive citrate cycle is possible in *Hbt. salinarum*

Since genes for the complete TCA cycle are present in the genomes of haloarchaea, and the enzyme activities for all of the corresponding enzymes have been demonstrated in *Hbt. salinarum* (Aitken & Brown, 1969; Hubbard & Miller, 1972; Kerscher & Oesterhelt, 1981a,b; Gradin *et al.*, 1985), only the irreversible enzymes for the reductive direction were examined in this study. All enzymes accomplishing the reversible steps could be found in the genomes of *Hbt. salinarum* and *Nmn. pharaonis* (Table 5.4). In *Nmn. moolapensis*, the ATP-citrate lyase gene is interrupted by two stop codons so converting it to a (non-functional) pseudogene. Neither paralogs nor homologues for this enzyme could be found in the genome, but it is possible that other enzymes with a similar substrate specificity could bridge this step, since all other genes for this cycle are present in the *Nmn. moolapensis* genome.

Reversal of the TCA cycle normally occurs under anaerobic growth conditions, but *Nmn. pharaonis* is only able to grow to a high cell density under aerobic conditions. However, local anaerobic conditions due to oxygen consumption in a rapidly growing culture might allow CO<sub>2</sub> fixation in this organism via the proposed pathway. Pyru-

Table 5.4: Homolog genes found in *Nmn. pharaonis*, *Hbt. salinarum* and *Nmn. moolapensis* encoding enzymes for the reductive citrate cycle.

Protein name	EC number	Accession number		
ATP citrate lyase/synthase	2.3.3.8	NP4244A	OE1942F	Nmlp_2832
2-oxoglutarate:ferredoxin oxidoreductase	1.2.7.3	NP1232A	OE1710R	Nmlp_3098
		NP1234A	OE1711R	Nmlp_3489
		NP3012A		Nmlp_3490
				Nmlp_3698
succinate dehydrogenase	1.3.99.1	NP4264A	OE2865R	Nmlp_1978
		NP4266A	OE2866R	Nmlp_1979
		NP4268A	OE2867R	Nmlp_1980
		NP4270A	OE2868R	Nmlp_1981
isocitrate dehydrogenase (NADP+) ferredoxins (iron-sulphur proteins)	1.1.1.42 -	NP2430A	OE3634F	Nmlp_2982
		NP0494A	OE1658F	Nmlp_1852
		NP1272A	OE4217R	Nmlp_2556
		NP3692A	OE4324R	Nmlp_2737
		NP3792A	OE4496R	Nmlp_3291
		NP4568A	OE4583F	Nmlp_3770
		NP4586A		Nmlp_3934
		NP4918A		Nmlp_1791

Ordered locus tags (protein) of *Nmn. pharaonis* start with "NP", those of *Hbt. salinarum* begin with "OE" while the tags for *Nmn. moolapensis* are abbreviated with "Nmlp".

vate:ferredoxin oxidoreductase, which is responsible for conversion of acetyl-CoA into pyruvate, was also found. Again, an open question is the reversibility of the oxidative decarboxylation of pyruvate and oxoglutarate. Both enzymes, which were purified and characterized by Kerscher & Oesterhelt (1981b) in *Hbt. salinarum*, are dependent on iron-sulphur proteins that mediate electron transfer (Kerscher & Oesterhelt, 1977). These enzymes use 2Fe-2S ferredoxin *fdx* as a coenzyme, with a redox potential of -345 mV (Kerscher *et al.*, 1976), while the iron sulphur centers of the enzymes themselves have redox potentials of -390, -515, and -540 mV (Pieulle *et al.*, 1997). It is therefore likely that the reverse reactions would be very slow in comparison to the rapid forward reactions (to succinyl- and acetyl-CoA). To overcome this large difference in redox potential, another ferredoxin, *fer4* 3Fe-4S, could be used. It has two redox potentials of -340 and -520 mV (unpublished results of Oesterhelt, Kerscher and Cammack) and is highly homologous to the 3Fe-4S type ferredoxin of *Thermoplasma acidophilum* (Kerscher *et al.*, 1982; Wakabayashia *et al.*, 1983).

Table 5.5: Genes found in *Nmn. pharaonis*, *Hbt. salinarum* and *Nmn. moolapensis* encoding enzymes of the reductive glycine cleavage system.

Protein name	EC number	Accession number		
glycine dehydrogenase (P-protein)	1.4.4.2	NP4594A	OE3274R	-
		NP4596A	OE3275R	
aminomethyltransferase (T-protein)	2.1.2.10	NP0436A	OE3278R	Nmlp_3564
		NP4774A		
dihydrolipoamide dehydrogenase (L-protein)	1.8.1.4	NP0104A	OE4116F	Nmlp_2291
hydrogen carrier protein (H-protein)	-	NP4772A	OE3277R	Nmlp_2988
serine/glycine hydroxymethyltransferase	2.1.2.1	NP2050A	OE3036F	Nmlp_3079

Ordered locus tags (protein) of *Nmn. pharaonis* start with "NP", those of *Hbt. salinarum* begin with "OE" while the tags for *Nmn. moolapensis* are abbreviated with "Nmlp".

### 5.2.1.6 Reductive condensation of carbon dioxide by the glycine cleavage system

In Bacteria and in mitochondria of animals and plants oxidative decarboxylation can be catalyzed by the glycine cleavage system (Kikuchi, 1973). Glycine is catabolized by attaching a lipoyl group to a conserved lysine residue while the carboxyl carbon is released as CO<sub>2</sub> and the methylene carbon as N<sup>5</sup>, 10-methylenetetrahydrofolate (Bender, 1985) (Glycine + H<sub>4</sub>folate + NAD<sup>+</sup>  $\rightleftharpoons$  5,10-methylene-H<sub>4</sub>folate + CO<sub>2</sub> + NH<sub>3</sub> + NADH + H<sup>+</sup>). The complex consists of four different proteins: (i) glycine dehydrogenase (P-protein), (ii) H-carrier protein (H-protein), (iii) dihydrolipoyl dehydrogenase (L-protein), (iv) aminomethyltransferase (T-protein). The H-protein shuttles the methylamine group of glycine from the P-protein to the T-protein. The glycine cleavage system's multienzyme complex is readily reversible, and can together with serine hydroxymethyltransferase catalyze the reductive condensation of carbon dioxide and ammonium with serine to yield two molecules of glycine (Bender, 1985; Andreesen, 1994). Archaea could use this multienzyme complex in the reverse direction in conjunction with CO<sub>2</sub> fixation pathway. Except for the missing P-protein in *Nmn. moolapensis*, all genes for the complex and the serine/glycine hydroxymethyltransferase could be detected in *Nmn. pharaonis*, *Hbt. salinarum* and *Nmn. moolapensis* (Table 5.5).

While the genes for P-, T-, and H-protein are organized in a single gene cluster in *Hbt. salinarum* (OE3274R-OE3278R), the corresponding genes in *Nmn. pharaonis* and *Nmn. moolapensis* are scattered throughout the whole genome. In *Nmn. moolapensis*,

only a paralog of the T-protein, a so called "homolog to T-protein", is encoded in the genome which is indeed present in *Nmn. pharaonis* too, but only in addition to the T-protein itself. This could indicate a non-functional glycine cleavage system in *Nmn. moolapensis*. Hence, *Hbt. salinarum* possesses the highest probability for a functional CO<sub>2</sub> assimilation by glycine biosynthesis via the glycine cleavage system.

## 5.2.2 Stable isotope labeling with <sup>13</sup>C carbonate in *Nmn. pharaonis*

In analogy to subsection 3.2.2, *Nmn. pharaonis* was grown in minimal medium either in presence of unlabeled carbon sources, U-<sup>13</sup>C<sub>2</sub> acetate or <sup>13</sup>C carbonate. Growth with <sup>13</sup>C carbonate and <sup>12</sup>C acetate took place under complete exclusion of natural air. A minimal medium was prepared in an anaerobic chamber filled with N<sub>2</sub> (95 %) and H<sub>2</sub> (5 %) to avoid assimilation of CO<sub>2</sub> from natural air. During growth, the medium was flushed automatically with synthetic air (N<sub>2</sub> 80 %, O<sub>2</sub> 20 %) for 5 min once an hour. Under these conditions cells could only fix the labeled CO<sub>2</sub> dissolved in the medium.

### 5.2.2.1 NMR spectra showing possible CO<sub>2</sub> fixation

2D FHSQC NMR measurements were performed on the lipids from *Nmn. pharaonis* grown on three differently labeled carbon sources: (A) unlabeled acetate and carbonate, (B) U-<sup>13</sup>C<sub>2</sub> acetate and unlabeled carbonate, (C) unlabeled acetate and <sup>13</sup>C carbonate. As shown in Figure 5.8 (A), traces of the naturally abundant carbon-13 were readily detectable in lipids from cells grown on unlabeled carbon sources. In panel (B), the addition of <sup>13</sup>C-acetate has greatly enhanced the labeling of lipids compared to that seen in panel (A). All unlabeled carbons of the isoprenoid chain were substituted for carbon-13. In the final spectrum (C), the level of enrichment of <sup>13</sup>C was between that seen in experiments (A) and (B). Initially, it was assumed that <sup>13</sup>C enrichment by incorporation of <sup>13</sup>CO<sub>2</sub> had occurred. Thus assimilation of inorganic carbon and further processing of the labeled carbon to lipids was possible in this halophilic archaeon. However, the amount and quality of the extracted lipids as well as the measurement itself can vary between the different samples. Hence, signals were integrated (the procedure is described in detail in section 2.5.8.1) and normalized values compared again in Table 5.6. In Figure 5.9 the integrated peaks from Figure 5.8-C,



showed a higher enrichment than the natural abundance of Figure 5.8-A measured in the unlabeled sample.

Comparison of the unlabeled sample with the  $^{13}\text{CO}_2$  sample showed that the average enrichment per C-atom in the labeled sample has increased by 20.6 % (calculated with the arithmetic mean of enrichment of all C-atoms per sample). This number also fits a rough estimation from the comparison of spectrum (A) with (C) in Figure 5.8 with the naked eye. This leads to the conclusion that although  $\text{CO}_2$  fixation took place, most of the metabolized carbon was incorporated from the non-labeled acetate, which is typical for a heterotrophic (or facultative autotrophic) organism.

It should be noted that the result of the ability or inability to assimilate  $^{13}\text{CO}_2$ , strongly depends on its environment and growth conditions. The genetic predisposition (the phylogeny) of an organism provides the basis if a pathway can be used. But the constraints of the occupied niche (the ecology) is at least as important as the phylogeny. This also means, that if the organism is cultured in the laboratory in a medium and under conditions which are suboptimal for  $\text{CO}_2$  fixation, it will use a different source than inorganic carbon for biosynthesis of building blocks. Oren (1994) estimates that only 5 % of cell carbon may derive from  $\text{CO}_2$  in heterotrophic microorganisms. This might be true if  $\text{CO}_2$  fixation mediated by carboxylation reactions only are taken into account. This study demonstrates, that a halophilic organism might use an autotrophic  $\text{CO}_2$  pathway. This also explains the higher account of incorporation of carbons from  $\text{CO}_2$  into biomolecules. The fraction of  $\text{CO}_2$  can be even higher, since only enrichment in lipids was investigated and it is not known how high the ratio of carbons from  $\text{CO}_2$ , distributed over the whole metabolic network, is.

Since an enrichment with  $^{13}\text{C}$  of every carbon could be measured in the NMR spectrum, a mixture of differently labeled lipids was the product of the introduced label by sodium carbonate. Regardless of which type of  $\text{CO}_2$  fixation pathway was used by the organism, they all lead to the production of acetyl-CoA. This means that the mevalonate pathway was supplied with 20 % labeled (derived from  $\text{CO}_2$ ) and 80 % unlabeled (derived from acetyl-CoA supplied in the medium) acetate molecules.

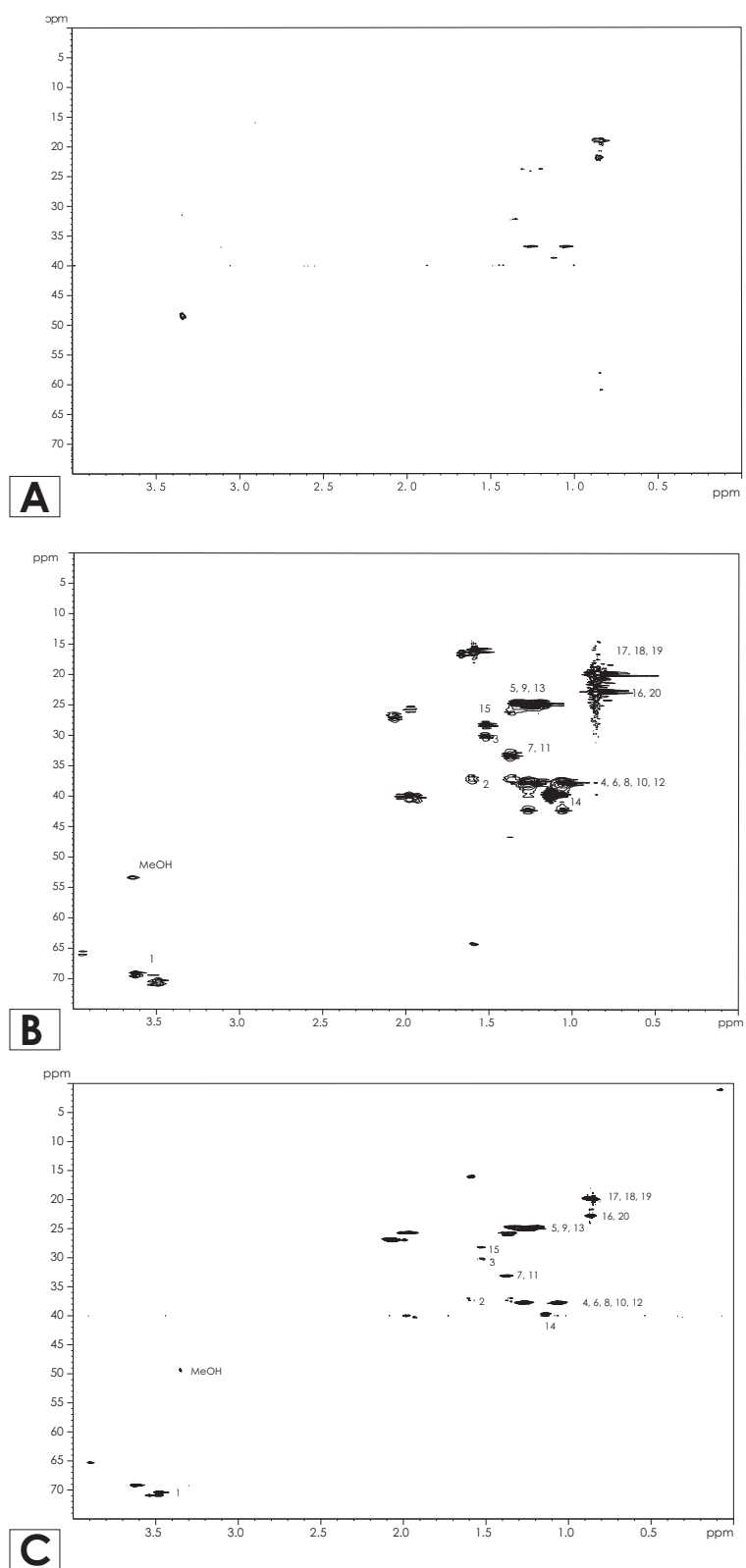


Figure 5.8: Comparison of NMR spectra of lipids extracted from cells grown in the presence of (A) unlabeled carbon sources, (B) U-<sup>13</sup>C<sub>2</sub> acetate or (C) <sup>13</sup>C carbonate.

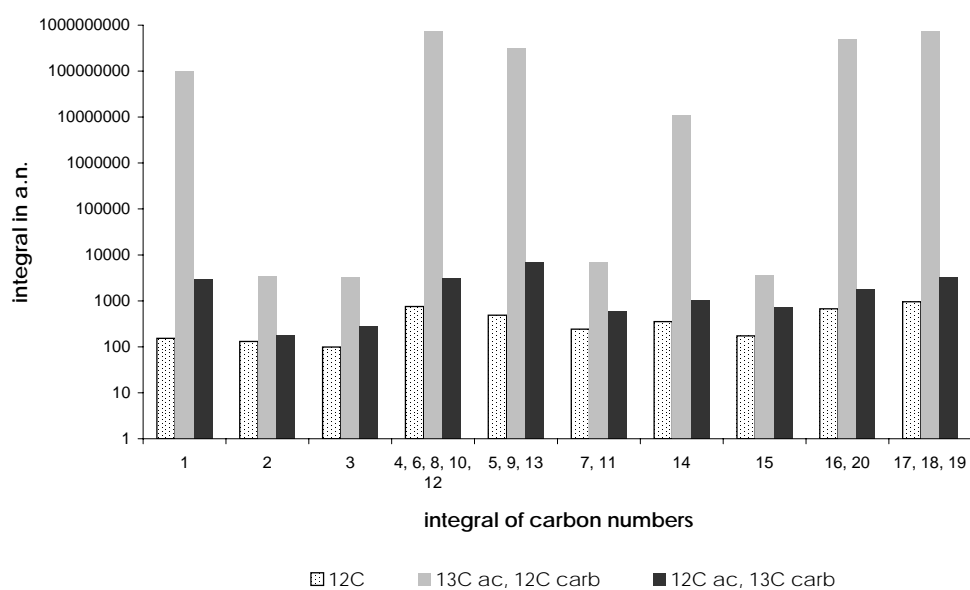


Figure 5.9: Integrated NMR signals after normalization of nonlabeled lipids ( $^{12}\text{C}$ ), labeled lipids from  $^{13}\text{C}$  acetate or  $^{13}\text{C}$  carbonate. A slight, but consistent increase of  $^{13}\text{C}$  enrichment in every carbon position in the  $^{13}\text{C}$  carbonate sample was detected. Data is shown in logarithmic scale.

Table 5.6: Integrated all ("a") and positive ("+") signals of FHSQC spectra of lipids from *Nmn. pharaonis* grown in presence of U- $^{13}\text{C}_2$  acetate or  $^{13}\text{C}$  carbonate.

integral	carbon #	$^{12}\text{C}$		$^{13}\text{C}$ ac., $^{12}\text{C}$ carb.		$^{12}\text{C}$ ac., $^{13}\text{C}$ carb.	
		a	+	a	+	a	+
1	MeOH	1161.2	1535.2	17374	18010	1311.8	2718.6
3	17, 18, 19	3034.9	3303.5	7.2593e+05	8.92E+09	30653	36994
5	16, 20	1929.7	2318.1	4.6055e+05	5.92E+09	16927	21163
7	5, 9, 13	1349	1690.3	3.3866e+05	3.87E+09	74118	79233
9	15	183.75	597.41	24740	43871	5500	8504.5
11	3	122.17	341,88	39014	40610	1328	3236,8
13	7, 11	507.51	837.84	72408	83746	5555.3	6991.6
15	2	213.99	451.59	41472	42234	-279.15	546.04
17	4, 6, 8, 10, 12	2179.9	2606.6	8.6499e+05	9.06E+09	31292	35260
19	14	793.48	1225.6	1.3106e+05	1.33E+08	8121.7	12181
21	1	280.09	530.23	1.1282e+05	1.19E+09	23754	33598

normalization by:

	(1) MeOD ("+" values)	(2) concentration in $^1\text{H}$ spectrum
$^{12}\text{C}$	100 %	100 %
$^{13}\text{C}$ ac., $^{12}\text{C}$ carb.	8.52 %	23 %
$^{12}\text{C}$ ac., $^{13}\text{C}$ carb.	56.00 %	200 %

### 5.2.2.2 GC/MS derived data does not confirm carbon incorporation from $\text{CO}_2$ in *Nmn. pharaonis*

The same lipid samples of *Nmn. pharaonis* were analyzed by GC/MS after splitting off the polar head group. The lipid spectra of cells grown in the presence of (i)  $^{12}\text{C}$  acetate,  $^{12}\text{C}$  carbonate, (ii)  $^{12}\text{C}$ , acetate  $^{13}\text{C}$  carbonate or (iii)  $^{13}\text{C}$  acetate,  $^{12}\text{C}$  carbonate are shown in Figure 5.10. Surprisingly, no incorporation of labeled carbons derived from  $^{13}\text{C}$  carbonate could be observed in the second spectrum, (ii). The two other spectra, in which carbons were derived from non-labeled (i) or labeled (iii) acetate, showed the same mass patterns and shifts, as measured and described in Figure 3.24. If significant  $\text{CO}_2$  fixation had taken place, comparable to labeling with acetate, an interference of carbon-12 patterns should be seen. However, this was not the case.

In subsection 4.2.1 the incorporation of the label into the carbon skeleton of amino acids was analyzed. In cells grown in the presence of unlabeled acetate and  $^{13}\text{C}$  carbonate, again no incorporation of  $^{13}\text{C}$  into any amino acid could be detected by MS. Unfortunately, NMR experiments in this case could not be performed due to technical difficulties.

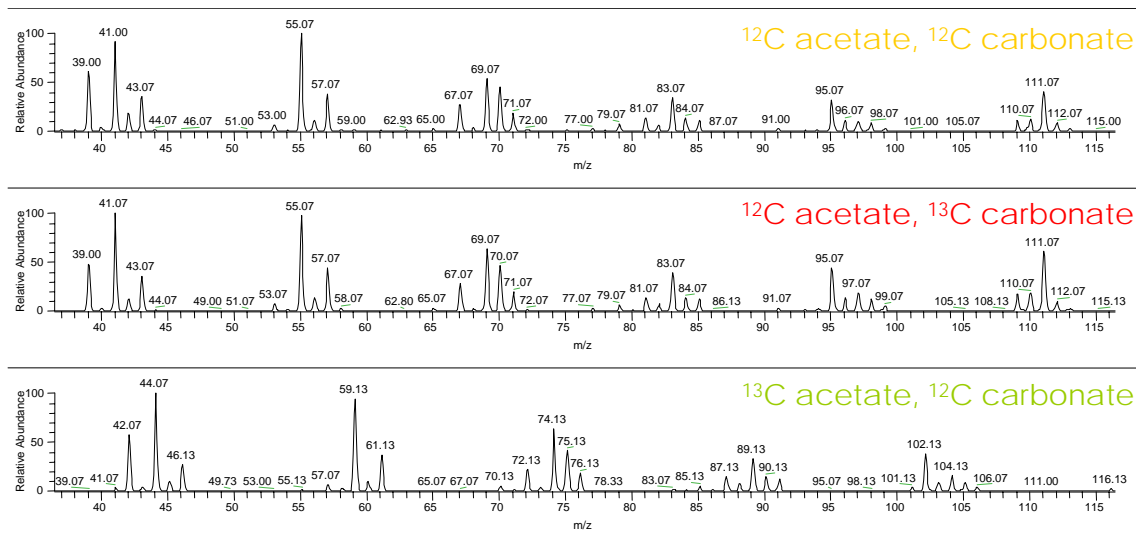


Figure 5.10: GC/MS spectra of lipids with incorporated carbons from (i)  $^{12}\text{C}$  acetate,  $^{12}\text{C}$  carbonate, (ii)  $^{12}\text{C}$  acetate  $^{13}\text{C}$  carbonate, (iii)  $^{13}\text{C}$  acetate,  $^{12}\text{C}$  carbonate. There was no influence of  $^{13}\text{C}$  sodium carbonate visible on the mass patterns of isoprenoids in spectra by GC/MS.

Why it is not possible to measure the incorporation of labeled carbons from  $\text{CO}_2$  by GC/MS in analogy to NMR? If the sample concentration were increased, the column would be overloaded and lose sensitivity. 20% of increased  $^{13}\text{C}$  enrichment by  $\text{CO}_2$  might be too low to detect significant intermediate-peaks. Mixed labeling patterns in Figure 5.10 were expected in comparison to the clear patterns measured of the unlabeled sample.

Another possibility for the discrepancy between NMR and GC/MS results might be that the enrichment of up to 20% with  $^{13}\text{C}$  is in fact lower due to variations while normalization of the raw data. Since the first step of normalization was performed by comparing the signal intensity of methanol (part of the solvent) of each sample, variations in volume due to evaporations are theoretically possible. But the NMR experiment was always started immediately after dissolving the lipid and besides from that all samples were measured under the same conditions with the same NMR program (implying that during the measurement itself, evaporation took place in every sample equally).

But this was not the only experiment, in which MS and NMR delivered different results for the same samples regarding signal intensities. Another example for the

discrepancy of the NMR and MS could be observed in subsection 3.2.2. There, the incorporation of unlabeled carbons from lysine in combination with labeled carbons from acetate in the medium was detected by NMR and GC/MS. Since lysine was added in different concentrations (5, 10, 30 mM) to the medium, a decreasing signal with increasing concentration of lysine could be measured with both methods. While the spectra, measured by NMR could already show an effect at the concentration of 20 mM  $^{12}\text{C}$  lysine (Figure 3.18), no mixed patterns could be observed in spectra of the same sample measured by GC/MS (Figure 3.25). The highest concentration (30 mM) of lysine was necessary to prove the incorporation of  $^{12}\text{C}$  carbons in lipids. This strongly confirms the high sensitivity of NMR.

Another advantage of NMR in this study is that the peaks of the carbon atoms of the lipid were annotated before by Ekiel *et al.* (1986) and could be compared to results of the literature. The spectra of the isoprenoids received from the MS could not be compared to literature nor to an external standard. Due to no availability of a reasonable standard (e.g. mevalonate), peaks measured in the chromatograms could not be allotted to specific compounds.

Since the NMR technique proved its supremacy also with its sensitivity in other experiments, it is save to assume that *Nmn. pharaonis* was able to perform  $\text{CO}_2$  fixation.

The regulation of autotrophic carbon metabolism and central carbohydrate metabolism in archaea is still not fully investigated. One example in heterotrophic archaea is the regulation of the futile cycling of glycolysis and gluconeogenesis. Most of the autotrophic archaea are facultative autotrophs and specifically downregulate the enzymes that are required for  $\text{CO}_2$  fixation when organic substrates (such as acetate) are available (Ramos-Vera *et al.*, 2009). In the case of *Nmn. pharaonis*, it would also be interesting to know how it regulates the transcription of its genes responsible for  $\text{CO}_2$  fixation and other carbohydrate pathways.

Another question is why should cells metabolize  $\text{CO}_2$  at all, if they have other readily assimilable organic carbon sources (e.g. acetate) available in the medium? The thermoacidophilic archaeon *Metallosphaera sedula* for example exhibits both chemoheterotrophic growth on organic carbon compounds and lithoautotrophic growth coupling sulfur or iron oxidation with assimilation of carbon dioxide. When succinate is added as the sole carbon source to the medium, the organism switches from autotrophic to heterotrophic growth and  $\text{CO}_2$  assimilation decreases or stops completely

Table 5.7: Genes of *Nmn. pharaonis* selected for transcription analysis.

Protein name	EC number	Protein	Accession number
AMP phosphorylase	2.4.2.-	NP3958A	<i>deoA</i>
type III RuBisCO	4.1.1.39	NP2770A	<i>rbcL</i>
adenine phosphoribosyltransferase	2.4.2.7, 2.4.2.22	NP1254A, NP1426A	<i>apt_2</i> , <i>apt_1</i>
ribose-1,5-biphosphate isomerase	5.3.1.-	NP3202A	-
Housekeeping genes as positive control			
succinate dehydrogenase	1.3.99.1	NP4264A	<i>sdhA</i>
citrate (si)-synthase	2.3.3.1	NP1314A	<i>citZ</i>

As a positive control for the RT-PCR two housekeeping genes were chosen.

(Hügler, 2003). So another experiment with *Nmn. pharaonis* would be to reduce the present acetate concentration in the minimal medium and make the organism more or less dependent on assimilating CO<sub>2</sub>. It should be pointed out, that these proposed experiments would only show efficient CO<sub>2</sub> fixation under the assumption that the genes for a complete pathway are present and, more importantly, are transcribed and translated into functional enzymes. Further experiments with <sup>14</sup>C-bicarbonate and subsequent HPLC analysis of <sup>14</sup>C-labeled products in cell-free extracts could also give deeper insights into CO<sub>2</sub> fixation pathways.

### 5.2.3 Transcriptional analysis verifies active RuBisCO in *Nmn. pharaonis*

Since *Nmn. pharaonis* is the only one of the three studied halophilic organisms encoding the gene for the archaeal RuBisCO, transcriptional analyses by reverse transcription and subsequent polymerase chain reaction (RT-PCR) were performed on the corresponding genes. The focus of this study was on the biosynthesis pathways of ribulose 1,5-bisphosphate via the AMP recycling pathway (section 5.2.1.2). To test if the primers bind specifically to the proper sequence, a "Check-PCR" was carried out on genomic DNA, Figure 5.11 shows the PCR products amplified by these primers. Genes of interest, with the corresponding protein name, are listed in Table 5.7.

RNA was isolated from cells, grown to mid-log phase (OD ~ 50) and remaining DNA was removed by two rounds of DNase digestion (Figure 5.12). Although some DNA could be still amplified by PCR after 40 cycles, the RNA was assumed to be pure. Also in the negative sample a slight band was visible in the agarose-gel. The RNA sample

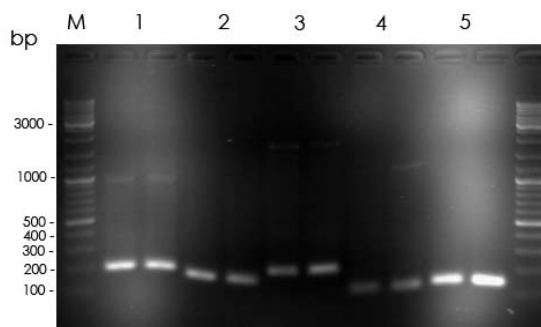


Figure 5.11: **Check-PCR of primers designed for RT-PCR.** Agarose gel separation of PCR products amplified from genomic DNA using primers targeting the following genes (with the expected size of fragment in brackets): (1) *deoA* (207 bp), (2) *rbcL* (187 bp), (3) *apt\_1* (238 bp), (4) *apt\_2* (137 bp) and (5) NP3202A (no gene name annotated) (145 bp). GeneRuler DNA Ladder Mix was used as a marker (M). As a template genomic DNA from *Nmn. pharaonis* from two different extractions (corresponding to the double lanes for every gene) was applied.

with the highest quality (verified using a Bioanalyzer) and sufficient concentration was transcribed into cDNA by reverse transcriptase. For this purpose, one of the oligonucleotides (the reverse primer) constructed for each gene was used (Table 2.20).

All cDNA fragments (whose sequence is unique for the particular gene) of the characteristic genes of the AMP-CO<sub>2</sub> fixation pathway could be amplified in the expected size. The sequence identity of the PCR-products was confirmed by gel extraction and subsequent sequencing of the fragment. Due to residual DNA-contamination, following incomplete DNA digestion with DNase, a band in the negative control (b) of the PCR fragments of *apt\_2* in Figure 5.13 is visible in a low intensity. Since the intensity of the bands are so much lower than the intensity of the cDNA based product (a), it has no influence on the results. Altogether, a transcript for every gene characteristic for the AMP-CO<sub>2</sub> fixation pathway could be detected, which confirms the hypothesis of CO<sub>2</sub> fixation in *Nmn. pharaonis*. Under aerobic conditions in the minimal medium the genes for adenine phosphoribosyltransferase (both paralogues), AMP phosphorylase, ribose-1,5-biphosphate isomerase and type III RuBisCO were definitely transcribed in *Nmn. pharaonis*. Thus pentose phosphate was converted to ribose 1,5-bisphosphate and further to 3-phosphoglycerate with concomitant CO<sub>2</sub> fixation. Since enzyme activity has been measured for glucose-6-phosphate dehydrogenase (recent experiments in cell extracts of *Hbt. salinarum*, unpublished by Daniela Breckau and Aitken & Brown, 1969) conversion of glucose-6-phosphate to gluconate



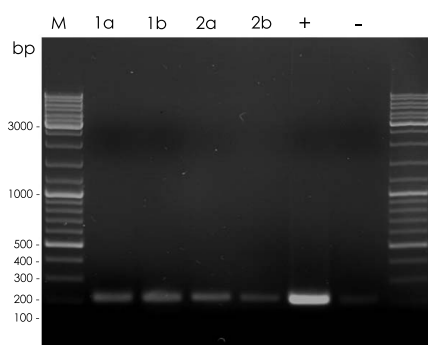


Figure 5.12: **Check-PCR with 40 cycles of extracted RNA analyzed by agarose gel-electrophoresis.** RNA samples (1) and (2) were extracted from two different cultures. (a) and (b) were separate extractions from the corresponding sample. GeneRuler DNA Ladder Mix was used as a marker (M). Positive control (+) was from genomic DNA and negative control (-) without any template. Applied primers for the Check-PCR was the primer-pair for amplifying part of the gene *sdhA*.

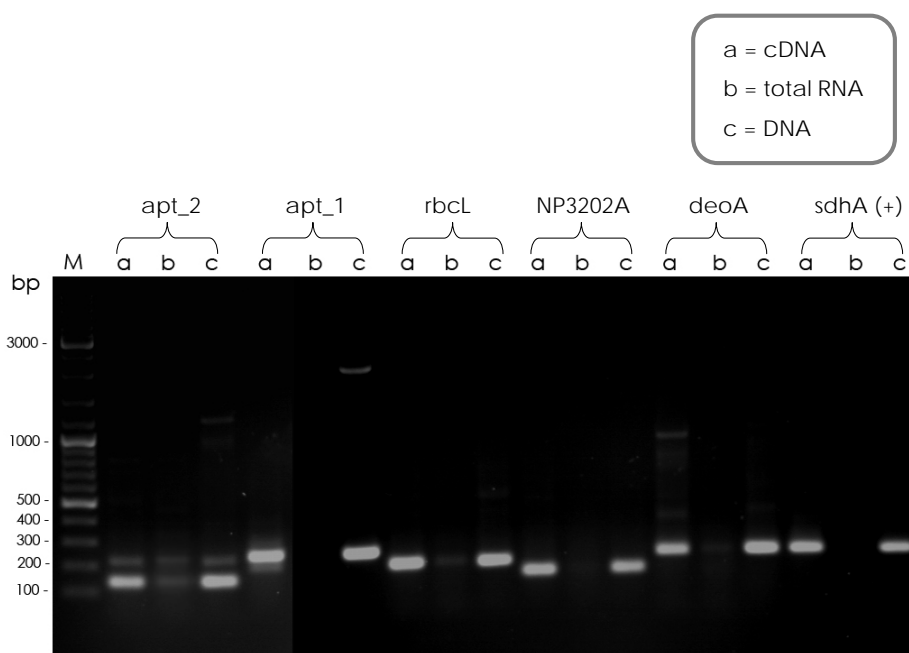





Figure 5.13: **Analysis of PCR products for genes involved in the AMP-CO<sub>2</sub> fixation pathway by agarosegel-electrophoresis.** As a template for the PCR products after 40 cycles (a) cDNA, (b) total RNA (as a negative control for DNA-contamination) and (c) genomic DNA (as a positive control) was used. GeneRuler DNA Ladder Mix was used as a marker (M). The same gene codes were already described in Table 5.7. *sdh* was used again as a positive control for the whole transcription analysis.

Table 5.8: Overview of possible fixation pathways in halophilic archaea.

Organism	Calvin cycle	Reductive acetyl-CoA pathway	3-hydroxy propionate cycle	Reductive citrate cycle	AMP-CO <sub>2</sub> fixation pathway	Glycine cleavage cycle
<i>Nmn. pharaonis</i>	not established in Archaea yet	missing CO-dehydrogenase/acetyl CoA synthase complex	CO <sub>2</sub> fixation via propionyl-CoA	no anaerobic conditions	proven by RT-PCR	no organisation in gene cluster for P-, T-, and H-proteins
<i>Hbt. salinarum</i>	id.	id.	id.		no RuBisCO	
<i>Nmn. moolapensis</i>	id.	id.	id.	no citrate lyase gene	no RuBisCO	no glycine dehydrogenase gene

Probability for a functional pathway:  high  low  moderate

The table summarizes all formerly described and discussed CO<sub>2</sub> fixation pathways in halophilic archaea. Every pathway was evaluated in *Nmn. pharaonis*, *Hbt. salinarum* and *Nmn. moolapensis* regarding literature references, genome annotation data and experimental results. "id." means identical comments in one column (for all three organisms).

6-phosphate must take place. From a genomic view, this still presents a missing link in this pathway, because no homologs for this enzyme could be found in any of the sequenced haloarchaea. It is possible that similar enzymes (e.g. glucose-dehydrogenase) with a lower substrate specificity take over this reaction. This also influences the biosynthesis pathway of riboses. The gene for 6-phospho-glucono lactonase is also missing but an alternative pathway could operate by synthesis of gluconate by the aforementioned glucose-6-phosphate dehydrogenase and then conversion to gluconate 6-phosphate by an alternative sugar kinase.

In future, enzyme activity assays of the archaeal RuBisCO in cell extracts or with the purified enzyme could verify its presence and significance in the metabolism of *Nmn. pharaonis* and would lead to more conclusions regarding its function.

A summary of all potential pathways in each organism is given in Table 5.8.

## 5.3 Conclusions

Representatives of halophilic archaeal species with distinct capabilities to gain energy were examined for key enzymes of the known autotrophic CO<sub>2</sub> fixation pathways.

Some pathways could be excluded in all three organisms, *Nmn. pharaonis*, *Hbt. salinarum* and *Nmn. moolapensis* such as the Calvin cycle and the reductive acetyl-CoA pathway.

Homology comparison of enzymes involved in classical as well as alternative CO<sub>2</sub> fixation pathways was performed. It can be concluded that Euryarchaeota exhibit a mosaic of surprisingly many possible CO<sub>2</sub> assimilation pathways.

*Nmn. pharaonis* is the only one of the three investigated organisms capable of employing an alternative AMP-CO<sub>2</sub> fixation pathway since a RuBisCO gene could be found. The pathway could not be reconstructed completely, but it presents one meaningful option for the carboxylating function of the RuBisCO, whose role in other archaea still remains elusive (Berg *et al.*, 2010). *Nmn. pharaonis* might also fix CO<sub>2</sub> via propionyl-CoA, which would explain the alkaline growth conditions.

In *Hbt. salinarum*, the responsible genes for the glycine cleavage system are organized in one gene cluster and therefore this organism also has a high probability for a functional reversible pathway if the growth conditions are suitable.

The only possibility for *Nmn. moolapensis* to assimilate CO<sub>2</sub> known so far is via propionyl-CoA. Nevertheless, *Nmn. moolapensis* has the lowest potential for CO<sub>2</sub> fixation based on genomic data.

The organism *Nmn. pharaonis* was chosen for investigation using <sup>13</sup>C labeling experiments because it is able to grow on a single carbon source, such as acetate, unlike the well-studied halophilic archaeon *Hbt. salinarum*. This greatly simplifies several experimental protocols, in particular those based on stable isotope labeling.

NMR experiments showed an incorporation of labeled bicarbonate into isoprenoids. Nonetheless, confirmation of the CO<sub>2</sub> fixation by mass spectrometry is pending due to sensitivity reasons. However, the NMR technique seemed to be the more reliable method and therefore the best choice for metabolic analysis in this study. It is assumed

that due to the heterotrophy of this organism only a minor part of carbon is derived from CO<sub>2</sub> and moreover incorporated into isoprenoids.

These results demonstrate that there are different possibilities of acquisition of cellular carbon from inorganic carbon in the metabolism of halophilic archaea, which need to be further analyzed. The study shows that the map of the metabolic landscape in haloarchaea is definitely more diverse than previously thought. Genome sequence data will be highly valuable for reconstructing potential pathways in other organisms in the future. Other aspects such as the dependence on growth conditions decide, if and which pathways are working in a given species.

Further analysis of determining the phylogenetic roots based on the mentioned key enzymes in each pathway would help to understand the early evolution of life and lead to a hypothetical chronology of events in the cellular carbon metabolism.

## 6 Genomic and metabolic features of *Nmn. moolapensis*

### 6.1 Introduction

#### 6.1.1 Haloarchaeal retinal proteins

Retinal proteins (RP) are a family of integral membrane proteins which share a common structure consisting of seven trans-membrane helices. These form a channel through which ions can move or signals be transmitted. They contain a covalently attached retinal chromophore (via a protonated Schiff base linkage) linked to a lysine residue in the seventh helix of the protein. Following light absorption, the retinal undergoes isomerization, which induces protein structural alterations, that allow the RP to function in ion transport or signal transmission (see Schäfer *et al.* (1999) and references therein). RP are found in all three domains of cellular life and serve many functions including ion tolerance, phototaxis and light perception, such as the rhodopsins in the human eye.

In haloarchaea, retinal proteins with different functions are found: bacteriorhodopsin (BR), which uses light energy to pump protons outside the cell; halorhodopsin (HR), which transports chloride ions into the cell; and sensory rhodopsins (SRI and SRII), which do not pump ions but relay signals to the interior of the cell, and these are used for phototaxis in motile species (reviewed by Oesterhelt (1998)). In Figure 6.1 an overview of haloarchaeal retinal proteins and their function is shown schematically.

Light activation of BR triggers a photocycle in which retinal is isomerized from all-trans to 13-cis and back, accompanied by de- and reprotonation of the Schiff base and conformational changes in the protein. This leads to proton release to the extracellular space against the membrane potential, followed by proton uptake from the intracellular space. Following their concentration gradient, the extruded protons flow back into the

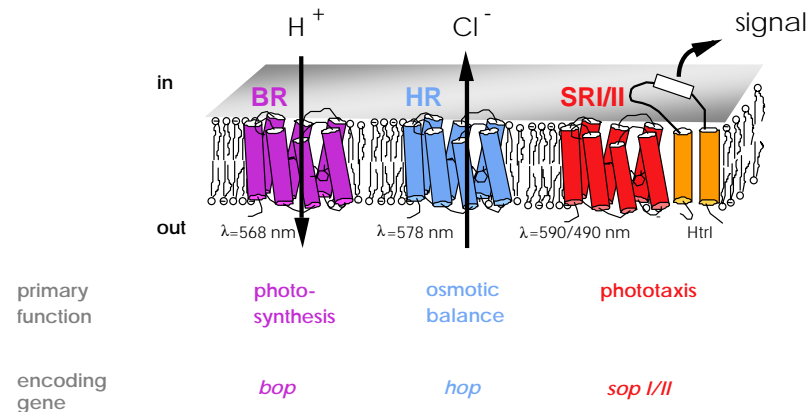


Figure 6.1: **Overview of haloarchaeal retinal proteins.** Their primary function and corresponding genes are written beneath the diagram and the absorption maximum of each retinal protein is given. BR: bacteriorhodopsin, HR: halorhodopsin, SR: sensory rhodopsin. Adapted from (Oesterhelt, 1999).

cell via the membrane ATPase thereby driving ATP synthesis (Oesterhelt, 1999). The transmembrane electrochemical proton gradient also drives other reactions such as the transport of specific metabolites.

In *Hbt. salinarum* for example, BR is packed tightly into 2D arrays, forming patches of purple membrane (PM) (Stoeckenius & Rowen, 1967). The trimeric arrangement of BR and the formation of the crystalline patches require lipid molecules at defined positions. The PM itself consists of 75% (w/w) BR and of 25% (w/w) lipids (Sumper *et al.*, 1976). NMR studies showed that there are 2 glycolipids and 6 phospholipids per BR molecule and that S-TGD-1 (glycolipid sulphate) is the only glycolipid (Renner *et al.*, 2005). The glycolipid sulphate plays an important role in the purple membrane by stabilizing the trimeric arrangement of BR (Essen *et al.*, 1998). This trimeric arrangement of BR in a hexagonal lattice is due to protein-protein interactions and protein-lipid interactions (Krebs *et al.*, 1997).

The function of the crystalline lattice structure in the purple membrane comprises the stabilization of the chromophore, which undergoes a specific conformational change from an all-trans-type to a 13-cis-retinal.

The second retinal protein HR acts as a light-driven inward-directed chloride pump (Schobert & Lanyi, 1982). As in the case of proton pumping by BR, chloride pumping

changes the membrane potential and thus energizes the system. However, this cannot lead to sustained photophosphorylation, as the halobacterial ATPase specifically uses protons for ATP synthesis. Rather, it is thought that the active import of chloride ions by the action of HR helps to maintain the high intracellular chloride concentrations required for osmotic balance of the cells especially during growth.

The retinal proteins SRI and SRII are the phototactic receptors of halophilic cells, which can recognize three light colors (reviewed by Oesterhelt (1998)). SRI is a photochromic receptor that detects orange (attracting response)- and UV-light (phobic response) and SRII detects blue light (phobic response). Instead of pumping ions, SRI and SRII transmit signals to their cognate transducers HtrI and HtrII, respectively. The 13-cis form of retinal signals the activated state which is forwarded along the signal transduction cascade by HtrI and HtrII. The signal activates autophosphorylation of the histidine kinase CheA, the first component of a two-component regulatory system. The phosphate groups are then transferred to CheY, the second component of the two-component system, which targets the flagellar motor switch (Oesterhelt & Marwan, 2005).

Retinal-based proton pumps are also known to be wide-spread among eubacteria, fungi, and even eukaryotes (Spudich, 2006). The genome of the bacterium *Salinibacter ruber*, for example, contains xanthorhodopsin that uses salinixanthin to harvest light energy in a wider spectral range than is possible with retinal alone (Balashov *et al.*, 2005). The protein is used for transmembrane proton transport (Balashov & Lanyi, 2007; Lanyi & Balashov, 2008). Thus, it is a light-driven proton pump similar to BR (Oesterhelt & Stoeckenius, 1971) and the archaeorhodopsins (Y.Mukohata, 1999) of the archaea, the proteorhodopsins of planktobacteria (Béjà *et al.*, 2001), and leptosphaeria rhodopsin of a eukaryote (Waschuk *et al.*, 2005), but with two chromophores.

### **6.1.2 Osmoprotection in halophiles by compatible solutes and inorganic cations**

Cells in all three kingdoms have evolved different strategies to adjust to increased external salt concentrations and to counteract the external osmotic pressure. Most

halophilic bacteria, e.g. *Halomonas elongata*, maintain osmotic balance by amassing compatible osmolytes such as glycerol, glycine-betaine or ectoine (Grammann *et al.*, 2002). They can also tolerate some turgor pressure and resist outside changes in salt concentration because they have cell walls made of peptidoglycan.

In general, organic molecules used for osmotic balance are accumulated by uptake or *de novo* synthesis. Numerous compatible solutes are known, including polyols like glycerol and arabinol, sugars and derivatives, amino acids and derivatives, betaines, and ectoines and occasionally peptides suitably altered to remove charges (Galinski, 1995).

Halophilic archaea such as *Hbt. salinarum* and *Nmn. pharaonis*, follow another route called: the "salt-in" strategy. To maintain positive turgor in hypertonic surroundings, high concentrations of inorganic ions (e.g. potassium) are accumulated in the cytosol. The salt-in strategy has been only detected in halophilic archaea of the order *Halobacteriales* and the anaerobic halophilic bacteria of the order *Haloanaerobiales*.

The high intracellular salt concentrations force all enzymes and structural cell components to function under these conditions (Lanyi, 1974; Eisenberg *et al.*, 1992). Indeed, haloarchaeal enzymes are typically halophilic, requiring high salt concentrations in order to function. For these species, compatible solute accumulation for osmoadaptive reasons has only recently been considered. Surprisingly, *Hbt. salinarum* was found to accumulate L-glutamate and glycine betaine inside the cell (Kokoeva *et al.*, 2002) and in haloalkaliphilic archaea, a novel disaccharide, 2-sulfotrehalose, could be detected as a compatible solute (Desmarais *et al.*, 1997).

### **6.1.3 *Nmn. moolapensis* and its comparison to other halophilic archaea**

The genome of the recently isolated and characterized extremely halophilic archaeon *Nmn. moolapensis* (Burns *et al.*, 2009) has been sequenced and partly annotated in the course of this study. Although *Nmn. moolapensis* shows a high 16S rRNA similarity of 97.5% to *Nmn. pharaonis* (Burns *et al.*, 2009), it exhibits different phenotypic properties and shows low DNA-DNA hybridization values. The focus in this study was on the metabolic differences between this neutrophilic species and the alkaliphilic member of this genus, *Nmn. pharaonis*, which grows in salt saturated soda lakes, at pH 11. New ether lipids were detected in *Nmn. moolapensis* and are described in subsection 3.2.1.



The following sections present a comparative analysis of the genetic and metabolic characteristics of *Nmn. moolapensis*, including the osmotic strategy for balancing the external osmotic pressure.

## 6.2 Results and discussion

### 6.2.1 Conclusions of the genome of *Nmn. moolapensis* and comparison to its haloalkaliphilic relative *Nmn. pharaonis*

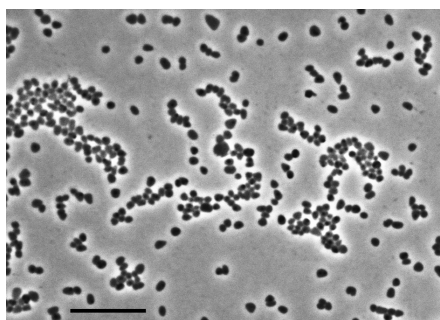


Figure 6.2: **Phase contrast micrograph of *Nmn. moolapensis*** (Burns *et al.*, 2009). The scale bar represents 10  $\mu\text{m}$ .

The complete genome sequence of *Nmn. moolapensis* (DSM 18674) was determined and subsequently annotated in several steps: (a) gene prediction using Reganor (McHardy *et al.*, 2004), (b) start codon validation, (c) automatic function prediction by Metanor (Goesmann *et al.*, 2005), (d) improvement of function prediction by comparison to *Nmn. pharaonis* and (e) curation of enzyme assignments in a manual procedure supported by Priam (Claudel-Renard *et al.*, 2003). The complete annotation procedure was executed in the

context of HaloLex, a web-based genome information system (Pfeiffer *et al.*, 2008a).

*Nmn. moolapensis* has no plasmids and contains a single chromosome of 2.9 Mb with a G+C content of 64.5%. In comparison to the chromosome of *Nmn. pharaonis* this is 0.32 Mb larger and about 1% higher in G+C content. The number of predicted ORFs (2850) is 167 more than that of the *Nmn. pharaonis* chromosome, but *Nmn. pharaonis* carries plasmids of 36 and 131 kb size, making the total number of predicted ORFs in both species very close to each other. Both species have a single ribosomal RNA operon but differ in the number of tRNA genes (46 versus 53) (Dyall-Smith *et al.*, 2010).

For gene prediction, Reganor from the GenDB package (Meyer *et al.*, 2003) was used. The program Reganor integrates data from two other gene predictors, Critica (Badger & Olsen, 1999) and Glimmer (Delcher *et al.*, 1999), taking advantage of the knowledge about strengths and weaknesses of the underlying programs. Critica detects similarity-

supported genes and is very stringent which results in a highly reliable set of ORFs, which are relatively incomplete. In contrast, Glimmer is a sensitive and sophisticated ab initio predictor working with a training set. The ORF set is much more complete but there is a tendency towards overprediction. The Glimmer performance depends on the quality of the training set, which is a critical issue for GC-rich genomes. Reganor selects all ORFs predicted by Critica because of the reliability of their prediction. The Critica ORFs are also used for training Glimmer, which ensures a good performance of Glimmer. Glimmer ORFs with a sufficiently high score are then added to regions not yet annotated as coding, thus making sure that overlapping ORFs are avoided.

Gene starts were validated by analyzing blastp results vs. ORF sets from completely sequenced haloarchaea for which gene starts had previously been manually curated. This is necessary as gene starts for GC-rich genomes are frequently incorrectly assigned. The procedure is described in the publication about HaloLex (Pfeiffer *et al.*, 2008a).

An automatic function prediction was performed using Metanor (Goesmann *et al.*, 2005) from the GenDB package, which integrates data from blast searches vs. complete genomes with other data, e.g. from domain databases. Besides *Nmn. pharaonis*, the annotation of *Hbt. salinarum* and *Hqr. walsbyi* has been extensively manually curated.

Function prediction could be improved by comparing *Nmn. moolapensis* to the closely related *Nmn. pharaonis*. A major advantage of this approach was the known high quality of the *Nmn. pharaonis* function annotation (Falb *et al.*, 2008). Orthologs of the two species were detected by identification of bidirectional best blast pairs (BBB). It was found that 67.6% proteins of *Nmn. moolapensis* have an ortholog in *Nmn. pharaonis* and the ortholog pairs have an average 67% amino acid sequence identity. Thus, annotation transfer from *Nmn. pharaonis* to *Nmn. moolapensis* was considered to be highly reliable. In addition to the 67.6% of annotated proteins with assigned cluster of orthologous groups (COG) (Tatusov *et al.*, 2000), 15.3% coding sequences showed blast hits, which were not bidirectional and 17% could not show any blast hit with a better E-value than  $e^{-4}$ .

Such proteins (17%) which do not have an ortholog in *Nmn. pharaonis* were compared to halophilic archaea (orthologs or paralogs). 7.4% of the total proteins (2850) were grouped to another COG and 9.6% proteins no homologs in any organism could be found. ORFs without any BLAST hit are strain-specific genes (e.g. originated from

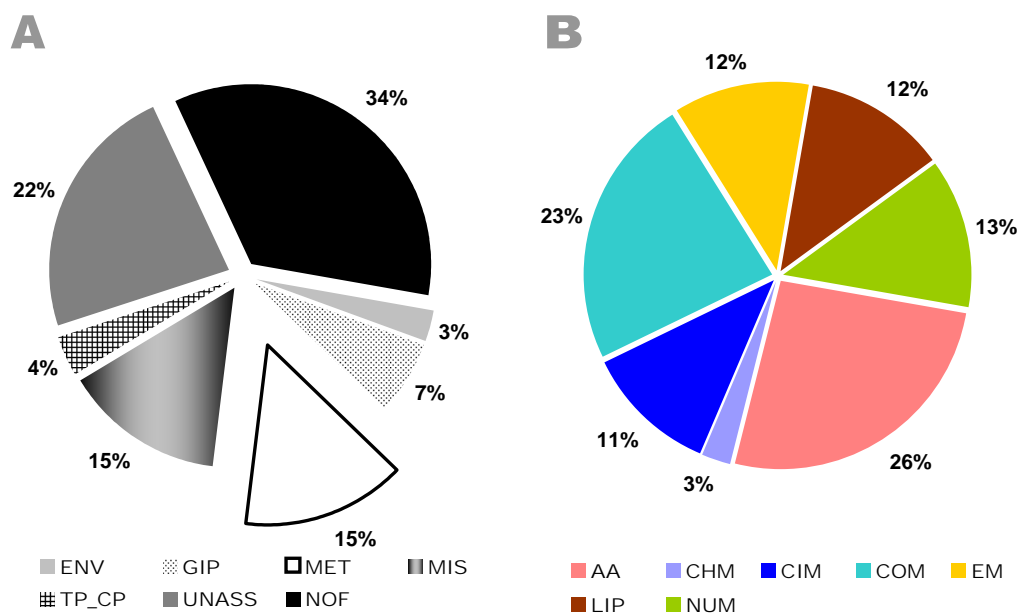


Figure 6.3: **Function categories (A) and function classes (B) for the classification of *Nmn. moolapensis* proteins.** In (A) distribution of proteins in function superclasses are shown. In (B) the function superclass for metabolism (MET) is expanded in function classes. Legend (function superclasses are written in bold): **MET** metabolism - AA amino acid metabolism, CHM carbohydrate metabolism, CIM central intermediary metabolism, COM coenzyme metabolism, EM energy metabolism, LIP lipid metabolism; **GIP** genetic information processing, **TP\_CP** transport and cellular processes, **ENV** environmental information processing, **MIS** miscellaneous functions, **UNASS** unassigned function, **NOF** no functional superclass

horizontal gene transfer) and their functions have to be investigated experimentally in future. Sometimes functions of strain-specific genes can be predicted by looking at their context within the genome.

Each protein was assigned to a functional category (Tatusov *et al.*, 1997). The specific function of proteins of *Nmn. moolapensis* was determined together with F. Pfeiffer and M. Dyll-Smith (both, MPI of Biochemistry, Dep. Oesterhelt). The proteins belong to the functional categories metabolism (15%), transport and cellular processes (4%), genetic information processing (7%), environmental information processing (3%), and miscellaneous (including general function, 15%). For the remaining proteins no particular functions could be determined: unassigned proteins (22%, including conserved hypothetical and hypothetical proteins) and proteins without a

function class (34%). Since the manual annotation has not been finished yet completely, the fraction of proteins without a function class (34%, "NOF" = no function class) is still high (Figure 6.3). However, since the distribution of proteins into function superclasses fit well to those annotated in *Nmn. pharaonis* (Falb, 2005), it is assumed that most of the proteins without function classes are hypothetical proteins and therefore the portion of proteins belonging to the function superclass "unassigned" (UNASS) will increase after finishing annotation. In the genome of *Nmn. pharaonis*, 42% of the proteins belong to this class (Falb *et al.*, 2005).

Regarding the 67.6% of BBB hits in the genomes of *Nmn. moolapensis* and *Nmn. pharaonis*, this value is consistent with the close phylogenetic relationship between the *Natronomonas* strains, as deduced from 16S rRNA gene sequences, and with their classification as separate species within the same genus.

Annotation of genes, which is based on homology searches in already published genomes, is only useful if gene prediction quality for the related reference species is sufficient. Since the genome of *Nmn. pharaonis* was annotated in the same department (Falb *et al.*, 2005), it is known that protein annotation transfer comes from a reliable source. Thus, after automatic validation of genes, only few discrepancies had to be checked manually.

### **6.2.1.1 Comparison and synteny analysis of retinal protein genes with associated regulators in halophilic archaea**

Prokaryotes often organize their genes in operons, a type of gene regulation, that enables them to regulate the expression of multiple genes depending on environmental conditions. In Bacteria, genes of related function, such as those forming metabolic pathways, are commonly found closely together on the genome. This is also the case in Archaea, for example the *pst*-operon in *Hbt. salinarum*, which is polycistronic and encodes genes for phosphate-specific transport (Furtwängler *et al.*, 2010).

The gene arrangement regarding retinal protein genes and their regulators were compared between *Nmn. moolapensis*, *Nmn. pharaonis* and *Hbt. salinarum* R1, highlighting differences and concluding back to their functions.

Table 6.1: **Genes encoding retinal proteins and associated regulators in *Nmn. moolapensis*.**

Accession number	Gene	Protein name
Nmlp_3721	bop	bacteriorhodopsin
Nmlp_1290	hop	halorhodopsin
Nmlp_2165	sopI	sensory rhodopsin I
Nmlp_1291	blp	bacterioopsin-linked protein blp
Nmlp_1294	bat	bacterioopsin activator
Nmlp_3577	brp	bacteriorhodopsin-related protein
Nmlp_1292	blh	brp-like protein
Nmlp_1110	boa_1	probable transcription regulator boa1
Nmlp_1964	boa_2	probable transcription regulator boa_2
Nmlp_3119	boa_3	probable transcription regulator boa_3
Nmlp_3792	boa_4	probable transcription regulator boa_4
Nmlp_1541	brz	probable brz

*Nmn. moolapensis* possesses all the genes for retinal proteins (*bop*, *hop*, *sop*), while *Nmn. pharaonis* lacks *bop*, the gene for bacteriorhodopsin (BR) (Table 6.1). In particular, the presence of the *bop* gene explained the phototrophic growth of *Nmn. moolapensis* with pyruvate (Burns *et al.*, 2009) as carbon source. In Figure 6.4, all previously known haloarchaeal opsins from completely sequenced genomes are compared in a phylogenetic tree to the bacterial opsin xanthorhodopsin (Xop) (from *Salinibacter ruber*) (Baliga *et al.*, 2004).

It can be noticed in the phylogenetic tree in Figure 6.4 that Xop I of *Har. marismortui* build sequence similarities to the archaeal Bop clade, while the sequence of Xop I showed high homologies to archaeal Sop proteins.

The other haloarchaeal rhodopsins are divided into three clades: Bop, Sop and Hop. Bop of *Nmn. moolapensis* showed the highest homology to bacteriorhodopsin sequence of *Hbt. salinarum*. *Hqr. walsbyi* (both, the type strain and C 23) is the only haloarchaeon possessing two *bop* genes, whose protein sequences are included in the Bop clade.

While *Nmn. pharaonis* encodes a type II sensory rhodopsin (*sop II*), the *sop* gene from *Nmn. moolapensis* clearly clusters with *sop I* genes and not with *sop II*. No *sop II* homologue was found in the genome of *Nmn. moolapensis*. Only the gene for the halorhodopsin (*hop*) in *Nmn. moolapensis* exhibited the highest similarity to the corresponding homologue of *Nmn. pharaonis*.

A close examination of the genomic contexts of retinal protein genes and their associated regulators in *Nmn. moolapensis* revealed a synteny more closely related to that of

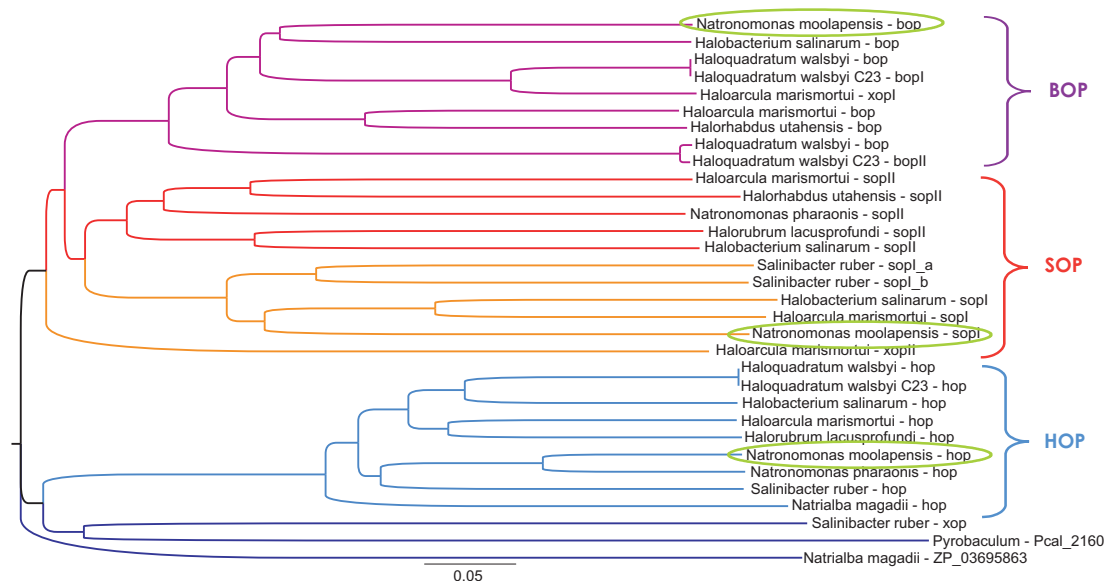


Figure 6.4: **Phylogenetic tree of all known haloarchaeal retinal proteins from sequenced genomes.** The length of the scale bar (0.05) represents 6% amino acid sequence distinction. Bop: bacteriorhodopsin, Hop: halorhodopsin, Sop: sensory rhodopsin, Xop: xanthorhodopsin

*Nmn. pharaonis*. For instance, the gene for halorhodopsin (*hop*) in *Nmn. moolapensis* is surrounded by the related genes *blp*, *blh*, *bat* as it is in *Nmn. pharaonis* (Figure 6.5, part A). In *Hbt. salinarum* it is the *bop* gene that is embedded in such a gene cluster (Figure 6.5, part B).

In Figure 6.6, the genome location of the *sop* gene in *Nmn. moolapensis* is compared to that of *Hbt. salinarum*. Both organisms encode a type I *sop* gene with its adjacent transducer *htrI*.

In part B of Figure 6.6, the location of a probable *brz* gene (Tarasov *et al.*, 2008) in the *Nmn. moolapensis* genome is shown. This is a regulator of the *bop* gene. It is not, as seen in *Hbt. salinarum*, located before the *bop* gene (Figure 6.5, part B). Therefore, the question arises, if the gene is a transcription regulator of *bop* or if it has more than one or another regulatory function. Nevertheless, the assumed *brz* gene (Nmlp\_1541) showed high homologies to *brz* in *Hrd. utahensis* (41% sequence identities) and in *Hbt. salinarum* (37%). *Nmn. pharaonis*, in contrast, does not possess a *brz* gene.

In the phylogenetic tree (Figure 6.4) halophilic rhodopsins were compared among each other. It could be shown that *Har. marismortui* is encoding two xanthorhodopsins

which show close homologies to the archaeal rhodopsins (Bop and Sop) but no homologies to the bacterial xanthorhodopsin. The protein of this formally functionally unpredictable opsin gene, named *xopII* (Baliga *et al.*, 2004), was analyzed recently by Nakao *et al.* (2010). It is classified as a new class of sensory rhodopsin (SR III) with a very weak proton-pumping activity whose direction is the same as that of bacteriorhodopsin, a typical light-driven proton pump.

Recently, Bop II of *Hqr. walsbyi*, strain C23 has been found not to pump protons, and its actual function in the cell has yet to be determined (Chii-Shen Yang, National Taiwan University, personal communication to Mike Dyll-Smith).

It could be shown that *Nmn. moolapensis* is encoding a *bop* gene, while no genes for this rhodopsin could be found in the *Nmn. pharaonis* genome (Falb *et al.*, 2005). Sharma *et al.* (2007) investigated the gene arrangement of BR, of genes for its biogenesis and of those important for retinal synthesis among haloarchaea. It was reported that both, gene gain by lateral gene transfer and gene loss contributed to the patchy distribution of BR among haloarchaeal lineages. The genetic mobility of the *bop* gene is also an issue in the *Natronomonas* genus. This genus is not the only case in which patchy distribution of Bop took place even at the genus level. For example, Kamekura (1998) documented that some *Halorubrum* species lack Bop.

Assuming that the different functional types of rhodopsins found in the haloarchaea today were already present in the common ancestor of this group (Ihara *et al.*, 1999), it does not surprise that BR is present in the genome of *Nmn. moolapensis*. The corresponding absence of it in *Nmn. pharaonis* can be explained by adaptation to a different (alkaline) ecological niche where BR functionality was not necessary to survive. This is consistent with the theory of a "habitat genome" (Legault *et al.*, 2006; McCarren & DeLong, 2007; Sharma *et al.*, 2007), a pool of genes useful for the adaptation to a particular set of environmental constraints.

The reason for the loss of the *bop* gene in *Nmn. pharaonis* and also the loss of the glycolipid, crucial for the purple membrane stability (Essen *et al.*, 1998; Renner *et al.*, 2005) (further discussions in subsection 3.2.1) is unclear, as soda lakes are just as sun-exposed as other hypersaline lakes. A possible scenario is that the ancestor of *Nmn. pharaonis* had a functional purple membrane, but that the high external pH was a selective factor in loss of the surface glycolipid, and the consequent loss of



function of BR led to its loss from this lineage. It is less likely that selection was due to the inefficiency of proton pumping by BR into the highly alkaline environment, as it has been previously shown that respiration in this organism results in proton-pumping (and not sodium-pumping) for ATP production via the membrane ATPase (Dyall-Smith *et al.*, 2010).

Another example for gene mobility in *Natronomonas* genus is the variable presence of the sensory rhodopsin Sop in the two species. Only *sop I* is encoded in the genome of *Nmn. moolapensis* and only *sop II* in the genome of *Nmn. pharaonis*. It seems that the different distribution of haloarchaeal rhodopsin ion pump genes in the *Natronomonas* genus is only one of many examples in the haloarchaeal group.

Sop I directs phototaxis of the cell into those wavelengths of light where BR absorbs maximally and can be used most efficiently (Oesterhelt, 1998). Since *Nmn. pharaonis* lacks BR, the photoattractant response which is mediated by this type of sensory rhodopsin did no longer take place and might lead to a loss of Sop I in *Nmn. pharaonis*. The same reason could probably force *Nmn. moolapensis* to keep the *sop I* in the genome or to gain it by lateral gene transfer from another species. Why Sop II, whose expression protects the cell from harmful photo-oxidative damage, is not present in the *Nmn. moolapensis* genome can only be speculated about. The distant relation of the Sop proteins of the two species probably reflects differences in selection pressure related to phototaxis acting in their different environments.

The analysis of the rhodopsin gene mobility in this chapter showed that lateral gene transfer as well as multiple independent losses between the species took place in the evolutionary history of the genus *Natronomonas*.

Among the haloarchaeal species harboring a *bop* gene, only a few were shown to produce large amounts of BR in culture (Sugiyama *et al.*, 1994; Kamekura *et al.*, 1998; Yatsunami *et al.*, 2000). In some species, the *bop* gene appears to be present but not expressed (Kamekura *et al.*, 1998). Furthermore, it could be shown that not all BR-producing haloarchaea produce purple membranes (Oren, 2002b) which are formed by trimeric patches of BR placed on a crystal lattice (Grigorieff *et al.*, 1995; Kimura *et al.*, 1997). Whether BR is expressed in *Nmn. moolapensis* and a purple membrane is formed was also analyzed and further results are described in subsection 6.2.2.2.

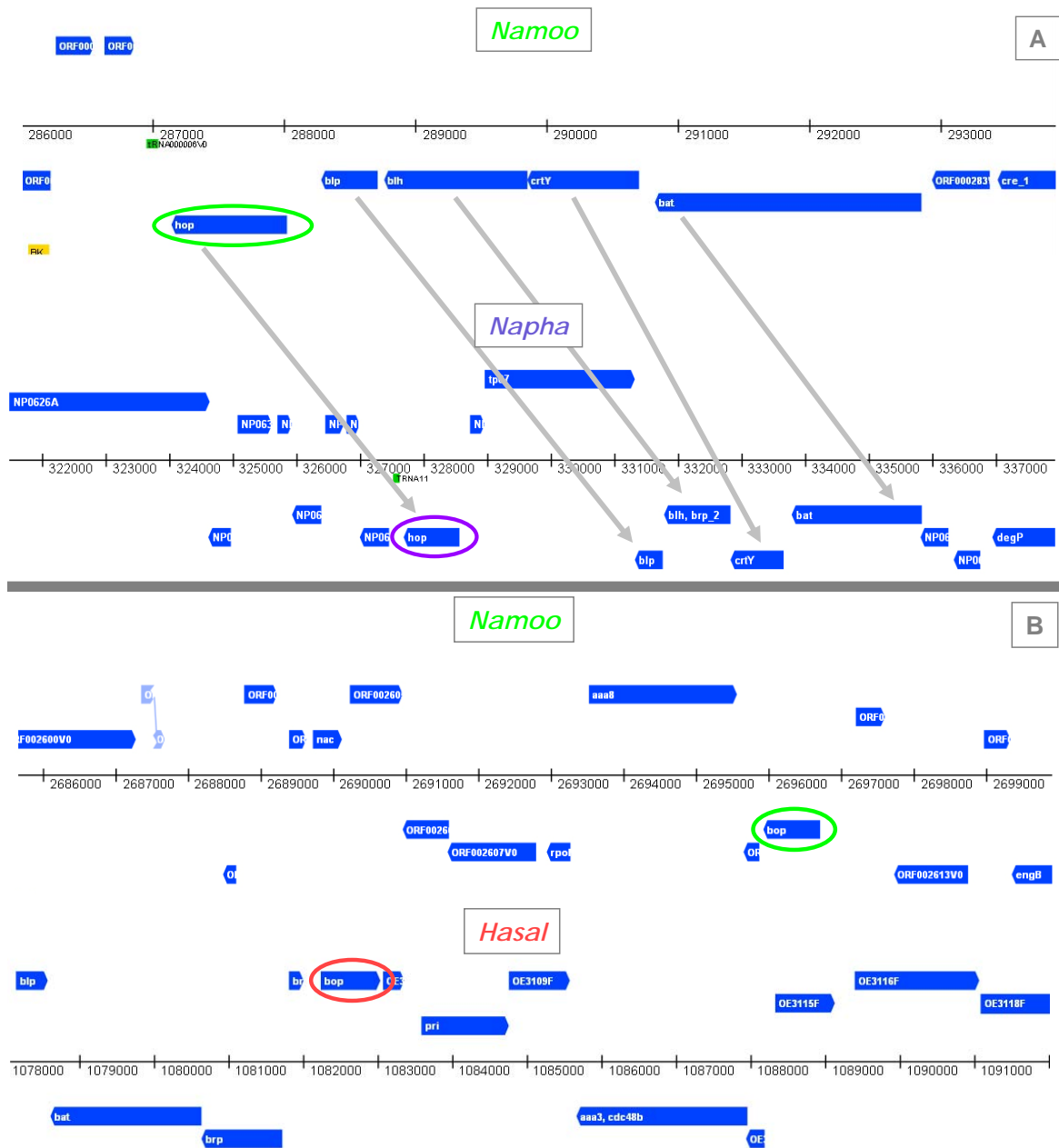


Figure 6.5: **Genome location of retinal genes and genes involved in their regulatory network in *Nmn. moolapensis*: bacteriorhodopsin and halorhodopsin. A:** The *hop* gene of *Nmn. moolapensis* (green encircled) is adjacent to genes involved in the BR regulatory network similar to the *hop* gene in *Nmn. pharaonis* (magenta encircled). The same genes (*blp*, *blh*, *crtY* and *bat*) are encoded in the *Hbt. salinarum* genome adjacent to the *bop* gene. **B:** Position of *bop* in *Nmn. moolapensis* genome (green encircled) in comparison to *bop* in *Hbt. salinarum* genome (red encircled).

In summary, the genome sequence of *Nmn. moolapensis* was determined and compared to that of its haloalkaliphilic relative, *Nmn. pharaonis*, in order to understand how these species diverged, particularly in relation to their differing pH optima. The genome of *Nmn. moolapensis* will be accessible through HaloLex ([www.halolex.mpg.de](http://www.halolex.mpg.de)) after finishing the annotation progress and submitting it to the EMBL database.

Although *Nmn. moolapensis* possesses the same genes for retinal proteins and their regulators (except *sopII*) as in *Hbt. salinarum*, their synteny is more related to the corresponding genes encoded in the genome of *Nmn. pharaonis*. Whether the genes for bacteriorhodopsin, halorhodopsin and sensory rhodopsin in *Nmn. moolapensis* are regulated in a similar way to those in *Hbt. salinarum*, has to be investigated by transcription studies in the future. It is not yet understood how the transcription of the *bop* gene in *Nmn. moolapensis* is regulated, given its location away from the usual cluster of associated genes. It is indeed functional, as shown later by phototrophic growth and translation of *bop* in subsection 6.2.2.

In Table 6.2 further differences and similarities between *Nmn. moolapensis* and related halophilic archaea regarding their genomes, lipids, retinal proteins and growth are summarized.

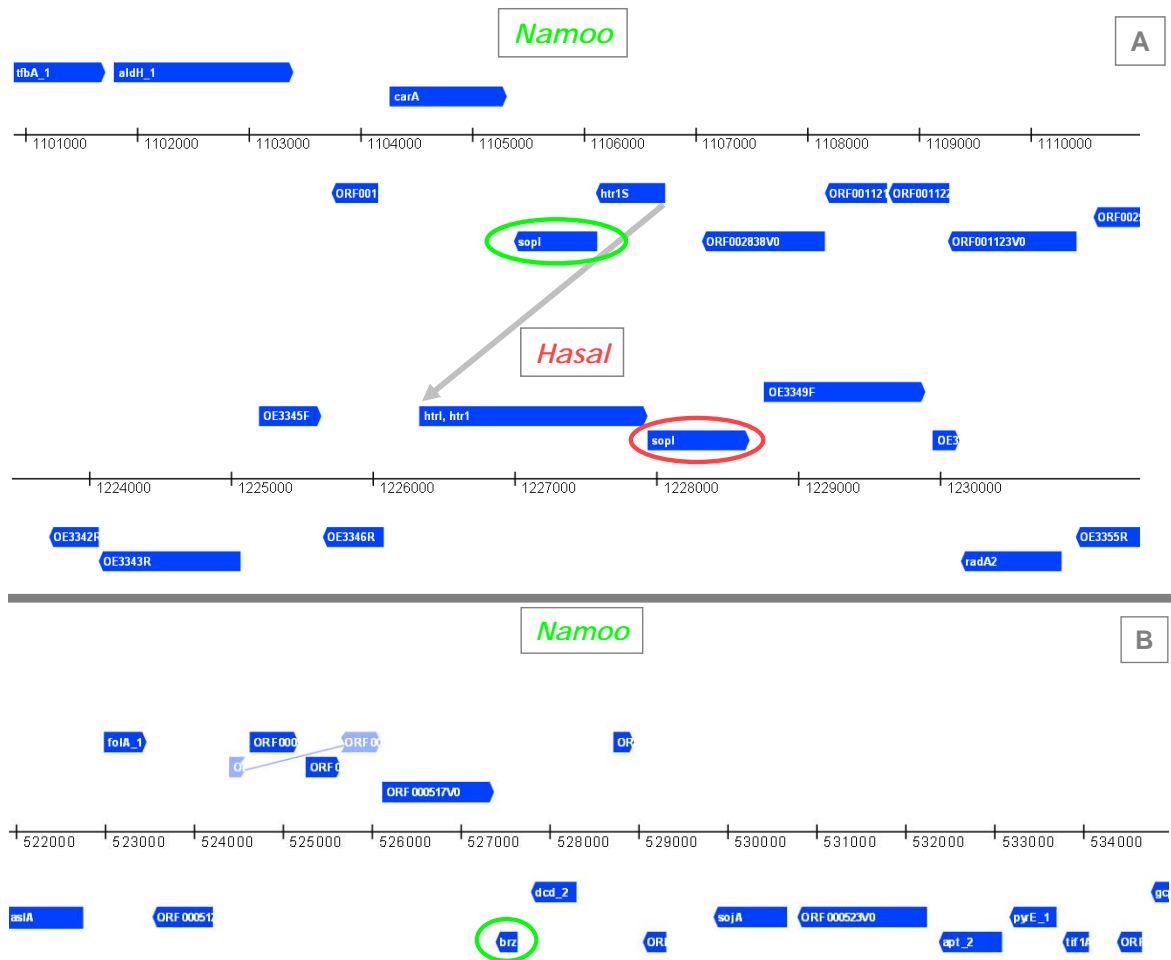


Figure 6.6: **Genome location of retinal genes and regulators in *Nmn. moolapensis*: sensory rhodopsin and transcription regulator *brz*.** **A:** The location of the *sop* gene in the genomes of *Nmn. moolapensis* (green encircled) and *Hbt. salinarum* (red encircled) is similar. **B:** The *brz* gene (green encircled) in *Nmn. moolapensis* is not located in the *bop* cluster.

Table 6.2: Genomic and physiologic comparison of *Nmn. moolapensis* to *Nmn. pharaonis* and *Hbt. salinarum* R1.

	<i>Nmn. moolapensis</i>	<i>Nmn. pharaonis</i>	<i>Hbt. salinarum</i> R1
<b>Isolation</b>	solar saltern crystallizer pond (Australia)	soda lake (Egypt)	salted fish
<b>Salt optimum [M]</b>	3.5	3.5	4-5
<b>pH</b>	6.0 – 8.5	8.5 – 11	7
<b>Genome size [Mb]</b>	2.92	2.60	2.72
<b>GC content [%]</b>	65.0	63.4	68.0
<b># plasmids</b>	0	2	4
<b>rRNA operons</b>	1	1	1
<b><i>fla</i> genes (motility)</b>	yes	yes	yes
<b>Glycolipids</b>	unknown glycolipid	no glycolipids	S-TGD
<b>Retinal proteins</b>	1 Bop, 1 Hop, 1 Sop (I)	0 Bop, 1 Hop, 1 Sop (II)	1 Bop, 1 Hop, 2 Sop (I,II)
<b>Growth</b>	chemoorganotrophic (aerobic, dark), phototrophic (O <sub>2</sub> -lim., light)	chemoorganotrophic (aerobic, dark)	chemoorganotrophic (aerobic, dark), phototrophic (O <sub>2</sub> -lim., light), fermentative (aerobic/anaerobic, dark)

Bop: bacteriorhodopsin, Hop: halorhodopsin, Sop: sensory rhodopsin, S-TGD: sulfated triglycosyldiphytanyl-glycerol. Data of *Hbt. salinarum* R1 and *Nmn. pharaonis*: Falb (2005).

### 6.2.1.2 Metabolic pathway comparison in the genus *Natronomonas*

Using PRIAM (Claudel-Renard *et al.*, 2003), an automatic enzyme detection method, it is possible to compare the metabolic potential between different species. In this way, gene complements of the two *Natronomonas* species were compared with each other, as described in Methods (subsubsection 2.6.4.2). Retrieved KEGG maps, processed with PRIAM, were compared and cases where enzymes were present in *Nmn. moolapensis* or *Nmn. pharaonis* but absent in the other were re-checked for accuracy. Different and common metabolic features between *Nmn. moolapensis* and *Nmn. pharaonis* are summarized in the next paragraphs concerning the archaeal respiratory chain, the amino acid and the cofactor metabolism.

**Respiratory chain** A classical electron transport chain, which can be seen in mitochondria, consists of four membrane-bound complexes. This enzymatic series produces a proton gradient across the membrane and catalyzes redox reactions. The four complexes are: NADH dehydrogenase (I), succinate dehydrogenase (II), ubiquinone-cytochrom c reductase (III) and the cytochrome c oxidase (IV).

*Nmn. moolapensis* grows best aerobically in the dark (subsection 6.2.2). The components of the respiratory chain as derived from genome analysis were compared to those of *Nmn. pharaonis* (Falb *et al.*, 2008) in order to obtain a pathway profile.

While no *nuo* genes encoding for subunits of the NADH dehydrogenase in halophiles and other aerobic archaea (Falb, 2005) could be found in the genome of *Nmn. moolapensis*, genes for the NADH dehydrogenase type II were present.

All *sdh* genes were found clustered in the order *sdhCDBA* for the second complex succinate dehydrogenase. The genes for the electron transfer flavoprotein (*etf*) were also detected.

Genes belonging to the cluster for menaquinone synthesis could be detected in the *Nmn. moolapensis* genome.

Neither *Natronomonas* species encode *pet* genes, which are assumed to encode for complex III in other haloarchaea (Falb *et al.*, 2008). A *cba* gene cluster coding for subunits of a cytochrome  $ba_3$ -type oxidase was present, and the genes were most similar to homologues in *Nmn. pharaonis*.

For the fourth complex, the corresponding *cox* genes for all subunits were encoded in the genome. ATP-synthase components could be identified (*atp* genes) which use the resultant proton-motive force to generate ATP.

A list of all involved genes can be seen in Table S5 and an overview of all complexes involved in the respiratory chain of the genus *Natronomonas* is presented in Figure 6.7.

Since the *nuo* cluster encoding the NADH acceptor module of the type I NADH dehydrogenase complex was not complete, as in other haloarchaeal genomes, it is assumed that NADH dehydrogenase type II (*ndh*) is able to feed electrons derived from NADH into the respiratory transport chain as complex I, but cannot translocate protons across the membrane.

In most halophilic archaea, electrons originating from NADH dehydrogenase as well as from Sdh and Etf complexes are transferred to menaquinone (Falb *et al.*, 2008).

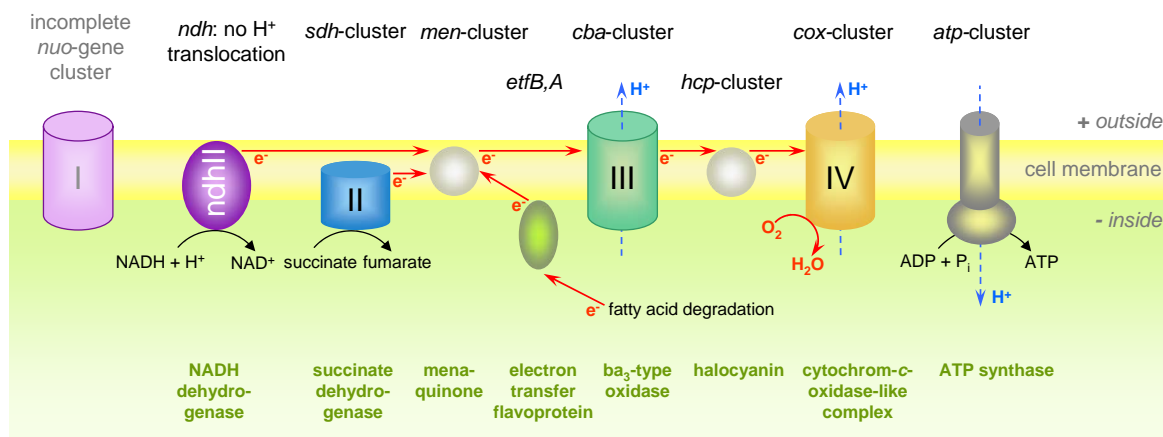


Figure 6.7: **Proposed respiratory chain for the genus *Natronomonas*.** The electron flow from NADH, succinate and fatty acid degradation through the transport chain to oxygen, which is reduced to water is indicated with red arrows. The electron transport chain is used to pump protons (blue arrows) from the cytoplasm across the cell membrane. This electrochemical gradient allows the ATP synthase to use the flow of protons through the enzyme back into the matrix to generate ATP from adenosine diphosphate (ADP) and inorganic phosphate ( $P_i$ ). Genome data of the *Nmn. pharaonis* genome were extracted from Falb *et al.* (2008).

Compared to *Nmn. pharaonis*, the *men* genes in *Nmn. moolapensis* were clustered into two groups: *menDF* form one group and *menECAB* a separate group.

The cytochrome  $ba_3$ -type oxidase interacts with the copper protein halocyanin in order to transport electrons in *Nmn. pharaonis* (Mattar *et al.*, 1994). For mediating the electron transfer step between menaquinone to halocyanin, a novel type of complex III is assumed (Falb, 2005). Fewer halocyanin genes (3 paralogs) could be found in *Nmn. moolapensis* than in *Nmn. pharaonis*.

In summary, *Nmn. moolapensis* showed similar components of the respiratory chain like *Nmn. pharaonis*. Apart from complex I, a complete respiratory chain could be detected in *Nmn. moolapensis*, since all other components are present in the genome.

**Biosynthesis of amino acids** Mapping the gene sets to the amino acids biosynthesis pathways did not reveal any significant differences. This is not surprising since both *Natronomonas* species are capable of growing in defined media including only a single carbon source, acetate for *Nmn. pharaonis* (Gonzalez *et al.*, 2010) and pyruvate for *Nmn. moolapensis* (Burns *et al.*, 2009). Therefore, both species have the ability to

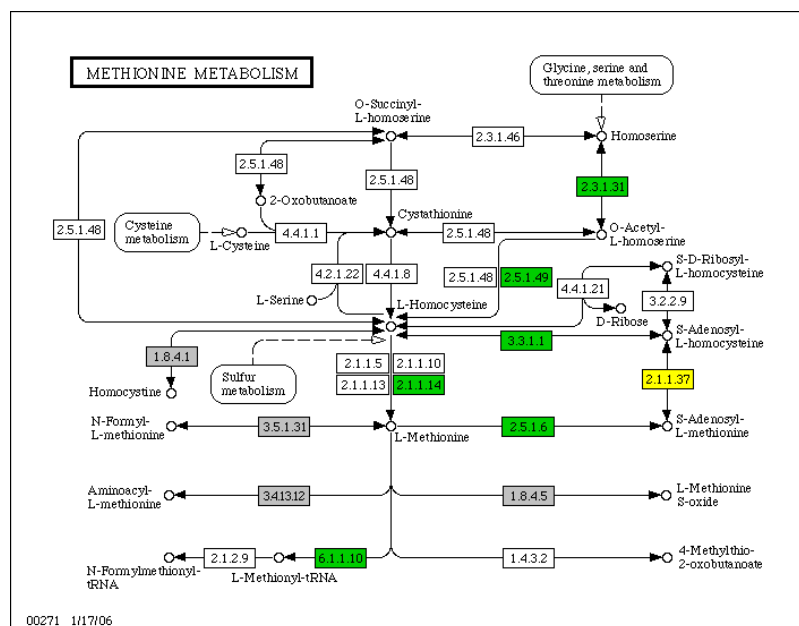


Figure 6.8: **Methionine metabolism in *Nmn. moolapensis* in a KEGG map and annotated with PRIAM.** Color code of boxes: green - PRIAM prediction above E-value of  $10^{-30}$ , yellow - PRIAM prediction below E-value of  $10^{-30}$ , grey - EC without proteins in ENZYME database.

synthesize all amino acids.

Only the biosynthesis of methionine showed some differences. In *Nmn. pharaonis*, methionine is biosynthesized from homoserine to O-acetyl-L-homoserine and then to the methionine precursor, L-homocysteine. No genes for the cystathionine synthase/lyase (*metB/C*) were detected in the *Nmn. moolapensis* genome, so conversion of cysteine or O-succinyl-L-homoserine does not appear to be possible. It is assumed that methionine is synthesized from homoserine (with glycine, serine and threonine as precursors) via O-acetyl-L-homoserine and L-homocysteine. All annotated genes of the *met* cluster are listed in Table S5 and the corresponding KEGG map is shown in Figure 6.8.

**Cofactor metabolism** Most of the prokaryotic organisms are capable of synthesizing cofactors *de novo*. Halophilic archaea seem to possess different capabilities for cofactor synthesis and reveal many gaps in biosynthetic pathways where enzyme genes are replaced by still unknown non-orthologous genes (Falb *et al.*, 2008).

*Nmn. moolapensis* possesses the same capabilities for cofactor synthesis as its al-



kaliphilic relative except for biotin. Furthermore, *Nmn. moolapensis* shows genes for biosynthesis of thiamine (*thi*), menaquinone (*men*), coenzymeA (*pan*, *coa*), pyridoxal 5-phosphate (vitamin B<sub>6</sub>), riboflavin (*rib*), tetrahydrofolate (*fol*), molybdopterin (*moa*, *moe*, *mob*), hemes (*hem*), cobamide (*cob*) and nicotinamide nucleotides (*nad*) (Table S5).

Genes for menaquinone, which are involved in the respiratory chain (see Figure 6.7), were not clustered together on the genome in *Nmn. moolapensis*, but split into two groups (*menDF* and *menECAB*). In other haloarchaea such as *Nmn. pharaonis* or *Hbt. salinarum*, these genes are found in one cluster.

There are three different pathways for biosynthesis of ubiquinone known: (i) with tyrosine as a precursor or chorismate via (ii) the *coq* cluster or (iii) the *ubi* gene cluster. However, only two genes of the *ubi* gene cluster and none of the *coq* gene cluster were encoded in *Nmn. moolapensis*, similar to *Nmn. pharaonis*.

The biotin gene cluster (*bioDFB*) found in *Nmn. pharaonis* could not be detected in the *Nmn. moolapensis* genome. This fits to the fact that biotin has to be supplied (Burns *et al.*, 2009) to the medium, which is described in subsection 5.2.1.4. *Hbt. salinarum* as well as *Hqr. walsbyi* lack genes for biotin and it has to be added to their growth media. It might be also possible that yet unassigned genes (functional equivalents that are not homologous to the known enzymes) detected in many sequenced halophiles encode an alternative biosynthesis pathway (Falb, 2005).

In general it is to note that the presence of enzymes (especially key enzymes) of a pathway, should be interpreted as an indicator for the possibility of an active pathway in an organism, but not as proof of its existence. This implies that the substrate specificity of particular enzymes belonging to large families cannot be predicted from sequence comparison alone and therefore additional experiments, such as enzyme activity assays, are important to confirm genomic data. Nevertheless, genomic annotation provides a fundamental basis for further biochemical studies and allows to obtain an overview of the metabolic potential of an organism, which was the concept of the analysis presented in this chapter. Approximately 90 archaeal genomes are now available in the NCBI database, considerably extending our ideas about the distribution of metabolic pathways in archaea (Berg *et al.*, 2010). Moreover, analyzing archaeal genomes is also a matter of shedding light on early evolution. Van der Oost & Siebers (2007) give a number of examples of archaeal genomes where gene duplication result

in two paralogues, one of which maintains its original function and another that is relieved from selection pressure and can rapidly evolve or reach another function.

## 6.2.2 Energy metabolism in *Nmn. moolapensis*

Since the neutrophilic species *Nmn. moolapensis* and the alkaliphilic member (and type species) of this genus, *Nmn. pharaonis*, grow in such different environments, investigation of energy metabolism of *Nmn. moolapensis* was also a focus of this work. The presence of BR suggested phototrophic growth. Moreover, homologs for all enzymes involved in the biosynthesis of retinal could be detected (Table S5).

Absence of genes for ADI pathway and archaeal RuBisCO indicated that arginine fermentation and CO<sub>2</sub> fixation (at least not catalyzed by the RuBisCO) are not possible.

### 6.2.2.1 Different illuminations showed phototrophic growth of *Nmn. moolapensis*

*Nmn. moolapensis* was grown under different conditions to investigate the capabilities of growing phototrophically or fermentatively. Anaerobic conditions were set by either flushing cultures with nitrogen (+N<sub>2</sub>) before closing the flask with a plug to make it airtightly or without nitrogen so that the culture still has an air reservoir above the medium.

It was observed that the cells were not able to grow under absolute anaerobic conditions in the dark, but they did grow in the dark when they had the air reservoir available (Figure 6.9). Fermentation, as a mode of energy conservation under anaerobic conditions, did not occur in this synthetic medium (DBCM2), which confirmed the genome annotation, that the gene cluster for the ADI pathway (arginine fermentation pathway) is incomplete in the *Nmn. moolapensis* genome. The inability to use arginine as the sole carbon source has been already detected by Burns *et al.* (2009).

Both *Natronomonas* strains could reach about the same maximum cell density at stationary phase when growing aerobically in the dark. Sometimes, cells of *Nmn. moolapensis* started to form flocks and stopped growing under aerobic conditions - in the light. Reasons for this are unclear.

Figure 6.9 also summarizes growth under different light sources (with or without filter: yellow or white light) and initial oxygen levels (with or without initial nitrogen

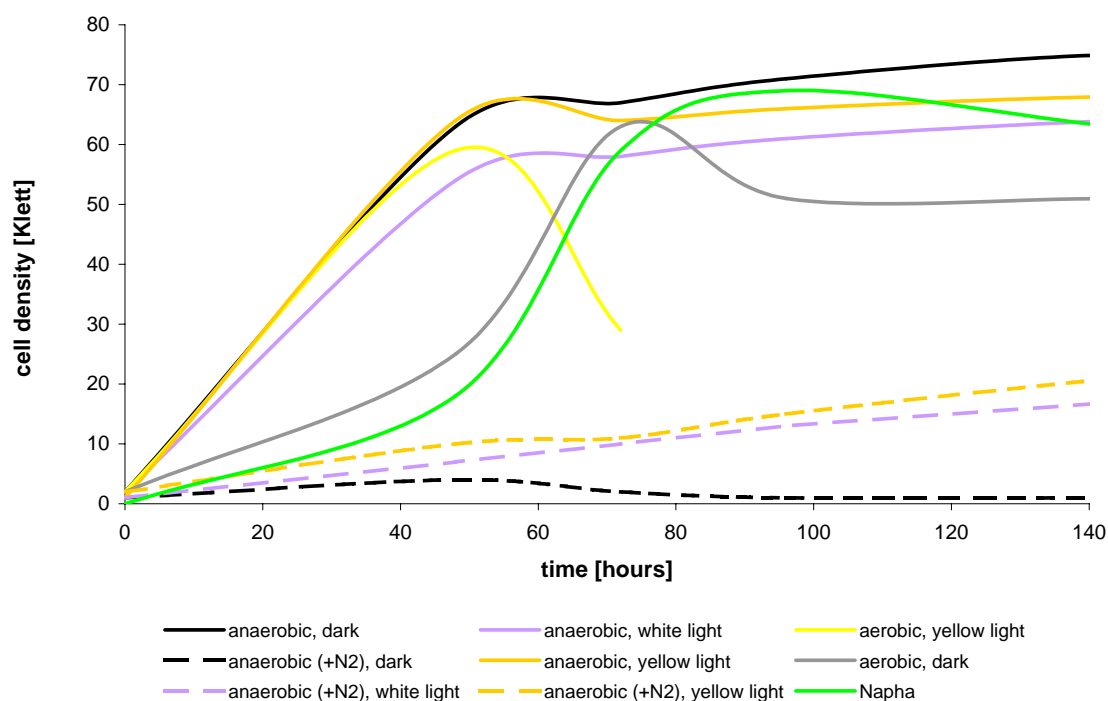


Figure 6.9: **Growth curves of *Nmn. moolapensis*, growing under different conditions.** Aerobic and anaerobic growth was compared to growth in the dark and different illumination (yellow and white light). After flushing the culture with nitrogen, providing strict anaerobic conditions, growth slowed down significantly. Thus growth at strict anaerobic conditions in the dark (black, dashed) was not possible while growth at moderate anaerobic conditions (black) took place. *Nmn. moolapensis* could also grow at strict anaerobic conditions in white as well as yellow light. *Nmn. pharaonis*, which was grown aerobically in the dark was taken as a reference.

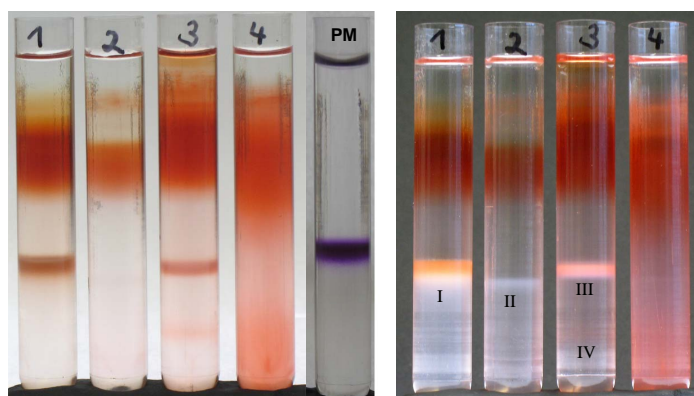


Figure 6.10: **Sucrose gradients of *Nmn. moolapensis* membranes.** Growth conditions: (1) anaerobic, yellow light + N<sub>2</sub>, (2) anaerobic, white light + N<sub>2</sub>, (3) anaerobic, yellow light, (4) aerobic, dark, PM: purple membrane (*Hbt. salinarum*). A broad red-colored band, probably containing bacterioruberin, is visible in the upper half of each gradient. In the anaerobically grown cultures a distinct band appears at about the same height as seen for the purple membrane. Left and right photos show the same samples with different backgrounds. Roman numerals mark bands.

flushing). It was observed that without initial nitrogen flushing, cultures grew faster in white light than in yellow light, but both reached the same density at stationary phase. *Nmn. moolapensis* could still grow under these strict anaerobic conditions during illumination. This indicates that *Nmn. moolapensis* can grow phototrophically, and photosynthesis can take place. In the next chapter the cell membrane of *Nmn. moolapensis* was investigated in more detail.

#### 6.2.2.2 Sucrose gradients of cell membranes resulted in differently colored bands

To investigate if *Nmn. moolapensis* can produce a purple membrane like *Hbt. salinarum* (Oesterhelt, 1972, 1975) cell membranes were analyzed by density centrifugation on a sucrose gradient. Cultures were grown (1) anaerobically under yellow light and with initial nitrogen flushing (+ N<sub>2</sub>), (2) anaerobically with white light + N<sub>2</sub>, (3) anaerobically with yellow light and (4) aerobically in the dark (Figure 6.10). In all anaerobic cultures, bands of different colors (orange, white and pink) and sizes were observed. Only in the aerobic culture no distinct band was visible. A white band in gradient number (2) became visible if the gradients were illuminated in front of a black background. In number (3), a second faint band beneath the main band could be seen.

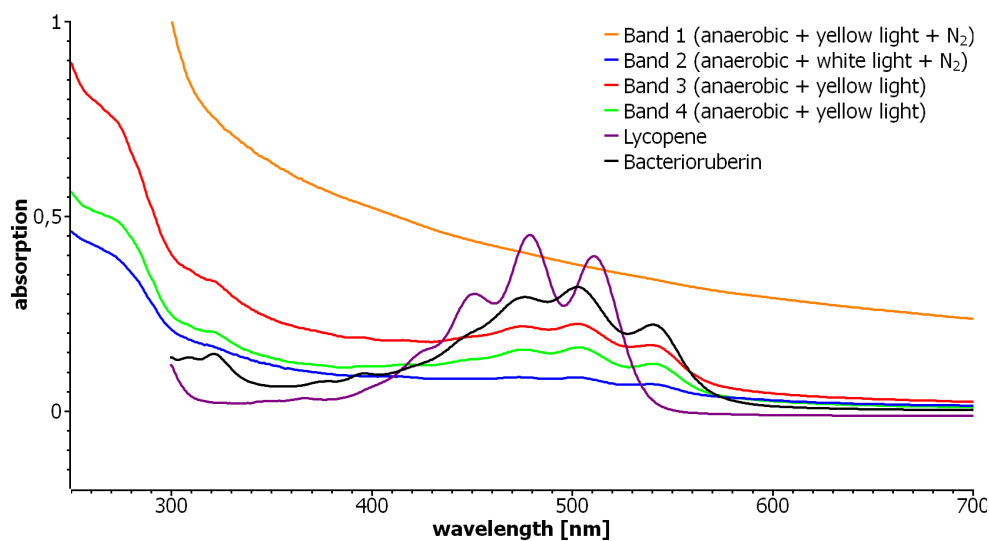


Figure 6.11: **Absorption spectra of isolated membrane bands from sucrose gradient of *Nmn. moolapensis*.**

Bands from the sucrose gradient were extracted with a pasteur pipette and UV/vis spectra were taken (Figure 6.11). Slight peaks matching to bacterioruberin were visible in the spectrum. In addition, lycopene and bacterioruberin were measured as a reference. The membrane bands 3 and 4, deriving from the culture grown anaerobically in yellow light showed a higher absorption than band 2 and 1. Neither lycopene nor absorption for BR (with bound retinal: 560 nm) could be detected. If the concentration of BR in the extracted membrane band is too low, the absorption maximum of it can also be hidden by the measured absorption spectrum of bacterioruberin.

Finally, proteins from the extracted bands were precipitated, separated by PAGE and analyzed by NanoLC-MS/MS. Bacteriorhodopsin could be identified by several unique peptides in the extracted membranes by MS/MS.

In the colors of the membranes in each gradient, major differences were apparent. None of the *Nmn. moolapensis* membranes appeared purple like the PM of *Hbt. salinarum* and the membrane extracted from the culture growing anaerobically with white light was even white. It was not expected that only slight changes in growth conditions (flushing with nitrogen or no flushing, white/yellow light) would have such a major effect on the regulation of membrane biosynthesis. The halobacterial membrane derives its purple color from the light absorbing retinal chromophore when it is covalently bound to the BR. The Bop protein of *Nmn. moolapensis* shares

54 % sequence identity with Bop of *Hbt. salinarum*. This also implies that there must be differences in the structure of the two compared proteins. Nevertheless, the protein with the highest sequence homology to the Bop protein of *Hbt. salinarum* is the Bop protein of *Nmn. moolapensis*. This can be seen in the phylogenetic tree in Figure 6.4.

Despite many different growth conditions, no purple membrane could be detected in a sucrose gradient for *Nmn. moolapensis*.

In *Halorubrum* sp. *aus-2*, the light-driven proton pump archaerhodopsin-2 was identified and found to form a claret membrane (Uegaki *et al.*, 1991). The significant color difference between the purple membrane and the claret membrane is due to the presence of the reddish pigment bacterioruberin in the latter membrane (Yoshimura & Kouyama, 2008). Although most members of *Halobacteriaceae* possess C 50 carotenoids of bacterioruberin groups (Dundas & Larsen, 1962), no trace of carotenoid is present, however, in the purple membrane of *Hbt. salinarum* (Kushwaha *et al.*, 1976b). Yoshimura & Kouyama (2008) proposed that bacterioruberin plays an important structural role for the trimerization of the archaerhodopsin in addition to the glycolipids (Essen *et al.*, 1998). Although no intense spectra for ruberins could be measured in *Nmn. moolapensis*, it is possible that this organism can also incorporate an additional carotenoid in the BR. A more sensitive method for the determination of this would be to measure the absorbance of a dried membrane film.

Another important question is whether different glycolipids are used by *Hbt. salinarum* and *Nmn. moolapensis* for stabilization of the trimeric BR proteins. Since *Hbt. salinarum* uses a glycolipid with three hexoses and *Nmn. moolapensis* only with one attached hexose (Figure 3.9), the BR activity could be modified due to probable changes in trimerization of the protein.

A recently developed method allows direct lipid analysis by MALDI mass spectrometry in intact membranes, without prior extraction/separation steps (Angelini *et al.*, 2010). This could help to analyze the membrane bands from the sucrose gradient directly and quickly gaining more information about their lipid components.

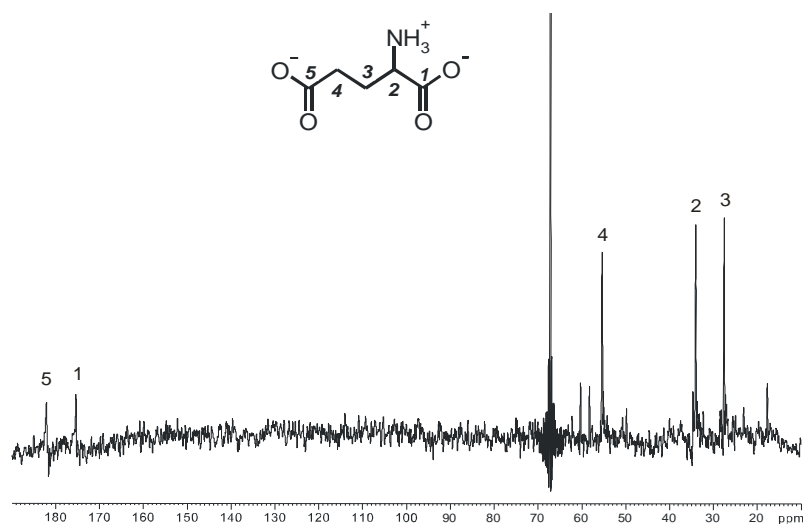


Figure 6.12: **NMR spectrum of extracted solutes of *Nmn. moolapensis*.** Glutamate was detected as the sole compatible solute in cytoplasmic extracts of *Nmn. moolapensis*.

### 6.2.3 NMR revealed glutamate as the sole compatible solute

*Nmn. moolapensis* was grown in the synthetic medium DBCM2 (Table 2.10) with pyruvate as the sole carbon source. Cytoplasmic extracts were isolated with ethanol and examined by natural abundance <sup>13</sup>C NMR. Also NMR spectra of *Nmn. pharaonis* and *Hbt. salinarum* were measured and compared. 2-sulfotrehalose has been demonstrated to be an osmolyte used by several haloalkaliphilic archaea including *Nmn. pharaonis* (Desmarais *et al.*, 1997). Whether *Nmn. moolapensis* is also capable of synthesizing this sulfated sugar or if it accumulates glutamate inside the cell like *Hbt. salinarum* (Kokoeva *et al.*, 2002) was examined in this study.

Surprisingly, 2-sulfotrehalose was not detected under the present conditions (aerobic growth in minimal or synthetic medium) neither in *Nmn. pharaonis* nor in *Nmn. moolapensis* or *Hbt. salinarum*. The only compatible solute detected in NMR analysis was glutamate (Figure 6.12). The use of glutamate inside the cell, balancing the electrical state of the cytoplasm in addition to chloride and the counterion potassium, is consistent with the results of Kokoeva *et al.* (2002) for *Hbt. salinarum*.

Moreover, it can be stated that there are no differences in the use of compatible solutes between neutrophilic and alkaliphilic haloarchaea if they are grown under the same conditions (aerobic incubation in the dark).

It was shown that all of the mentioned organisms were able to synthesize glutamate *de novo* in response to osmotic stress. This implies that synthesis of compatible solutes is very dependent on the composition of the growth medium, which could explain the differences in the spectrum of *Nmn. pharaonis* to those measured by Desmarais *et al.* (1997). Further studies are needed to compare the solute response of *Nmn. moolapensis* to other halophiles relating to different salt concentrations (high salt and low salt conditions).

### 6.3 Conclusions

The genome of the neutrophilic *Nmn. moolapensis* was elucidated and compared to its alkaliphilic relative *Nmn. pharaonis* and the neutrophilic *Hbt. salinarum* to analyze how species diverged in relation to their differing pH optima.

A comparison and synteny analysis of retinal protein genes with associated regulators was performed and could show among other things, that the synteny of retinal protein genes in *Nmn. moolapensis* is more related to the corresponding genes in the *Nmn. pharaonis* genome than in the *Hbt. salinarum* genome. Rearrangements to these genomes and genetic mobility of some retinal protein genes (e.g. *bop*) can be seen as adaptations to different ecological niches (e.g. high external pH) and explain their different possibilities to gain energy.

Comparing the metabolic potentials of *Nmn. moolapensis* and *Nmn. pharaonis* with PRIAM (Claudel-Renard *et al.*, 2003), a method for automated enzyme detection in fully sequenced genome, showed that only a few single genes were absent/present in the respective genome, without any influence on a whole pathway. Therefore, it was concluded that the program PRIAM is rather helpful for genome comparisons between organisms not closely related.

Significant differences could only be detected in the biotin biosynthesis with *Nmn. moolapensis* lacking all necessary genes, and methionine metabolism, which differs in *Nmn. moolapensis*.



Genes for energy metabolism were investigated manually revealing major differences between the two species. It could be verified that the detected *bop* gene, not present in the alkaliphilic species, was expressed in *Nmn. moolapensis* under different growth conditions, resulting in variably colored membranes. While no purple membrane could be detected, phototrophic growth was possible.

It was also concluded that reasons for the different color of the membrane in comparison to the purple membrane in *Hbt. salinarum* might be the incorporation of glycolipids other than the S-TGD-1. Another reason could be the different amino acid sequences of bacteriorhodopsin or the presence of an additional pigment, like ruberin inside the protein.

Glutamate was detected as a compatible solute inside the cell of *Nmn. moolapensis*, confirming *de novo* synthesis of this amino acid. Moreover, it could be demonstrated that at similar growth conditions *Nmn. moolapensis*, *Nmn. pharaonis* and *Hbt. salinarum* accumulate glutamate inside the cell. This shows that there are no differences between neutrophilic and alkaliphilic haloarchaea in osmolyte biosynthesis in response to osmotic stress and that its biosynthesis depends very much on the composition of the growth medium.

Overall, *Nmn. moolapensis* is a useful model organism for the comparative study of archaeal microbes that thrive in environments varying widely in pH. Based on this study, future work on comparative analysis of retinal proteins in the different organisms can broaden the knowledge about their biosynthesis and regulation.



## 7 Supplementary material

Table S1: **Protein sequence analysis of lysine decarboxylase.** In the genome annotation of *Hrd. utahensis* a gene (Huta\_1965) annotated as a possible lysine decarboxylase was found. Amino acid sequence homology searches in HaloLex - Blast were performed. The cut-off for e-value was  $1e - 25$ .

<b>Organism</b>	<b>ORF</b>	<b>e-value</b>
<i>Har. marismortui</i>	rrnAC2888	$6e - 38$
<i>Nmn. pharaonis</i>	NP0552A	$1e - 35$
<i>Nmn. moolapensis</i>	ORF002891V0	$2e - 34$
<i>Hqr. walsbyi</i>	HQ2000A	$3e - 32$
<i>Hmc. mukohataei</i>	Hmuk_1012	$5e - 32$
<i>Hrr. lacusprofundi</i>	Hlac_0814	$3e - 31$
<i>Nab. magadii</i>	Nmag_1975	$9e - 27$
<i>Htg. turkmenica</i>	Htur_3727	$1e - 26$
<i>Hfx. volcanii</i>	HVO_1628	$1e - 25$

## 7 Supplementary material

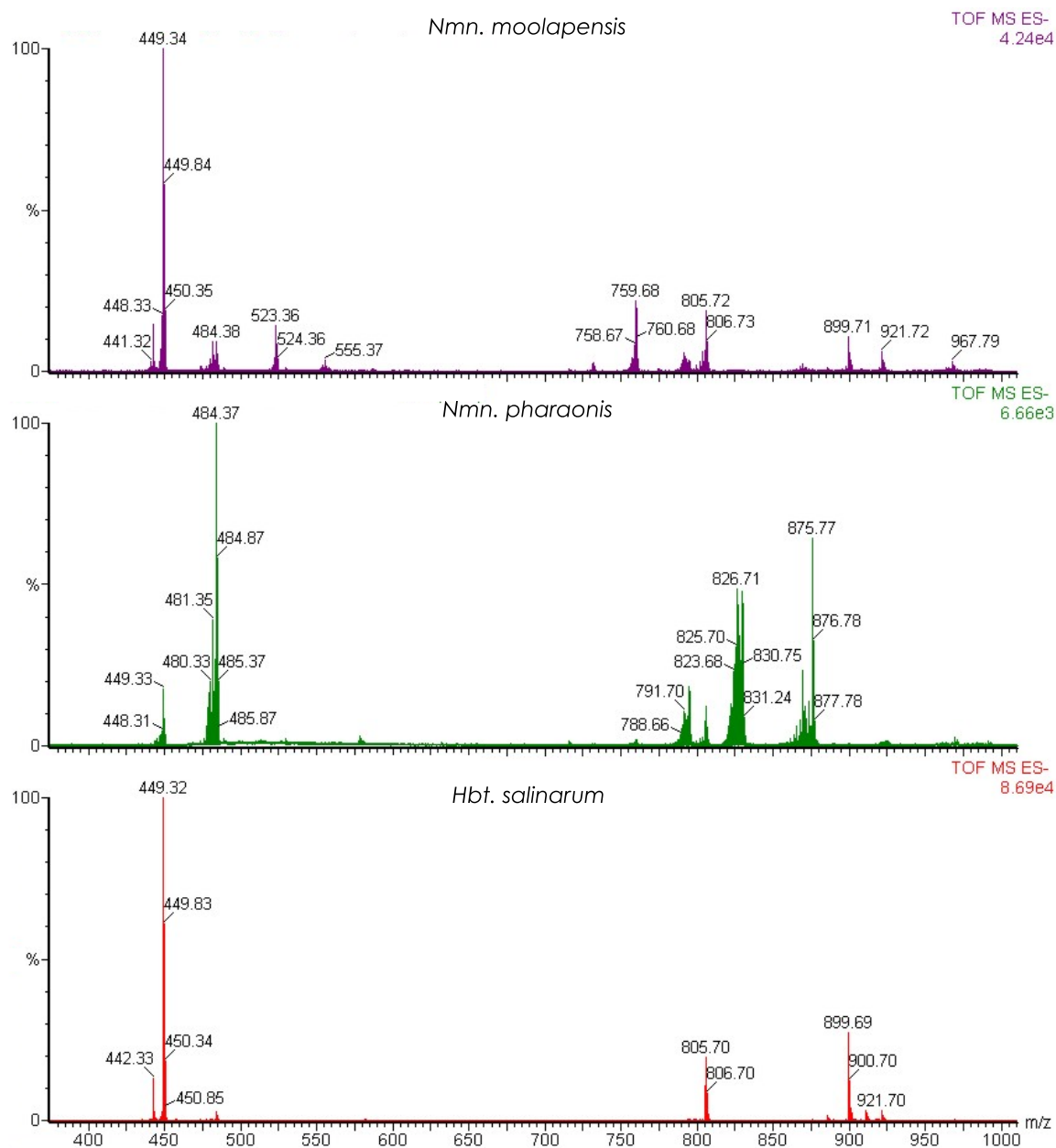
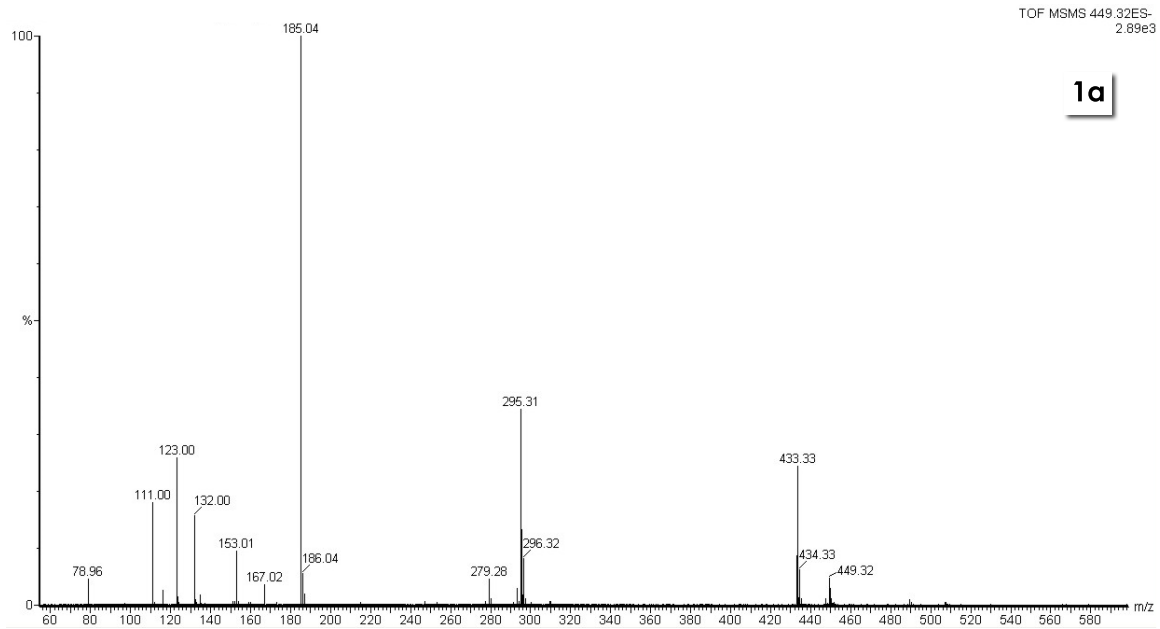
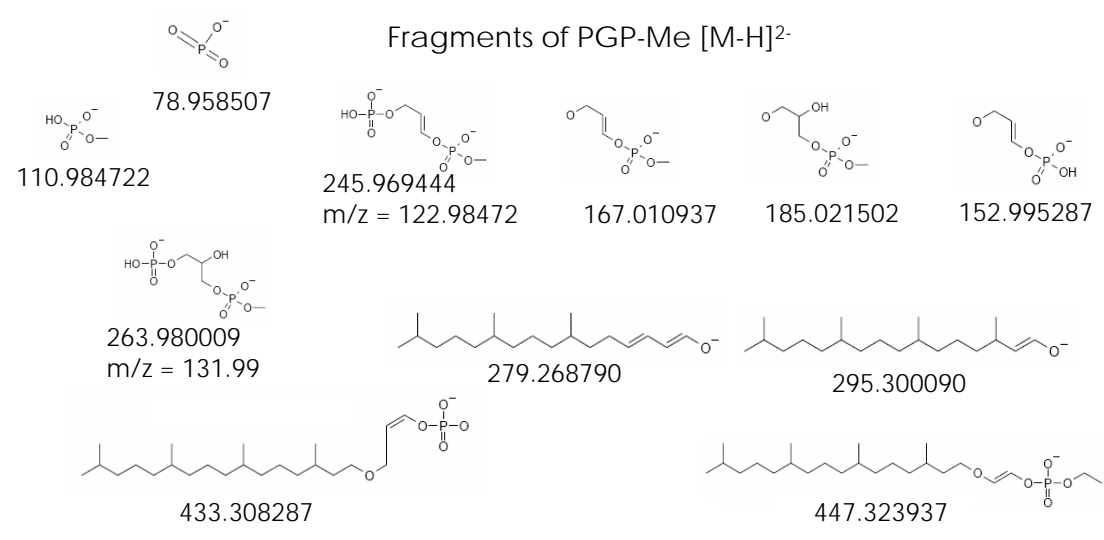


Figure S1: Comparison of total lipid extracts by ESI-MS. Spectra show sharp peaks for *Hbt. salinarum* but peaks with satellites for *Nmn. moolapensis* and most intense for *Nmn. pharaonis*. These satellites are of lower mass and might correspond to unsaturated isoprenoids as even mass differences were observed.

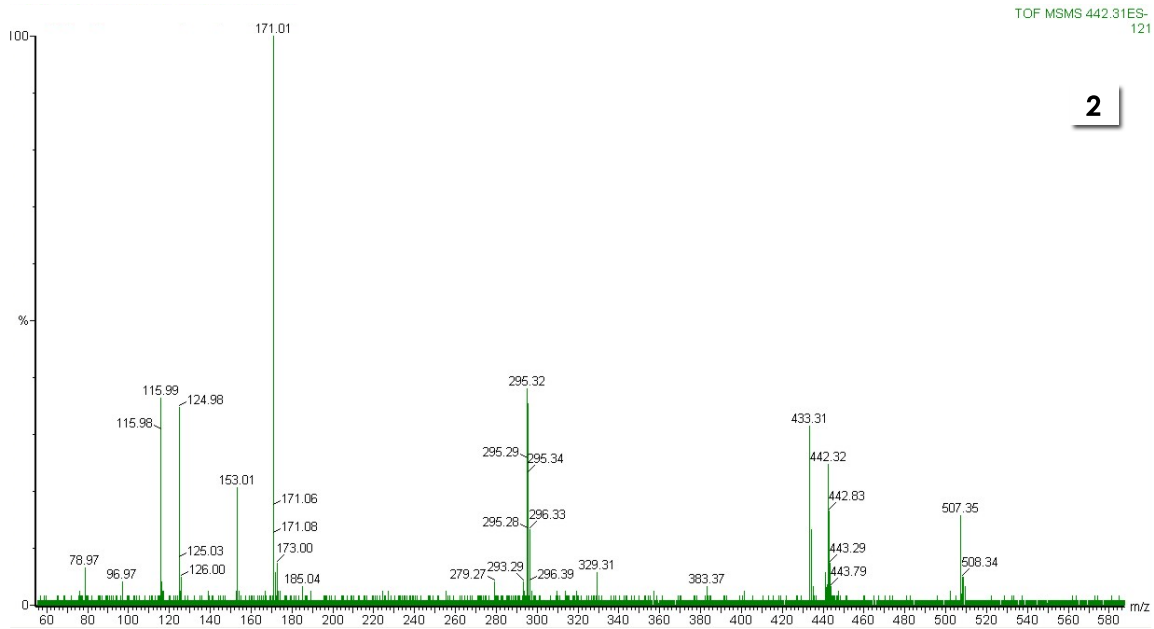


**1a**

Fragments of PGP-Me [M-H]<sup>2-</sup>

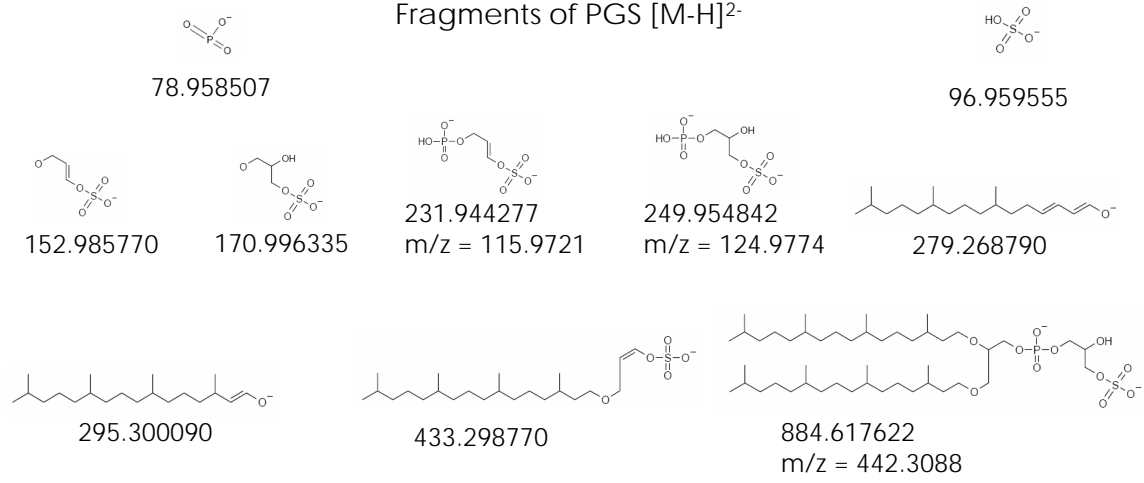




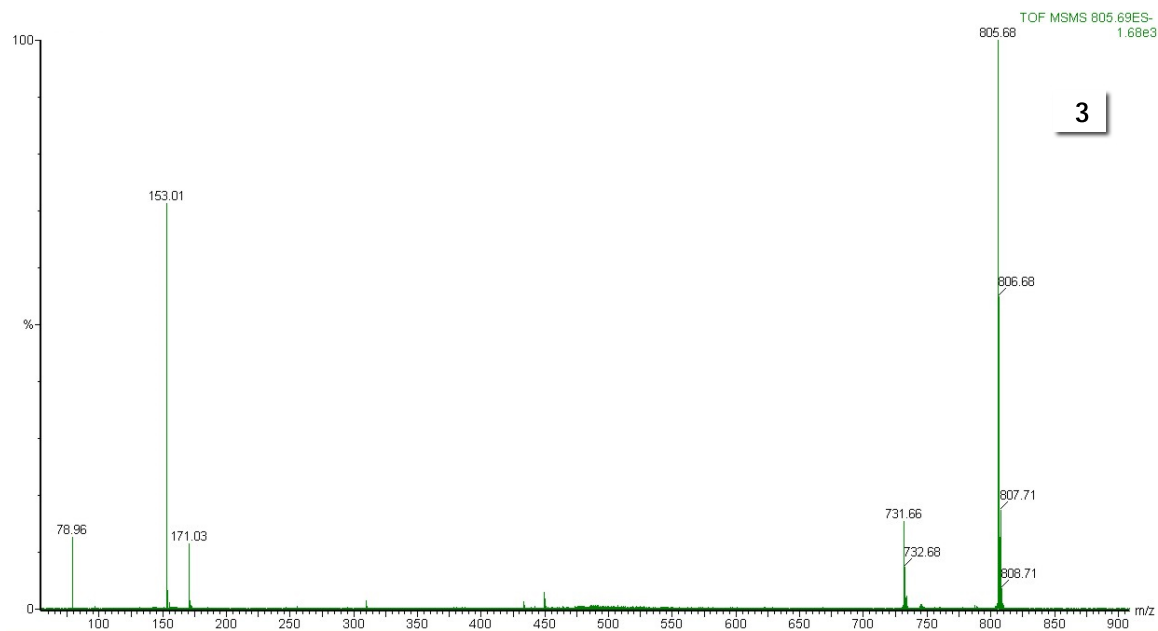


2

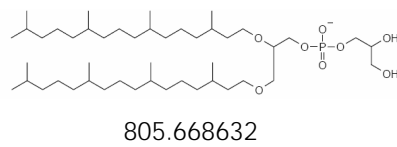
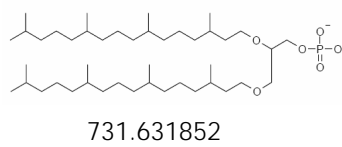
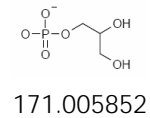
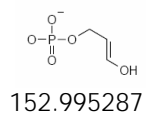
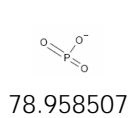
Fragments of PGS [M-H]<sup>2-</sup>



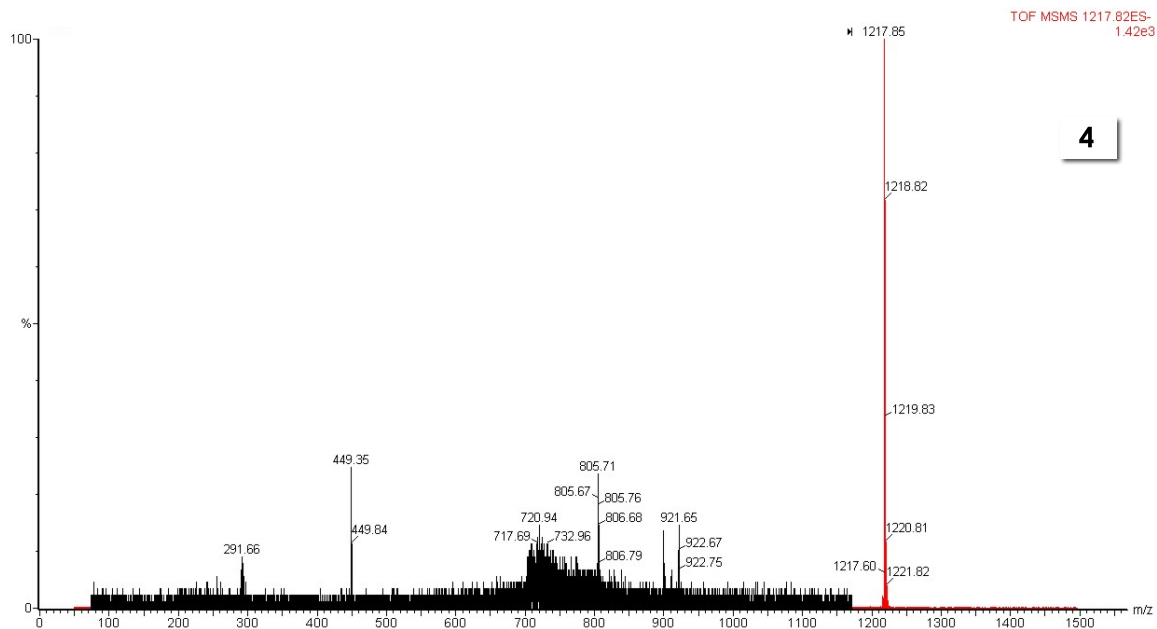
7 Supplementary material



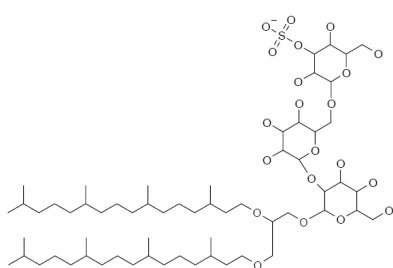
Fragments of PG [M-H]<sup>-</sup>



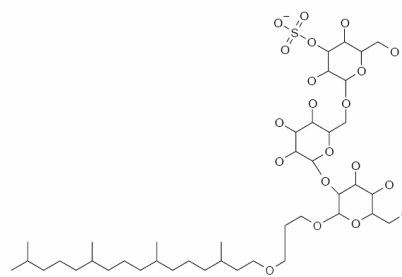




Fragments of S-TGD [M-H]<sup>-</sup>

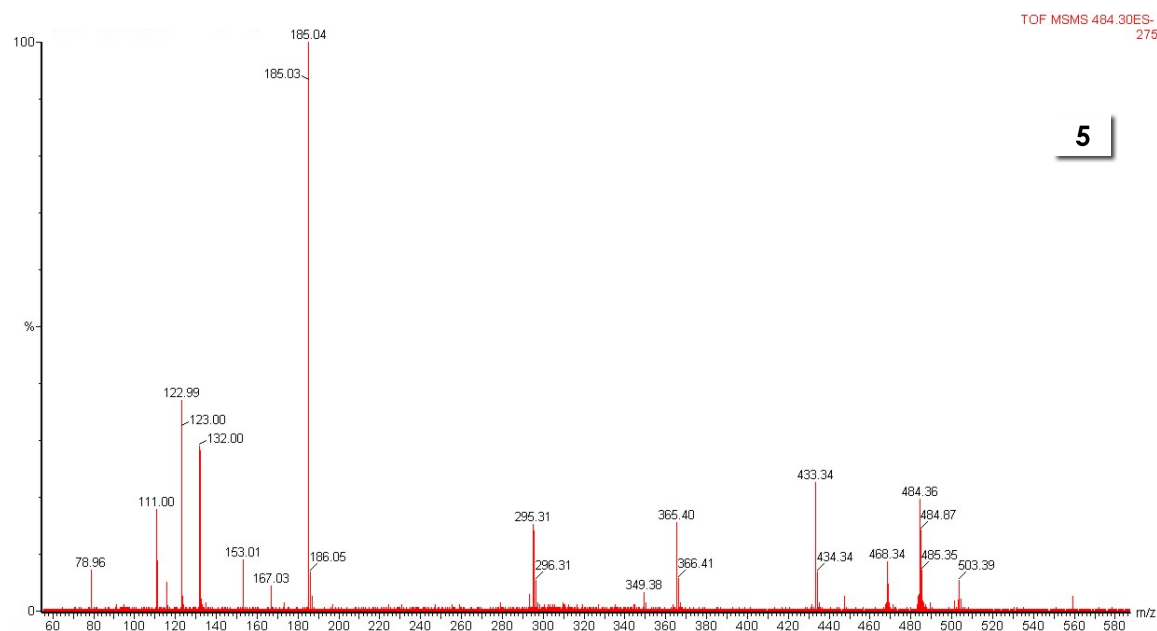


1217.780810



921.472895

## 7 Supplementary material



Fragments of PGP-Me [M-H]<sup>-</sup> C<sub>20</sub>-C<sub>25</sub>

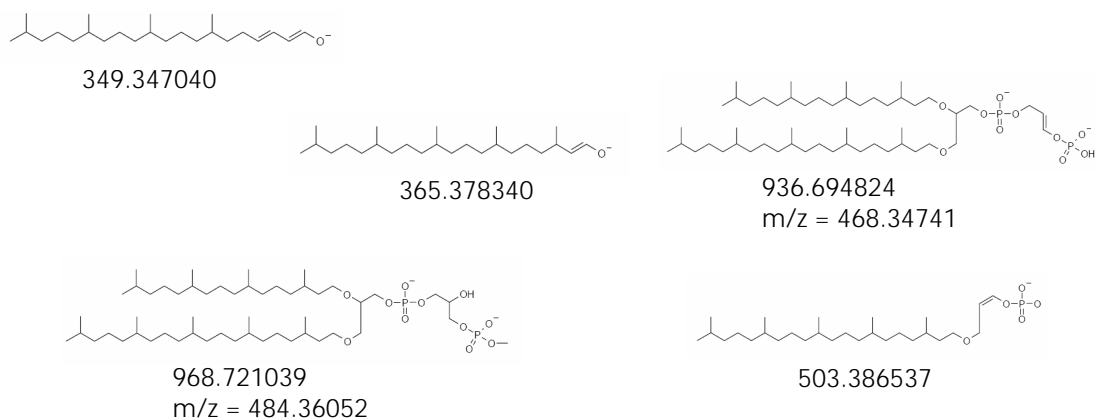
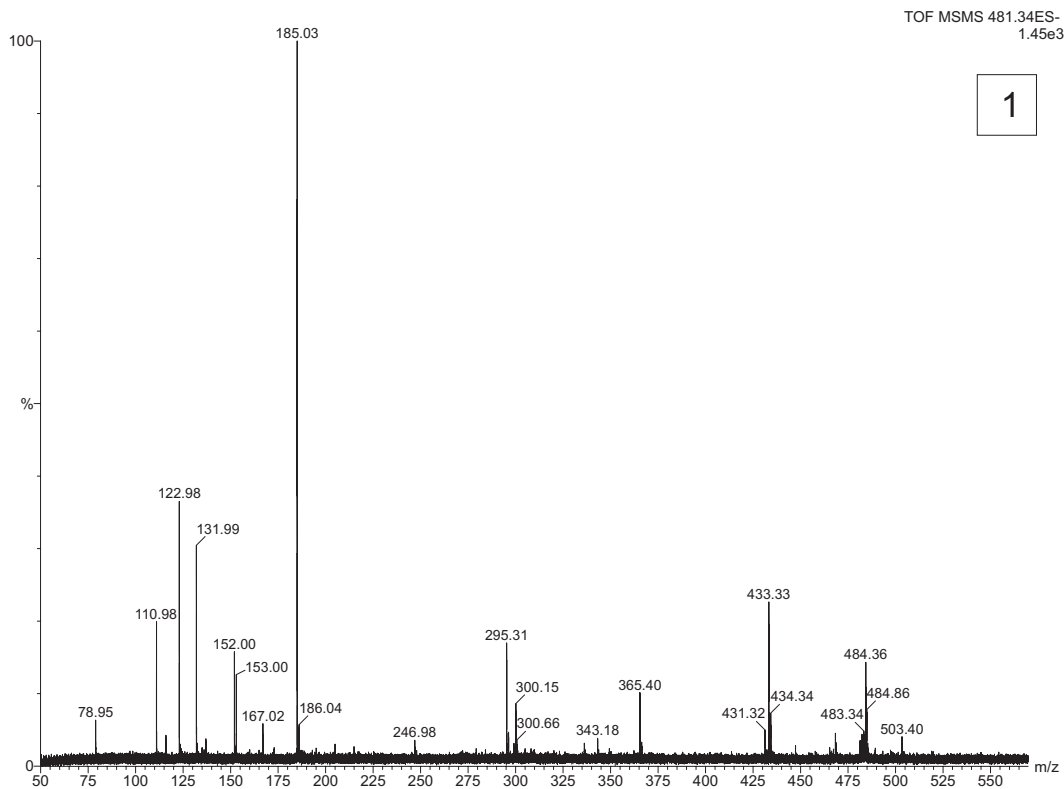
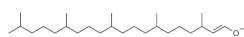


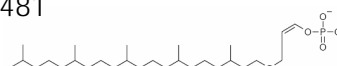
Figure S2: **Catalogue of lipid fragments from MS/MS spectra.** Fragments of the following ions were analyzed and the respective structures proposed (**1-4**: from total lipid extract of *Hbt. salinarum* and **5**: from total lipid extract of *Nmn. pharaonis*). **1a** PGP-Me doubly charged ion, **1b** PGP-Me singly charged ion, **2** PGS doubly charged ion, **3** PG singly charged ion, **4** S-TGD-1 singly charged ion, **5** PGP-Me doubly charged with a C<sub>20</sub> and a C<sub>25</sub> isoprenoid. The exact calculated mass of each fragment is written beneath the structure.



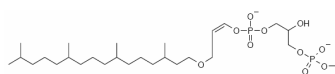
MS/MS fragments of peak 481



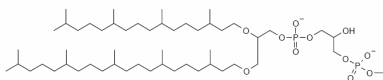
365.378340



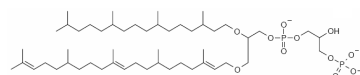
503.386537



600.319224  
m/z = 300.1596

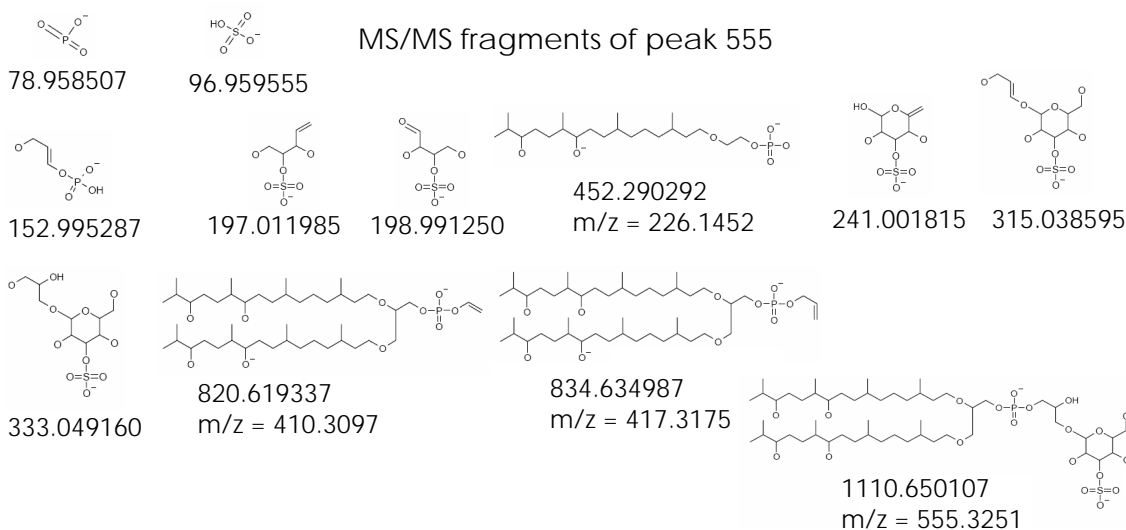
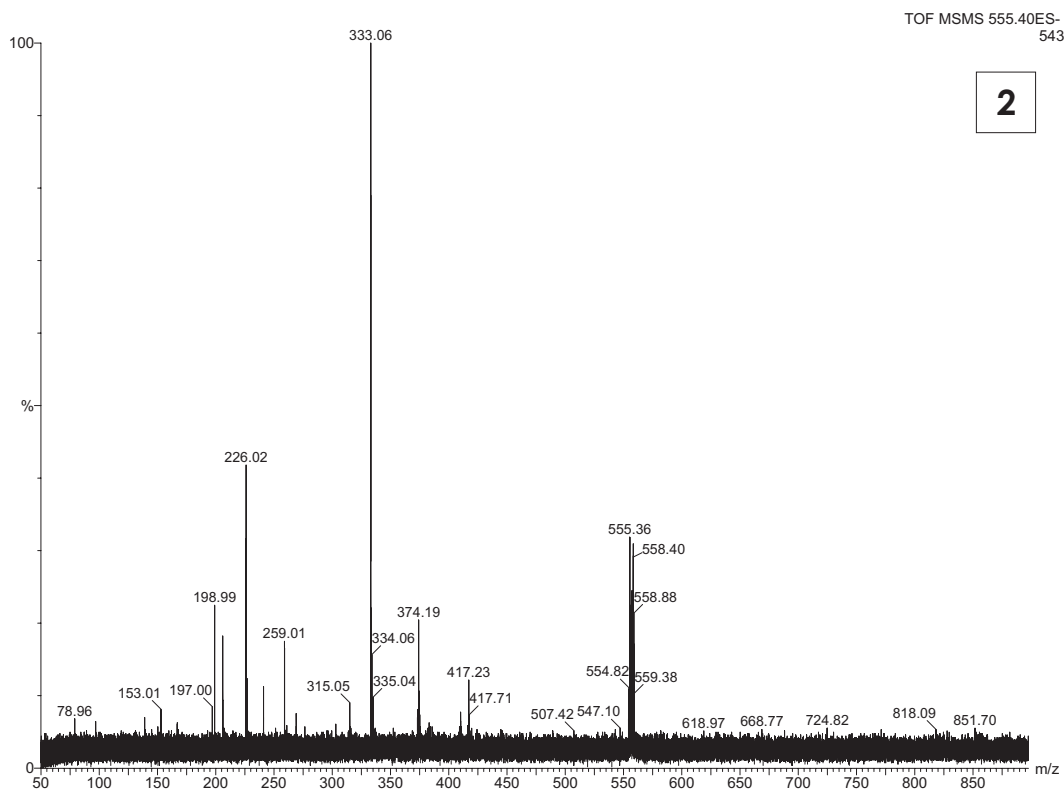


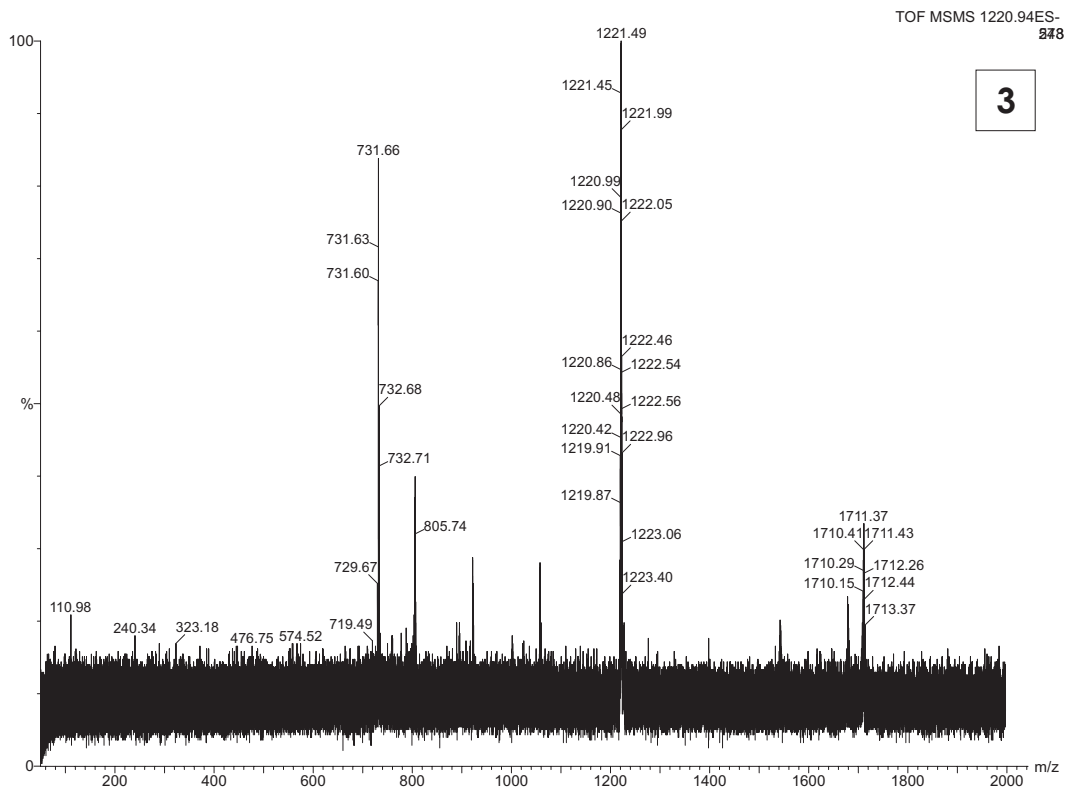
968.721039  
m/z = 484.3605



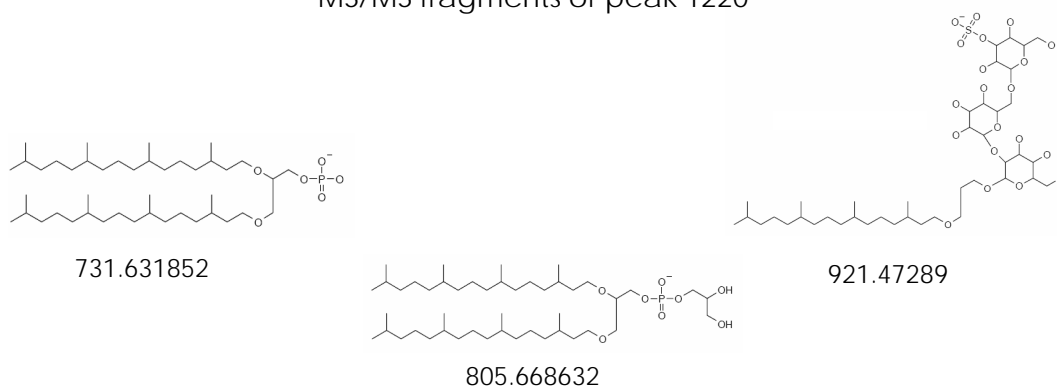
962.674089  
m/z = 481.3371

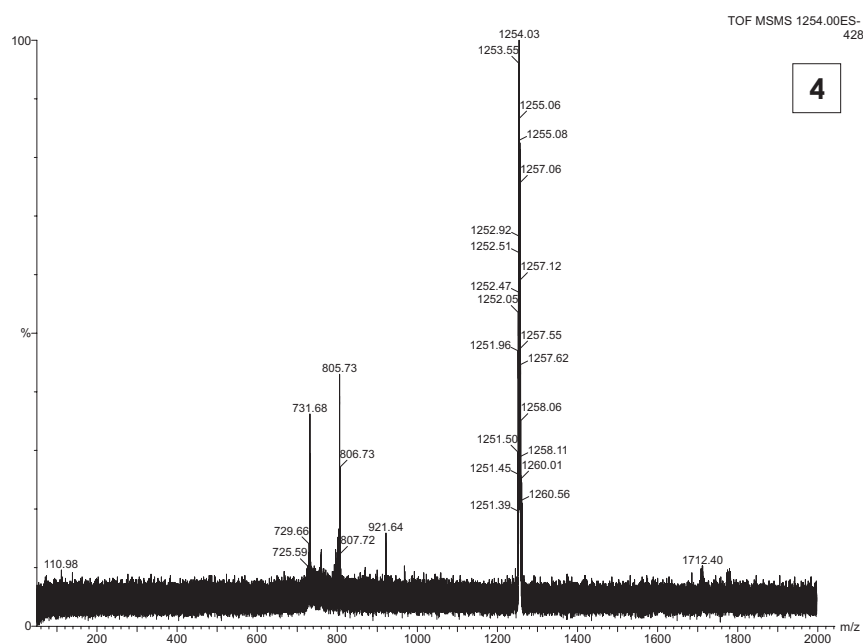
# 7 Supplementary material





MS/MS fragments of peak 1220





MS/MS fragments of peak 1254

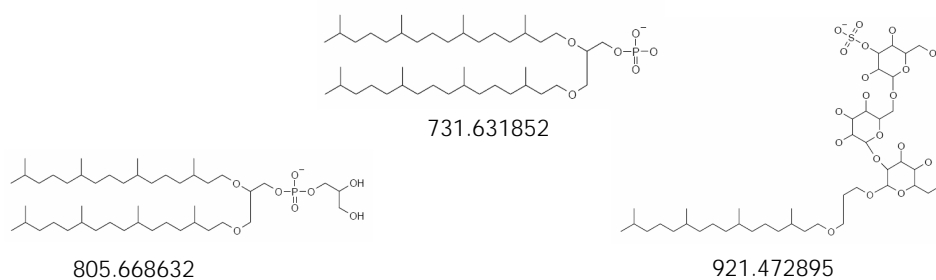


Figure S3: **Lipid fragments from MS/MS spectra of unknown MS peaks in *Nmn. moolapensis*.** For lipid characterization in *Nmn. moolapensis* the fragments of the following MS peaks were analyzed: **(1)** doubly charged ion 481 amu; **(2)** doubly charged ion 555 amu; **(3)** singly charged ion 1220 amu; **(4)** singly charged ion 1254 amu. Peak 481 amu might be an unsaturated form of the lipid PGP-Me C<sub>20</sub>-C<sub>25</sub> and peak 555 amu might be the tetra-hydroxy form of the new glycolipid in *Nmn. moolapensis*. Due to the singly charged precursors and very stable molecule in the spectra **(3)** and **(4)** they are more difficult to interpret and only structures of a few fragments could be proposed.

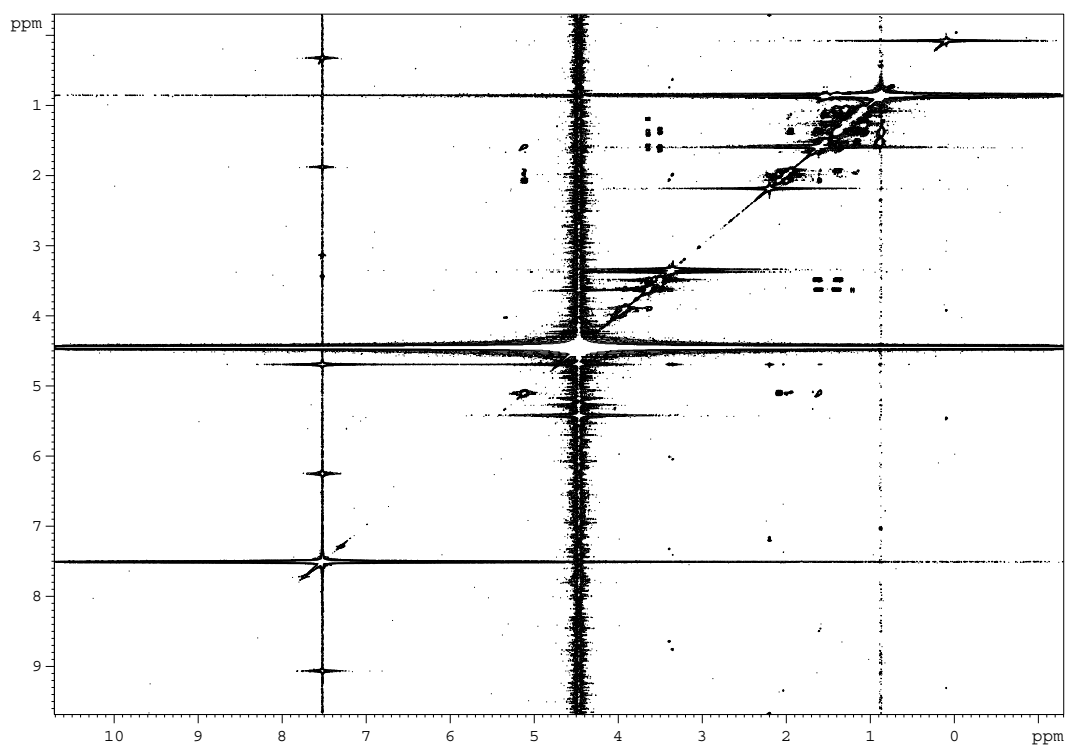


Figure S4: 2D proton-COSY experiment of fully <sup>13</sup>C labeled lipids.

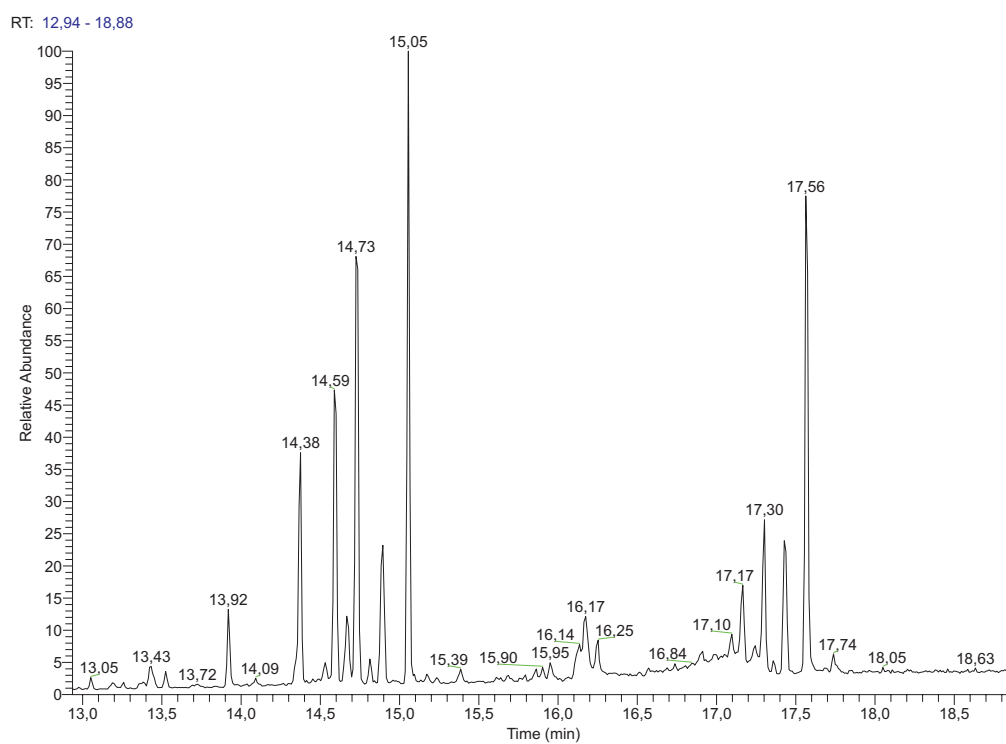


Figure S5: Chromatogram of a typical GC/MS measurement of isoprenoids.



Table S2: Summary of arginine and ornithine uptake experiments in *Hbt. salinarum*.

glycerol	light	CO <sub>2</sub>	arg	orn	arg/orn	Δorn	Δarg
+	+	24	+	-	1,71	4,52	7,72
+	-	0	+	-	2,30	3,32	7,63
+	+	0	+	-	2,65	3,07	8,13
-	+	24	+	-	2,94	3,52	10,34
-	+	0	+	-	3,27	3,61	11,81
-	-	0	+	-	2,82	3,88	10,94
-	+	-	+	+	\	0,00	12,36
-	+	-	-	+	\	7,96	\
-	-	-	-	+	\	8,47	\
-	+	-	+	-	6,02	2,63	15,86
-	-	-	+	-	7,55	2,02	15,26
-	-	-	+	+	4,64	3,00	13,89
-	-	24	+	+	\	0,00	12,12
+	+	-	+	-	2,48	5,43	13,48
+	-	-	+	-	1,43	6,95	9,96
+	+	24	+	-	2,03	5,53	11,23
+	+	0	+	-	1,85	7,15	13,20
+	-	0	+	-	2,78	4,83	13,41
-	+	-	+	-	0,86	8,79	7,60
-	-	-	+	-	1,52	5,38	8,16
-	+	24	+	-	1,54	4,73	7,29
-	+	0	+	-	1,11	6,25	6,93
-	-	0	+	-	1,68	4,24	7,14
+	+	-	+	+	\	\	10,85
+	-	-	+	+	\	0,00	9,17
+	+	24	+	+	\	0,00	11,50
+	+	-	-	+	\	7,30	\
+	-	-	-	+	\	8,85	\
-	+	-	+	+	\	0,00	12,02
-	-	-	+	+	\	\	9,51
-	+	24	+	+	\	0,00	9,57
-	+	-	-	+	\	7,76	\
-	-	-	-	+	\	7,76	\

Each uptake experiment is listed with its particular parameters and experiments measured in parallel are separated by horizontal lines. Cultures grown on glycerol in the synthetic medium are marked with a "+". Cell suspensions which were illuminated during the uptake experiment are marked with a "+" in the "light"-column and those which have grown anaerobically since the start of the experiment with a "0" and after 24 h with a "24". Either 0.5 % arginine, 0.5 % ornithine or both was added to the basal salt medium (" +/- "). The intracellular change of concentration [fmol/fl] of ornithine (Δorn) and arginine (Δarg) and the ratio were calculated under the assumption that no degradation or incorporation into proteins took place. Indeterminable values due to measurement inaccuracies were indicated with a "\".

## 7 Supplementary material

QUANTIFIED PROTEINS				
AccNo	ProtName	Ratio	SD %	Count
OE5208R	(OE5208R) arginine deiminase (EC 3.5.3.6)	29,70	18,33	4
OE3580R	(OE3580R) threonine--tRNA ligase (EC 6.1.1.3)	13,16	3,74	2
OE4305R	(OE4305R) ABC-type dipeptide transport system periplasmic dipeptide-binding protein	10,29	0,60	2
OE4759F	(OE4759F) cell surface glycoprotein precursor	9,75	1,72	2
OE1584R	(OE1584R) conserved protein	9,72	2,29	4
OE3724F	(OE3724F) phosphoribosylaminoimidazolesuccinocarboxamide synthase (EC 6.3.2.6)	9,64	1,27	2
OE4198F	(OE4198F) alanine--tRNA ligase (EC 6.1.1.7)	8,88	2,68	2
OE3524F	(OE3524F) pyridoxine biosynthesis protein	8,56	1,57	3
OE2622R	(OE2622R) pyruvate--ferredoxin oxidoreductase (EC 1.2.7.1) beta chain (pyruvate dehydrogenase	7,72	0,69	2
OE1711R	(OE1711R) oxoglutarate--ferredoxin oxidoreductase (EC 1.2.7.3) alpha chain (alpha-ketoglutarate--	7,43	1,02	3
OE2304F	(OE2304F) DNA topoisomerase (ATP-hydrolyzing) (EC 5.99.1.3) chain A	7,21	0,47	2
OE1770F	(OE1770F) DNA double-strand break repair ATPase	6,33	2,79	4
OE3807R	(OE3807R) oligoendopeptidase	6,19	3,34	3
OE1737R	(OE1737R) dnaK-type molecular chaperone hsp70	6,12	0,23	2
OE2623R	(OE2623R) pyruvate--ferredoxin oxidoreductase (EC 1.2.7.1) alpha chain (pyruvate dehydrogenase	6,11	1,38	4
OE1623F	(OE1623F) adenylosuccinate lyase (EC 4.3.2.2)	5,71	0,47	2
OE4742R	(OE4742R) DNA-directed RNA polymerase (EC 2.7.7.6) chain B"	5,58	1,30	7
OE3308F	(OE3308F) malate dehydrogenase (oxaloacetate decarboxylating) (EC 1.1.1.40)	5,21	1,72	3
OE4718F	(OE4718F) ribonuclease R homolog	5,09	0,49	2
OE5205R	(OE5205R) ornithine carbamoyltransferase (EC 2.1.3.3), catabolic	4,42	1,87	2
OE2579F	(OE2579F) adenylosuccinate synthase (EC 6.3.4.4)	4,35	2,21	2
OE3934R	(OE3934R) citrate (si)-synthase (EC 2.3.3.1) (formerly EC 4.1.3.7)	3,83	2,18	2
OE3177F	(OE3177F) pyruvate carboxylase (EC 6.4.1.1)	3,56	1,00	2
OE3691F	(OE3691F) probable anthranilate phosphoribosyltransferase (EC 2.4.2.18)	3,56	1,25	3
OE1522F	(OE1522F) aspartyl-tRNA(Asn) amidotransferase (EC 6.3.5.-) chain B	3,27	0,97	3
OE2138F	(OE2138F) probable acyl/butyryl-CoA dehydrogenase (EC 1.3.99.-)	3,14	2,62	2
OE3940F	(OE3940F) conserved protein	2,79	1,32	2
OE3168R	(OE3168R) pyridoxal phosphate-dependent aminotransferase (acetylornithine transaminase homol	2,26	0,23	2
OE5212F	(OE5212F) SMC-like protein sph1	1,90	0,44	3
OE4741R	(OE4741R) DNA-directed RNA polymerase (EC 2.7.7.6) chain B'	1,87	2,08	2
OE3571R	(OE3571R) GMP synthase (glutamine-hydrolyzing) (EC 6.3.5.2), subunit B	1,38	0,58	2
OE3922R	(OE3922R) glutamate--ammonia ligase (EC 6.3.1.2)	0,70	0,18	2
OE2871F	(OE2871F) probable 3-hydroxyacyl-CoA dehydrogenase (EC 1.1.1.157)	0,55	0,37	2
OE3580R	(OE3580R) threonine--tRNA ligase (EC 6.1.1.3)	0,44	0,17	3

Figure S6: Overview of all quantified proteins using the ICPL method.

Table S3: Enzymes encoded in *Nmn. pharaonis* (Napha) and *Hbt. salinarum* (Hasal) capable of CO<sub>2</sub> fixation.

ORFs	Protein name	Enzymes	Reactions
Napha			
NP0106A	prephenate dehydratase	4.2.1.51	L-Arogenate $\rightleftharpoons$ L-Phenylalanine + H <sub>2</sub> O + CO <sub>2</sub> ; Prephenate $\rightleftharpoons$ Phenylpyruvate + H <sub>2</sub> O + CO <sub>2</sub>
NP1088A, NP1124A	precorrin-6Y C5,15-methyltransferase	2.1.1.132	Cobalt-dihydro-precorrin 6 + S-Adenosyl-L-methionine $\rightleftharpoons$ Cobalt-precorrin 8 + S-Adenosyl-L-homocysteine + CO <sub>2</sub>
NP0132A, NP1772A	malate dehydrogenase	1.1.1.40	(S)-malate + NADP <sup>+</sup> $\rightleftharpoons$ pyruvate + CO <sub>2</sub> + NADPH
NP5302A	L-threonine-O-3-phosphate decarboxylase	4.1.1.81	L-Threonine O-3-phosphate $\rightleftharpoons$ D-1-Aminopropan-2-ol O-phosphate + CO <sub>2</sub>
NP4484A	pyruvoyl-dependent arginine decarboxylase	4.1.1.19	L-Arginine $\rightleftharpoons$ Agmatine + CO <sub>2</sub>
NP1646A	diaminopimelate decarboxylase	4.1.1.20	meso-2,6-Diaminoheptanedioate $\rightleftharpoons$ L-Lysine + CO <sub>2</sub>
NP3358A	prephenate dehydrogenase	1.3.1.12	Prephenate + NAD <sup>+</sup> $\rightleftharpoons$ 3-(4-Hydroxyphenyl)pyruvate + CO <sub>2</sub> + NADH + H <sup>+</sup>
NP3166A	indole-3-glycerol-phosphate synthase	4.1.1.48	1-(2-Carboxyphenylamino)-1'-deoxy-D-ribulose 5'-phosphate Indoleglycerol phosphate + CO <sub>2</sub> + H <sub>2</sub> O
NP2430A	$\rightleftharpoons$ isocitrate dehydrogenase	1.1.1.42	Oxalosuccinate $\rightleftharpoons$ 2-Oxoglutarate + CO <sub>2</sub>
NP4506A, NP4830A	carbamoyl-phosphate synthase	6.3.5.5	2 ATP + L-Glutamine + HCO <sub>3</sub> <sup>-</sup> + H <sub>2</sub> O $\rightleftharpoons$ 2 ADP + Orthophosphate + L-Glutamate + Carbamoyl phosphate
NP2286A, NP2290A	phosphoribosylaminoimidazole carboxylase	4.1.1.21	1-(5-Phospho-D-ribosyl)-5-amino-4-imidazolecarboxylate $\rightleftharpoons$ Aminoimidazole ribotide + CO <sub>2</sub>
NP4774A	aminomethyltransferase (glycine cleavage system protein T)	2.1.2.10	5,10-Methylenetetrahydrofolate + NH <sub>3</sub> + CO <sub>2</sub> + NADH + H <sup>+</sup> $\rightleftharpoons$ Glycine + Tetrahydrofolate + NAD <sup>+</sup>
NP3710A, NP4944A, NP4946A,	formate dehydrogenase	1.2.1.2	Formate + NAD <sup>+</sup> $\rightleftharpoons$ H <sup>+</sup> + CO <sub>2</sub> + NADH

NP4960A, NP4962A NP2770A	ribulose-bisphosphate carboxylase	4.1.1.39	D-Ribulose 1,5-bisphosphate + CO <sub>2</sub> + H <sub>2</sub> O => 3-Phospho-D-glycerate
NP4044A, NP4046A NP1232A, NP1234A, NP3012A	pyruvate-ferredoxin oxidoreductase  oxoglutarate-ferredoxin oxidoreductase	1.2.7.1  1.2.7.3	Oxidized ferredoxin + Pyruvate + CoA <=> Reduced ferredoxin + Acetyl-CoA + CO <sub>2</sub>  Oxidized ferredoxin + 2-Oxoglutarate + CoA <=> Reduced ferredoxin + Succinyl-CoA + CO <sub>2</sub>
NP1194A	tyrosine decarboxylase	4.1.1.25	L-tyrosine <=> tyramine + CO <sub>2</sub>
NP2562A	probable 5-oxopent-3-ene-1,2,5- tricarboxylate decarboxylase 3	4.1.1.68	5-oxopent-3-ene-1,2,5-tricarboxylate <=> 2-oxohept-3-enedioate + CO <sub>2</sub>
NP3464A, NP4250A, NP4252A, NP4364A, NP4368A NP1580A	propionyl-CoA carboxylase carboxyltransferase  diphosphomevalonate decarboxylase	6.4.1.3  4.1.1.33	ATP + propanoyl-CoA + HCO <sub>3</sub> <sup>-</sup> <=> ADP + phosphate + (S)-methylmalonyl-CoA  ATP + (R)-5-diphosphomevalonate <=> ADP + phosphate + isopentenyl
Hasal			
OE2563R	SEPHCHC synthase	2.5.1.64	2-Oxoglutarate + Thiamin diphosphate <=> Succinate semialdehyde-thiamin diphosphate anion + CO <sub>2</sub>
OE1469F	indole-3-glycerol-phosphate synthase	4.1.1.48	1-(2-Carboxyphenylamino)-1'-deoxy-D-ribose 5'-phosphate <=> Indoleglycerol phosphate + CO <sub>2</sub> + H <sub>2</sub> O
OE3634F	isocitrate dehydrogenase (NADP+)	1.1.1.42	Oxalosuccinate <=> 2-Oxoglutarate + CO <sub>2</sub>
OE3363F	probable orotidine-5'-phosphate decarboxylase	4.1.1.23	Orotidine 5'-phosphate <=> UMP + CO <sub>2</sub>
OE3634F	isocitrate dehydrogenase (NADP+)	1.1.1.42	Isocitrate + NADP+ <=> 2-Oxoglutarate + CO <sub>2</sub> + NADPH + H+

OE3554F,	carbamoyl-phosphate synthase	6.3.4.16	ATP + NH <sub>3</sub> + CO <sub>2</sub> + H <sub>2</sub> O =>
OE3556R			ADP + Orthophosphate + Carbamoyl phosphate
OE5206R	carbamate kinase	2.7.2.2	ATP + NH <sub>3</sub> + CO <sub>2</sub> => ADP + Carbamoyl phosphate
OE2770F	prephenate dehydrogenase	1.3.1.12,	Prephenate + NAD <sup>+</sup> <=>
		1.3.1.52,	3-(4-Hydroxyphenyl)pyruvate + CO <sub>2</sub> + NADH + H <sup>+</sup>
		1.3.1.43	
OE1951F,	phosphoribosylaminoimidazole carboxylase	4.1.1.21	1-(5-Phospho-D-ribose)-5-amino-4-imidazolecarboxylate
OE1952F			<=> Aminoimidazole ribotide + CO <sub>2</sub>
OE1710R,	oxoglutarate-ferredoxin oxidoreductase	1.2.7.3	Reduced ferredoxin + Succinyl-CoA + CO <sub>2</sub>
OE1711R			<=> Oxidized ferredoxin + 2-Oxoglutarate + CoA
OE3278R	aminomethyltransferase (glycine cleavage system protein T)	2.1.2.10	5,10-Methylenetetrahydrofolate + NH <sub>3</sub> + CO <sub>2</sub> + NADH + H <sup>+</sup> => Glycine + Tetrahydrofolate + NAD <sup>+</sup>
OE3648F	nicotinate-nucleotide pyrophosphorylase	2.4.2.19	Pyridine-2,3-dicarboxylate + 5-Phospho-alpha-D-ribose 1-diphosphate => Nicotinate D-ribonucleotide + Pyrophosphate + CO <sub>2</sub>
OE4117F	prephenate dehydratase	4.2.1.91,	Prephenate <=> Phenylpyruvate + H <sub>2</sub> O + CO <sub>2</sub>
		4.2.1.51	
OE1498R	tyrosine decarboxylase	4.1.1.25	L-tyrosine <=> tyramine + CO <sub>2</sub>
OE1893F	diphosphomevalonate decarboxylase	4.1.1.33	ATP + (R)-5-diphosphomevalonate <=> ADP + phosphate + isopentenyl
OE1939F,	propionyl-CoA carboxylase carboxyltransferase	6.4.1.3	ATP + propanoyl-CoA + HCO <sub>3</sub> <sup>-</sup> <=>
OE3175F,			ADP + phosphate + (S)-methylmalonyl-CoA
OE3177F			
OE3259F	L-threonine-O-3-phosphate decarboxylase	4.1.1.81	L-Threonine O-3-phosphate <=> D-1-Aminopropan-2-ol O-phosphate + CO <sub>2</sub>
OE3803R	pyruvoyl-dependent arginine decarboxylase	4.1.1.19	(S)-Malate + NADP <sup>+</sup> <=> Pyruvate + CO <sub>2</sub> + NADPH + H <sup>+</sup>

OE3308F malate dehydrogenase

1.1.1.40 (S)-malate + NADP+ = pyruvate + CO2 + NADPH

---

Table S5: Genes of *Nmn. moolapensis* annotated for pathway comparison.

Protein name	EC number	Accession number	Gene
<b>Respiratory chain</b>			
NADH dehydrogenase-like complex subunit A	1.6.5.-	Nmlp_3415	nuoA
NADH dehydrogenase-like complex subunit B	1.6.5.-	Nmlp_3416	nuoB
NADH dehydrogenase-like complex subunit CD	1.6.5.-	Nmlp_3417	nuoCD
NADH dehydrogenase-like complex subunit H	1.6.5.-	Nmlp_3418	nuoH
NADH dehydrogenase-like complex subunit I	1.6.5.-	Nmlp_3419	nuoI
NADH dehydrogenase-like complex subunit J1	1.6.5.-	Nmlp_3421	nuoJ1
NADH dehydrogenase-like complex subunit J2	1.6.5.-	Nmlp_3422	nuoJ2
NADH dehydrogenase-like complex subunit K	1.6.5.-	Nmlp_3423	nuoK
NADH dehydrogenase-like complex subunit L	1.6.5.-	Nmlp_3424	nuoL
NADH dehydrogenase-like complex subunit M	1.6.5.-	Nmlp_3425	nuoM
NADH dehydrogenase-like complex subunit N	1.6.5.-	Nmlp_3426	nuoN
probable NADH dehydrogenase	1.6.99.3	Nmlp_2475	ndh
succinate dehydrogenase subunit C	1.3.99.1	Nmlp_1978	sdhC
succinate dehydrogenase subunit D	1.3.99.1	Nmlp_1979	sdhD
succinate dehydrogenase subunit B	1.3.99.1	Nmlp_1980	sdhB
succinate dehydrogenase subunit A	1.3.99.1	Nmlp_1981	sdhA
electron transfer flavoprotein beta subunit	1.3.99.1	Nmlp_1192	etfB
electron transfer flavoprotein alpha subunit	1.3.99.1	Nmlp_1193	etfA
2-succinyl-5-enolpyruvyl-6-hydroxy -3-cyclohexene-1-carboxylic-acid synthase	2.2.1.9	Nmlp_2003	menD
isochorismate synthase	5.4.4.2	Nmlp_2004	menF
O-succinylbenzoic acid-CoA ligase	6.2.1.26	Nmlp_3070	menE
O-succinylbenzoate synthase	4.2.1.-	Nmlp_3071	menC

1,4-dihydroxy-2-naphthoate octaprenyltransferase	2.5.1.-	Nmlp_3072	menA
naphthoate synthase	4.1.3.36	Nmlp_3073	menB
ba3-type terminal oxidase subunit	1.9.3.-	Nmlp_2478	cbaE
ba3-type terminal oxidase subunit	1.9.3.-	Nmlp_2479	cbaD
ba3-type terminal oxidase subunit II	1.9.3.-	Nmlp_2480	cbaB, coxB_2
ba3-type terminal oxidase subunit I	1.9.3.-	Nmlp_2481	cbaA, coxA_2
halocyanin	-	Nmlp_1066	hcp_4
halocyanin	-	Nmlp_1866	hcp_6
halocyanin	-	Nmlp_3218	hcp_1
cox-type terminal oxidase subunit I	1.9.3.-	Nmlp_3433	coxA
cox-type terminal oxidase subunit III	1.9.3.-	Nmlp_3436	coxC
cox-type terminal oxidase subunit II	1.9.3.-	Nmlp_3437	coxB

---

### Methionine metabolism

O-acetylhomoserine aminocarboxypropyltransferase (methionine synthase)	2.5.1.49	Nmlp_1414	metY_1
homoserine O-acetyltransferase	2.3.1.31	Nmlp_1415	metA
O-acetylhomoserine aminocarboxypropyltransferase (methionine synthase)	2.5.1.49	Nmlp_1417	metY_2
5-methyltetrahydropteroyltriglutamate-homocysteine S-methyltransferase (methionine synthase II)	2.1.1.14	Nmlp_2726	metE_1
5-methyltetrahydropteroyltriglutamate-homocysteine S-methyltransferase (methionine synthase II)	2.1.1.14	Nmlp_2727	metE_2
methionine-tRNA ligase	6.1.1.10	Nmlp_3239	metS

---

### Cofactor metabolism

#### Quinones

men cluster - part of respiratory chain - above probable prenyltransferase (homolog to 4-hydroxybenzoate)	2.5.1.-	Nmlp_1223	ubiA_3
--	---------	-----------	--------



octaprenyltransferase / homolog to protoheme IX farnesyltransferase)			
probable ubiquinone biosynthesis transmembrane protein 1	-	Nmlp_2768	ubiB_1
(S)-2,3-di-O-geranylgeranylglyceryl phosphate synthase	2.5.1.42	Nmlp_2958	ubiA_2
<hr/>			
Vitamin B group			
<hr/>			
thiamine-phosphate kinase	2.7.4.16	Nmlp_1170	thiL
hydroxyethylthiazole kinase	2.7.1.50	Nmlp_1983	thiM
thiamine-phosphate pyrophosphorylase	2.5.1.3	Nmlp_1984	thiE
thiamine biosynthesis enzyme ThiH 1	-	Nmlp_2441	thiH_1
thiamine biosynthesis enzyme ThiH 2	-	Nmlp_3320	thiH_2
phosphomethylpyrimidine kinase / thiamine biosynthesis protein thiN	2.7.4.7	Nmlp_3884	thiDN
proteasome-activating nucleotidase	-	Nmlp_1184	pan_1
proteasome-activating nucleotidase	-	Nmlp_1703	pan_2
3-methyl-2-oxobutanoate hydroxymethyltransferase	2.1.2.11	Nmlp_1971	panB
dephospho-CoA kinase	2.7.1.24	Nmlp_1098	coaE
phosphopantothenoylcysteine decarboxylase/ phosphopantothenate-cysteine ligase	4.1.1.36,6.3.2.5	Nmlp_2761	dfp, coaBC
pyridoxine biosynthesis protein glutaminase component	-	Nmlp_1256	pdxT
pyridoxine biosynthesis protein pyridoxal 5'-phosphate synthesis component	-	Nmlp_1352	pdxS, pyroA
<hr/>			
GTP-derived coenzymes			
<hr/>			
riboflavin synthase alpha subunit	2.5.1.9	Nmlp_1179	ribC
3,4-dihydroxy-2-butanone 4-phosphate synthase	5.4.99.-	Nmlp_1368	ribB_1
riboflavin synthase beta subunit	2.5.1.9	Nmlp_1952	ribE
(6,7-dimethyl-8-ribityllumazine synthase)			
5-amino-6-(5-phosphoribosylamino)uracil reductase	1.1.1.193	Nmlp_2212	ribG
dihydrofolate reductase	1.5.1.3	Nmlp_1535	folA_1
dihydropteroate synthase 2	2.5.1.15	Nmlp_2218	folP_2
dihydrofolate reductase	1.5.1.3	Nmlp_2593	folA_2

methylenetetrahydrofolate dehydrogenase / methenyltetrahydrofolate cyclohydrolase	1.5.1.5,3.5.4.9	Nmlp_3082	folD
folylpolyglutamate synthase/ 7,8-dihydropteroate reductase/ dihydropteroate synthase	6.3.2.17,2.5.1.15	Nmlp_3136	folCP
aminodeoxychorismate synthase component II	2.6.1.85	Nmlp_1106	pabB, trpE_2
aminodeoxychorismate synthase component I	2.6.1.85	Nmlp_1107	pabA, trpG_2
aminodeoxychorismate lyase	4.1.3.38	Nmlp_1108	pabC, ilvE_2
Molybdenum cofactor synthesis protein 2 large subunit	-	Nmlp_1167	moaE
molybdenum cofactor biosynthesis protein moaB1	-	Nmlp_1472	moaB_1
probable molybdenum cofactor biosynthesis protein moaB2	-	Nmlp_2626	moaB_2
molybdenum cofactor biosynthesis protein moaA	-	Nmlp_2842	moaA
molybdenum cofactor biosynthesis protein MoaC	-	Nmlp_2862	moaC
molybdopterin converting factor small subunit	-	Nmlp_3668	moaD_1
molybdopterin converting factor small subunit	-	Nmlp_3872	moaD_2
molybdenum cofactor biosynthesis protein moeB	-	Nmlp_1065	moeB
molybdenum cofactor biosynthesis protein moeA	-	Nmlp_2764	moeA_1
molybdenum cofactor biosynthesis protein moeA	-	Nmlp_2765	moeA_2
molybdopterin-guanine dinucleotide biosynthesis protein B	-	Nmlp_2139	mobB
probable molybdopterin-guanine dinucleotide biosynthesis protein A	-	Nmlp_3179	mobA
<hr/>			
Porphyrines			
transducer protein HemAT	-	Nmlp_1637	hemAT_1, htr10A
protoporphyrinogen oxidase	1.3.3.4	Nmlp_1876	hemY
transducer protein HemAT	-	Nmlp_2852	hemAT_2, htr10B
glutamyl-tRNA reductase	1.2.1.-	Nmlp_3270	hemA
hydroxymethylbilane synthase (porphobilinogen deaminase)	2.5.1.61	Nmlp_3494	hemC
uroporphyrin-III C-methyltransferase	2.1.1.107	Nmlp_3495	hemX, cysG2
uroporphyrinogen-III synthase	4.2.1.75	Nmlp_3496	hemD
glutamate-1-semialdehyde 2,1-aminomutase	5.4.3.8	Nmlp_3916	hemL
porphobilinogen synthase	4.2.1.24	Nmlp_3919	hemB

cobyrinic acid a,c-diamide synthase	-	Nmlp_1039	cbiA, cobB
nicotinate-nucleotide-dimethylbenzimidazole	2.4.2.21	Nmlp_1040	cobT
phosphoribosyltransferase			
precorrin-6Y C5,15-methyltransferase (decarboxylating)	2.1.1.132	Nmlp_1044	cbiE, cobL1
precorrin-8X methylmutase	5.4.1.2	Nmlp_1045	cbiC, cobH
cobalt chelatase, oxygen-dependent	4.99.1.-	Nmlp_1046	cobN
Cobalamin synthesis protein/P47K	-	Nmlp_2118	cobW
cobalamin (5'-phosphate) synthase	2.7.8.-	Nmlp_2449	cobS
GTP:adenosylcobinamide-phosphate guanylyltransferase	-	Nmlp_2450	cobY
L-threonine-O-3-phosphate decarboxylase	4.1.1.81	Nmlp_2451	cobD
cob(I)alamin adenosyltransferase	2.5.1.17	Nmlp_3671	cobO
cobyric acid synthase	6.3.1.-	Nmlp_3688	cbiP, cobQ
precorrin-3B C17-methyltransferase 2	2.1.1.131	Nmlp_3782	cbiH_2, cobJ_2
precorrin-3B C17-methyltransferase 1	2.1.1.131	Nmlp_3783	cbiH_1, cobJ_1
precorrin-4 C11-methyltransferase	2.1.1.133	Nmlp_3785	cbiF, cobM
precorrin-2 C20-methyltransferase	2.1.1.130	Nmlp_3786	cbiL, cobI
precorrin-8W decarboxylase	1.-.-.-	Nmlp_3787	cbiT, cobL2
<b>Other coenzymes</b>			
NAD(+) synthase (glutamine-hydrolyzing)	1 6.3.5.1	Nmlp_2208	nadE_1
quinolinate synthase A	4.1.99.-	Nmlp_2408	nadA
L-aspartate oxidase, quinolinate synthetase B	1.4.3.16	Nmlp_2409	nadB
nicotinate-nucleotide pyrophosphorylase (carboxylating)	2.4.2.19	Nmlp_2410	nadC
nicotinamide-nucleotide adenyltransferase	2.7.7.1	Nmlp_3853	nadM
<b>Retinal biosynthesis</b>			
geranylgeranyl-diphosphate	2.5.1.32	Nmlp_3029	crtB1
geranylgeranyltransferase (phytoene synthase)			
phytoene dehydrogenase (phytoene desaturase)	1.14.99.-	Nmlp_3026	crtI1

phytoene dehydrogenase (phytoene desaturase)	1.14.99.-	Nmlp_3576	crtI2
lycopene cyclase	1.14.-.-	Nmlp_1293	crtY
brp-like protein		Nmlp_1292	blh
bacteriorhodopsin-related protein	Nmlp_3577	brp	

---

# Bibliography

- Aitken, D. M. & Brown, A. D. (1969). Citrate and glyoxylate cycles in the halophil, halobacterium salinarium. *Biochim Biophys Acta*, **177** (2), 351–354.
- Aivaliotis, M., Oberwinkler, T., Damsma, G., Klee, K., Schlesner, M., Pfeiffer, F., Siedler, F., Lottspeich, F., & Oesterhelt, D. (2011). Arginine fermentation - a unique feature to gain energy in an extremophilic archaeon. *in preparation*, .
- Allers, T. & Mevarech, M. (2005). Archaeal genetics - the third way. *Nat Rev Genet*, **6** (1), 58–73.
- Altschul, S. F., Madden, T. L., Schäffer, A. A., Zhang, J., Zhang, Z., Miller, W., & Lipman, D. J. (1997). Gapped blast and psi-blast: a new generation of protein database search programs. *Nucleic Acids Res*, **25** (17), 3389–3402.
- Andreesen, J. R. (1994). Glycine metabolism in anaerobes. *Antonie Van Leeuwenhoek*, **66** (1-3), 223–237.
- Angelini, R., Babudri, F., Lobasso, S., & Corcelli, A. (2010). Maldi-tof/ms analysis of archaeobacterial lipids in lyophilized membranes dry-mixed with 9-aminoacridine. *J Lipid Res*, **51** (9), 2818–2825.
- Badger, J. & Olsen, G. (1999). Critica: coding region identification tool invoking comparative analysis. *Molecular Biology and Evolution*, **16**, 512–524.
- Baginsky, M. L. & Rodwell, V. W. (1967). Metabolism of pipercolic acid in a pseudomonas species. v. pipercolate oxidase and dehydrogenase. *J Bacteriol*, **94** (4), 1034–1039.
- Bailey, J. E. (1991). Toward a science of metabolic engineering. *Science*, **252** (5013), 1668–1675.
- Balashov, S. P., Imasheva, E. S., Boichenko, V. A., Anto, J., Wang, J. M., & Lanyi, J. K. (2005). Xanthorhodopsin: A proton pump with a light-harvesting carotenoid antenna. *Science*, **309**, 2061–2064.
- Balashov, S. P. & Lanyi, J. K. (2007). Xanthorhodopsin: Proton pump with a carotenoid antenna. *Cell Mol Life Sci*, **64** (18), 2323–2328.
- Baliga, N. S., Bonneau, R., Facciotti, M. T., Pan, M., Glusman, G., Deutsch, E. W., Shannon, P., Chiu, Y., Weng, R. S., Gan, R. R., Hung, P., Date, S. V., Marcotte, E., Hood, L., & Ng, W. V. (2004). Genome sequence of haloarcula marismortui: a halophilic archaeon from the dead sea. *Genome Res*, **14** (11), 2221–2234.
- Barker, H., Kahn, J., & Hedrick, L. (1982). Pathway of lysine degradation in fusobacterium nucleatum. *Journal of Bacteriology*, **152**, 201–207.
- Bender, D. (1985). *Amino Acid Metabolism*. John Wiley & Sons Ltd.
- Berg, I. A., Kockelkorn, D., Ramos-Vera, W. H., Say, R. F., Zarzycki, J., Hügler, M., Alber, B. E., & Fuchs, G. (2010). Autotrophic carbon fixation in archaea. *Nat Rev Microbiol*, **8** (6), 447–460.

## Bibliography

---

- Berg, J., Tymoczko, J., & Stryer, L. (2002). *Biochemistry. 5th edition.* chapter Amino Acids Are Made from Intermediates of the Citric Acid Cycle and Other Major Pathways, p. Section 24.2. W. H. Freeman and Company.
- Bhattacharjee, J. K. (1985). alpha-amino adipate pathway for the biosynthesis of lysine in lower eukaryotes. *Crit Rev Microbiol*, , **12** (2), 131–151.
- Bhaumik, S. R. & Sonawat, H. M. (1994). Pyruvate metabolism in halobacterium salinarium studied by intracellular <sup>13</sup>C nuclear magnetic resonance spectroscopy. *J Bacteriol*, , **176** (8), 2172–2176.
- Béjà, O., Spudich, E., Spudich, J., LeClerc, M., & DeLong, E. (2001). Proteorhodopsin phototrophy in the ocean. *Nature*, , **411**, 786–78.
- Bligh, E. G. & Dyer, W. J. (1959). A rapid method of total lipid extraction and purification. *Can J Biochem Physiol*, , **37** (8), 911–917.
- Bolhuis, H., Palm, P., Wende, A., Falb, M., Rampp, M., Rodriguez-Valera, F., Pfeiffer, F., & Oesterhelt, D. (2006). The genome of the square archaeon haloquadratum walsbyi : life at the limits of water activity. *BMC Genomics*, , **7**, 169.
- Boucher, Y. (2007). *Archaea: molecular and cellular biology*, chapter Lipids: Biosynthesis, Function, and Evolution, pp. 341–353. ASM Press, Washington, D.C.
- Boucher, Y., Kamekura, M., & Doolittle, W. F. (2004). Origins and evolution of isoprenoid lipid biosynthesis in archaea. *Mol Microbiol*, , **52** (2), 515–527.
- Burns, D. G., Janssen, P. H., Itoh, T., Minegishi, H., Usami, R., Kamekura, M., & Dyal-Smith, M. L. (2009). Natronomonas moolapensis sp. nov., two non-alkaliphilic isolates recovered from a solar saltern crystallizer pond. *Int J Syst Evol Microbiol*, , .
- Burton, N. P., Williams, T. D., & Norris, P. R. (1999). Carboxylase genes of sulfolobus metallicus. *Arch Microbiol*, , **172** (6), 349–353.
- Cavicchioli, R. (2006). Cold-adapted archaea. *Nat Rev Microbiol*, , **4** (5), 331–343.
- Chaban, B., Ng, S. Y. M., & Jarrell, K. F. (2006). Archaeal habitats—from the extreme to the ordinary. *Can J Microbiol*, , **52** (2), 73–116.
- Chang, Y. F. & Adams, E. (1974). D-lysine catabolic pathway in pseudomonas putida: interrelations with l-lysine catabolism. *J Bacteriol*, , **117** (2), 753–764.
- Chen, A., Zhang, D., & Poulter, C. D. (1993). (s)-geranylgeranylgeranyl glyceryl phosphate synthase. purification and characterization of the first pathway-specific enzyme in archaeobacterial membrane lipid biosynthesis. *J Biol Chem*, , **268** (29), 21701–21705.
- Claudel-Renard, C., Chevalet, C., Faraut, T., & Kahn, D. (2003). Enzyme-specific profiles for genome annotation: Priam. *Nucleic Acids Res*, , **31** (22), 6633–6639.
- Corcelli, A. (2009). The cardiolipin analogues of archaea. *Biochim Biophys Acta*, , **1788** (10), 2101–2106.
- Corcelli, A., Colella, M., Mascolo, G., Fanizzi, F. P., & Kates, M. (2000). A novel glycolipid and phospholipid in the purple membrane. *Biochemistry*, , **39** (12), 3318–3326.

- Corcelli, A., Lobasso, S., Palese, L. L., Saponetti, M. S., & Papa, S. (2007). Cardiolipin is associated with the terminal oxidase of an extremely halophilic archaeon. *Biochem Biophys Res Commun*, **354** (3), 795–801.
- Costilow, R. N. & Laycock, L. (1971). Ornithine cyclase (deaminating). purification of a protein that converts ornithine to proline and definition of the optimal assay conditions. *J Biol Chem*, **246** (21), 6655–6660.
- Cunin, R., Glansdorff, N., Piérard, A., & Stalon, V. (1986). Biosynthesis and metabolism of arginine in bacteria. *Microbiol Rev*, **50** (3), 314–352.
- Damsma, G. (2006). Investigation of the arginine deiminase pathway in halobacterium salinarum using proteomic tools. Master's thesis, Planck Institute of Biochemistry.
- Danson, M. J., Lambie, H. J., & Hough, D. W. (2007). *Archaea - Molecular and Cellular Biology*, chapter Central Metabolism, pp. 260 – 287. ASM Press.
- DasSarma, S. & Fleischmann, E. M., eds (1995). *Archaea: a Laboratory Manual*. Cold Spring Harbor Laboratory.
- Dauner, M. & Sauer, U. (2000). Gc-ms analysis of amino acids rapidly provides rich information for isotopomer balancing. *Biotechnol Prog*, **16** (4), 642–649.
- Davis, M. C. (1998). Making a living at the extremes. *Trends Biotechnol*, **16**, 102–104.
- Degani, H., Danon, A., & Caplan, S. R. (1980). Proton and carbon-13 nuclear magnetic resonance studies of the polar lipids of halobacterium halobium. *Biochemistry*, **19** (8), 1626–1631.
- Delcher, A., Harmon, D., Kasif, S., White, O., & Salzberg, S. (1999). Improved microbial gene identification with glimmer. *Nucleic Acids Research*, **27**, 4636–4641.
- DeLong, E. F. & Pace, N. R. (2001). Environmental diversity of bacteria and archaea. *Syst Biol*, **50** (4), 470–478.
- Desmarais, D., Jablonski, P. E., Fedarko, N. S., & Roberts, M. F. (1997). 2-sulfotrehalose, a novel osmolyte in haloalkaliphilic archaea. *J Bacteriol*, **179** (10), 3146–3153.
- Diehl, F., Grahlmann, S., Beier, M., & Hoheisel, J. D. (2001). Manufacturing dna microarrays of high spot homogeneity and reduced background signal. *Nucleic Acids Res*, **29** (7), E38.
- Dundas, I. D. & Larsen, H. (1962). The physiological role of the carotenoid pigments of halobacterium salinarium. *Arch. Microbiol.* **44**, 233–239.
- Dyall-Smith, M., ed (2009). *The Halohandbook - Protocols for haloarchaeal genetics*.
- Dyall-Smith, M., Pfeifer, F., Oberwinkler, T., Klee, K., Schuster, S., Rampp, M., & Oesterhelt, D. (2010). *Natronomonas moolapensis*: genomic insights into a neutrophilic member of a "haloalkaliphilic" genus. *in preparation*, .
- Eisenberg, H., Mevarech, M., & Zaccari, G. (1992). Biochemical, structural, and molecular genetic aspects of halophilism. *Adv Protein Chem*, **43**, 1–62.
- Ekiel, I., Smith, I. C., & Sprott, G. D. (1983). Biosynthetic pathways in methanospirillum hungatei as determined by 13c nuclear magnetic resonance. *J Bacteriol*, **156** (1), 316–326.

## Bibliography

---

- Ekiel, I., Sprott, G. D., & Patel, G. B. (1985). Acetate and CO<sub>2</sub> assimilation by methanotrophic consortia. *J Bacteriol*, **162** (3), 905–908.
- Ekiel, I., Sprott, G. D., & Smith, I. C. (1986). Mevalonic acid is partially synthesized from amino acids in *Halobacterium cutirubrum*: a <sup>13</sup>C nuclear magnetic resonance study. *J Bacteriol*, **166** (2), 559–564.
- Ellis, R. (1979). The most abundant protein on earth. *Trends Biochem. Sci.* **4**, 241–244.
- Essen, L., Siebert, R., Lehmann, W. D., & Oesterhelt, D. (1998). Lipid patches in membrane protein oligomers: crystal structure of the bacteriorhodopsin-lipid complex. *Proc Natl Acad Sci U S A*, **95** (20), 11673–11678.
- Evans, M. C., Buchanan, B. B., & Arnon, D. I. (1966). A new ferredoxin-dependent carbon reduction cycle in a photosynthetic bacterium. *Proc Natl Acad Sci U S A*, **55** (4), 928–934.
- Evershed, R. (1993). *Handbook of Derivatives for Chromatography* chapter Advances in silylation., pp. 51–108. K Blau and JM Halket.
- Ezaki, S., Maeda, N., Kishimoto, T., Atomi, H., & Imanaka, T. (1999). Presence of a structurally novel type ribulose-bisphosphate carboxylase/oxygenase in the hyperthermophilic archaeon, *Pyrococcus kodakaraensis* kod1. *J Biol Chem*, **274** (8), 5078–5082.
- Fagerquist, C. K., Neese, R. A., & Hellerstein, M. K. (1999). Molecular ion fragmentation and its effects on mass isotopomer abundances of fatty acid methyl esters ionized by electron impact. *J Am Soc Mass Spectrom*, **10** (5), 430–439.
- Falb, M. (2005). *Computational Genome and Pathway Analysis of Halophilic Archaea*. PhD thesis, Max-Planck-Institute of Biochemistry, Munich.
- Falb, M., Müller, K., Königsmaier, L., Oberwinkler, T., Horn, P., von Gronau, S., Gonzalez, O., Pfeiffer, F., Bornberg-Bauer, E., & Oesterhelt, D. (2008). Metabolism of halophilic archaea. *Extremophiles*, **12** (2), 177–196.
- Falb, M., Pfeiffer, F., Palm, P., Rodewald, K., Hickmann, V., Tittor, J., & Oesterhelt, D. (2005). Living with two extremes: conclusions from the genome sequence of *Natronomonas pharaonis*. *Genome Res*, **15** (10), 1336–1343.
- Finn, M. W. & Tabita, F. R. (2004). Modified pathway to synthesize ribulose 1,5-bisphosphate in methanogenic archaea. *J Bacteriol*, **186** (19), 6360–6366.
- Fothergill, J. C. & Guest, J. R. (1977). Catabolism of l-lysine by *Pseudomonas aeruginosa*. *J Gen Microbiol*, **99** (1), 139–155.
- Fredrickson, H. L., Rijpstra, W. I. C., Tas, A. C., van der Greef, J., LaVos, G. F., & de Leeuw, J. W. (1989). *Microbial mats: Physiological ecology of benthic microbial communities*, chapter Chemical characterization of benthic microbial assemblages, p. 455–468. American Society for Microbiology Washington DC.
- Fukuchi, S., Yoshimune, K., Wakayama, M., Moriguchi, M., & Nishikawa, K. (2003). Unique amino acid composition of proteins in halophilic bacteria. *J Mol Biol*, **327** (2), 347–357.



- Furtwängler, K., Tarasov, V., Wende, A., Schwarz, C., & Oesterhelt, D. (2010). Regulation of phosphate uptake via pst transporters in halobacterium salinarum r1. *Mol Microbiol*, , **76** (2), 378–392.
- Galinski, E. A. (1995). Osmoadaptation in bacteria. *Adv Microb Physiol*, , **37**, 272–328.
- Gerrard, W. & Lappert, M. F. (1952). Fission of mixed ethers by boron trichloride. *J. Chem. Soc.*, , 1486.
- Ghosh, M. & Sonawat, H. M. (1998). Kreb's tca cycle in halobacterium salinarum investigated by <sup>13</sup>c nuclear magnetic resonance spectroscopy. *Extremophiles*, , **2** (4), 427–433.
- Gibson, J. A. E., Miller, M. R., Davies, N. W., Neill, G. P., Nichols, D. S., & Volkman, J. K. (2005). Unsaturated diether lipids in the psychrotrophic archaeon halorubrum lacusprofundi. *Syst Appl Microbiol*, , **28** (1), 19–26.
- Goesmann, A., Linke, B., Bartels, D., Dondrup, M., Krause, L., Neuweger, H., Oehm, S., Paczian, T., Wilke, A., & Meyer, F. (2005). BrigeP—the bridge-based genome-transcriptome-proteome browser. *Nucleic Acids Res*, , **33** (Web Server issue), W710–W716.
- Gonzalez, O. (2009). *Reconstruction, Modeling & Analysis of Haloarchaeal Metabolic Networks*. PhD thesis, LMU München.
- Gonzalez, O., Gronau, S., Falb, M., Pfeiffer, F., Mendoza, E., Zimmer, R., & Oesterhelt, D. (2008). Reconstruction, modeling & analysis of halobacterium salinarum r-1 metabolism. *Mol Biosyst*, , **4** (2), 148–159.
- Gonzalez, O., Oberwinkler, T., Mansueto, L., Pfeiffer, F., Mendoza, E., Zimmer, R., & Oesterhelt, D. (2010). Characterization of growth and metabolism of the haloalkaliphile natronomonas pharaonis. *PLoS Comput Biol*, , **6** (6), e1000799.
- Gordon, D., Abajian, C., & Green, P. (1998). Consed: a graphical tool for sequence finishing. *Genome Res*, , **8** (3), 195–202.
- Gottschalk, G. (1986). *Bacterial metabolism*. Springer-Verlag,.
- Gradin, C., Hederstedt, L., & Baltscheffsky, H. (1985). Soluble succinate dehydrogenase from the halophilic archaeobacterium, halobacterium halobium. *Arch Biochem Biophys*, **239**, 200–205.
- Graham, D. E., Overbeek, R., Olsen, G. J., & Woese, C. R. (2000). An archaeal genomic signature. *Proc Natl Acad Sci U S A*, **97** (7), 3304–3308.
- Grammann, K., Volke, A., & Kunte, H. J. (2002). New type of osmoregulated solute transporter identified in halophilic members of the bacteria domain: Trap transporter teaabc mediates uptake of ectoine and hydroxyectoine in halomonas elongata dsm 2581(t). *J Bacteriol*, **184** (11), 3078–3085.
- Grey, V. L. & Fitt, P. S. (1976). An improved synthetic growth medium for halobacterium cutirubrum. *Can J Microbiol*, **22** (3), 440–442.
- Grigorieff, N., Beckmann, E., & Zemlin, F. (1995). Lipid location in deoxycholate-treated purple membrane at 2.6 a. *J Mol Biol*, **254** (3), 404–415.

- Gruhler, A., Olsen, J. V., Mohammed, S., Mortensen, P., Faergeman, N. J., Mann, M., & Jensen, O. N. (2005). Quantitative phosphoproteomics applied to the yeast pheromone signaling pathway. *Mol Cell Proteomics*, **4** (3), 310–327.
- Haas, D., Galimand, M., Gamper, M., & Zimmermann, A. (1990). *Pseudomonas* chapter Arginine network of *Pseudomonas aeruginosa*: specific and global controls, pp. 303–316. American Society for Microbiology Washington, D.C.
- Halket, J. (1993). *Handbook of derivatives for chromatography*, chapter Derivatives for Gas Chromatography-Mass Spectrometry, p. 297. Wiley, Chicheseter.
- Hampp, N. & Oesterhelt, D. (2004). *NanoBiotechnology*, chapter Bacteriorhodopsin and its potentials in technical applications, pp. 146 – 167. Wiley-Vch.
- Hancock, A. J. & Kates, M. (1973). Structure determination of the phosphatidylglycerosulfate (diether analog) from halobacterium cutirubrum. *J Lipid Res*, **14** (4), 422–429.
- Hanson, T. E. & Tabita, F. R. (2001). A ribulose-1,5-bisphosphate carboxylase/oxygenase (rubisco)-like protein from chlorobium tepidum that is involved with sulfur metabolism and the response to oxidative stress. *Proc Natl Acad Sci U S A*, **98** (8), 4397–4402.
- Hartmann, R. & Oesterhelt, D. (1977). Bacteriorhodopsin-mediated photophosphorylation in halobacterium halobium. *Eur J Biochem*, **77** (2), 325–335.
- Hartmann, R., Sickinger, H. D., & Oesterhelt, D. (1980). Anaerobic growth of halobacteria. *Proc Natl Acad Sci U S A*, **77** (7), 3821–3825.
- Hügler, M. (2003). *Autotrophe CO<sub>2</sub>-Fixierung in thermophilen Mikroorganismen*. PhD thesis, Universität Freiburg.
- Hügler, M., Huber, H., Stetter, K. O., & Fuchs, G. (2003). Autotrophic co<sub>2</sub> fixation pathways in archaea (crenarchaeota). *Arch Microbiol*, **179** (3), 160–173.
- Higashino, K., Fujioka, M., & Yamamura, Y. (1971). The conversion of l-lysine to saccharopine and alpha-amino adipate in mouse. *Arch Biochem Biophys*, **142** (2), 606–614.
- Hochuli, M., Patzelt, H., Oesterhelt, D., Wüthrich, K., & Szyperski, T. (1999). Amino acid biosynthesis in the halophilic archaeon haloarcula hispanica. *J Bacteriol*, **181** (10), 3226–3237.
- Holo, H. (1989). Chloroflexus aurantiacus secretes 3-hydroxypropionate, a possible intermediate in the assimilation of co<sub>2</sub> and acetate. *Arch Microbiol*, **151**, 252–256.
- Hüseyin, B. (2001). *Untersuchung der lipidvermittelten Kristallisation der Ionenpumpen Bacteriorhodopsin und Halorhodopsin aus Halobacterium Salinarum*. PhD thesis, LMU München.
- Hubbard, J. & Miller, A. (1972). Reversible inactivation of isocitrate dehydrogenase from an obligate halophile: changes in the secondary structure. *Arch Biochem Biophys*, **148**, 318–319.
- Ihara, K., Umemura, T., Katagiri, I., Kitajima-Ihara, T., Sugiyama, Y., Kimura, Y., & Mukohata, Y. (1999). Evolution of the archaeal rhodopsins: evolution rate changes by gene duplication and functional differentiation. *J Mol Biol*, **285** (1), 163–174.
- Ishii, M., Miyake, T., Satoh, T., Sugiyama, H., Oshima, Y., Kodama, T., & Igarashi, Y. (1996). Autotrophic carbon dioxide fixation in acidianus brierleyi. *Arch Microbiol*, **166** (6), 368–371.

- Jain, R., Rivera, M. C., & Lake, J. A. (1999). Horizontal gene transfer among genomes: the complexity hypothesis. *Proc Natl Acad Sci U S A*, , **96** (7), 3801–3806.
- Jansen, K., Stupperich, E., & Fuchs, G. (1982). Carbohydrate synthesis from acetyl coa in the autotroph methanobacterium thermoautotrophicum. *Archives of Microbiology*, , **132**, 355–364.
- Javor, B. (1988). Co<sub>2</sub> fixation in halobacteria. *Arch Microbiol*, , **149**, 433–440.
- Kamekura, M. (1998). Diversity of extremely halophilic bacteria. *Extremophiles*, , **2** (3), 289–295.
- Kamekura, M. & Kates, M. (1988). *Halophilic bacteria. Vol. II*, chapter Lipids of halophilic archaeobacteria, p. 25–54. CRC Press Boca Raton, FL.
- Kamekura, M. & Kates, M. (1999). Structural diversity of membrane lipids in members of halobacteriaceae. *Biosci Biotechnol Biochem*, , **63** (6), 969–972.
- Kamekura, M., Seno, Y., & Tomioka, H. (1998). Detection and expression of a gene encoding a new bacteriorhodopsin from an extreme halophile strain ht (jcm 9743) which does not possess bacteriorhodopsin activity. *Extremophiles*, , **2** (1), 33–39.
- Kanehisa, M. & Goto, S. (2000). Kegg: kyoto encyclopedia of genes and genomes. *Nucleic Acids Res*, , **28** (1), 27–30.
- Kates, M. (1993a). Biology of halophilic bacteria, part ii. membrane lipids of extreme halophiles: biosynthesis, function and evolutionary significance. *Experientia*, , **49** (12), 1027–1036.
- Kates, M. (1993b). *The Biochemistry of Archaea (Archaeobacteria)*, chapter Membrane lipids of Archaea, p. 261–295. Elsevier.
- Kates, M. (1996). Structural analysis of phospholipids and glycolipids in extremely halophilic archaeobacteria. *J. Microbiol. Meth.*, **25**, 113–128.
- Kates, M. & Kushwaha, N. (1978). *Energetics and Structure of Halophilic Microorganisms*, chapter Biochemistry of the lipids of extremely halophilic bacteria, pp. 461–480. Elsevier, Amsterdam, The Netherlands.
- Kates, M., Yengoyan, L. S., & Sastry, P. S. (1965). A diether analog of phosphatidyl glycerophosphate in halobacterium cutirubrum. *Biochim. Biophys. Acta*, , **98**, 252–268.
- Kellermann, J. (2008). Icp1–isotope-coded protein label. *Methods Mol Biol*, , **424**, 113–123.
- Kenealy, W. & Waselefsky, D. (1985). Studies on the substrate range of clostridium kluveri; the use of propanol and succinate. *Archives of Microbiology*, , **141**, 187–194.
- Kerscher, L., Nowitzki, S., & Oesterhelt, D. (1982). Thermoacidophilic archaeobacteria contain bacterial-type ferredoxins acting as electron acceptors of 2-oxoacid:ferredoxin oxidoreductases. *Eur J Biochem*, , **128** (1), 223–230.
- Kerscher, L. & Oesterhelt, D. (1977). Ferredoxin is the coenzyme of alpha-ketoacid oxidoreductases in halobacterium halobium. *FEBS Lett*, , **83** (2), 197–201.
- Kerscher, L. & Oesterhelt, D. (1981a). The catalytic mechanism of 2-oxoacid:ferredoxin oxidoreductases from halobacterium halobium. one-electron transfer at two distinct steps of the catalytic cycle. *Eur J Biochem*, , **116** (3), 595–600.

- Kerscher, L. & Oesterhelt, D. (1981b). Purification and properties of two 2-oxoacid:ferredoxin oxidoreductases from halobacterium halobium. *Eur J Biochem*, , **116** (3), 587–594.
- Kerscher, L., Oesterhelt, D., Cammack, R., & Hall, D. O. (1976). A new plant-type ferredoxin from halobacteria. *Eur J Biochem*, , **71** (1), 101–107.
- Kikuchi, G. (1973). The glycine cleavage system: composition, reaction mechanism, and physiological significance. *Mol Cell Biochem*, , **1** (2), 169–187.
- Kimura, Y., Vassilyev, D., Miyazawa, A., Kidera, A., Matsushima, M., Mitsuoka, K., Murata, K., Hirai, T., & Fujiyoshi, Y. (1997). Surface of bacteriorhodopsin revealed by high-resolution electron crystallography. *Nature*, , **389**, 206–211.
- Klebahn, H. (1919). *Die Schädlinge des Klippfisches*. Mitt. Inst. Allg. Botanik Hamburg.
- Königsmäier, L. (2006). Analysen des fettsäuremetabolismus in halophilen archaea. Master's thesis University of Salzburg.
- Koch, M. (2005). *Investigations on halobacterial transducers with respect to membrane potential sensing and adaptive methylation*. PhD thesis LMU München.
- Koga, Y., Kyuragi, T., Nishihara, M., & Sone, N. (1998). Did archaeal and bacterial cells arise independently from noncellular precursors? a hypothesis stating that the advent of membrane phospholipid with enantiomeric glycerophosphate backbones caused the separation of the two lines of descent. *J Mol Evol*, **46** (1), 54–63.
- Koga, Y. & Morii, H. (2005). Recent advances in structural research on ether lipids from archaea including comparative and physiological aspects. *Biosci Biotechnol Biochem*, **69** (11), 2019–2034.
- Koga, Y. & Morii, H. (2006). Special methods for the analysis of ether lipid structure and metabolism in archaea. *Anal Biochem*, **348** (1), 1–14.
- Koga, Y. & Morii, H. (2007). Biosynthesis of ether-type polar lipids in archaea and evolutionary considerations. *Microbiol Mol Biol Rev*, **71** (1), 97–120.
- Kokoeva, M. V., Storch, K.-F., Klein, C., & Oesterhelt, D. (2002). A novel mode of sensory transduction in archaea: binding protein-mediated chemotaxis towards osmoprotectants and amino acids. *EMBO J*, **21** (10), 2312–2322.
- Kolbe, M., Besir, H., Essen, L. O., & Oesterhelt, D. (2000). Structure of the light-driven chloride pump halorhodopsin at 1.8 Å resolution. *Science*, **288** (5470), 1390–1396.
- Kolog-Gulko, M. & Oesterhelt, D. (2010). How halobacterium salinarum synthesises aromatic amino acids? *in preparation*, .
- Krebs, M., Li, W., & Halambeck, T. (1997). Intramembrane substitutions in helix d of bacteriorhodopsin disrupt the purple membrane. *J. Mol. Biol.* **267**, 172–183.
- Kreimeyer, A., Perret, A., Lechaplais, C., Vallenet, D., Médigue, C., Salanoubat, M., & Weissenbach, J. (2007). Identification of the last unknown genes in the fermentation pathway of lysine. *J Biol Chem*. **282**, 7191–7.
- Krishnan, L. & Sprott, G. D. (2008). Archaeosome adjuvants: immunological capabilities and mechanism(s) of action. *Vaccine*, **26** (17), 2043–2055.

- Kushwaha, S. C., Kates, M., & Porter, J. W. (1976a). Enzymatic synthesis of c40 carotenes by cell-free preparation from halobacterium cutirubrum. *Can J Biochem*, **54** (9), 816–823.
- Kushwaha, S. C., Kates, M., & Stoeckenius, W. (1976b). Comparison of purple membrane from halobacterium cutirubrum and halobacterium halabium. *Biochim Biophys Acta*, **426** (4), 703–710.
- Lange, B. M., Rujan, T., Martin, W., & Croteau, R. (2000). Isoprenoid biosynthesis: the evolution of two ancient and distinct pathways across genomes. *Proc Natl Acad Sci U S A*, **97** (24), 13172–13177.
- Lanyi, J. K. (1974). Salt-dependent properties of proteins from extremely halophilic bacteria. *Bacteriol Rev*, **38** (3), 272–290.
- Lanyi, J. K. & Balashov, S. P. (2008). Xanthorhodopsin: a bacteriorhodopsin-like proton pump with a carotenoid antenna. *Biochim Biophys Acta*, **1777** (7-8), 684–688.
- Lattanzio, V. M. T., Corcelli, A., Mascolo, G., & Oren, A. (2002). Presence of two novel cardiolipins in the halophilic archaeal community in the crystallizer brines from the salterns of margherita di savoia (italy) and eilat (israel). *Extremophiles*, **6** (6), 437–444.
- Lechner, J., Wieland, F., & Sumper, M. (1985). Biosynthesis of sulfated saccharides n-glycosidically linked to the protein via glucose. purification and identification of sulfated dolichyl monophosphoryl tetrasaccharides from halobacteria. *J Biol Chem*, **260** (2), 860–866.
- Lefèvre, O., Mollova, N., & Longevialle, P. (1992). Reactivity of electron impact ionized large-ring cycloalkylamines. loss of  $cnh_{2n} + 1$ . alkyl radicals from long-chain aliphatic compounds with a terminal enamine or ester function (lipids). *Organic Mass Spectrometry*, **27**, 589 – 596.
- Legat, A., Gruber, C., Zangger, K., Wanner, G., & Stan-Lotter, H. (2010). Identification of polyhydroxyalkanoates in halococcus and other haloarchaeal species. *Appl Microbiol Biotechnol*, **87** (3), 1119–1127.
- Legault, B. A., Lopez-Lopez, A., Alba-Casado, J. C., Doolittle, W. F., Bolhuis, H., Rodriguez-Valera, F., & Papke, R. T. (2006). Environmental genomics of "haloquadratum walsbyi" in a saltern crystallizer indicates a large pool of accessory genes in an otherwise coherent species. *BMC Genomics*, **7**, 171.
- Lengeler, J., Drews, G., & Schlegel, H., eds (1999). *Biology of the Prokaryotes*. Blackwell Science, Oxford.
- Lillo, J. G. & Rodriguez-Valera, F. (1990). Effects of culture conditions on poly(beta-hydroxybutyric acid) production by haloferax mediterranei. *Appl Environ Microbiol*, **56** (8), 2517–2521.
- Ljungdahl, L. G. (1986). The autotrophic pathway of acetate synthesis in acetogenic bacteria. *Annu Rev Microbiol*, **40**, 415–450.
- Ma, Y., Galinski, E. A., Grant, W. D., Oren, A., & Ventosa, A. (2010). Halophiles 2010: life in saline environments. *Appl Environ Microbiol*, **76** (21), 6971–6981.
- Madern, D., Pfister, C., & Zaccai, G. (1995). Mutation at a single acidic amino acid enhances the halophilic behaviour of malate dehydrogenase from haloarcula marismortui in physiological salts. *Eur J Biochem*, **230** (3), 1088–1095.

## Bibliography

---

- Maeda, N., Kanai, T., Atomi, H., & Imanaka, T. (2002). The unique pentagonal structure of an archaeal rubisco is essential for its high thermostability. *J Biol Chem*, **277** (35), 31656–31662.
- Maeda, N., Kitano, K., Fukui, T., Ezaki, S., Atomi, H., Miki, K., & Imanaka, T. (1999). Ribulose bisphosphate carboxylase/oxygenase from the hyperthermophilic archaeon *Pyrococcus kodakaraensis* kod1 is composed solely of large subunits and forms a pentagonal structure. *J Mol Biol*, **293** (1), 57–66.
- Magrum, L. J., Luehrsen, K. R., & Woese, C. R. (1978). Are extreme halophiles actually "bacteria"? *J Mol Evol*, **11** (1), 1–8.
- Mancinelli, R. L. & Hochstein, L. I. (1986). The occurrence of denitrification in extremely halophilic bacteria. *FEMS Microbiol Lett*, **35**, 55–58.
- Margulies, M., Egholm, M., Altman, W. E., Attiya, S., Bader, J. S., Bemben, L. A., Berka, J., Braverman, M. S., Chen, Y.-J., Chen, Z., Dewell, S. B., Du, L., Fierro, J. M., Gomes, X. V., Godwin, B. C., He, W., Helgesen, S., Ho, C. H., Ho, C. H., Irzyk, G. P., Jando, S. C., Alenquer, M. L. I., Jarvie, T. P., Jirage, K. B., Kim, J.-B., Knight, J. R., Lanza, J. R., Leamon, J. H., Lefkowitz, S. M., Lei, M., Li, J., Lohman, K. L., Lu, H., Makhijani, V. B., McDade, K. E., McKenna, M. P., Myers, E. W., Nickerson, E., Nobile, J. R., Plant, R., Puc, B. P., Ronan, M. T., Roth, G. T., Sarkis, G. J., Simons, J. F., Simpson, J. W., Srinivasan, M., Tartaro, K. R., Tomasz, A., Vogt, K. A., Volkmer, G. A., Wang, S. H., Wang, Y., Weiner, M. P., Yu, P., Begley, R. F., & Rothberg, J. M. (2005). Genome sequencing in microfabricated high-density picolitre reactors. *Nature*, **437** (7057), 376–380.
- Matsubara, H. & Sasaki, R. M. (1969). High recovery of tryptophan from acid hydrolysates of proteins. *Biochem Biophys Res Commun*, **35** (2), 175–181.
- Mattar, S., Scharf, B., Kent, S. B., Rodewald, K., Oesterheld, D., & Engelhard, M. (1994). The primary structure of halocyanin, an archaeal blue copper protein, predicts a lipid anchor for membrane fixation. *J Biol Chem*, **269** (21), 14939–14945.
- McCarren, J. & DeLong, E. F. (2007). Proteorhodopsin photosystem gene clusters exhibit co-evolutionary trends and shared ancestry among diverse marine microbial phyla. *Environ Microbiol*, **9** (4), 846–858.
- McGenity, T. J., Gemell, R. T., Grant, W. D., & Stan-Lotter, H. (2000). Origins of halophilic microorganisms in ancient salt deposits. *Environ Microbiol*, **2** (3), 243–250.
- McHardy, A. C., Goesmann, A., Pühler, A., & Meyer, F. (2004). Development of joint application strategies for two microbial gene finders. *Bioinformatics*, **20** (10), 1622–1631.
- Menendez, C., Bauer, Z., Huber, H., Gad'on, N., Stetter, K. O., & Fuchs, G. (1999). Presence of acetyl coenzyme a (coa) carboxylase and propionyl-coa carboxylase in autotrophic crenarchaeota and indication for operation of a 3-hydroxypropionate cycle in autotrophic carbon fixation. *J Bacteriol*, **181** (4), 1088–1098.
- Meyer, F., Goesmann, A., McHardy, A. C., Bartels, D., Bekel, T., Clausen, J., Kalinowski, J., Linke, B., Rupp, O., Giegerich, R., & Pühler, A. (2003). Gendb—an open source genome annotation system for prokaryote genomes. *Nucleic Acids Res*, **31** (8), 2187–2195.
- Michal, G. (1999). *Biochemical Pathways: Biochemie-Atlas*. Spektrum Akademischer Verlag.

- Michel, H. & Oesterhelt, D. (1976). Light-induced changes of the pH gradient and the membrane potential in *Halobacterium salinarum*. *FEBS Lett*, **65** (2), 175–178.
- Moldoveanu, N. & Kates, M. (1988). Biosynthetic studies of the polar lipids of *Halobacterium cutirubrum*. *Biochim. Biophys. Acta*, **960**, 161–182.
- Montrone, M., Marwan, W., Grünberg, H., Musseleck, S., Starostzik, C., & Oesterhelt, D. (1993). Sensory rhodopsin-controlled release of the switch factor fumarate in *Halobacterium salinarum*. *Mol Microbiol*, **10** (5), 1077–1085.
- Morii, H. & Koga, Y. (2003). Cdp-2,3-di-o-geranylgeranyl-sn-glycerol:1-serine o-archaetidyltransferase (archaetidylserine synthase) in the methanogenic archaeon *Methanothermobacter thermoautotrophicus*. *J Bacteriol*, **185** (4), 1181–1189.
- Morii, H., Yagi, H., Akutsu, H., Nomura, N., Sako, Y., & Koga, Y. (1999). A novel phosphoglycolipid archaetidyl(glucosyl)inositol with two sesterterpanyl chains from the aerobic hyperthermophilic archaeon *Aeropyrum pernix* K1. *Biochim Biophys Acta*. **1436**, 426–36.
- Morth, S. & Tindall, B. J. (1985). Evidence that changes in the growth conditions affect the relative distribution of diether lipids in haloalkaliphilic archaeobacteria. *FEMS Microbiol. Lett.* **29**, 285–288.
- Mu, F., Williams, R. F., Unkefer, C. J., Unkefer, P. J., Faeder, J. R., & Hlavacek, W. S. (2007). Carbon-fate maps for metabolic reactions. *Bioinformatics*, **23** (23), 3193–3199.
- Mueller-Cajar, O. & Badger, M. R. (2007). New roads lead to rubisco in archaeobacteria. *Bioessays*, **29** (8), 722–724.
- Nakao, Y., Kikukawa, T., Shimono, K., Tamogami, J., Kimitsuki, N., Nara, T., Unno, M., Ihara, K., & Kamo, N. (2010). Photochemistry of a putative new class of sensory rhodopsin (sriii) coded by xop2 of haloarcular *Marismortui*. *J Photochem Photobiol B*, .
- Ng, W. V., Kennedy, S. P., Mahairas, G. G., Berquist, B., Pan, M., Shukla, H. D., Lasky, S. R., Baliga, N. S., Thorsson, V., Sbrogna, J., Swartzell, S., Weir, D., Hall, J., Dahl, T. A., Welti, R., Goo, Y. A., Leithauser, B., Keller, K., Cruz, R., Danson, M. J., Hough, D. W., Maddocks, D. G., Jablonski, P. E., Krebs, M. P., Angevine, C. M., Dale, H., Isenbarger, T. A., Peck, R. F., Pohlschroder, M., Spudich, J. L., Jung, K. W., Alam, M., Freitas, T., Hou, S., Daniels, C. J., Dennis, P. P., Omer, A. D., Ebhardt, H., Lowe, T. M., Liang, P., Riley, M., Hood, L., & DasSarma, S. (2000). Genome sequence of *Halobacterium* species nrc-1. *Proc Natl Acad Sci U S A*, **97** (22), 12176–12181.
- Nishihara, M. & Koga, Y. (1988). Quantitative conversion of diether or tetraether phospholipids to glycerophosphoesters by dealkylation with boron trichloride: a tool for structural analysis of archaeobacterial lipids. *J Lipid Res*, **29** (3), 384–388.
- Nishihara, M., Yamazaki, T., Oshima, T., & Koga, Y. (1999). sn-glycerol-1-phosphate-forming activities in archaea: separation of archaeal phospholipid biosynthesis and glycerol catabolism by glycerophosphate enantiomers. *J Bacteriol*, **181** (4), 1330–1333.
- Norris, P., Nixon, A., & Hart, A. (1989). *Microbiology of extreme environments and its potential for biotechnology* chapter Acidophilic, mineral-oxidizing bacteria: the utilization of carbon dioxide with particular reference to autotrophy in *Sulfolobus*, pp. 24–43. Elsevier, London, United Kingdom.
- Norton, C. F. (1992). Rediscovering the ecology of halobacteria. *ASM News*, , **58**, 363–367.

## Bibliography

---

- Oberwinkler, T. (2006). Analyse zum aminosäure- und isoprenoidstoffwechsel in halophilen archaea. Master's thesis, University of Salzburg, Austria.
- Oesterhelt, D. (1972). [the purple membrane from halobacterium halobium]. *Hoppe Seylers Z Physiol Chem*, , **353** (10), 1554–1555.
- Oesterhelt, D. (1975). The purple membrane of halobacterium halobium: a new system for light energy conversion. *Ciba Found Symp*, , (31), 147–167.
- Oesterhelt, D. (1976). Isoprenoids and bacteriorhodopsin in halobacteria. *Prog Mol Subcell Biol*, , **4**, 133–166.
- Oesterhelt, D. (1998). The structure and mechanism of the family of retinal proteins from halophilic archaea. *Curr Opin Struct Biol*, , **8** (4), 489–500.
- Oesterhelt, D. (1999). *Photosynthese*, chapter Photosynthese der zweiten Art: Die halophilen Archaea, pp. 146–161. Georg Thieme Verlag, Stuttgart, New York.
- Oesterhelt, D., Bräuchle, C., & Hampp, N. (1991). Bacteriorhodopsin: a biological material for information processing. *Q Rev Biophys*, , **24** (4), 425–478.
- Oesterhelt, D. & Krippahl, G. (1973). Light inhibition of respiration in halobacterium halobium. *FEBS Lett*, , **36** (1), 72–76.
- Oesterhelt, D. & Krippahl, G. (1983). Phototrophic growth of halobacteria and its use for isolation of photosynthetically-deficient mutants. *Ann Microbiol (Paris)*, , **134B** (1), 137–150.
- Oesterhelt, D. & Marwan, W. (2005). Salz in der suppe des lebens. *Biospektrum*, , , 60–62.
- Oesterhelt, D. & Stoeckenius, W. (1971). Rhodopsin-like protein from the purple membrane of halobacterium halobium. *Nat New Biol*, , **233** (39), 149–152.
- Olsen, J. V., de Godoy, L. M. F., Li, G., Macek, B., Mortensen, P., Pesch, R., Makarov, A., Lange, O., Horning, S., & Mann, M. (2005). Parts per million mass accuracy on an orbitrap mass spectrometer via lock mass injection into a c-trap. *Mol Cell Proteomics*, , **4** (12), 2010–2021.
- Oren, A. (1983). Bacteriorhodopsin-mediated co<sub>2</sub> photoassimilation in the dead sea. *Limnol. Oceanogr.*, **28**, 33–41.
- Oren, A. (1991). Anaerobic growth of halophilic archaeobacteria by reduction of fumarate. *J Gen Microbiol*, , **137**, 1387–1390.
- Oren, A. (1994). The ecology of extremely halophilic archaea. *FEMS Microbiol Rev*, , **13**, 415–440.
- Oren, A. (2000). *The Prokaryotes. A Handbook on the Biology of Bacteria: Ecophysiology, Isolation, Identification, Applications*, chapter Life at high salt concentrations. Springer - Verlag.
- Oren, A. (2002a). *Halophilic microorganisms and their environments*, chapter Hypersaline environments and their biota, pp. 393 – 394. Kluwer Academic Publishers.
- Oren, A. (2002b). *Halophilic microorganisms and their environments*, pp. 183–185. Kluwer Academic.
- Oren, A. (2002c). Diversity of halophilic microorganisms: environments, phylogeny, physiology, and applications. *J Ind Microbiol Biotechnol*, , **28** (1), 56–63.



- Oren, A. & Trüper, H. G. (1990). Anaerobic growth of halophilic archaeobacteria by reduction of dimethylsulfoxide and trimethylamine n-oxide. *FEMS Microbiol Lett*, , **70**, 33 – 36.
- Papes, F., Kemper, E. L., Cord-Neto, G., Langone, F., & Arruda, P. (1999). Lysine degradation through the saccharopine pathway in mammals: involvement of both bifunctional and monofunctional lysine-degrading enzymes in mouse. *Biochem J*, , **344 Pt 2**, 555–563.
- Penke, B., Ferenczi, R., & Kovács, K. (1974). A new acid hydrolysis method for determining tryptophan in peptides and proteins. *Anal Biochem*, , **60** (1), 45–50.
- Peretó, J., López-García, P., & Moreira, D. (2004). Ancestral lipid biosynthesis and early membrane evolution. *Trends Biochem Sci*, , **29** (9), 469–477.
- Petter, H. (1931). On bacteria of salted fish. *Proceedings Academy of Science, Amsterdam*, , **34**, 1417–1423.
- Pfeifer, F., Gregor, D., Hofacker, A., Plösser, P., & Zimmermann, P. (2002). Regulation of gas vesicle formation in halophilic archaea. *J Mol Microbiol Biotechnol*, , **4** (3), 175–181.
- Pfeifer, F., Krüger, K., Röder, R., Mayr, A., Ziesche, S., & Offner, S. (1997). Gas vesicle formation in halophilic archaea. *Arch Microbiol*, , **167** (5), 259–268.
- Pfeiffer, F., Broicher, A., Gillich, T., Klee, K., Mejía, J., Rampp, M., & Oesterhelt, D. (2008a). Genome information management and integrated data analysis with halolex. *Arch Microbiol*, , **190** (3), 281–299.
- Pfeiffer, F., Schuster, S. C., Broicher, A., Falb, M., Palm, P., Rodewald, K., Ruepp, A., Soppa, J., Tittor, J., & Oesterhelt, D. (2008b). Evolution in the laboratory: the genome of halobacterium salinarum strain r1 compared to that of strain nrc-1. *Genomics*, , **91** (4), 335–346.
- Phadwal, K. & Singh, P. K. (2003). Isolation and characterization of an indigenous isolate of dunaliella sp. for beta-carotene and glycerol production from a hypersaline lake in india. *J Basic Microbiol*, , **43** (5), 423–429.
- Pieulle, L., Magro, V., & Hatchikian, E. C. (1997). Isolation and analysis of the gene encoding the pyruvate-ferredoxin oxidoreductase of desulfovibrio africanus, production of the recombinant enzyme in escherichia coli, and effect of carboxy-terminal deletions on its stability. *J Bacteriol.*, **179**, 5684–5692.
- Poole, C., Sye, W., Singhawangcha, S., F Hsu, A. Z., Arfwidsson, A., & Vessman, J. (1980). New electroncapturing pentafluorophenyldialkylchlorosilanes as versatile derivatizing reagents for gas chromatography. *J. Chromatogr.*, **199**, 123–142.
- Pugh, E. L. & Kates, M. (1994). Acylation of proteins of the archaeobacteria halobacterium cutirubrum and methanobacterium thermoautotrophicum. *Biochim Biophys Acta*, , **1196** (1), 38–44.
- Ramos-Vera, W. H., Berg, I. A., & Fuchs, G. (2009). Autotrophic carbon dioxide assimilation in thermoproteales revisited. *J Bacteriol*, , **191** (13), 4286–4297.
- Rao, J. K. & Argos, P. (1981). Structural stability of halophilic proteins. *Biochemistry*, , **20** (23), 6536–6543.

## Bibliography

---

- Rawal, N., Kelkar, S. M., & Altekhar, W. (1988). Alternative routes of carbohydrate metabolism in halophilic archaeobacteria. *Indian J Biochem Biophys*, , **25** (6), 674–686.
- Renner, C., Kessler, B., & Oesterhelt, D. (2005). Lipid composition of integral purple membrane by <sup>1</sup>h and <sup>31</sup>p nmr. *J Lipid Res*, , **46** (8), 1755–1764.
- Rodriguez-Valera, F. (1992). *The Archaeobacteria: Biochemistry and Biotechnology*, chapter Biotechnological potential of halobacteria., pp. 135 – 147. Biochemical Society Symposium no. 58. Biochemical Society.
- Rodriguez-Valera, F., Ventosa, A., Juez, G., & Imhoff, J. F. (1985). Variation of environmental features and microbial populations with salt concentration in a multipond saltern. *Microb Ecol*, , **11**, 107–115.
- Rogers, P. J. & Morris, C. A. (1978). Regulation of bacteriorhodopsin synthesis by growth rate in continuous cultures of halobacterium halobium. *Arch Microb*, , **119**, 323 – 325.
- Rosa, M. D. & Gambacorta, A. (1988). The lipids of archaeobacteria. *Prog Lipid Res*, , **27** (3), 153–175.
- Rosa, M. D., Gambacorta, A., Nicolaus, B., Ross, H. N. M., Grant, W. D., & Bullock, J. D. (1982). An asymmetric archaeobacterial diether lipid from alkaliphilic halophiles. *J. Gen. Microbiol.*, **128**, 344–348.
- Rosa, M. D., Gambacorta, A., Nicolaus, B., Ross, N. M., & Grant, W. D. (1983). A c25:25 diether core lipid from archaeobacterial haloalkaliphiles. *J. Gen. Microbiol.*, **129**, 2333–2337.
- Rosa, M. D., Rosa, S. D., & Gambacorta, A. (1977). <sup>13</sup>c nmr assignments and biosynthetic data for the ether lipids of calderiella. *Phytochemistry*, , **16**, 1909–1912.
- Rothberg, J. M. & Leamon, J. H. (2008). The development and impact of 454 sequencing. *Nat Biotechnol*, , **26** (10), 1117–1124.
- Rothschild, L. J. & Mancinelli, R. L. (2001). Life in extreme environments. *Nature*, , **409** (6823), 1092–1101.
- Ruepp, A. & Soppa, J. (1996). Fermentative arginine degradation in halobacterium salinarium (formerly halobacterium halobium): genes, gene products, and transcripts of the arcrcab gene cluster. *J Bacteriol*, , **178** (16), 4942–4947.
- Sato, T., Atomi, H., & Imanaka, T. (2007). Archaeal type iii rubiscos function in a pathway for amp metabolism. *Science*, , **315** (5814), 1003–1006.
- Sauer, U., Lasko, D. R., Fiaux, J., Hochuli, M., Glaser, R., Szyperski, T., Wüthrich, K., & Bailey, J. E. (1999). Metabolic flux ratio analysis of genetic and environmental modulations of escherichia coli central carbon metabolism. *J Bacteriol*, , **181** (21), 6679–6688.
- Schauder, R., Widdel, F., & Fuchs, G. (1987). Carbon assimilation pathways in sulfate-reducing bacteria ii. enzymes of a reductive citric acid cycle in the autotrophic desulfobacter hydrogenophilus. *Arch Microbiol*, , **148**, 218–225.
- Schäfer, G. (1996). Bioenergetics of the archaeobacterium sulfolobus. *Biochim Biophys Acta*, , **1277** (3), 163–200.

- Schäfer, G., Engelhard, M., & Müller, V. (1999). Bioenergetics of the archaea. *Microbiol Mol Biol Rev*, , **63** (3), 570–620.
- Schäfer, S., Paalme, T., Vilu, R., & Fuchs, G. (1989). <sup>13</sup>C-nmr study of acetate assimilation in thermoproteus neutrophilus. *Eur J Biochem*, , **186** (3), 695–700.
- Schobert, B. & Lanyi, J. K. (1982). Halorhodopsin is a light-driven chloride pump. *J Biol Chem*, , **257** (17), 10306–10313.
- Schubert, B. A., Lowenstein, T. K., Timofeeff, M. N., & Parker, M. A. (2010). Halophilic archaea cultured from ancient halite, death valley, california. *Environ Microbiol*, , **12** (2), 440–454.
- Schwaiger, R. (2009). *Genespressions- und Protein-DNA-Interaktions-Studien des Aminosäure-Metabolismus und metallabhängiger Prozesse in Halobacterium salinarium R1*. PhD thesis, Max-Planck-Institut für Biochemie.
- Sharma, A. K., Walsh, D. A., Baptiste, E., Rodriguez-Valera, F., Doolittle, W. F., & Papke, R. T. (2007). Evolution of rhodopsin ion pumps in haloarchaea. *BMC Evol Biol*, , **7**, 79.
- Shevchenko, A., Wilm, M., Vorm, O., & Mann, M. (1996). Mass spectrometric sequencing of proteins silver-stained polyacrylamide gels. *Anal Chem*, , **68** (5), 850–858.
- Shiba, H., Kawasumi, T., Igarashi, Y., Kodama, T., & Minoda, Y. (1985). The co<sub>2</sub> assimilation via the reductive tricarboxylic acid cycle in an obligately autotrophic, aerobic hydrogen-oxidizing bacterium, hydrogenobacter thermophilus. *Arch Microbiol*, , **141**, 198–203.
- Shimada, H., Nemoto, N., Shida, Y., Oshima, T., & Yamagishi, A. (2002). Complete polar lipid composition of thermoplasma acidophilum ho-62 determined by high-performance liquid chromatography with evaporative light-scattering detection. *J Bacteriol*, , **184** (2), 556–563.
- Sims, R. P. A. & Larose, J. A. G. (1961). The use of iodine vapor as a general detecting agent in the thin layer chromatography of lipids. *Journal of the American Oil Chemists' Society*, , **39**, 232.
- Sklenar, V., Piotto, M., Leppik, R., & Saudek, V. (1993). Gradient-tailored water suppression for 1h-15n hsqc experiments optimized to retain full sensitivity. *J. Magn. Reson. A*, , **102**, 241–245.
- Smit, A. & Mushegian, A. (2000). Biosynthesis of isoprenoids via mevalonate in archaea: the lost pathway. *Genome Res*, , **10** (10), 1468–1484.
- Soderberg, T. (2005). Biosynthesis of ribose-5-phosphate and erythrose-4-phosphate in archaea: a phylogenetic analysis of archaeal genomes. *Archaea*, , **1** (5), 347–352.
- Soderberg, T., Chen, A., & Poulter, C. D. (2001). Geranylgeranylglyceryl phosphate synthase. characterization of the recombinant enzyme from methanobacterium thermoautotrophicum. *Biochemistry*, , **40** (49), 14847–14854.
- Soppa, J. (2006). From genomes to function: haloarchaea as model organisms. *Microbiology*, , **152** (Pt 3), 585–590.
- Spudich, J. L. (2006). The multitasking microbial sensory rhodopsins. *Trends Microbiol*, , **14** (11), 480–487.
- Stadtman, T. (1973). Lysine metabolism of clostridia. *Adv. Enzymol.*, **38**, 413–448.

## Bibliography

---

- Stan-Lotter, H., McGenity, T. J., Legat, A., Denner, E. B., Glaser, K., Stetter, K. O., & Wanner, G. (1999). Very similar strains of halococcus salifodinae are found in geographically separated permo-triassic salt deposits. *Microbiology*, , **145** ( Pt 12), 3565–3574.
- Stoeckenius, W. & Rowen, R. (1967). A morphological study of halobacterium halobium and its lysis in media of low salt concentration. *J Cell Biol*, , **34** (1), 365–393.
- Stupperich, E., Hammel, K., Fuchs, G., & Thauer, R. (1983). Carbon monoxide fixation into the carboxyl group of acetyl coenzyme a during autotrophic growth of methanobacterium. *FEBS Lett*, , **152**, 21–3.
- Sugiyama, Y., Yamada, N., & Mukohata, Y. (1994). The light-driven proton pump, cruxrhodopsin-2 in haloarcula sp. arg-2 (br+, hr-), and its coupled atp formation. *Biochim Biophys Acta*, , **1188** (3), 287–292.
- Sumper, M., Reitmeier, H., & Oesterhelt, D. (1976). Biosynthesis of the purple membrane of halobacteria. *Angew Chem Int Ed Engl*, , **15** (4), 187–194.
- Szyperski, T. (1995). Biosynthetically directed fractional 13c-labeling of proteinogenic amino acids. an efficient analytical tool to investigate intermediary metabolism. *Eur J Biochem*, , **232** (2), 433–448.
- Szyperski, T. (1998). 13c-nmr, ms and metabolic flux balancing in biotechnology research. *Q Rev Biophys*, , **31** (1), 41–106.
- Tabita, F. R., Hanson, T. E., Li, H., Satagopan, S., Singh, J., & Chan, S. (2007). Function, structure, and evolution of the rubisco-like proteins and their rubisco homologs. *Microbiol Mol Biol Rev*, , **71** (4), 576–599.
- Takayama, M. (1995). Metastable mclafferty rearrangement reaction in the electron impact ionization of stearic acid methyl ester. *International Journal of Mass Spectrometry and Ion Processes*, , **144**, 199–204.
- Tarasov, V. Y., Besir, H., Schwaiger, R., Klee, K., Furtwängler, K., Pfeiffer, F., & Oesterhelt, D. (2008). A small protein from the bop-brp intergenic region of halobacterium salinarum contains a zinc finger motif and regulates bop and crt1 transcription. *Mol Microbiol*, , **67** (4), 772–780.
- Tatusov, R. L., Galperin, M. Y., Natale, D. A., & Koonin, E. V. (2000). The cog database: a tool for genome-scale analysis of protein functions and evolution. *Nucleic Acids Res*, , **28** (1), 33–36.
- Tatusov, R. L., Koonin, E. V., & Lipman, D. J. (1997). A genomic perspective on protein families. *Science*, , **278** (5338), 631–637.
- Tebbe, A. (2005). *Das Proteom eines halophilen Archaeons und seine Antwort auf Änderung der Lebensbedingungen - Inventarisierung, Quantifizierung und posttranslationale Modifikationen*. PhD thesis, Max Planck Institut für Biochemie.
- Tebbe, A., Schmidt, A., Konstantinidis, K., Falb, M., Bisle, B., Klein, C., Aivaliotis, M., Kellermann, J., Siedler, F., Pfeiffer, F., Lottspeich, F., & Oesterhelt, D. (2009). Life-style changes of a halophilic archaeon analyzed by quantitative proteomics. *Proteomics*, , **9** (15), 3843–3855.
- Thompson, J. D., Higgins, D. G., & Gibson, T. J. (1994). Clustal w: improving the sensitivity of progressive multiple sequence alignment through sequence weighting, position-specific gap penalties and weight matrix choice. *Nucleic Acids Res*, , **22** (22), 4673–4680.

- Tindall, B. (1985). Qualitative and quantitative distribution of diether lipids in haloalkaliphilic archaeobacteria. *Syst. Appl. Microbiol.*, **6**, 243–246.
- Tindall, B., Ross, H., & Grant, W. (1984). Natronobacterium gen. nov. and natronococcus gen. nov., two new genera of haloalkaliphilic archaeobacteria. *Syst Appl Microbiol*, , **5**, 41–57.
- Twelmeyer, J. (2007). *Etablierung der DNA-Mikroarray-Transkriptom-Analyse für Halobacterium salinarum R1*. PhD thesis, LMU München.
- Uda, I., Sugai, A., Kon, K., Ando, S., Itoh, Y. H., & Itoh, T. (1999). Isolation and characterization of novel neutral glycolipids from thermoplasma acidophilum. *Biochim Biophys Acta*, , **1439** (3), 363–370.
- Uda, I., Sugai, A., Shimizu, A., Itoh, Y. H., & Itoh, T. (2000). Glucosylcaldarchaetidylglycerol, a minor phosphoglycolipid from thermoplasma acidophilum. *Biochim Biophys Acta*, , **1484** (2-3), 83–86.
- Uegaki, K., Sugiyama, Y., & Mukohata, Y. (1991). Archaeorhodopsin-2, from halobacterium sp. aus-2 further reveals essential amino acid residues for light-driven proton pumps. *Arch. Biochem. Biophys.*, **286**, 107–110.
- Upasani, V. N., Desai, S. G., Moldoveanu, N., & Kates, M. (1994). Lipids of extremely halophilic archaeobacteria from saline environments in india: a novel glycolipid in natronobacterium strains. *Microbiology*, , **140** ( Pt 8), 1959–1966.
- Valentine, D. L. (2007). Adaptations to energy stress dictate the ecology and evolution of the archaea. *Nat Rev Microbiol*, , **5** (4), 316–323.
- van der Oost, J. & Siebers, B. (2007). *Archaea*, chapter Evolution, Physiology and Molecular Biology, pp. 247–259. Blackwell.
- Ventosa, A. & Nieto, J. J. (1995). Biotechnological applications and potentialities of halophilic microorganisms. *World J Microbiol Biotechnol*, , **11**, 85 – 94.
- Wakabayashia, S., Fujimotoa, N., Wadaa, K., Matsubaraa, H., Kerscher, L., & Oesterheld, D. (1983). Amino acid sequence of a ferredoxin from thermoacidophilic archaeobacteria, thermoplasma acidophilum. *Febs Letters*, , **162**, 21–24.
- Waschuk, S., Jr, A. B., Shi, L., & Brown, L. (2005). Leptosphaeria rhodopsin: Bacteriorhodopsin-like proton pump from a eukaryote. *PNAS*, , **102**, 6879–6883.
- Watson, G. M., Yu, J. P., & Tabita, F. R. (1999). Unusual ribulose 1,5-bisphosphate carboxylase/oxygenase of anoxic archaea. *J Bacteriol*, , **181** (5), 1569–1575.
- Wächtershäuser, G. (1990). Evolution of the first metabolic cycles. *Proc Natl Acad Sci U S A*, , **87** (1), 200–204.
- Weik, M., Patzelt, H., Zaccai, G., & Oesterheld, D. (1998). Localization of glycolipids in membranes by in vivo labeling and neutron diffraction. *Mol Cell*, , **1** (3), 411–419.
- White, R. H. (2003). The biosynthesis of cysteine and homocysteine in methanococcus jannaschii. *Biochim Biophys Acta*, , **1624** (1-3), 46–53.

## Bibliography

---

- Wimmer, F., Oberwinkler, T., Bisle, B., Tittor, J., & Oesterhelt, D. (2008). Identification of the arginine/ornithine antiporter arcD from halobacterium salinarum. *FEBS Lett*, , **582** (27), 3771–3775.
- Woese, C. R. & Fox, G. E. (1977). The concept of cellular evolution. *J Mol Evol.*, **1**, 1–6.
- Woo, K.-L. & Chang, D.-K. (1993). Determination of 22 protein amino acids as n(o)-tert.-butyldimethylsilyl derivatives by gas chromatography. *Journal of Chromatography A*, , **638**, 97–107.
- Yamanishi, Y., Mihara, H., Osaki, M., Muramatsu, H., Esaki, N., Sato, T., Hizukuri, Y., Goto, S., & Kanehisa, M. (2007). Prediction of missing enzyme genes in a bacterial metabolic network. reconstruction of the lysine-degradation pathway of pseudomonas aeruginosa. *FEBS J*, , **274** (9), 2262–2273.
- Yatsunami, R., Kawakami, T., Ohtani, H., & Nakamura, S. (2000). A novel bacteriorhodopsin-like protein from haloarcula japonica strain tr-1: gene cloning, sequencing, and transcript analysis. *Extremophiles*, , **4** (2), 109–114.
- Y.Mukohata, K. Ihara, T. T. Y. S. (1999). Halobacterial rhodopsins. *J. Biochem.*, **125**, 649–657.
- Yoshimura, K. & Kouyama, T. (2008). Structural role of bacterioruberin in the trimeric structure of archaerhodopsin-2. *J Mol Biol*, , **375** (5), 1267–1281.

# Appendix

## Abbreviations

aa	amino acid(s)
amu	atomic mass unit = unified atomic mass unit (u)
a. n.	absolute number
ATP	adenosine triphosphate
BBB	bidirectional best blast
BCA	bicinchoninic acid
bp	base pair(s)
BPG	biphosphatidylglycerol
BLAST	Basic Local Alignment Search Tool
BR/Bop	bacteriorhodopsin
DBCM2	
cDNA	complementary DNA
CID-MS	collision-induced dissociation mass spectra
ca	circa
COSY	correlated spectroscopy
DEPC	diethylpyrocarbonate
DAP	diaminopimelate
dept	distortionless enhancement by polarization transfer
DHA	dihydroxyacetone
DHAP	dihydroxyacetone phosphate
DMAPP	isomer dimethylallyl diphosphate
dNTPs	mixture dATP, dTTP, dCTP, dGTP
DTT	1,4-Dithiothreitol
EDTA	ethylenediaminetetraacetic acid
e.g.	for example
E-value	expect value
ESI	electrospray ionisation
FA	formic acid
FGPPS	farnesylgeranyl diphosphate synthase
FHSQC	Fast Heteronuclear Single Quantum Coherence
GC/MS	gas chromatography mass spektrometry
GGGP	geranylgeranylglyceryl phosphate
GGPPS	geranylgeranyl diphosphate synthase
<i>Hasal</i>	<i>Halobacterium salinarum</i>
<i>Hbt. salinarum</i>	<i>Halobacterium salinarum</i>
HMG-CoA	3-hydroxy-3-methylglutaryl-CoA
HPLC	high-performance liquid chromatography
HR/Hop	halorhodopsin
<i>Hrr. lacusprofundi</i>	<i>Halorubrum lacusprofundi</i>

## Appendix

---

Htr	halobacterial transducer
ICPL	Isotope Coded Protein Labeling
IDI	isopentenyl diphosphate isomerases
InChI	International Chemical Identifier
i.e.	that is
IPP	isopentenyl diphosphate
kDa	kilodalton
KEGG	Kyoto Encyclopedia of Genes and Genomes
LC	liquid chromatography
M	molar
MALDI	matrix-assisted laser desorption/ionization
MeCN	acetonitrile
MGM	modified growth medium for haloarchaea
MS	mass spectrometry
<i>Namoo</i>	<i>Natronomonas moolapensis</i>
<i>Nmn. moolapensis</i>	<i>Natronomonas moolapensis</i>
<i>Napha</i>	<i>Natronomonas pharaonis</i>
<i>Nmn. pharaonis</i>	<i>Natronomonas pharaonis</i>
N	number
NMR	nuclear magnetic resonance
NTC	non-template control reaction
OD <sub>600</sub>	optical density at 600 nm
ORF	open reading frame
P	pellet
PA	phosphatidic acid
PAGE	polyacrylamide gel electrophoresis
PCR	polymerase chain reaction
PG	phosphatidyl glycerol
PGP	phosphatidyl glycerophosphate
PGS	Phosphatidylglycerosulfate
PM	purple membrane
PP	pentose phosphate
PP <sub>i</sub>	inorganic diphosphate
PRPP	5-phosphoribosyl 1-pyrophosphate
ppm	parts per million
RIN	RNA integrity number
RP	Retinal proteins
rpm	revolutions per minute
rt	room temperature (20 - 23 °C)
RT-PCR	reverse transcription polymerase chain reaction
RuBisCO	Ribulose-1,5-bisphosphate-carboxylase/-oxygenase
SN	supernatant
SDS	sodium dodecyl sulfate
SILAC	stable isotope labeling with amino acids in cell culture
Sop	sensory rhodopsin
SW	salt water
TCA	trichloroacetic acid (for protein precipitation) or tricarboxylic acid (Krebs cycle)
TFA	trifluoroacetic acid
THF	tetrahydrofuran



---

TLC	thin layer chromatography
TOF	time-of-flight
Tris	tris(hydroxymethyl)aminomethane
vs.	versus
v/v	volume per volume
wt	wild type
w/v	weight per volume

## Publications

Parts of this work were published previously or are in preparation for publication:

Oberwinkler T. and Oesterhelt D. (2007) CO<sub>2</sub> Fixation in Halophilic Archaea. *Talk at the Archaea Symposium* ("SPP1112"), Schmitten near Frankfurt

Falb M., Müller K., Königsmaier L., Oberwinkler T., Horn P., von Gronau S., Gonzalez O., Pfeiffer F., Bornberg-Bauer E. and Oesterhelt D. (2008) Metabolism of halophilic archaea. *Extremophiles* (12), 177-196

Wimmer F., Oberwinkler T., Bisle B., Tittor J. and Oesterhelt D. (2008) Identification of the arginine/ornithine antiporter ArcD from *Halobacterium salinarum*. *FEBS Lett* (582), 3771-3775

Schwaiger R., Furtwängler K., Oberwinkler T. and Oesterhelt D (2008) Insights into Transcriptional Regulation and Pathway Analysis of Halophilic Archaea. *Poster presentation at the International Congress of Genetics*, Berlin

Aivaliotis M., Oberwinkler T., Klee K., Damsma G., Schlesner M., Siedler F., Pfeiffer F., Lottspeich F. and Oesterhelt D. (2008) Arginine Fermentation – a Unique Feature to Gain Energy in an Extremophilic Archaeon. *Poster presentation at the Interaction Proteome Summer School "From Functional Proteomics to Systems Biology"*, Spetses, Greece

Oberwinkler T., Bista M., Siedler F., Pfeiffer F. and Oesterhelt D. (2009) Metabolic Labeling Studies on Halophilic Membrane Lipids. *Poster presentation at the FEBS-EMBO Lecture Course: Biomembranes*, Corsica, France

Oberwinkler T., Bista M., Gonzales O., Siedler F., Pfeiffer F. and Oesterhelt D. (2009) Metabolic Studies in the Halophilic Archaeon *N. pharaonis*. *Poster presentation at the Gordon Research Conference: Archaea*, New Hampshire, USA

Gonzalez O., Oberwinkler T., Mansueto L., Pfeiffer F., Mendoza E., Zimmer R. and Oesterhelt D. (2010) Characterization of growth and metabolism of the haloalkaliphile *Natronomonas pharaonis*. *PLoS Comput Biol* e1000799

Oberwinkler T., Dyall-Smith M., Pfeiffer F., Siedler F. and Oesterhelt D. (2010) Genomic and metabolic features of a new halophilic archaeon, *Nmn. moolapensis*, and comparison to its haloalkaliphilic relative *Nmn. pharaonis*. *Poster presentation at the Halophiles Conference*, Beijing, China

Aivaliotis M., Oberwinkler T., Damsma G., Klee K., Pfeiffer F., Siedler F., Lottspeich F. and Oesterhelt D. (2011) Arginine fermentation - a unique feature to gain energy in an extremophilic archaeon. *in preparation*

Oberwinkler T., Dyall-Smith M., Pfeiffer F., Siedler F. and Oesterhelt D. (2011) Lipid Metabolism of Halophilic Archaea. *in preparation*

---

## Danksagung

Mein Dank gilt...

Meinem Doktorvater Prof. Dr. Dieter Oesterhelt, der mich begeisternd in die salzige Welt dieser extremen Lebensformen eingeführt und meine Neugierde durch stets hilfreiche Diskussionen weiter geschürt hat.

Frau Prof. Dr. Helga Stan-Lotter für die Ermutigung mich überhaupt am MPI für Biochemie zu bewerben, Erfahrungen am NASA Ames Research Institute sammeln zu dürfen und die Bereitschaft als Zweitgutachterin einzutreten.

Mike Dyall-Smith mit Familie für seine motivierende Art, seinem Interesse und das erste Korrekturlesen.

Meinen stets hilfsbereiten, unterhaltsamen und empatischen Kollegen Rita Schwaiger, Katarina Furtwängler, Daniela Breckau, Susanne von Gronau, Arthur Miller, Wilfried Staudinger, Mirit Kologulko, Florian und Bettina Wimmer, Peter Palm, Christoph Schwarz und Michalis Aivaliotis, die mir den Laboralltag versüßten.

Dem Massenspektrometrie-Team mit Frank Siedler, Sigrid Bauer, Beatrix Scheffer und Barbara Dahners für ihre Unterstützung während den Messungen, Diskussionen und die Bereitstellung der Massenspektrometrie-Infrastruktur.

Der Bioinformatik-Gruppe mit Friedhelm Pfeiffer, Orland Gonzalez, Loc Mansueto, Alberto Marin-Sanguino, Ricardo del Rosario und Markus Rampp für die Einführung in die Genomannotation, zahlreiche Diskussionen über Stoffwechsel und Erklärungen.

Michal Bista, Marcin Krajewski und Sergio Cadamuro für ihre verständliche Einführung in die NMR-Technik und ihre Unterstützung bei der Spektrenauswertung.

Matthias Schlesner für wertvolle Tipps, Anregungen, Diskussionen während der Arbeit und nicht zuletzt sein geduldiges Korrekturlesen am Ende.

Wolfgang Strasshofer für die unermüdlichen Aminosäure Analysen und der gesamten Core-Facility.

Martin Grininger, Mathias Enderle und Barbara Mulinacci für nette Gespräche und sportliche Aktivitäten.

Meinen Kollegen und "Mädls": Kathrin Klee, Judith Müller, Mandy Büttner, Elisabeth Weidinger, Silvia Fassbender und meiner lieben "Zenzi" - Cäcilia Köstler.

Frau Haack für die Hilfe in allen möglichen organisatorischen Belangen und Silvia Haslbeck für stets saubere Labormaterialien.

Allen anderen Mitarbeitern der "OE-Abteilung" für die angenehme Atmosphäre und allen Weggeführten, die ich während Konferenzen und Workshops kennenlernen durfte und mich mit weiterer Inspiration versorgten.

Zuletzt allen, die nicht unmittelbar beteiligt waren, ohne die diese Arbeit jedoch nicht zustande gekommen wäre:

Meinen Freundinnen Elisabeth Wernig, Melina Defner und Alexandra Kollmitzer aus Klagenfurt, Gudrun Trinker aus Salzburg und Lisa Königsmaier aus Linz für ihre langjährige Freundschaft, Erleben von schönen Momenten, Zuhören und einfach Dasein.

Meinen Bionik-Freunden Severin Ehret und Carmen Zlaner, die mit mir ihre Begeisterung für eine noch recht unbekanntete Wissenschaft teilen.

Meinen Eltern, Bruder, Großeltern und der restlichen Familie in Österreich und Deutschland für ihre Unterstützung in jeglicher Form.

Meinem Freund Martin für das kostbare Leben ausserhalb des Instituts.



---

## Curriculum vitae

### OBERWINKLER Tanja Margret (Mag. Biol.)

Geburtsdatum \* 11.04.1983, Fürstenfeldbruck, Deutschland  
Staatsangehörigkeit Österreich, Deutschland

#### BERUFSERFAHRUNG

- 09.2006 – 10.2006 Stipendiatin des "Planetary Biology Internships" am NASA Ames Research Center, USA
- 01.2005 – 06.2005 Werksstudentin bei Prokaria Ltd., Island
- 07.2004 – 08.2004 Praktikantin am Max Planck Institut für Molekulare Genetik, Berlin, Deutschland
- 07.2003 – 08.2003 Praktikantin an der Landesanstalt für veterinärmedizinische Untersuchungen, Ehrental, Österreich

#### SCHUL- UND AUSBILDUNG

- seit 11.2006 Promotion am Max Planck Institut für Biochemie, Martinsried, Deutschland  
DISSERTATION: „Metabolic and Genomic Annotations in Halophilic Archaea“  
Betreuer: Prof. Dr. Dieter Oesterhelt, Abteilung Membranbiochemie
- 11.2004 – 06.2006 Diplomstudium Genetik und Biotechnologie, Paris-Lodron Universität Salzburg, mit Schwerpunkt Bioinformatik und Mikrobiologie  
07.2006: Diplomprüfung (Mag. Biol./MSc) mit Auszeichnung (Note: 1.0)  
08.2005 – 05.2006: Diplomarbeit „Analyse zum Aminosäure- und Isoprenoidstoffwechsel in halophilen Archaea“, Max Planck Institut für Biochemie, Martinsried
- 01.2005 – 06.2005 Auslandssemester an der University of Iceland in Reykjavik, Island
- 09.2001 – 11.2004 Bakkalaureatsstudium Genetik und Molekularbiologie, Paris-Lodron Universität Salzburg, Österreich  
11.2004: Abgabe von vier Bakkalaureatsarbeiten
- 09.1993 – 07.2001 Bundesrealgymnasium Viktring, Österreich mit Schwerpunkt Bildnerische Erziehung  
06.2001: Matura (Reifeprüfung) mit ausgezeichnetem Erfolg (Note: 1.5)
- 09.1989 – 07.1993 Volksschule, Ponfeld, Österreich

München, 1. Oktober 2010